

**PROCESS-INDUCED
DISORDERS IN DRUG POWDERS
FOR INHALATION**



DOCTORAL THESIS
SUBMITTED IN FULFILLMENT OF THE REQUIREMENTS
FOR THE DEGREE OF
DOCTOR IN NATURAL SCIENCE
AT THE CHRISTIAN ALBRECHT UNIVERSITY, KIEL, GERMANY

by

Thorsten Nicolas Müller

Kiel 2015

Referee: Prof. Dr. Hartwig Steckel

Co-Referee: Prof. Dr. Thomas Kunze

Date of exam: 10.07.2015

Accepted for publication: 10.07.2015

sgd. Prof. Dr. Wolfgang J. Duschl (Dean)

Research articles contributing to this thesis:

Thorsten Müller¹, Regina Scherließ¹, Jörg Schiewe², Rüdiger Smal¹, Claudius Weiler², Hartwig Steckel¹

Applicability of a one-step DVS method for the determination of amorphous amounts for further different hydrophilic and hydrophobic drugs

Eur. J. of Pharm. and Biopharm., 94 (2015) 333-341

Thorsten Müller¹, Regina Krehl¹, Jörg Schiewe², Claudius Weiler², Hartwig Steckel¹

Influence of small amorphous amounts in hydrophilic and hydrophobic APIs on storage stability of dry powder inhalation products

Eur. J. of Pharm. and Biopharm., 92 (2015) 130-138

Thorsten Müller¹, Jörg Schiewe², Rüdiger Smal¹, Claudius Weiler², Markus Wolkenhauer², Hartwig Steckel¹

Measurement of low amounts of amorphous content in hydrophobic active pharmaceutical ingredients with dynamic organic vapor sorption

Eur. J. of Pharm. and Biopharm., 92 (2015) 102-111

Conference contributions:

Müller, T., Schiewe, J., Weiler, C., Steckel, H.,

Usability of a one-step DVS method for the determination of amorphous amounts in hydrophilic and lipophilic active pharmaceutical ingredients,

8th Polish-German Symposium, Kiel, Germany (2015)

Müller, T., Krehl, R., Schiewe, J., Weiler, C., Steckel, H.,

The influence of amorphous amounts in active pharmaceutical ingredients on the aerodynamic particle size distribution and on storage stability,

Drug Delivery to the Lungs 25, Edinburgh, Scotland (2014)

Müller, T., Schiewe, J., Weiler, C., Steckel, H.,

Detecting low amounts of amorphous content in hydrophobic active pharmaceutical ingredients,

Controlled Release Society, Germany Local Chapter, Kiel, Germany (2014)

Müller, T., Schiewe, J., Weiler, C., Steckel, H.,

Detecting low amounts of amorphous content in hydrophobic active pharmaceutical ingredients,

9th World Meeting of Pharmaceutics, Biopharmaceutics and Pharmaceutical Technology, Lisbon, Portugal (2014)

Müller, T., Schiewe, J., Smal, R., Weiler, C., Steckel, H.,

Preparation and characterization of crystalline, semi-crystalline and fully amorphous powders of hydrophilic and lipophilic active pharmaceutical ingredients,

Drug Delivery to the Lungs 24, Edinburgh, Scotland (2013)

*“Tradition ist eine Laterne, der Dumme hält sich an ihr fest,
dem Klugen leuchtet sie den Weg“*

George Bernard Shaw

Lack of a specific mark or a reference to a trademark or a patent does not imply that this work or part of it can be used or copied without copyright permission.

Table of Contents

TABLE OF CONTENTS	I
LIST OF FIGURES	VII
LIST OF TABLES	XII
LIST OF FORMULA SYMBOLS	XIV
LIST OF ABBREVIATIONS	XVII
1 INTRODUCTION AND OBJECTIVES	1
1.1 Introduction	1
1.2 Objectives	4
2 THEORETICAL BACKGROUND	6
2.1 Human respiratory tract	6
2.2 Achievements and challenges of pulmonary drug delivery	6
2.2.1 Drug application devices	7
2.2.1.1 Nebulizers	7
2.2.1.2 Pressurized metered-dose inhalers (pMDIs)	7
2.2.1.3 Dry powder inhalers (DPIs)	8
2.2.1.4 Soft mist inhalers (SMIs)	8
2.2.2 Formulation strategies in dry powder inhalers (DPIs)	8
2.2.3 Interparticulate interactions in DPIs - Agglomeration behavior of solid particles	9
2.2.4 Aerodynamic behavior of particles in the laminar/turbulence air flow....	10
2.2.5 Deposition behavior of inhalable particles within the respiratory tract ...	12
2.3 Crystallinity and physical stability of amorphous systems	13
2.3.1 Thermodynamic state	13

2.3.2	Glass transition ($T_{g\ mix}$) of amorphous mixtures	15
3	MATERIALS AND METHODS	17
3.1	Materials.....	17
3.1.1	Selection of the model active pharmaceutical ingredients (APIs)	17
3.1.1.1	Ipratropium bromide (ITB)	17
3.1.1.2	Formoterol fumarate (FF)	18
3.1.1.3	Salbutamol sulphate (SBS)	18
3.1.1.4	Ciclesonide (CS)	19
3.1.1.5	Budesonide (BS)	20
3.1.1.6	Glibenclamide (GC).....	20
3.1.2	Selection of the excipient	22
3.1.2.1	α -Lactose-monohydrate	22
3.1.3	Selection of inhalation devices.....	23
3.1.3.1	DPI - Easyhaler [®]	23
3.1.3.2	DPI - HandiHaler [®]	23
3.2	Methods	25
3.2.1	Preparation of fully amorphous and semi-crystalline samples.....	25
3.2.1.1	Ball-milling (BM)	25
3.2.1.2	Spray-drying (SD).....	25
3.2.1.3	Freeze-drying (FD)	26
3.2.1.4	Quench-cooling (QC).....	27
3.2.1.5	Jet-milling (JM)	27
3.2.1.6	Mixing tests with glass beads (Turbula blender)	28
3.2.2	Other manufacturing processes	28
3.2.2.1	Blending of samples with different amorphous amounts (for calibration curves and validation)	28
3.2.2.2	Conditioning	29

3.2.2.3	Blending powder for inhalation/Dissolution testing (Turbula blender).....	29
3.2.3	Methods for characterization and analysis of amorphous content	31
3.2.3.1	Dynamic vapor sorption (DVS)	31
3.2.3.2	X-ray powder diffraction (XRPD)	32
3.2.3.3	Differential scanning calorimetry (DSC).....	32
3.2.3.4	Temperature-modulated differential scanning calorimetry (TMDSC)	33
3.2.3.5	Hyper-differential scanning calorimetry (Hyper-DSC)	33
3.2.3.6	Dynamic mechanical analysis (DMA)	33
3.2.4	Methods for powder and particle characterization	35
3.2.4.1	Particle size distribution (PSD) determined by laser diffraction analysis ..	35
3.2.4.2	Density measurement.....	36
3.2.4.3	Scanning electron microscopy (SEM)	36
3.2.4.4	Inverse gas chromatography (iGC)	37
3.2.4.5	Surface area determined by Brunauer, Emmett and Teller (BET) method.	38
3.2.4.6	Residual moisture determined by infrared scale (IR)	39
3.2.5	Methods for blend characterization and <i>in-vitro</i> deposition behavior	39
3.2.5.1	Determination of blend homogeneity	39
3.2.5.2	High performance liquid chromatography (HPLC)	39
3.2.5.3	Cascade impactor - Next Generation Impactor (NGI)	40
3.2.5.4	Cascade impactor - Andersen Cascade Impactor (ACI)	42
3.2.6	Methods for dissolution behavior	42
3.2.6.1	Paddle apparatus with membrane holder (Dissolution testing)	42
3.2.6.2	Optimization of drug deposition on the filter membrane (ACI)	43
3.2.6.3	Solubility measurements - Saturation solubility	43
3.2.7	Design of Experiments (DoE)	44
4	RESULTS AND DISCUSSION	45
4.1	Amorphous content and estimation of stability behavior	45

4.1.1	Fully amorphous samples	45
4.1.1.1	Ball-milling process	45
4.1.1.2	Spray-drying process	48
4.1.1.3	Freeze-drying process	49
4.1.1.4	Quench-cooling method.....	50
4.1.2	Stability assessment of the amorphous APIs and shelf-life	51
4.1.3	Semi-crystalline samples	57
4.1.3.1	Jet-milling process	57
4.1.3.2	Mixing tests with glass beads	59
4.2	Additional physico-chemical characterization of the crystalline starting material.....	60
4.3	Development of a one-step Dynamic vapor sorption (DVS) method for the calculation of amorphous amounts	61
4.3.1	Case study of Ciclesonide (CS).....	64
4.3.1.1	Water moisture sorption isotherms - Influence on the absorption behavior and the need for organic solvents	65
4.3.1.2	Organic solvent screening - Influence on absorption behavior.....	66
4.3.1.3	Determination of the optimal vapor (p/p_0) value	69
4.3.1.4	Temperature robustness - Design of Experiments (DoE).....	70
4.3.1.5	Influence of particle size/surface on the absorption behavior.....	72
4.3.1.6	Validation of the organic one-step DVS method based on the ICH Guideline Q2 (R1).....	77
4.3.1.7	Schematic absorption behavior of hydrophilic and hydrophobic samples with polar and nonpolar solvents	79
4.3.2	Applicability to other model APIs.....	80
4.3.2.1	Adaption for hydrophobic model drugs (BS/GC).....	81
4.3.2.2	Adaption for hydrophilic model drugs (ITB/FF/SBS).....	87
4.3.3	Conclusion I.....	88

4.3.4	Usability of the one-step method on selected powder samples	89
4.3.5	Conclusion II	95
4.4	Aerodynamic investigations: Influence of different amorphous amounts on the de-agglomeration and deposition behavior	96
4.4.1	Study 1: Lactose, SBS, CS and the Easyhaler®	97
4.4.1.1	Bulk powder and blend characterization.....	98
4.4.1.2	Impaction analysis	102
4.4.1.3	Schematic model based on NGI results - Influence on FPF (Study 1)	107
4.4.2	Study 2: Glass beads, SBS, CS and HandiHaler®	111
4.4.2.1	Bulk powder and blend characterization.....	112
4.4.2.2	Impaction analysis	114
4.4.2.3	Schematic model based on NGI results (Study 2)	120
4.4.3	Conclusion III	121
4.5	Dissolution testing.....	122
4.5.1	Bulk powder and blend characterization	124
4.5.2	Optimization of the phosphate buffer as dissolution media for CS	126
4.5.3	Optimization of the dose collection for SBS and CS with the Andersen Cascade Impactor (ACI)	129
4.5.4	Burst release and poor solubility	133
4.5.5	Conclusion IV.....	137
5	OVERALL CONCLUSION AND FUTURE PERSPECTIVES	139
6	SUMMARY.....	141
7	SUMMARY (GERMAN).....	143
8	APPENDIX.....	145
8.1	Methods	145

8.1.1	Quantification of API content - HPLC	145
8.1.1.1	Salbutamol sulphate	145
8.1.1.2	Ciclesonide.....	146
8.2	Materials.....	147
8.3	Raw data.....	149
8.3.1	Validation of High Performance Liquid Chromatography (HPLC) methods for SBS and CS.....	149
8.3.2	Selected XRPD diagrams	152
8.3.3	Selected DSC diagrams	155
8.3.4	Selected TMDSC diagrams	157
8.3.5	Selected organic moisture sorption isotherms by DVS.....	159
8.3.6	Delivered dose (Easyhaler [®]) of the NGI Study 1	160
9	REFERENCES	162
	DANKSAGUNG.....	178
	LEBENS LAUF.....	179
	ERKLÄRUNG NACH § 8 DER PROMOTIONSORDNUNG	180

List of figures

Figure 1: Simplified schematic interactions between carrier particle and micronized API modified from Pilcer et al., 2012.....	9
Figure 2: Agglomerate of spray-dried Ciclesonide particles	11
Figure 3: Mechanisms of stress to de-agglomerate particles by air flow modified from Weiler et al., 2008	11
Figure 4: Division of the respiratory system linked to the overlapping deposition principles in the lung modified from Meier et al., 1981	12
Figure 5: Differences between the crystalline and the amorphous state	14
Figure 6: Temperature-dependence of liquid and crystalline state	15
Figure 7: Chemical structure of Ipratropium bromide	17
Figure 8: Chemical structure of Formoterol.....	18
Figure 9: Chemical structure of Salbutamol	18
Figure 10: Chemical structure of Ciclesonide (pro-drug) and ester hydrolyzes	20
Figure 11: Chemical structure of Budesonide.....	20
Figure 12: Chemical structure of Glibenclamide	21
Figure 13: Tomahawk-like particle shape of lactose and agglomerated needle-like SBS crystals.....	22
Figure 14: Disaccharide lactose (condensation of D-galactose and D-glucose).....	23
Figure 15: Cross-sectional view of the reservoir based Easyhaler [®] and de-agglomeration principle.....	23
Figure 16: HandiHaler [®] as capsule based model inhalation device.....	24
Figure 17: Movement of grinding chamber in ball-mill process.....	25
Figure 18: Freeze-drying profile: time depending change of temperature and pressure.....	26
Figure 19: Transformation of crystalline to amorphous material by quench-cooling.....	27
Figure 20: Schematic structure of the jet-mill (JM)	27
Figure 21: Rotation of the Turbula mixer	28
Figure 22: Set-up of the DVS-HT: Giving the option for testing 10 samples and application of organic solvents.....	31
Figure 23: Structure of the evacuated X-ray tube	32
Figure 24: Principle of temperature-modulated heating rate.....	33
Figure 25: Viscoelastic behavior of amorphous samples.....	34
Figure 26: Relationship between elastic modulus, storage modulus and loss modulus.....	35
Figure 27: Cumulative volume-based particle size distribution.....	36

Figure 28: Schematic of inverse gas chromatography (iGC).....	37
Figure 29: Set-up of an open NGI with collection cups.....	41
Figure 30: Modified Andersen Cascade Impactor with filter stage for dose collection.....	42
Figure 31: Paddle apparatus with membrane holder.....	43
Figure 32: Solid bridges of a sintered ball-milled API.....	46
Figure 33: Comparison of fully amorphous and fully crystalline APIs.....	47
Figure 34: Difference in surface morphology: Comparison of rough and smooth spheres.....	49
Figure 35: Freeze-dried, porous SBS sample.....	50
Figure 36: DSC measurement of the hydrophilic APIs.....	50
Figure 37: DSC measurement of the hydrophobic APIs.....	51
Figure 38: Glass transition of amorphous APIs dependent on molecular weight.....	52
Figure 39: Adsorption behavior of fully crystalline APIs.....	53
Figure 40: Absorption behavior of fully amorphous APIs.....	54
Figure 41: Temperature influence on amorphous ball-milled CS and BS samples.....	55
Figure 42: Humidity influence on amorphous ball-milled CS and BS samples.....	55
Figure 43: Temperature robustness of an amorphous SBS sample.....	56
Figure 44: Influence of one grinding cycle on particle size (SBS).....	58
Figure 45: Influence of the number of grinding cycles on the peak intensity in XRPD.....	59
Figure 46: Blends with small and big glass beads.....	59
Figure 47: Comparison of different methods to determine amorphous content of CS.....	62
Figure 48: DMA measurement of fully amorphous CS.....	63
Figure 49: DMA measurement for 15% amorphous content (CS).....	64
Figure 50: Water moisture sorption isotherms of hydrophilic and hydrophobic samples.....	65
Figure 51: Increase of absorption behavior/re-crystallization to different organic solvents....	67
Figure 52: Decrease of glass transition due to solvent type and quantity (Gordon-Taylor)....	69
Figure 53: Influence of the p/p_0 value (isopropanol) on the stability of amorphous amounts.	70
Figure 54: Temperature-robustness of the developed DVS method.....	71
Figure 55: Integration of measured absorption values in the model.....	72
Figure 56: Influence of particle size on the absorption behavior.....	73
Figure 57: Influence of amorphous state localized on the surface and inside the particle.....	74
Figure 58: Mass specific surface and absorption behavior of different amorphous samples... 74	74
Figure 59: Influence of particle shape on SD and BM samples for CS.....	76
Figure 60: TMDSC measurement of spray-dried and ball-milled CS samples.....	76
Figure 61: Estimation of LOQ based on baseline absorption of crystalline material for CS... 78	78

Figure 62: One-step DVS method for CS in detail	78
Figure 63: Schematic absorption behavior modified from Weiler et al., 2008	79
Figure 64: Overview of the DVS-method development: Production, test measurement and calculation	80
Figure 65: Organic solvent screening for BS (JM1 Gc3).....	81
Figure 66: BS calibration curves measured with different solvent types and intensity levels.	82
Figure 67: Organic solvent screening for GC (JM1 Gc3).....	83
Figure 68: GC calibration curves measured with different solvent types	84
Figure 69: Optimized one-step DVS method for the calculation of amorphous parts (CS, BS and GC)	84
Figure 70: Hydrophobic starting material and the conditioned samples with isopropanol.....	85
Figure 71: Micronized powders compared to conditioned samples with isopropanol.....	86
Figure 72: Further organic solvent storages for BS and GC	86
Figure 73: Optimized one-step DVS method for the calculation of amorphous parts (ITB, FF and SBS).....	88
Figure 74: Calibration curves of all investigated APIs for the calculation of amorphous amounts	89
Figure 75: Increase of mass absorption of the single blends of CS in dependence to the vapor value	91
Figure 76: Alternative method for the preparation of homogenous mixtures of amorphous amounts	92
Figure 77: Overview of the absorption behavior of SBS samples	94
Figure 78: Overview of the absorption behavior of CS samples	95
Figure 79: Design of Study 1: Investigation of the influence of different amorphous amounts in hydrophilic and hydrophobic APIs on the de-agglomeration and aerodynamic deposition behavior.....	97
Figure 80: Relation of the cumulative distribution of SBS particles - Study 1.....	99
Figure 81: Relation of the cumulative distribution of CS particles - Study 1	100
Figure 82: SEM pictures of the conditioned SBS samples - Study 1.....	101
Figure 83: SEM pictures of the conditioned CS samples - Study 1	101
Figure 84: Deposition behavior of SBS and CS blends with different amorphous amounts after 1 day of storage at 45% RH - Study 1	102
Figure 85: Deposition behavior of SBS and CS blends with different amorphous amounts after 180 days of storage at 45% RH - Study 1	103

Figure 86: Change of fine particle fraction for amorphous SBS blends (storage over 6 months at 45% RH and RT) - Study 1	104
Figure 87: Change of fine particle fraction for amorphous CS blends (storage over 6 months at 45% RH and RT) - Study 1	106
Figure 88: Blends of SBS 2 and SBS 3 after storage at 45% RH for 6 months (A) overview and (B) magnification - Study 1	107
Figure 89: De-agglomeration model of SBS (A) at the beginning of storage (B) during storage at 45% RH.....	108
Figure 90: Degradation of strong hydrogen bridge bonds (SBS) during storage at 45%	109
Figure 91: De-agglomeration model during inhalation for CS (A) smooth and (B) rough API particle surface	110
Figure 92: Degradation of weak hydrogen bridge bonds (CS) during storage at 45% RH....	110
Figure 93: Design of Study 2: Investigation of the influence of different amorphous amounts in hydrophilic and hydrophobic APIs on the de-agglomeration and aerodynamic deposition behavior.....	111
Figure 94: Formulated glass beads with a concentration of 0.6% API.....	112
Figure 95: SEM pictures of glass beads without (A) and with API (B).....	114
Figure 96: Deposition behavior of SBS and CS blends with different amorphous amounts after 1 day of storage at 45% RH - Study 2	115
Figure 97: Deposition behavior of SBS and CS blends with different amorphous amounts after 180 days of storage at 45% RH - Study 2.....	116
Figure 98: Change of fine particle fraction for amorphous SBS blends (storage over 6 months at 45% RH and RT) - Study 2 in comparison to study 1.....	116
Figure 99: Change of fine particle fraction for amorphous CS blends (storage over 6 months at 45% RH and RT) - Study 2 in comparison to study 1.....	118
Figure 100: SEM pictures of the thin API-film on the surface of glass beads formulation with (A) SBS and (B) CS	120
Figure 101: Change of crystal shape during the mixing process	120
Figure 102: Press-on forces on different types of carrier (lactose/glass bead) modified from de Boer et al., 2006	121
Figure 103: Overview of the dissolution testing	123
Figure 104: SEM pictures of the bulk powders for SBS.....	125
Figure 105: SEM pictures of the bulk powders for CS	125
Figure 106: Solubility test of CS by adding different and various amounts of surfactants ...	126

Figure 107: Adding of 0.5% Plasdone [®] for higher solubility of CS samples	128
Figure 108: Adding of 0.05% SDS for higher solubility of CS samples	129
Figure 109: Impaction of SBS blends in dependence to multi dosing (HandiHaler [®]).....	130
Figure 110: Impaction of CS blends in dependence to multi dosing (HandiHaler [®]).....	130
Figure 111: Impaction of SBS blends in dependence to multi dosing (Easyhaler [®]).....	131
Figure 112: Impaction of CS blends in dependence to multi dosing (Easyhaler [®]).....	132
Figure 113: Equal doses of both blends because of different actuations applied with the Easyhaler [®]	132
Figure 114: Absolute amount of each SBS blend dissolved over 4 hours	133
Figure 115: Residual amounts of each SBS blend on the watch glass and on the membrane	134
Figure 116: Release profiles of the SBS blends with different amorphous amounts.....	135
Figure 117: Absolute amount of the CS blends dissolved after 4 hours	136
Figure 118: Residual amounts of each CS blend on the watch glass and membrane	137
Figure 119: Time-depending diffusions layer of SBS and CS	138
Figure 120: HPLC signal/noise ratio of both APIs	150

List of tables

Table 1: Glass transition temperature of the used solvents	16
Table 2: Typical characteristics of the hydrophilic model drugs	19
Table 3: Typical characteristics of the hydrophobic model drugs	21
Table 4: Overview of the produced and tested mixtures.....	30
Table 5: Important parameter of the analysis of variance (ANOVA).....	44
Table 6: Optimized ball-mill parameters for BS	46
Table 7: Parameters for all APIs in the ball-milling process for the production of fully amorphous samples	47
Table 8: Influence of longer grinding times on CS samples	48
Table 9: Characterization of successful produced fully amorphous spray-dried powders.....	49
Table 10: Overview of the investigated APIs by DSC measurement	51
Table 11: Influence of the number of grinding cycles on the particle size distribution.....	57
Table 12: Physico-chemical characterization of crystalline starting material.....	60
Table 13: Physico-chemical characteristics of the polar and nonpolar solvents.....	66
Table 14: Experimental observations of the organic solvent screening.....	68
Table 15: DoE to investigate the factors amorphous content (1) and temperature (2)	71
Table 16: Evaluation of the DoE - Temperature robustness	72
Table 17: Powder characterization of investigated samples	75
Table 18: Final parameters for all hydrophobic APIs for the determination of amorphous content by DVS	85
Table 19: Final parameters for all hydrophilic APIs for the determination of amorphous content	88
Table 20: Process standard deviation and process coefficient of variation of the calibration curves of the developed DVS methods	90
Table 21: Absorption values of different amorphous blends at 0.1 p/p_0 and 0.3 p/p_0	91
Table 22: Determination of the amorphous content of micronized powders.....	93
Table 23: PSD and amorphous content of the conditioned SBS and CS samples - Study 1....	98
Table 24: Content uniformity of the blended inhalable mixtures - Study 1.....	100
Table 25: NGI results of both SBS blends with lactose - Study 1	105
Table 26: NGI results of both CS blends with lactose - Study 1	106
Table 27: PSD and amorphous content of the conditioned SBS and CS samples - Study 2..	113
Table 28: Content uniformity of the blended inhalable mixtures - Study 2.....	113
Table 29: NGI results of both SBS blends with glass beads - Study 2	117

Table 30: NGI results of both CS blends with glass beads - Study 2	119
Table 31: PSD and amorphous content of the conditioned SBS and CS samples for the dissolution testing.....	124
Table 32: Content uniformity of the blended inhalable mixtures for the dissolution testing.	124
Table 33: Screening for an optimized solubility of CS powder samples	127
Table 34: HPLC linearity of different SBS and CS amounts.....	149
Table 35: HPLC recovery rates of both APIs in the accuracy test series.....	150
Table 36: Closeness of agreement between a series of measurements for the precision	151
Table 37: Robustness of SBS and CS HPLC analytics up to 5 days	152

List of formula symbols

a	Intercept
A	Surface area of nitrogen molecule [m ²]
A_H	Material-specific Hamaker constant [J]
b	slope of curve
C_C	Cunningham correction factor [-]
C_p	Specific heat capacity [J/g · °C]
γ	Surface tension [N/m]
d	Particle diameter [m]
d_{ae}	Aerodynamic diameter [m]
d_{geo}	Geometric diameter [m]
$Diff$	Diffusion coefficient
δ	Phase angle [°]
ε	Strain [N/m ²]
f	Frequency [Hz]
F_{CF}	Capillary force [N]
F_R	Resistance force [N]
F_{vdW}	Van der Waals force [N]
g	Gravitational acceleration [m/s ²]
G^*	Elastic modulus [Pa]
G'	Storage modulus [Pa]
G''	Loss modulus [Pa]
η	Viscosity [Pa · s]
ΔH	Enthalpy [J]
θ	Contact angle [°]
k	Boltzmann's constant [J/K]
K	Constant
N_A	Avogadro constant [mol ⁻¹]
n_{ads}	Amount of absorbed gas [mol/g]
m_{dry}	mass dry [g]
n_m	Monolayer [mol/g]

m_{wet}	mass wet [g]
Q_3	Cumulative volume-based distribution [%]
R_I	Radius of sphere [m]
Re	Reynolds number [-]
ρ_a	Air density [kg/m ³]
ρ_p	Particle density [kg/m ³]
ρ_0	H ₂ O density [kg/m ³]
π	3.14159
S_m	Mass-specific surface area [m ² /g]
Stk	Stokes' number
S_v	Volume-specific surface area [m ² /cm ³]
S_{x0}	Process standard deviation
σ	Stress [μ m/m]
T	Temperature [K]
T_c	Re-crystallization temperature [K]
T_g	Glass transition [K]
$T_{g\ mix}$	Glass transition of binary mixture [K]
T_K	Kauzmann temperature [K]
T_m	Melting point [K]
T_o	Onset temperature of the melting point [K]
T_p	Period [s]
Δt	Temporal phase shift
V	Air velocity [m/s]
v_{rel}	Relative velocity [m/s]
V_S	Setting velocity [m/s]
V_{x0}	Process coefficient of variation [%]
X	Measure of length [m]
x_{Aggl}	Diameter of the agglomerate [μ m]
X_S	Dynamic shape factor
x_{10}	Particle diameter < 10% particle volume [μ m]
x_{50}	Particle diameter < 50% particle volume [μ m]

x_{90}	Particle diameter < 90% particle volume [μm]
ω	Angular frequency [s^{-1}]
w	Weight fraction [%]

List of abbreviations

ACI	Andersen Cascade Impactor
API	Active pharmaceutical ingredient
APSD	Aerodynamic particle size distribution
AUC	Area under the curve
BET	Brunauer, Emmett and Teller
BM	Ball-milling
BS	Budesonide
CFC	Chlorofluorocarbon
COPD	Chronic obstructive pulmonary disease
CS	Ciclesonide
CV	Coefficient of variation
DD	Delivered dose
ddH ₂ O	double distilled water
DMA	Dynamic mechanical analysis
DoE	Design of experiments
DPI	Dry powder inhaler
DSC	Differential scanning calorimetry
DVS	Dynamic vapor sorption
F	Filter stage
FD	Freeze-drying
FF	Formoterol fumarate
FID	Flame ionization detector
FPD	Fine particle dose
FPF	Fine particle fraction
GC	Glibenclamide
Gc	Grinding cycle
GSD	Geometric standard deviation
HFA	Hydrofluoroalkane
HPLC	High performance liquid chromatography
HPMC	Hydroxylpropyl methyl cellulose

ICH	International Conference on Harmonisation
ICS	Inhaled corticosteroid
iGC	Inverse gas chromatography
IMC	Isothermal microcalorimetry
IR	Infrared scale
ITB	Ipratropium bromide
JM	Jet-milling
LABA	Long-acting β_2 -adrenoceptor agonist
LOQ	Limit of quantification
MMAD	Mass median aerodynamic diameter
NGI	Next Generation Impactor
PBS	Phosphate buffered saline
Ph. Eur.	Pharmacopoeia Europaea
pMDI	Pressurized metered-dose inhaler
PSD	Particle size distribution
QC	Quench-cooling
RH	Relative humidity
rpm	rounds per minute
RSD	Relative standard deviation
RT	Room temperature
SABA	Short-acting β_2 -adrenoceptor agonist
SAMA	Short-acting muscarinergic antagonist
SBS	Salbutamol sulphate
Sccm	Standard cubic centimeter per minute
SD	Spray-drying
sd	Standard deviation
SDS	Sodium dodecyl sulfate
SEM	Scanning electron microscopy
SMI	Soft mist inhaler
TCD	Thermal conductivity detector
TMDSC	Temperature modulated differential scanning calorimetry

USP United States Pharmacopoeia

XRPD X-ray powder diffraction

1 INTRODUCTION AND OBJECTIVES

1.1 Introduction

Inhalation products are routinely used in the therapy of the local treatment of respiratory diseases [1]. The focus of attention is on diseases such as bronchial asthma, chronic obstructive pulmonary disease (COPD), cystic fibrosis or lung cancer [2]. Thereby, different drug application devices such as nebulizers, pressurized metered-dose inhalers (pMDIs) and dry powder inhalers (DPIs) are used for an efficient delivery of the active pharmaceutical ingredients (APIs) to the lung [3]. Anticholinergic bronchodilators, β_2 -adrenoceptor agonists and inhalable corticosteroids are usually prescribed for the benefit of the patients [4].

DPIs are especially well established on the market and thereby arouse a great interest. For this type of device formulation strategies revolve around carrier or carrier-free systems [5]. On the one hand the micronized API (particle size about 5 μm) is formulated with coarse carrier particles ($> 100 \mu\text{m}$) in a binary mixture. On the other hand spheroids (soft aggregates) are manufactured by controlled agglomeration (spheronisation) of micronized particles [6]. In both cases the dispersion of these agglomerates (drug-to-drug/drug-to-carrier) is generated by induced air turbulences through grids/rotators, shearing forces and particle collisions to achieve a significant amount of drug depositing in the lungs.

In general, an extended understanding of the particle structure and de-agglomeration behavior of the micronized API is needed to optimize these formulations. Several physico-chemical parameters have to be determined which have an influence on the detachment of the drug from the carrier (powder flow, particle size, shape, surface morphology, contact area, hygroscopicity) [7–9]. A specific parameter for inhalable products is the aerodynamic diameter (d_{ae}) of the API. It takes the particle shape/particle density into account and it should be in the range of 0.5 μm and 5.0 μm for an efficient pulmonary drug delivery [10]. APIs which contain particles larger than 5.0 μm might impact in the upper airways and thus boost side effects. Formulation strategies such as “particle engineering” focus on a high fine particle fraction (FPF: % of delivered dose $< 5\mu\text{m}$) which is characterized by a narrow particle size distribution (PSD), good flow and dispersion properties of the excipient and the API [11].

Furthermore, it is well-documented in the literature that standard pharmaceutical operations such as intensive blending, milling and also sieving can induce structural changes [12] and cause disruption in the crystal structure (amorphous content) to the surface of both, excipients and active pharmaceutical ingredients. These mentioned disorders in the surface structure

have a high affinity to water vapor [13] and might induce a lowering in the glass transition temperature [14] which can lead to a re-crystallization process of the thermodynamic unstable amorphous amounts. These conditions can affect processing, performance and the product stability [15]. In any case, the kinetics of process induced disorders are only partly understood. In addition, finding a reliable method to accurately determine the amorphous content in pharmaceutical powders down to a level $< 1\%$ is still a challenge. The need of quantifying, monitoring and controlling amorphous parts is therefore absolutely essential.

First studies demonstrated that the performance of inhalation powder blends is significantly affected when amorphous lactose is added to the carrier lactose for the simulation of the before mentioned disorders [16,17]. It is assumed that the micronization of the APIs lead to post-operational relaxation in the inhalable mixtures inducing particle size changes and re-crystallization effects.

Nevertheless, the exact imitation of process-induced disorders is hardly to achieve as the quality of the structural changes may differ. It is well known that there are different states of amorphicity depending on the conducted process. So far fully amorphous samples were prepared by spray-drying [18], freeze-drying [19] or quench cooling [20]. Subsequently these purely amorphous materials were mixed with crystalline material to produce calibration curves.

However, various analytical techniques can be used when addressing the issue of the determination of amorphous content in a powder. Over the years different papers have been published using traditional analytical techniques such as Powder X-ray Diffraction (XRPD) and Differential Scanning Calorimetry (DSC) (limit of detection: 5-10%) [21]. Furthermore, near infrared spectroscopy was used to differentiate between amorphous and crystalline states by evaluating the peak intensity and shifts in the known fingerprint regions of the spectra (limit of detection: 1%) [22]. In conclusion all these bulk analytical techniques measure the properties of the sample as a whole and thus the amorphous content becomes a small part of the total signal [23]. Furthermore, studies using isothermal microcalorimetry (IMC) were published (limit of detection: 1%) [24]. One disadvantage of this technique is that a potential re-crystallization of the amorphous solid may not be detected due to the time required to equilibrate the sample [25]. This equilibration process in the isothermal microcalorimetry takes place unmonitored for nearly 1 hour. Furthermore, no data can be recorded confirming that amorphous amounts remain stable in this period of time.

Amorphous parts which might act as “reactive spots” on the surface can be determined especially in hydrophilic samples by water moisture sorption isotherms [26]. In their review Sheokand et al. divided the DVS-methods into three main groups for the quantification of amorphous amounts [15]. Equilibrium moisture uptake (based on absorption), water uptake method (based on re-crystallization) and residual weight (based on solvated solvent) method are in focus. For hydrophobic material, which is chemically more stable against water vapor and the change in crystallinity is self-limiting, only a few approaches (DVS) are available which focus on organic solvents. For example Mackin et al. used acetone as a solvent (for benzyl ether derivative) and Samra et al. used mixtures of ethanol/water and ethanol/n-propanol in their investigations with hydrophobic terfenadine [25,27].

1.2 Objectives

This thesis focuses on the production and evaluation of amorphous amounts, the development of a detection method (< 1%) especially for more hydrophobic APIs based on absorption techniques (Dynamic vapor sorption) and on the influence of amorphous amounts on the de-agglomeration behavior over a defined storage time (six months). Furthermore, the applicability of a dissolution testing system (Andersen Cascade Impactor and USP paddle apparatus 2) for inhalable blends is investigated determining the influence of different amorphous amounts on dissolution behavior.

Firstly, the work schedule consists of the preparation of semi-crystalline and fully amorphous samples by using different technologies and the investigation of the process conditions. The focus is set on methods such as ball-milling, spray-drying, freeze-drying and quench cooling for the establishment of purely amorphous material. On the contrary, the generation of small proportions of amorphous forms mainly localized on the surface of the particles is performed by jet-milling and intensive blending (simulation with glass beads). Furthermore, the influence of these process-induced disorders on the stability and shelf-life is investigated.

In the second part the establishment and the qualification of DVS sorption methods that enable the quantification of amorphous parts down to a level of < 1% are performed. Firstly, hydrophilic and hygroscopic APIs such as Ipratropium bromide, Formoterol fumarate and Salbutamol sulphate are investigated and moisture sorption isotherms are determined, respectively. Afterward, hydrophobic APIs such as Ciclesonide, Budesonide and Glibenclamide are evaluated. Thereby, a change from polar (water) to nonpolar organic solvents is necessary to increase the affinity of the drug to the solvent (organic solvent screening). Finally, the method is meant to be simplified as much as possible because the development of a one-step measurement is desired. The determination of the optimal vapor (p/p_0) value and the adjustment of the temperature are required. In addition, the influence of amorphous quality, particle size and surface on the absorption behavior is investigated. To complete the described method a validation of the one-step DVS method based on the ICH Guideline Q2 (R1) is performed. Hereby, the linearity, precision and the limit of quantification (LOQ) are investigated. The applicability of all six model APIs is tested and a general guidance for the adaptation of the method to other drugs is established. Finally, the calculation of the amorphous amounts in the unknown samples and the energy-dependent introduction of an amorphous phase onto solid surfaces are desired to be feasible. In addition, the extent of amorphous parts depending on the material properties (melting point, hydrophobicity) is evaluated.

The thematic field of inhalation addresses the impact of amorphous content in API/lactose blends on the physical stability (six months). The focus is set on process conditions that introduce amorphous amounts to the API and on the investigation of the re-crystallization process for these inhalable blends. Of great interest is the diversified behavior of hydrophilic and hydrophobic samples. Furthermore, inert glass beads replace the hydrophilic lactose as a model carrier.

The completion of the work schedule involves the dissolution testing. The applicability of a dissolution test system (Andersen Cascade Impactor and USP paddle apparatus 2) is investigated for hydrophilic and hydrophobic active pharmaceutical ingredients. The objective is to evaluate the influence of different amorphous amounts in inhalation powders on the dissolution rate.

2 THEORETICAL BACKGROUND

2.1 Human respiratory tract

The respiratory system is essential for supplying the organism with oxygen and removing carbon dioxide. It is mainly responsible for pulmonary ventilation and the movement of air into and out of the lungs [28]. Depth of respiration and breathing frequency is regulated by a complex and specific regulatory system [29].

Basically, the airways are divided into two major regions, the upper and lower respiratory tracts. The first part includes the nasal passages, throat, pharynx and the larynx. The lower tract is divided into the trachea, bronchi, bronchioles and the alveoli (attractive respiratory region [30]). These subdivisions facilitate gaseous exchange to blood vessels which is enabled by the very large surface area (80-90 m²) and thin absorption membranes (0.1-0.2 μm) of the lung [31]. Furthermore, high lung perfusion (5-6 l/min) allows a rapid distribution of molecules [29].

Figure 4 shows the division of the respiratory system and the relationship between particle size and lung deposition. In chapter 2.2.4 the general deposition principles (impaction, sedimentation and diffusion) are illustrated.

2.2 Achievements and challenges of pulmonary drug delivery

The efficient delivery of active pharmaceutical ingredients (APIs) to the lung by inhalation products depends on several parameters which include the formulation (flowability, particle size, shape, surface), the inhaler device (nebulizers, pressurized metered-dose inhalers (pMDIs) and dry powder inhalers (DPIs)), the metering system (capsule, multi-unit dose or reservoir dose) and the patient's inhalation technique (e.g. flow rate) [32]. A specific parameter for inhalation products is the aerodynamic diameter (d_{ae}) of the API. It takes account of the particle shape/particle density and it should be in the range of 0.5 μm and 5.0 μm for efficient pulmonary drug delivery [33]. This value is defined by the equation 2.1, where d_{geo} is the geometric diameter, ρ_p and $\rho_0 = 1 \text{ g/cm}^3$ are the particle and unit densities, respectively and X_S is the dynamic shape factor. Large porous particles might have the same aerodynamic behavior as smaller particles with higher density.

$$d_{ae} = d_{geo} \cdot \sqrt{\frac{\rho_p}{\rho_0 \cdot X_S}} \quad 2.1$$

For very small particles (0.1-0.3 μm) the Cunningham correction factor (C_C) needs to be introduced [34]. APIs which exhibit larger particle size might impact in upper airways and thus boost side effects. Consequently, the efficiency of the treatment of respiratory diseases such as bronchial asthma, chronic obstructive pulmonary disease (COPD), cystic fibrosis or lung cancer can be lowered. Formulation strategies such as “particle engineering” focus on a high fine particle fraction (FPF: % of delivered dose < 5 μm) by supplying a narrow particle size distribution (PSD), good flow and dispersion properties of the excipient and the API [35]. An interest in the systemic drug delivery has emerged recently [36] and promotes the potential for the entry of peptides, proteins, antibiotics or vaccines over the lung. Affrezza[®], for example, is an inhalable insulin which improves the blood sugar control in adult patients with diabetes (MannKind Corporation) [37]. Recently, Adasuve[®] (Ioxapine), an inhalation powder has been approved for the acute treatment of agitation associated with schizophrenia or bipolar disorders in adults (Alexza Pharmaceuticals).

2.2.1 Drug application devices

In general, drug application devices can be distinguished into four main groups.

2.2.1.1 Nebulizers

Nebulizers are used for solution- and suspension-based medications. The aerosolization is performed by a vibrating mesh (Mesh nebulizers), ultrasonic transducer (Ultrasonic nebulizers) or by compressed air (Jet nebulizers) [38]. These types are effective in aerosol delivery in children (mouthpiece or facemask) [39]. One main disadvantage is the high price and furthermore the need for maintenance of the equipment and consequent supervision during drug application [40]. Also the droplet size might be affected by changes in temperature, as well as the concentration of the nebulizing solution in the reservoir during the inhalation process [41].

2.2.1.2 Pressurized metered-dose inhalers (pMDIs)

pMDIs are formulated as solutions or suspensions. Aerosol delivery from pMDI is a complex process involving the discharge and the atomization of a pressurized propellant-based formulation following a rapid evaporation of volatile components [42]. Mainly the propellant (e.g. HFA), semi-volatile cosolvents (e.g. ethanol), non-volatile excipients (e.g. surfactant lipids) and the API are formulated [43]. In the past, environmentally damaging chlorofluorocarbon propellants (CFCs) were used [44], however, today these are replaced by more harmless propellants of hydrofluoroalkane-type (HFAs). Typically pMDIs are robust to chemical

degradation but suffer from various physical instability, including flocculation, sedimentation or creaming and wall losses [45]. pMDIs may be used in combination with a spacer device for inhalation of steroids and for asthma treatment in children.

2.2.1.3 Dry powder inhalers (DPIs)

DPIs offer various designs for mouthpieces, air inlet channels and aerosolization chambers leading to differences in aerodynamic characteristics [46]. On the market, different concepts are present, such as capsule- or blister-based formulations that can either be inserted manually into the device by the patient or are irreversibly inserted during manufacturing. Commonly, the API is formulated with coarse carrier particles (e.g. mannitol or lactose) to improve flowability and dispersibility [32]. The dispersion energy is generated by the inhalation pattern (flow rate, volume and breath-holding time) [47]. The disadvantages of this treatment are the moisture sensitivity [48] and electrostatic charging [49]. In general, DPIs are physically stable and more harmless to the environment [50]. These properties are interesting and lucrative for further DPI-developments in the future. In this study the focus is set on DPIs. This type of inhaler is used in various investigations to determine the influence on particle deposition and dissolution behavior of amorphous parts in micronized powders.

2.2.1.4 Soft mist inhalers (SMIs)

The Respimat[®], a so-called SMI, produces a slow aerosol cloud (< 10 m/s) which results in higher lung deposition due to facilitation of slow-breathing maneuver [51]. This SMI generates small particles over a longer duration (1.5 s) which, in particular, is an advantage for patients with lower flow rate and volume. The aerosol is generated by pressing a metered amount of liquid through a nozzle system (250 bar) forming two jets disintegrating into fine droplets (Soft Mist[™]) by collision [52]. One disadvantage is the high price of the SMIs compared to other devices.

2.2.2 Formulation strategies in dry powder inhalers (DPIs)

In general, the API (about 5 μm) is formulated with carrier particles (about 250 μm) to a binary mixture [53]. Thereby, interactions between API-API and/or API-carrier are present of different kind and degree (Chapter 2.2.3). A further approach to increase the drug deagglomeration is the addition of micronized carrier particles (fines). This ternary mixture facilitates the saturation of high-energy binding sites on the carrier by the fine particles (active site hypothesis), protect the drug particles against high press-on forces (buffer hypothesis) and

trigger the formation of API-carrier agglomerates (agglomeration hypothesis) [54–58]. These phenomena might enable a better dispersibility of the API. Another formulation strategy concerns with carrier-free systems. Hereby, for example spheroids (soft aggregates) are manufactured by controlled agglomeration (spheronisation) of micronized particles [32].

2.2.3 Interparticulate interactions in DPIs - Agglomeration behavior of solid particles

Interparticulate interactions (cohesion of drug-drug and adhesion of drug-carrier) occur mostly on DPIs and are dominated by physical forces and interactions [59]. Physical forces can be divided into binding mechanisms with or without material bridges which were described by Schubert et al. [60,61]. The solid bridges include behaviors such as sintering induced by temperature (Figure 1, a) and particles which are melted together due to re-crystallization processes of amorphous regions (b). Liquid bridges that are mostly generated by water vapor are based on an adsorption layer between particles (capillary forces, e).

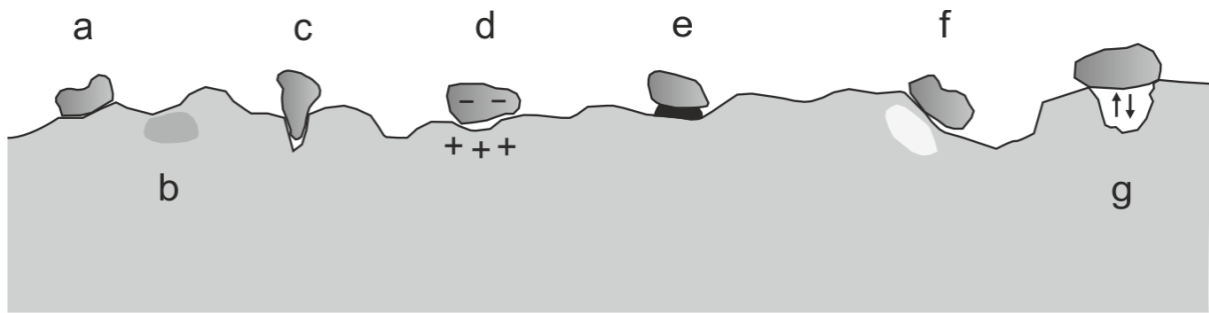


Figure 1: Simplified schematic interactions between carrier particle and micronized API modified from Pilcer et al., 2012

These capillary forces (F_{CF}) arise when the formation of liquid concave-shaped menisci (meniscus force) around the contact area of two neighboring particles (radius of sphere R_1 and R_2) come into existence [62]. In this calculation the surface tension γ and the contact angle θ are taken into account (Equation 2.2) [63].

$$F_{CF} = - \frac{4 \cdot \pi \cdot R_1 \cdot R_2 \cdot \gamma \cdot \cos \theta}{R_1 + R_2} \quad 2.2$$

Van der Waals forces (f), electrostatic charges (d), and mechanical interlocking (c) are dominated by physical forces without material bridges. Van der Waals forces (F_{vdW}) occur once dipole interactions are induced, the separation distance between particles is sufficiently small (< 100 nm) and the size of the particle is small (< 10 μ m). Equation 2.3 shows the calculation by Hamaker (sphere and sphere), where A_H represents the material-specific Hamaker constant,

R is the radius of a sphere ($R = 2 R_1 \cdot R_2 / (R_1 + R_2)$) and x is the distance of both particles [60,64].

$$F_{vdW} = \frac{A_H \cdot R}{16 \cdot \pi \cdot x^2} \quad 2.3$$

Electrostatic charge arises by direct surface contact and charge transfer between donor and acceptor particles. Triboelectrification describes the electrostatic charging by a short collision or by intense friction [65]. Contact charging is classified into three main parts (metal-metal, metal-insulators or insulator-insulators) [66]. In summary, the extent of Van der Waals forces (F_{vdW}), electrostatic charges and capillary forces (F_{CF}) are dependent on the materials [67]. Other interactions are based on chemical forces such as acid-base interaction forces (g) or hydrogen bonding. Hydrogen bonding is based on the Coulomb interaction between negative charge of a free electron pair and the partially exposed positive charge of a proton [68].

Furthermore, particle size, shape [69], surface properties (adhering particles, roughness) [70], press-on forces during the mixing process [71] and the relative humidity (RH) [72] show an enormous effect on agglomeration behavior. Nevertheless, in optimal powder formulations adhesive forces and de-agglomeration forces have to be balanced. These interactions have to be strong enough to guarantee homogenous, stable powder blends and on the other hand weak enough to enable the separation forces during inhalation to detach a substantial fraction of drug dose from carrier particles [71]. In general, several of these described effects are reinforced and mechanisms may overlap.

2.2.4 Aerodynamic behavior of particles in the laminar/turbulence air flow

Mostly, the dispersion of these agglomerates (drug-to-drug/drug-to-carrier) is generated by induced air turbulences through grids/rotators, shearing forces and particle collisions. In this case the physical stress has to dominate the adhesive forces [73]. These complex mechanisms can be enhanced by optimized formulation, well-designed devices and a good inhalation practice. Figure 2 shows an example for an agglomerated powder (spray-dried Ciclesonide particles) which might de-agglomerate into single particles for an effective therapy.

Flow forces and the mechanism of stress to de-agglomerate particles are divided into four categories (Rumpf and Raasch, 1962) and can be described individually. Figure 3a demonstrates the effect of a linear flow. The maximal stress (resistance force F_R) is present if a stationary particle/agglomerate is accelerated in the air stream.

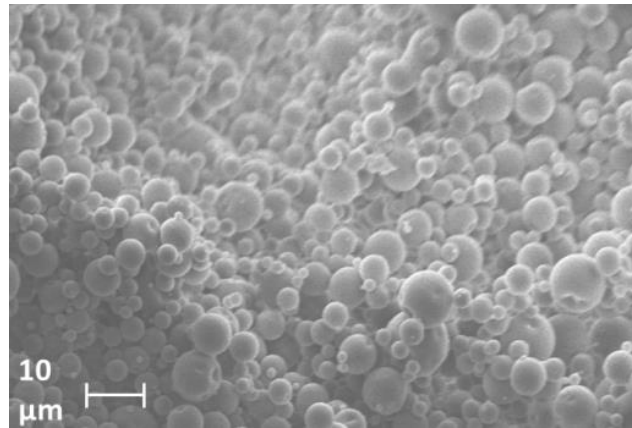


Figure 2: Agglomerate of spray-dried Ciclesonide particles

This flow condition is generally associated with turbulence and shear flows. The resistance force (F_R) is calculated on the relative velocity (v_{rel}), air density (ρ_a), the diameter of the agglomerate (x_{Aggl}) and air viscosity (η) (Equation 2.4, 2.5).

$$F_R = \frac{\pi}{8} \cdot \rho_a \cdot v_{rel}^2 \cdot x_{Aggl}^2 \cdot Re \quad 2.4$$

$$Re = \frac{v_{rel} \cdot x_{Aggl} \cdot \rho_a}{\eta} \quad 2.5$$

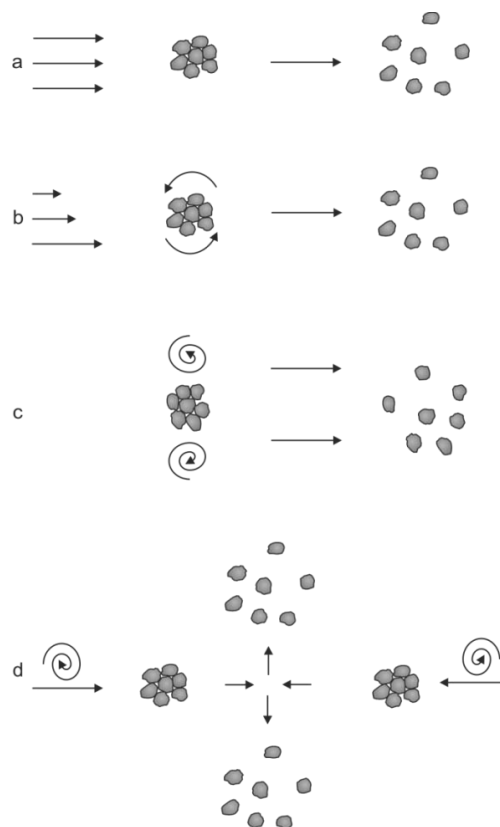


Figure 3: Mechanisms of stress to de-agglomerate particles by air flow modified from Weiler et al., 2008

Part b (Figure 3) describes the rotation of the agglomerate in the shear flow. In addition, to the direct effect of stress, the shear flow causes an additional rotation of the particles by its center. This leads to the reinforcement of centrifugal forces and tensile stresses which facilitates the de-agglomeration. Mechanism c (Figure 3) is based on turbulences which are caused by shear stress and velocity fluctuations. These turbulence transport processes influence the rate of the mixing processes, lead to changes in the particle size and reinforce the acceleration of particle agglomerates [73]. The effect of impact processes is explained in part d (Figure 3). Hereby, particle-particle agglomerates or particle-wall collisions are caused by high particle concentrations and turbulences. This exchange of impulses may lead to dispersion or deformation of the agglomerates.

2.2.5 Deposition behavior of inhalable particles within the respiratory tract

Once the API is de-agglomerated from the surface of the carrier, the focus is brought to the particle deposition in the lung. The intensity of each lung deposition mechanism in the airways varies with the particle parameters (diameter and density), morphometric parameters (airway radius, branching angle and gravity angle) and breathing parameters (residence time or particle velocity) [74]. Figure 4 shows the three main overlapping deposition principles in the lung (impaction/sedimentation/diffusion).

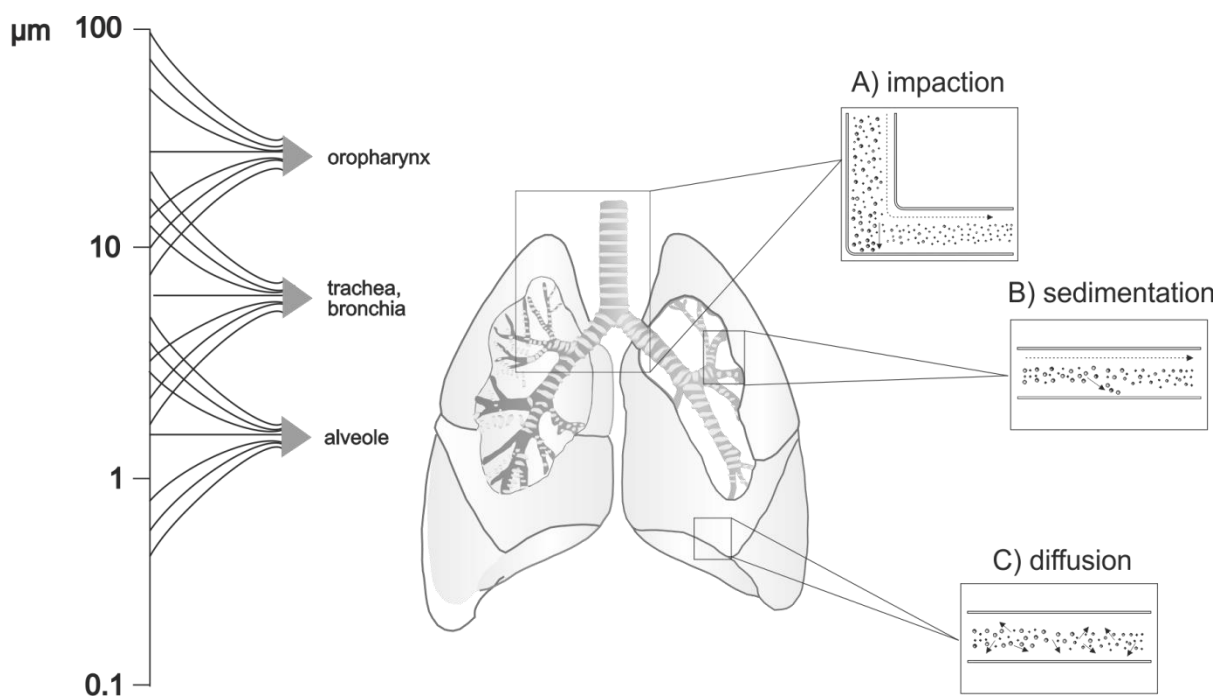


Figure 4: Division of the respiratory system linked to the overlapping deposition principles in the lung modified from Meier et al., 1981

Larger particles ($> 10 \mu\text{m}$) are impacted in the upper airways of the lung due to inertial separation and centrifugal force (Figure 4 A) and, thus, may not follow the air stream [75]. Once impacted to the mucus of the lung, the particles are removed by ciliary clearance [76]. The dimensionless Stokes' number (Stk) describes the probability of particle deposition in the airways via impaction (Equation 2.6). The higher the Stokes' number the more particles will be impacted. Thereby, the particle density (ρ_p), the particle diameter (d), air velocity (V), air viscosity (η) and the airway radius (R) are involved.

$$Stk = \frac{\rho_p \cdot d^2 \cdot V}{18 \cdot \eta \cdot R} \quad 2.6$$

Sedimentation (Figure 4 B) is a time-dependent physical process in which particles settle down depending on their gravitational forces [77]. In this case, lung deposition can be increased by breathing maneuvers (e.g. breath-holding) [78]. Stokes' law can be used to calculate the setting velocity (V_s), where ρ_a is the density of air and g is the gravitational acceleration (Equation 2.7). For very small particles a correction factor (Cunningham C_C) is applied to Stokes' law.

$$V_s = \frac{(\rho_p - \rho_a) \cdot d^2 \cdot g}{18 \cdot \eta} \quad 2.7$$

Diffusion (Figure 4 C) occurs when small particles ($\leq 0.5 \mu\text{m}$) undergo a random motion in the air stream due to the collision with gas molecules [77]. This mechanism is also known as the Brownian motion and is correlated to the particle size and can be described by the Stokes-Einstein equation 2.8, where $Diff$ is the diffusion coefficient, k is the Boltzmann's constant and T is the temperature. The Brownian motion increases with decreasing particle size and becomes an important mechanism for particle deposition in the deep lung [78].

$$Diff = \frac{k \cdot T}{3 \cdot \pi \cdot \eta \cdot d} \quad 2.8$$

2.3 Crystallinity and physical stability of amorphous systems

2.3.1 Thermodynamic state

Pharmaceutical solids can be present in crystalline or amorphous forms. Regarding the crystalline state, the constituent atoms or molecules are arranged repetitiously in a specific three-

dimensional array. Whereas in the case of amorphous materials, the atoms or molecules are randomly placed, comparable to a liquid [78].

Figure 5 shows the comparison of the crystalline form (lattice structure with a high degree of order and with a defined melting point T_m) and the amorphous form (without near-order and with glass transition T_g). Amorphous amounts can be prepared by rapid precipitation, cooling or lyophilization. Furthermore, amorphous regions are especially created on the surface of particles during high-energetic processes (such as milling, blending and even sieving) [79]. These regions have a huge potential to change during handling and storage and should be controlled and limited to a minimal level. The metastable state tends to change over time, initiated by changes in relative humidity and/or temperature [80].

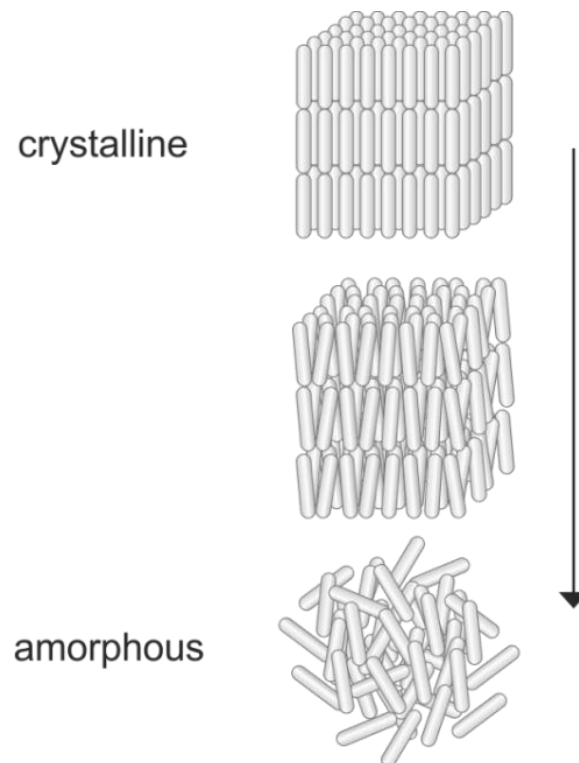


Figure 5: Differences between the crystalline and the amorphous state

In 1910 W. Ostwald introduced the concept of metastable state and the increase in the potential free energy [81]. Later, Kauzmann investigated the temperature-dependent decrease in configurational entropy of the liquid and the crystalline state [82]. The diagram (Figure 6) shows that a crystalline material turns into the liquid phase at its melting point (T_m) when the temperature increases. As soon as the liquid is rapidly 'supercooled' the metastable, amorphous form is built at the glass transition T_g ('glassy state') [83]. This time-dependent intermediate state has a higher potential free energy that may promote the transformation from an unstable to a more stable product. The 'glassy state' tries to re-establish an energetic equilib-

rium and reach the crystalline state again. This can be achieved by water uptake due to storage at higher relative humidities.

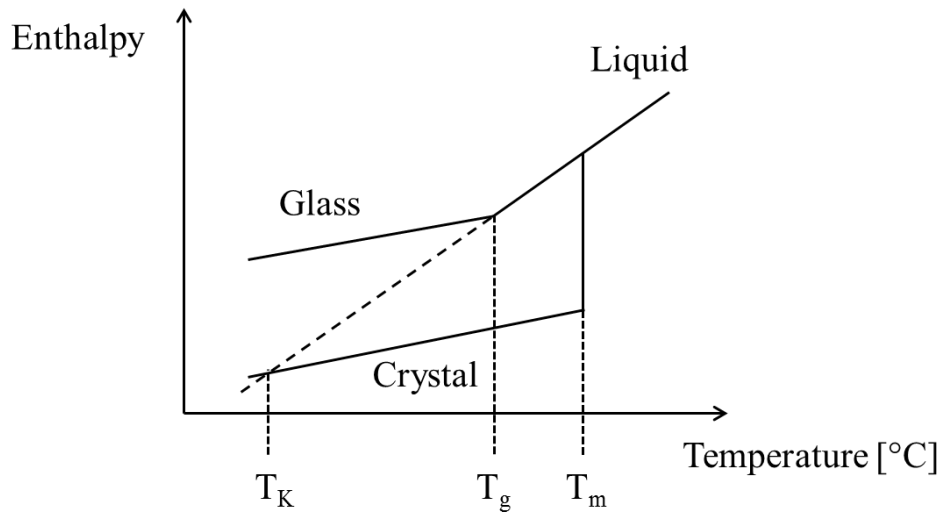


Figure 6: Temperature-dependence of liquid and crystalline state

As a result of the higher content of water the molecular mobility increases (plasticizer effect) and the glass transition temperature is reduced. This facilitates the spontaneous re-crystallization [84]. By extrapolation to lower temperatures the liquid state has a lower enthalpy than the crystal state. The Kauzmann temperature is located (T_K) at this intersection point at which the difference in entropies becomes zero.

2.3.2 Glass transition ($T_{g\ mix}$) of amorphous mixtures

The binary mixture of amorphous materials (API/API or API/solvent) is also defined by a common glass transition ($T_{g\ mix}$) [85]. The intended application is capable of determining glass transitions of a mixture (two components) or to determine the interaction between a sample and humidity upon vapor absorption. This behavior can be described by the Gordon-Taylor-equation (2.9, 2.10), where w_1 or w_2 is the weight fraction of the single component, T_{g1} or T_{g2} is the glass transition of the single component (powder or water), K is the constant and ρ_1 or ρ_2 is the true density of the pure component.

$$T_{g\ mix} = \frac{(w_1 \cdot T_{g1}) + (K \cdot w_2 \cdot T_{g2})}{w_1 + (K \cdot w_2)} \quad 2.9$$

$$K = \frac{\rho_1 \cdot T_{g1}}{\rho_2 \cdot T_{g2}} \quad 2.10$$

The glass transition temperature ($T_{g\ mix}$) of the sample is decreased if more water is adsorbed due to the low T_g of water. This behavior might initialize an earlier re-crystallization of the amorphous amounts. In summary, the determination of the glass transition behavior is a powerful tool for the understanding of the quantification of water mobility in products and for controlling the shelf-life of products [86].

The published value of the T_g of water is 136 K [87]. For the other solvents (methanol, ethanol, isopropanol and ethyl acetate) the T_g was estimated by calculating T_g with equation 2.11 under consideration of the melting temperature (T_m) of the pure substance [88]. Table 1 shows an overview of the glass transitions (T_g) of the used solvents.

$$T_g = \frac{2}{3} \cdot T_m \quad 2.11$$

Table 1: Glass transition temperature of the used solvents

SOLVENT	T_g [K]
Water	136
Methanol	116
Ethanol	104
Isopropanol	122
Ethyl acetate	126
Methylene chloride	118

3 MATERIALS AND METHODS

3.1 Materials

For this investigation, six different active pharmaceutical ingredients (APIs) were chosen as model drugs due to their varying physico-chemical properties (e.g. lipophilicity, solubility and hygroscopicity). These are thought to allow a substantial view on different research issues. Mostly, these APIs are for inhalation application.

One issue is the production of fully amorphous and semi-crystalline APIs. The main objective is to develop tailored methods for the quantification of the amorphous content in these different hydrophilic and hydrophobic APIs by applying an individually dynamic vapor sorption technique. Finally, the influence of amorphous amounts is determined by storage stability tests (6 months) and the dissolution behavior analyzed.

3.1.1 Selection of the model active pharmaceutical ingredients (APIs)

3.1.1.1 Ipratropium bromide (ITB)

Ipratropium bromide (ITB, Ph. Eur. 8), an anticholinergic bronchodilator [89], is routinely used in the treatment of respiratory diseases such as bronchial asthma and chronic obstructive pulmonary disease (COPD) [90]. The competitive antagonism prevents constriction of the bronchioles. ITB is part of the short-acting muscarinic antagonists (SAMAs) substance class [91]. This API (e.g. marketed product Atrovent N[®] [92]) is available as a well-established pMDI formulation. The dosage is about 20 µg per inhalation. Furthermore, ITB is characterized by a very good solubility and high affinity to water vapor (Chapter 4.1.2). Figure 7 shows the chemical structure of this model drug (molecular weight: 430.4 g/mol, one stereogenic center).

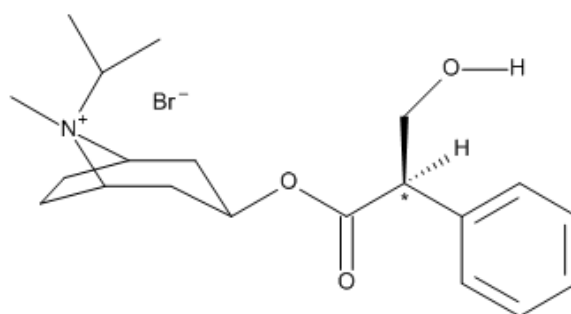


Figure 7: Chemical structure of Ipratropium bromide

3.1.1.2 Formoterol fumarate (FF)

Formoterol fumarate (FF, Ph. Eur. 8) belongs to the group of the long-acting β_2 -adrenoceptor agonists (LABAs) and is mainly used for the regular treatment of COPD [93]. It leads to the relaxation of the smooth muscle of the bronchioles and therefore to an extension of certain airways. In the literature, it is described to be 10-20 times more potent than SBS [94]. FF can be found as a mono or combined preparation (e.g. combined with Budesonide) on the market. This potent API is applied with low doses (12 μg) in a capsule based DPI formulation (Foadil[®], Novartis). Figure 8 shows the structural formula (molecular weight: 478.5 g/mol, two stereogenic centers).

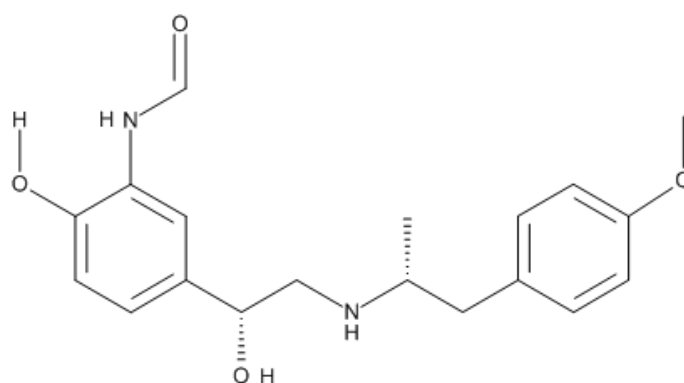


Figure 8: Chemical structure of Formoterol

3.1.1.3 Salbutamol sulphate (SBS)

Salbutamol sulphate (SBS, Ph. Eur. 8) belongs to the substance class of short-acting β_2 -adrenoceptor agonists (SABAs) and is routinely used in the treatment of respiratory diseases such as bronchial asthma [95,96]. On the market it is available as a pMDI (dose: 100 μg), DPI (dose: 200-400 μg) as well as solutions for nebulization (dose: 0.5-5.0 mg/ml). Figure 9 shows the chemical structure of SBS (molecular weight: 576.7 g/mol).

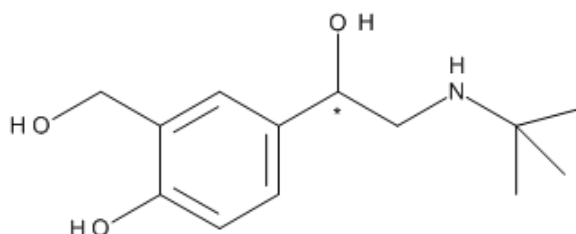


Figure 9: Chemical structure of Salbutamol

Mostly, racemic mixture (1:1 ratio) are marketed, in which the R-enantiomer (levalbuterol) shows more beneficial effects [97]. The S-enantiomer can increase airway hyperactivity and boost the airways smooth muscle contractility in response to allergens [98]. In addition, com-

binations with ITB (Combivent[®]) are available (SAMAs/SABAs) [99]. This API was chosen as the most important representatives of the hydrophilic category. Further investigations were performed to study the influence of amorphous amounts on the aerodynamic deposition and dissolution behavior.

Table 2 shows an overview of typical characteristics of the three used hydrophilic model drugs.

Table 2: Typical characteristics of the hydrophilic model drugs

API	ITB	FF	SBS
Molecular weight [g/mol]	430.4	478.5	576.7
Solubility	Soluble in H ₂ O	Slightly soluble in H ₂ O	Soluble in H ₂ O
Melting point [°C] [*]	237.9 ± 0.4	143.7 ± 1.1	210.7 ± 0.4 282.8 ± 0.5
Water content [%] [*]	3.65	2.28	0.47
Lipophilicity [LogP] (Source: DrugBank)	-1.80	1.06	0.34
Drug class	SAMA	LABA	SABA
Market product	Atrovent N [®]	Foradil [®]	Ventolin [®]
Dose [µg]	20	12	100

^{*} measured

3.1.1.4 Ciclesonide (CS)

A major focus has been put on Ciclesonide (CS, Ph. Eur. 8), a hydrophobic API, in this study (amorphous amounts, aerodynamic, deposition and dissolution behavior). It has a molecular weight of 540.7 g/mol, belongs to the inhaled corticosteroids (ICSs) and improves lung function in patients with mild-to-moderate persistent asthma [100]. CS is a pro-drug and is converted to its pharmacologically active metabolite (desisobutyryl-ciclesonide) in the lungs by the endogenous esterase [101]. This on-site activation (Figure 10) results in a 100-fold greater relative glucocorticoid receptor binding affinity [102]. A commercial product on the market is the MDI Alvesco[®] (typical dose: 80-160 µg). Unfortunately, these ICS are generally underused due to lack of compliance (no instant effect) and steroid fear but this third generation type shows an improved therapeutic index and pharmacologic profile [103]. It can be shown

that CS has a low water affinity due to its hydrophobic characteristic and therefore has an enormous stability for the amorphous amounts (Chapter 4.1.2).

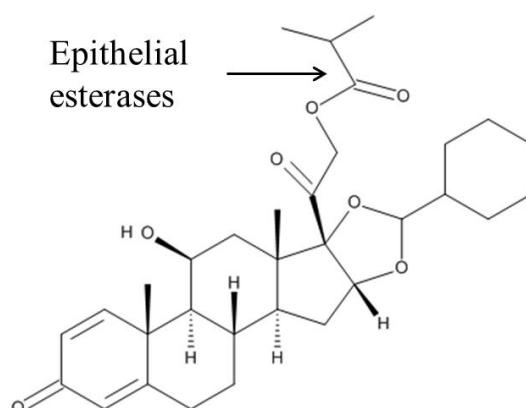


Figure 10: Chemical structure of Ciclesonide (pro-drug) and ester hydrolyzes

3.1.1.5 Budesonide (BS)

Budesonide (BS, Ph. Eur. 8) is an inhalable corticosteroid (ICS) which is recommended as the first-line treatment for patients with persistent asthma [104]. This effective medication is characterized by reducing airway inflammation and mucus production [105]. Figure 11 shows the chemical structure of BS (molecular weight: 430.5 g/mol). This API is available as a single preparation (Pulmicort[®] Turbohaler[®], AstraZeneca) or in combinations with Formoterol (ICS/LABA) because of synergistic effects [106]. Typically, it is marketed with doses of 200-400 μg . Nevertheless, it was demonstrated that it has a higher affinity to water and amorphous amounts are less stable compared to hydrophobic CS.

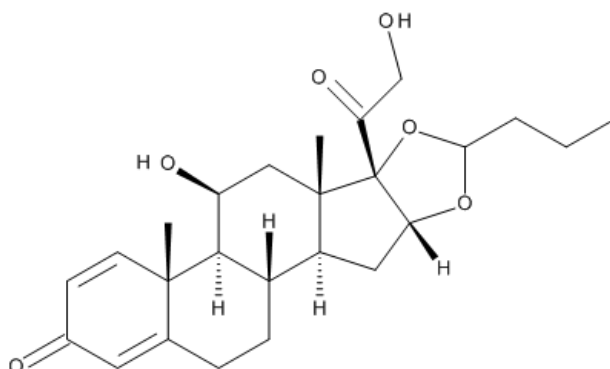


Figure 11: Chemical structure of Budesonide

3.1.1.6 Glibenclamide (GC)

Glibenclamide (GC, Ph. Eur. 8) was chosen as the final hydrophobic model API which is not applied in the inhalation field but primarily processed as tablets (Euglucon N[®], typical dose:

3500 µg) and used in peroral therapy. This hypoglycemic drug is applied to treat type 2 diabetes [107]. The activity is based on the depolarization of pancreatic beta cells and the release of insulin to control diabetes [108]. The structural formula is shown in figure 12 (molecular weight: 494.0 g/mol). As a result of its good biomembrane permeability and its very poor water solubility, it is rated as a class II drug of the Biopharmaceutics Classification System [109].

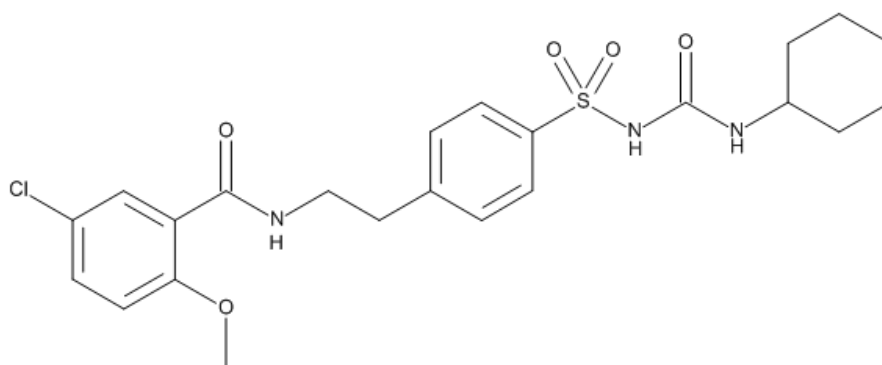


Figure 12: Chemical structure of Glibenclamide

Table 3 shows a summary of physico-chemical characteristics of the used hydrophobic APIs, respectively.

Table 3: Typical characteristics of the hydrophobic model drugs

API	CS	BS	GC
Molecular weight [g/mol]	540.7	430.5	494.0
Solubility	Insoluble in H ₂ O	Insoluble in H ₂ O	Insoluble in H ₂ O
Melting point [°C] [*]	210.4 ± 0.2	260.4 ± 2.1	173.1 ± 1.5
Water content [%] [*]	0.46	0.38	0.29
Lipophilicity [LogP] (Source: DrugBank)	5.32	2.73	3.78
Drug class	ICS	ICS	Antidiabetic
Market product	Alvesco [®]	Pulmicort [®]	Euglucon N [®]
Dose [µg]	80-160	200-400	3500

^{*} measured

3.1.2 Selection of the excipient

3.1.2.1 α -Lactose-monohydrate

α -Lactose-monohydrate (Respitose[®] SV003, $x_{50} = 57.9 \pm 0.2 \mu\text{m}$, Ph. Eur. 8) was kindly provided by DFE pharma (Goch, Germany) and was used as carrier in the studies to investigate aerodynamic deposition and dissolution behavior with SBS and CS. Commonly, α -lactose-monohydrate is used in marketed DPI products [110] because these carrier particles have a safe toxicological profile and are physically/chemically stable. A further advantage is the availability on the market and the inexpensive purchase [59].

In general, the carrier particle size for lactose is between 40 μm and up to 200 μm . It is characterized by a tomahawk-like particle shape [111]. Figure 13 shows this typical structure (blends with SBS as model drug) which may facilitate the detachment of the drug during inhalation. The magnification (B) demonstrates the agglomeration of API crystal needles on the surface. After preparing a stable homogeneous powder blend with the API (typically in a ratio of 1:67.5 (w/w) [112]), the drug particles should be de-agglomerated and re-dispersed during the inhalation process [113].

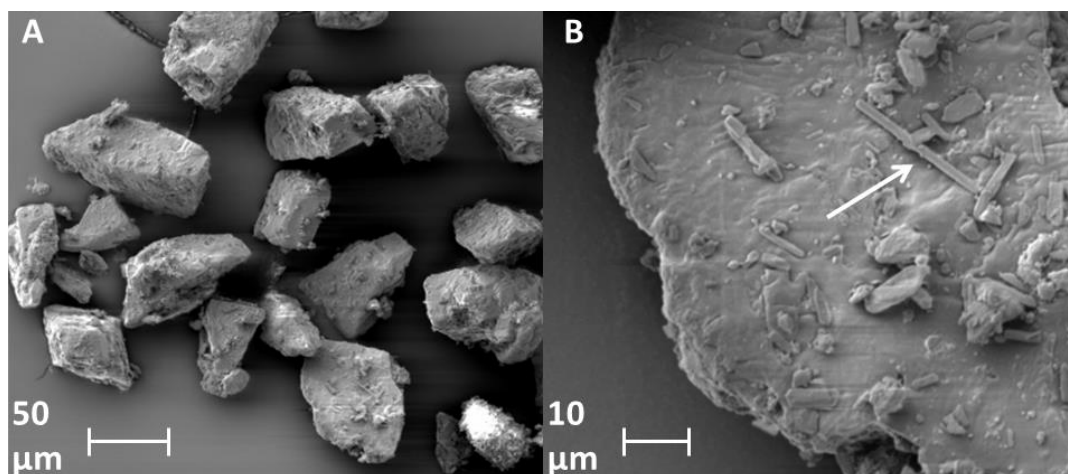


Figure 13: Tomahawk-like particle shape of lactose and agglomerated needle-like SBS crystals

Figure 14 shows the two monomers (D-galactose and D-glucose) of lactose which are linked β -1-4-glycosidic. The production is carried out using milk or whey as starting material in industrial scale. Lipids, proteins and minerals are removed by pasteurization, microfiltration, ion exchange and ultimately lactose is crystallized [114].

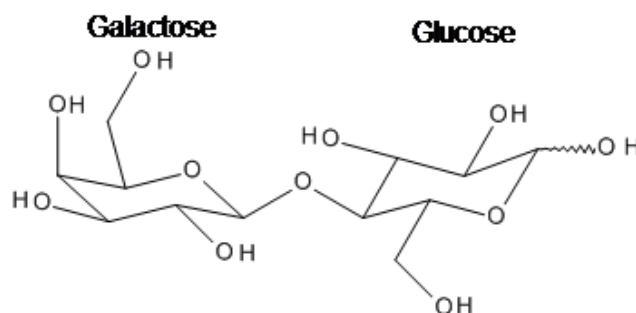


Figure 14: Disaccharide lactose (condensation of D-galactose and D-glucose)

3.1.3 Selection of inhalation devices

3.1.3.1 DPI - Easyhaler[®]

In this thesis, the Easyhaler[®] (Hexal) was used for aerodynamic investigations, storage stability tests of amorphous blends (Next Generation Impactor) and for the preparation of certain powder fractions for dissolution testing (membranes with fine particles, Andersen Cascade Impactor). Figure 15 shows a cross-sectional view of the reservoir based inhaler and the de-agglomeration principle during the inhalation. A defined amount of the powder blend is metered (volumetric) by the rotary gate feeder. The drug release and the de-agglomeration from the carrier lactose are induced by the patient's air flow (dispersion energy) during inhalation.

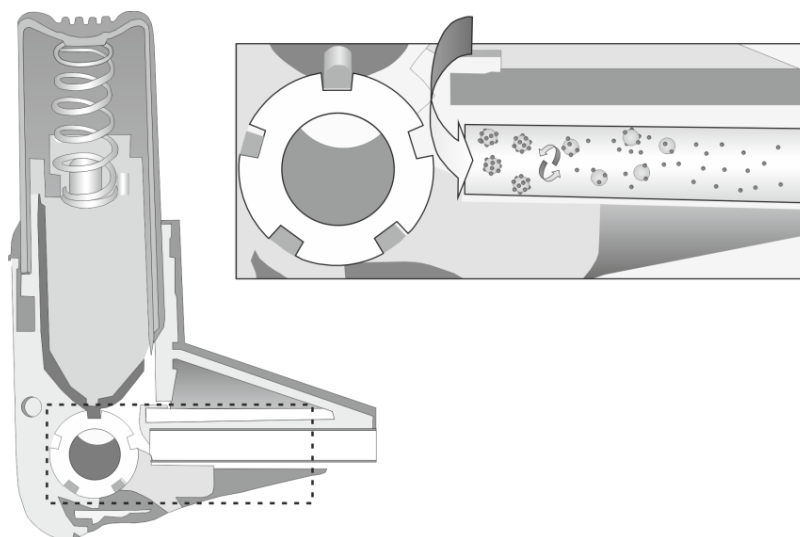


Figure 15: Cross-sectional view of the reservoir based Easyhaler[®] and de-agglomeration principle

3.1.3.2 DPI - HandiHaler[®]

The HandiHaler[®] (Boehringer Ingelheim, figure 16) was used for the aerodynamic investigations and storage stability tests with the API mixed with glass beads (Next Generation Impactor). In this case the better dosage of the glass beads was significant compared to the res-

ervoir based Easyhaler[®]. The API de-agglomeration of the glass beads is facilitated mainly when the powder leaves the capsules by generated turbulences after piercing the capsule (30 ± 2 mg) and starting the inhalation process [92].

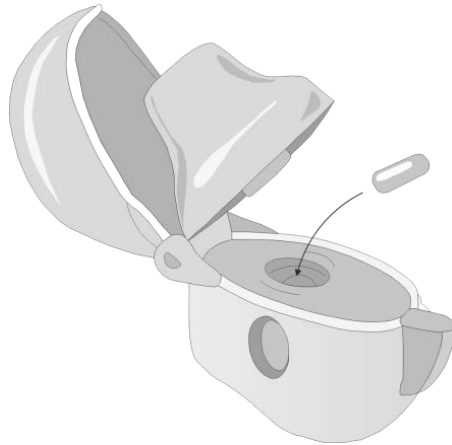


Figure 16: HandiHaler[®] as capsule based model inhalation device

3.2 Methods

3.2.1 Preparation of fully amorphous and semi-crystalline samples

Four methods to produce fully amorphous powders and two procedures for low amorphous samples were evaluated. In this case study, all six model APIs with different physico-chemical characteristics were tested.

3.2.1.1 Ball-milling (BM)

The principle of this ball-mill is based on the opposing rotation of the grinding vessel and the counterweight/sun wheel (Figure 17). The crystal structure is transformed and the grinding process leads to amorphization due to friction and impact forces of the grinding balls [115,116].

Crystalline APIs were ball-milled in zirconium oxide grinding jars (500 ml) containing a defined number of zirconium oxide grinding balls (30 mm) using a Retsch PM 100 mill (Haan, Germany). The grinding time, the rotation speed and the filling level was adjusted for each API, respectively. During the process the temperature (cold storage room: 1-3 °C) was monitored. To avoid re-crystallization after milling the fully amorphous samples were stored over phosphorous pentoxide (P_2O_5).

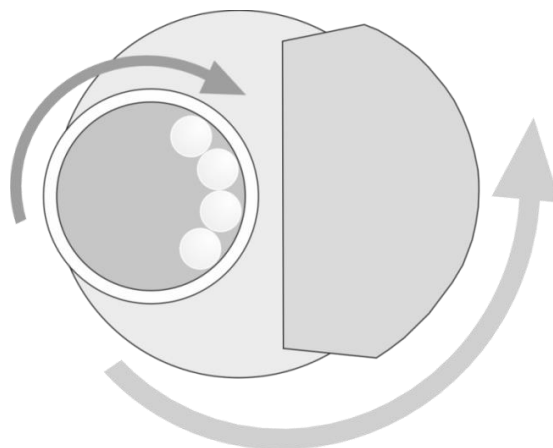


Figure 17: Movement of grinding chamber in ball-mill process

3.2.1.2 Spray-drying (SD)

Initially, the atomization (dual nozzle) of the solution with defined solid concentration takes place in the spray-drying process. By supplying a heat flow on the formed droplets the solvent is quickly removed mostly resulting in amorphous solid particles at the end of the drying process.

Amorphous SBS was produced by spray-drying a 5% (*w/w*) aqueous solution with a Büchi Mini Spray Dryer B-290 (Flawil, Switzerland). An inlet air temperature of 150-151 °C, an outlet temperature of 80-82 °C, feed flow of 4.5 ml/min and an aspiration of 100% was used. Amorphous CS and BS were prepared by spray drying a 5% (*w/w*) methylene chloride solution at an inlet air temperature of 50-51 °C, an outlet temperature of 34-35 °C, feed flow of 3.75 ml/min and an aspiration of 100%. To avoid re-crystallization the amorphous samples were stored over P₂O₅.

3.2.1.3 Freeze-drying (FD)

In the freeze-drying process ice crystals (water) sublime directly into the gaseous state without intermediate appearance of a liquid phase. Amorphous powders are formed by drying of the frozen solution under vacuum. Amorphous ITB and SBS were prepared by freeze drying of a 2% (*w/w*) aqueous solution with a Christ alpha 1-4 freeze dryer (Osterode, Germany). First the fluid was applied by means of a burette into liquid nitrogen (Dewar vessel, 50 ml); the frozen balls were sieved and frozen at -30 °C in the freeze dryer for 15 minutes. Afterward, vacuum was applied (2.56 mbar) and the primary drying process was started at -10 °C and continued for 40 hours. Then the secondary drying at 0.0001 mbar was started at +10 °C and lasted for 20 hours. The time depending change of temperature and pressure is shown in figure 18. To avoid re-crystallization the amorphous samples were stored over P₂O₅.

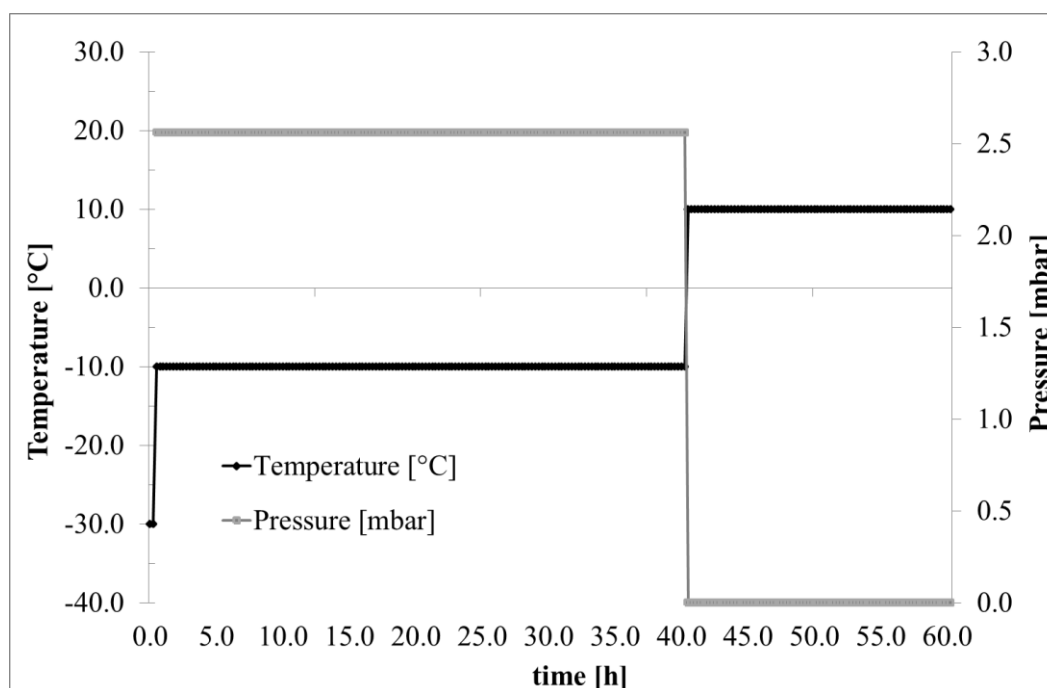


Figure 18: Freeze-drying profile: time depending change of temperature and pressure

3.2.1.4 Quench-cooling (QC)

In general, the melting of the crystal lattice of the respective sample and the sudden conversion of the melt into liquid nitrogen ($-196\text{ }^{\circ}\text{C}$) leads to the formation of amorphous substances [117].

1 g of GC was weighed into an aluminium cup (Figure 19) and melted on a Kofler-heat bench (Wagner Munz, Munich, Germany) at $220\text{ }^{\circ}\text{C}$ or $230\text{ }^{\circ}\text{C}$. The melt was carefully transferred into liquid nitrogen. The amorphous powder was sieved ($425\text{ }\mu\text{m}$) and stored over P_2O_5 to avoid re-crystallization.

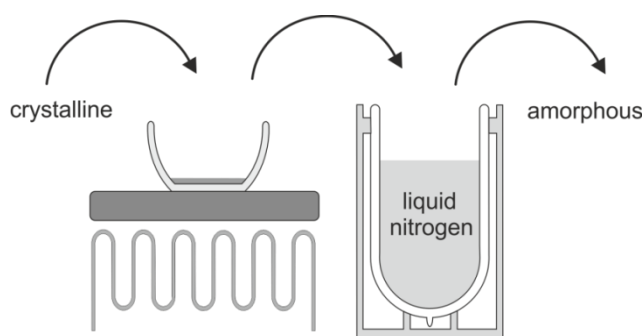


Figure 19: Transformation of crystalline to amorphous material by quench-cooling

3.2.1.5 Jet-milling (JM)

In a mill, the material is mechanically cracked, whereby small amorphous regions are formed at the point of rupture carried out by high speed particle-particle or particle-wall collisions [118]. Once a certain degree of comminution is achieved the material leaves the grinding chamber because of the decreasing centrifugal forces. The powder sample can be collected by a filter or a cyclone. Figure 20 shows the schematic structure of the jet-mill used in this study.

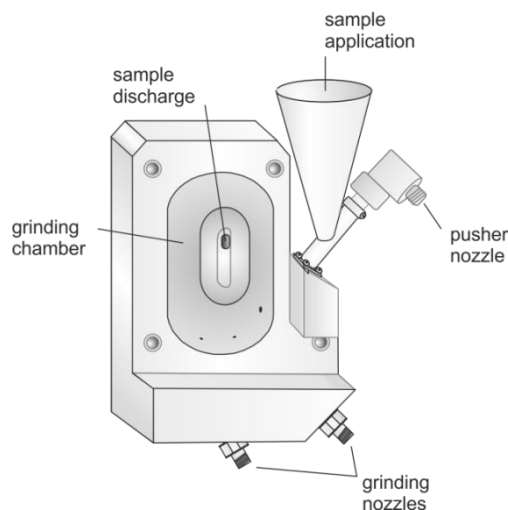


Figure 20: Schematic structure of the jet-mill (JM)

5 g of each crystalline API was jet-milled (JM1) using the Jet-O-Mizer Modell 00 (Fluid Energy Aljet, Plumsteadville, USA). The grinding pressure was adjusted to 8.0 bar (pure nitrogen of quality 2.8) and up to three grinding cycles (Gc 1-3) were performed by repeating this procedure. In further experiments the grinding pressure was changed to lower pressures (JM2 = 2 bar, JM3 = 3 bar and JM4 = 4 bar). To avoid re-crystallization the partly amorphous samples were stored over P_2O_5 .

3.2.1.6 Mixing tests with glass beads (Turbula blender)

The powder and the admixed glass beads are mechanically strained by the rotation of the mixer. The powders and its crystal lattices are physically stressed by the induced impact forces of the glass beads.

The powder blends with crystalline API (1 g) and glass beads (24 g, 0.25 mm or 4.0 mm, Roth, Karlsruhe, Germany) were accurately weighed into a stainless steel container by using the double sandwich method (8 g beads/0.5 g API/8 g beads/0.5 g API/8 g beads). All blends were prepared with a Turbula blender (W.A. Bachofen AG, Basel, Switzerland). The mixing speed (42 rpm) and the mixing time (45 min) were fixed. Figure 21 shows the rotation of the Turbula mixer. After the blending process the glass beads were separated by an air jet sieve (time: 3 minutes; pressure: 3.000 Pa; mesh size: 150 μm) and a cyclone (Hosokawa Alpine, Augsburg, Germany).



Figure 21: Rotation of the Turbula mixer

3.2.2 Other manufacturing processes

3.2.2.1 Blending of samples with different amorphous amounts (for calibration curves and validation)

Firstly, powder blends (5 g, filling level of the mixing vessel: 30%) with fully amorphous (e.g. ball-milled or freeze-dried) API (0.1%, 0.15%, 0.2%, 0.25%, 0.5%, 2.0%, 5.0%, 8.0% and 15.0%) and crystalline API were sieved (mesh size: 500 μm) and then accurately weighed

into a stainless steel container by using the double sandwich method. All blends were prepared with a Turbula mixer (W.A. Bachofen AG, Basel, Switzerland). The mixing speed (42 rpm) and the mixing time (3×15 min and after every 15 min sieved with the 500 μm sieve) did remain unchanged. For micronized, crystalline starting materials (e.g. FF or BS) an electrostatics discharge stick (Haug GmbH, Leinfelden, Germany) had to be used in order to guarantee a homogeneous mixture by removing electrostatic charge from the powder.

3.2.2.2 Conditioning

In general, the amorphous samples (e.g. micronized powders or blends) were stored over P_2O_5 in a desiccator (volume 2.4 l, room temperature) to avoid re-crystallization.

Different amorphous amounts in powder samples (aerodynamic investigations/dissolution testing) were produced on the basis of different storage conditions (solvent and vapor). To avoid re-crystallization after the milling process (JM1 Gc1 and JM1 Gc3) the amorphous samples were stored over P_2O_5 in a desiccator, respectively (are named: SBS 1/SBS 2 or CS 1/CS 2). The hydrophobic CS sample (JM1 Gc3) was stored over 10 ml isopropanol for 2 hours (CS 3) and the other half of the hydrophilic SBS sample (JM1 Gc3) was stored over saturated KCl solution at 85% RH for 16 hours (SBS 3) in order to re-crystallize the main amorphous parts (volume 2.4 l, room temperature).

To determine the influence of storage stability all produced powder blends (lactose or glass beads with SBS 2/SBS 3 and CS 2/CS 3) were stored open in a petri dish at room temperature and at 45% RH in a desiccator (volume: 2.4 l). After defined time points (1 day, 1 week, 2 weeks, 1 month, 3 months and 6 months) the aerodynamic particle size distribution of each blend was investigated.

In order to investigate the surface of the hydrophobic samples and the interaction with organic solvent, these samples were stored over 10 ml methanol or isopropanol (BS), isopropanol (CS) and isopropanol or methylene chloride (GC). The samples were compared by SEM analysis after 2 hours of storage in a desiccator (volume: 2.4 l, room temperature).

3.2.2.3 Blending powder for inhalation/Dissolution testing (Turbula blender)

Powder blends (NGI, Study 1, chapter 4.4.1) with micronized amorphous or crystalline API (SBS 2/SBS 3 or CS 2/CS 3, 0.25 g) and α -lactose-monohydrate (24.75 g) were firstly sieved (mesh size: 500 μm) and then accurately weighed into a stainless steel container by using the double sandwich method (8.25 g/0.125 g/8.25 g/0.125 g/8.25 g). All blends were prepared

with a Turbula mixer (W.A. Bachofen AG, Basel, Switzerland). The mixing speed (42 rpm) and the mixing time (3×15 min and after every 15 min sieved with the 500 μm sieve) did retain unchanged. Finally, two blends for every API with low and high amorphous amounts were produced, respectively (Table 4).

Powder blends (NGI, Study 2, chapter 4.4.2) with micronized amorphous or crystalline API (SBS 2/SBS 3 or CS 2/CS 3, 0.15 g) and glass beads (24.85 g, 0.25 mm, Roth, Karlsruhe, Germany) were prepared using the same conditions. Finally, two blends for every API with low and high amorphous amounts were produced, respectively (Table 4).

Powder blends (ACI, Dissolution testing, chapter 4.5) with micronized amorphous or crystalline API (SBS 1/SBS 2/SBS 3 or CS 1/CS 2/CS 3, 0.25 g) and α -lactose-monohydrate (24.75 g) were prepared using the same conditions. Finally, three blends for every API with low, middle and high amorphous amounts were produced, respectively (Table 4).

Table 4: Overview of the produced and tested mixtures

Conditioning process	Amorphous content	Carrier type	Area of application
SBS 1	middle	Lactose	Dissolution testing
SBS 2	high	Lactose	NGI, Study 1
SBS 2	high	Lactose	Dissolution testing
SBS 2	high	Glass bead	NGI, Study 2
SBS 3	low	Lactose	NGI, Study 1
SBS 3	low	Lactose	Dissolution testing
SBS 3	low	Glass bead	NGI, Study 2
CS 1	middle	Lactose	Dissolution testing
CS 2	high	Lactose	NGI, Study 1
CS 2	high	Lactose	Dissolution testing
CS 2	high	Glass bead	NGI, Study 2
CS 3	low	Lactose	NGI, Study 1
CS 3	low	Lactose	Dissolution testing
CS 3	low	Glass bead	NGI, Study 2

3.2.3 Methods for characterization and analysis of amorphous content

3.2.3.1 Dynamic vapor sorption (DVS)

Amorphous powders adsorb water molecules not only on the surface also by absorption into the material. The mass of adsorbed and absorbed solvent depends on the solvent used and the adjusted relative humidity (p/p_0). Screening vapor sorption measurements were conducted with a DVS-1, Surface Measurement Systems Ltd., London, UK using a gravimetric method to determine the humidity-dependent increase in mass (1 sample). For all screening measurements water was used as a solvent to determine moisture sorption isotherms of crystalline starting materials and fully amorphous samples. Furthermore, the contrasting increase of mass between hydrophilic and hydrophobic APIs was investigated. For all measurements the p/p_0 value was increased from 0.0 p/p_0 to 0.9 p/p_0 (steps 0.1 p/p_0), then again decreased to 0.0 p/p_0 (steps 0.1 p/p_0) and finally the cycle was repeated a second time. The equilibrium criteria for each step was reached after no further mass change was detected within four single mass data points.

All other dynamic vapor sorption measurement was conducted with a DVS-HT, Surface Measurement Systems Ltd., London, UK using a gravimetric method to determine the humidity-dependent increase of mass (up to 10 samples) in order to classify the amorphous content after a calibration with known amorphous amounts (Figure 22).

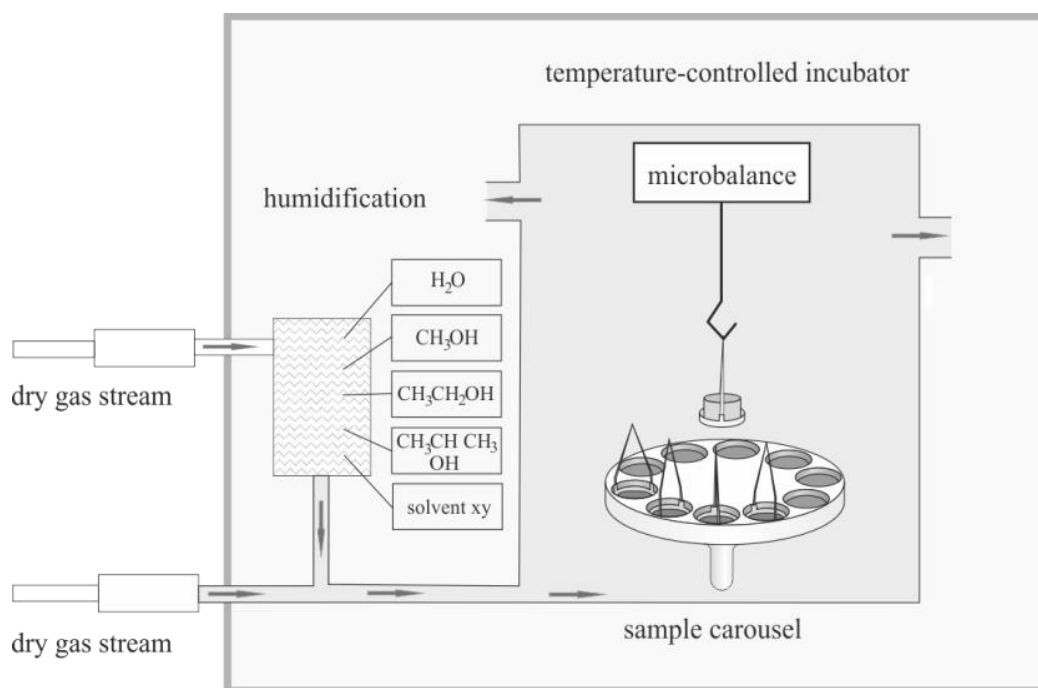


Figure 22: Set-up of the DVS-HT: Giving the option for testing 10 samples and application of organic solvents

For each hydrophilic and hydrophobic API individual parameters were used. Different solvents (polar and nonpolar) and different p/p_0 values (0.05 p/p_0 up to 0.5 p/p_0) were adjusted for screening measurements, respectively. Hydrophilic APIs were measured with ddH₂O and hydrophobic APIs were screened with ddH₂O, methanol, ethanol, isopropanol, ethyl acetate, methylene chloride, acetone and hexane (mean \pm sd).

3.2.3.2 X-ray powder diffraction (XRPD)

X-rays are generated in an evacuated X-ray tube. A high voltage is applied at the cathode (Wolfram), whereby electrons are released and accelerated in the direction of the metal anode (Figure 23). This kinetic energy is mainly converted into thermal energy while only a small fraction is emitted as X-rays.

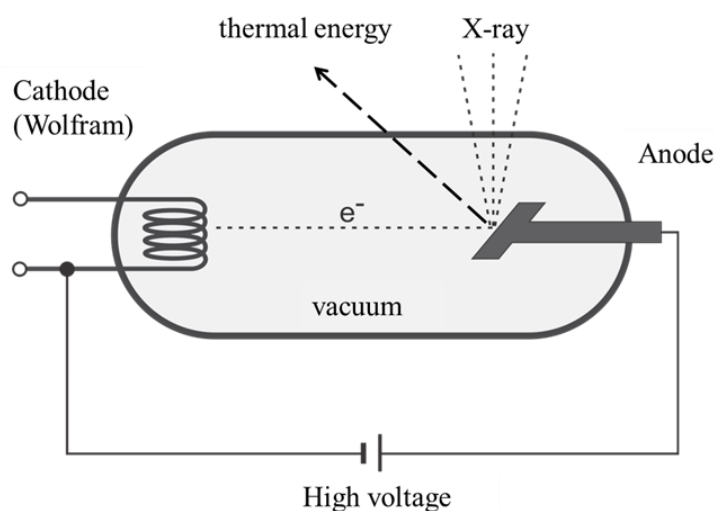


Figure 23: Structure of the evacuated X-ray tube

XRPD is used for identifying the structure of a crystal lattice by measuring the angles and intensities of the diffracted beams (Ph. Eur. 8, 2.9.33). All powders were examined by X-ray powder diffraction (XRPD, Stoe&Cie GmbH, Darmstadt, Germany) to investigate the state of crystallinity of the samples. The X-ray Cu anode was operated at a voltage of 40 kV and strength of 30 mA. The samples were measured in the range of 8-35° at a step rate of $2\theta = 0.05^\circ$ with 2 seconds measuring time per step.

3.2.3.3 Differential scanning calorimetry (DSC)

In order to determine the re-crystallization temperature and the melting temperature the samples were analyzed by differential scanning calorimetry (Perkin Elmer PYRIS Diamond DSC, Massachusetts, USA). The differential heat flow between the sample and the reference cell is determined during a temperature-time-program of the measurement. For the measurement

2-3 mg of powder was accurately weighed into pierced aluminum DSC pans. The samples were investigated at a heating rate of $10\text{ }^{\circ}\text{C min}^{-1}$ under a nitrogen flow of 20 ml min^{-1} between $0\text{ }^{\circ}\text{C}$ and $300\text{ }^{\circ}\text{C}$. The calculation of melting temperature (T_m), onset temperature (T_o), re-crystallization temperature (T_c), the corresponding event area [mJ] and enthalpy (ΔH) was carried out by PYRIS software 3.8 (Perkin Elmer) (mean \pm sd).

3.2.3.4 Temperature-modulated differential scanning calorimetry (TMDSC)

A modulated temperature DSC (Perkin Elmer PYRIS Diamond DSC, Massachusetts, USA) was used to determine in triplicate the change in heat capacity (ΔC_p) and to measure the glass transition temperature (T_g) of the samples (Figure 24) (mean \pm sd). 5-6 mg of powder was filled into pierced aluminum DSC pans. All samples were measured at a heating rate of $5\text{ }^{\circ}\text{C min}^{-1}$, amplitude of $3\text{ }^{\circ}\text{C}$ and an isothermal length of 1 minute under a nitrogen flow of 20 ml min^{-1} between $0\text{ }^{\circ}\text{C}$ and $150\text{ }^{\circ}\text{C}$.

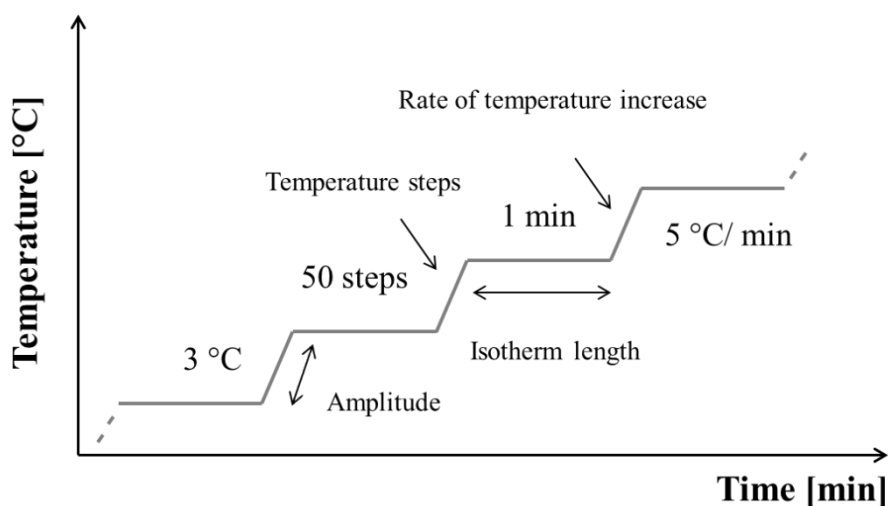


Figure 24: Principle of temperature-modulated heating rate

3.2.3.5 Hyper-differential scanning calorimetry (Hyper-DSC)

In order to determine the re-crystallization temperature (T_c) and the melting point (T_m) Hyper-DSC (Perkin Elmer PYRIS Diamond DSC, Massachusetts, USA) was used. 2-3 mg of powder was accurately weight into pierced aluminum DSC pans. The samples were run at a heating rate of $300\text{ }^{\circ}\text{C min}^{-1}$ under a nitrogen flow of 20 ml min^{-1} between $-80\text{ }^{\circ}\text{C}$ and $280\text{ }^{\circ}\text{C}$.

3.2.3.6 Dynamic mechanical analysis (DMA)

Dynamic mechanical analysis (DMA) is mainly used to determine structure, morphology and viscoelastic behavior of polymers but also for the analysis of crystalline and amorphous mate-

rials [119]. 15 mg of powder was accurately weighed into aluminum pockets. These powder pockets show a time-dependent deformation (strain ε) under sinusoidal mechanical stress σ (Figure 25). The measurement was carried out using a temperature gradient (heating rate of $5\text{ }^{\circ}\text{C min}^{-1}$ and temperature range of $40\text{ }^{\circ}\text{C}$ to $230\text{ }^{\circ}\text{C}$) and a Frequency of 1 Hz. The strain is correlated to the viscosity of the sample [120]. Herewith, the elastic modulus (G^*) and $\tan \delta$ can be calculated (Figure 26). They are composed of the storage modulus (G' , mechanical energy which is stored in shear and elongation experiment) and the loss modulus (G'' , converted mechanical energy into heat energy). The behavior of the sample during mechanical stress can be divided into 3 main parts.

Case 1: Elastic behavior: sample (crystalline) reacts without delay to the force ($\Delta\delta = 0$)

Case 2: Viscous behavior: sample reacts with the most delay to the force ($\Delta\delta = 90^{\circ}$)

Case 3: Viscoelastic behavior: sample (amorphous) reacts in between case 1 and case 2

$$(0^{\circ} < \Delta\delta < 90^{\circ})$$

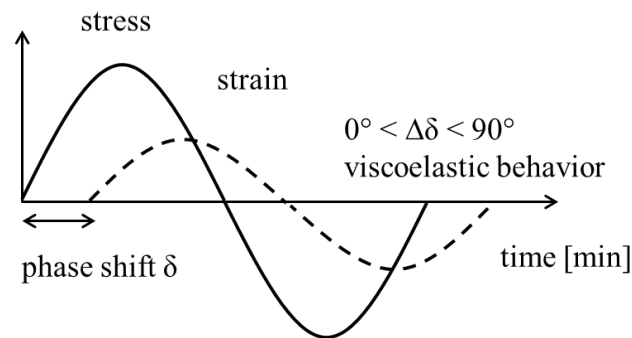


Figure 25: Viscoelastic behavior of amorphous samples

Equation 3.1 shows the calculation of the phase angle δ considering the temporal phase shift (Δt) and the angular frequency (ω , equation 3.2). Here, the frequency (f) and the period (T_p) are included in the calculation.

$$\delta = \Delta t \cdot \omega \quad 3.1$$

$$\omega = 2\pi \cdot f = \frac{2\pi}{T_p} \quad 3.2$$

The storage modulus (G' , equation 3.3) and the loss modulus (G'' , equation 3.4) are calculated from the maximum values of the stress σ and strain ε taking account of the phase angle δ .

$$G' = \frac{\sigma_{max}}{\epsilon_{max}} \cdot \cos \delta \quad 3.3$$

$$G'' = \frac{\sigma_{max}}{\epsilon_{max}} \cdot \sin \delta \quad 3.4$$

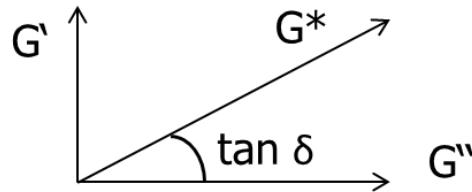


Figure 26: Relationship between elastic modulus, storage modulus and loss modulus

3.2.4 Methods for powder and particle characterization

3.2.4.1 Particle size distribution (PSD) determined by laser diffraction analysis

A parallel laser beam is diffracted by particles located in the measuring zone resulting in a unique diffraction pattern from which a PSD is calculated (Ph. Eur. 8, 2.9.31). The diffracted light is recorded on a multi-element photodetector after it has been focused by a Fourier lens. The diffraction angle is proportional to the particle size and can be described mathematically by the Mie- or Fraunhofer-theory [121].

The particle size distribution (PSD) of the samples was determined by the Sympatec Helium-Neon Laser Optical System (HELOS[®], Sympatec GmbH, Clausthal-Zellerfeld, Germany) with the dry dispersion module RODOS[®]. The powders were dispersed into the measuring zone by compressed air (3 bar). A R2 lens (focal length: 50 mm and measuring range: 0.25 μm up to 87.50 μm) or a R5 lens (focal length: 500 mm and measuring range: 0.50 μm up to 875.00 μm) were used depending on the expected particle size. The calculation of the volumetric particle diameter was done with Windox 5 software based on FREE (Fraunhofer Enhanced Evaluation). The cumulative volume-based distribution (Q_3), the values of x_{10} , x_{50} , x_{90} and the specific surface area (S_v) are determined in triplicate and specified as the characteristic parameters (Figure 27). On basis of the equation 3.5 the Span is calculated which represents the width of the particle size distribution (mean \pm sd).

$$Span = \frac{x_{90} - x_{10}}{x_{50}} \quad 3.5$$

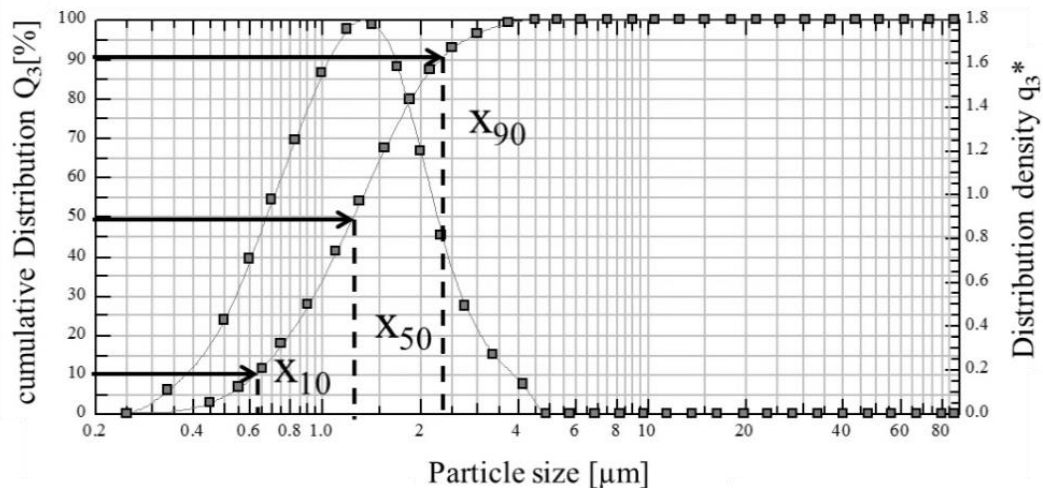


Figure 27: Cumulative volume-based particle size distribution

3.2.4.2 Density measurement

The density of the powder samples is determined by gas pycnometry. The principle is based on the displacement of a gas as a result of the volume of the sample. The solid density can be determined due to the pressure rise and the known mass of the powder sample (Ph. Eur. 8, 2.9.23). Because of the smallest atoms among the noble gases and the ability to cover the smallest open pores (true density) helium (inert test gas) is specified.

The true density was measured with a Helium-pycnometer (Pycnomatic ATC, Porotec, Hofheim, Germany). A suitable amount of powder was accurately weight into the vessel, followed by a ten-fold determination. Every powder was analyzed three times (mean \pm sd).

3.2.4.3 Scanning electron microscopy (SEM)

An electron beam is thermionically emitted from a cathode (Wolfram), accelerated and focused in the direction of the sample. Thereby, signals due to the interaction of the sample and electron beam are detected. The recording of the samples up to a magnification of 100,000 is possible due to the shorter wavelength of the electron beam.

By using a scanning electron microscope (SEM) the particle and surface morphology powders were investigated. The samples (non-conductive) were prepared by fixing the powder on a carbon sticker and coating the sample with gold using a BAL-TEC SCP 050 Sputter Coater (Leica Instruments, Wetzlar, Germany). The samples were visualized with a Zeiss Ultra 55 plus (Carl Zeiss NTS GmbH, Oberkochen, Deutschland) using the SE-2 detector and a working voltage of 2 kV.

3.2.4.4 Inverse gas chromatography (iGC)

Alkanes are separately injected into a standard column packed with the solid sample and the retention time of the vapor is measured by a flame ionization detector, respectively. The retention times changes due to interactions with the powder as a function of surface and bulk properties.

The dispersive surface energy was determined by means of inverse gas chromatography (Surface Measurement Systems Ltd., SMS, London, UK). At least 100 mg powder was packed into a pre-silanized glass column, with an inner diameter of 3 mm and length of 30 cm, with silanized glass wool. The columns were compacted using the iGC column packer (SMS, London, UK) at a medium intensity (corresponds to level 6) for 10 min and conditioned for 2 hours at 0% RH and 303 K to remove impurities and physisorbed water. Different alkanes (decane, nonane, octane, heptane and hexane) were injected three times. The flame ionization detector (FID) was used to measure the highest surface energy of the samples. The dispersive part of the surface energy was calculated (3-fold) with help of the iGC software (SMS, London, UK) for all starting materials of each API (mean \pm sd). A detailed illustration of the calculations is described by Ylä-Mäihänen et al. [122]. Figure 28 shows the schematic set-up of the inverse gas chromatography.

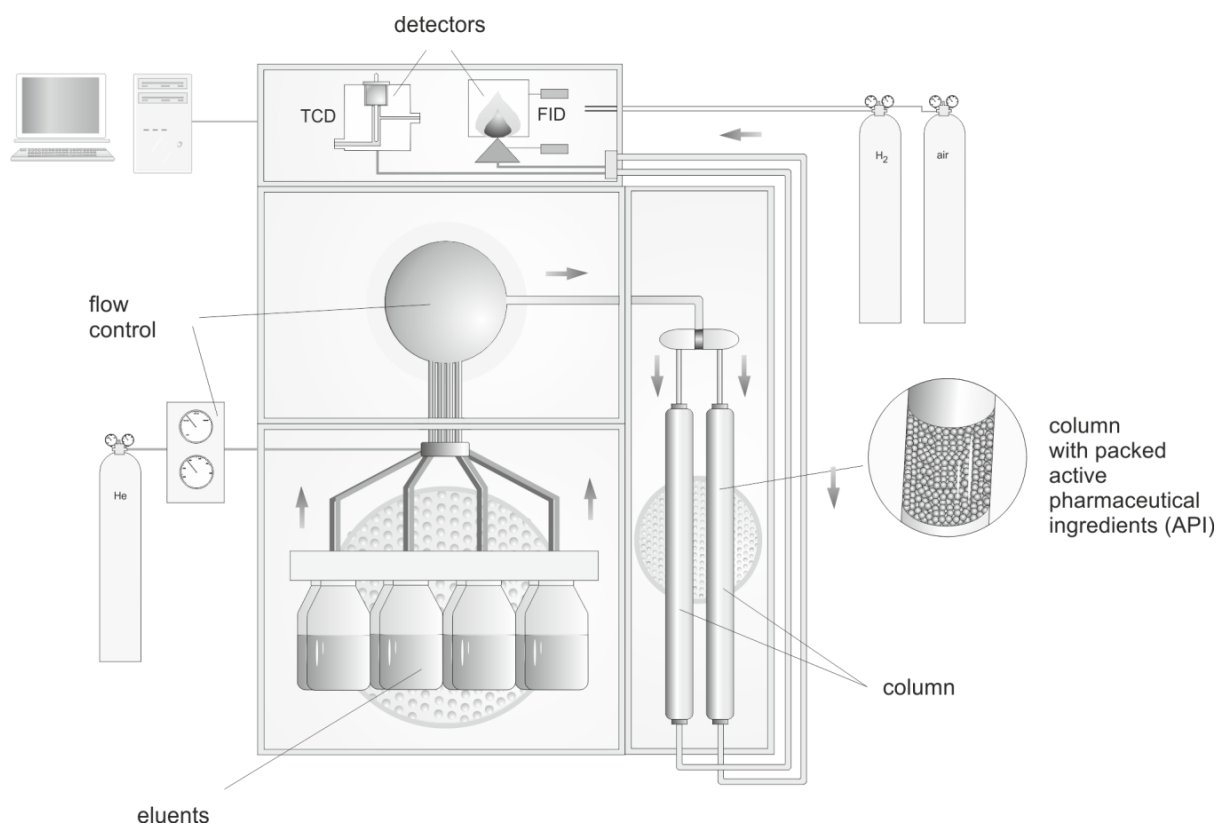


Figure 28: Schematic of inverse gas chromatography (iGC)

3.2.4.5 Surface area determined by Brunauer, Emmett and Teller (BET) method

The determination of the specific surface is performed by a gas adsorption method (Ph. Eur. 8, 2.9.26). The principle is based on the physical adsorption of inert gas molecules (nitrogen) onto solid surfaces [123]. The amount in which the surface is coated by a monolayer of adsorbed nitrogen is determined. The mass-specific surface (S_m) is calculated based on the surface area of nitrogen molecules and the sample mass.

The specific surface area (SSA) was measured under vacuum using the nitrogen adsorption BET method with a Gemini 2360 system (Micromeritics Instrument Corporation, Norcross, USA). All samples (weight > 300 mg) were evacuated in a VacPrep 061 (Micromeritics Instrument Corporation, Norcross, USA) for at least 24 hours at 40 °C to remove adherent substances from the surface. Glass beads were weighed in the reference cell to reduce the volume difference between the sample and the reference cell. Therefore the true density was measured with the Pycnomatic ATC (Porotec, Hofheim, Germany) to obtain an adequate volume of glass beads. Eleven relative pressures between 0.05 p/p_0 and 0.3 p/p_0 were used in the measurement (liquid nitrogen, T = 77 K) and the molar amount of adsorbed gas (n_{ads}) is determined. Every sample was analyzed in triplicate (mean \pm sd). Thereafter, the monolayer can be calculated using the BET equation (Brunauer, Emmett and Teller, equation 3.6).

$$\frac{p/p_0}{n_{ads} \cdot (1 - p/p_0)} = \frac{1}{n_m \cdot K} + \frac{K - 1}{n_m \cdot K} \cdot p/p_0 \quad 3.6$$

The monolayer n_m (Equation 3.7) and the constant K (Equation 3.8) are calculated from the intercept ($a = 1 / n_m \cdot K$) and the slope ($b = (K - 1) / (n_m \cdot K)$) by plotting the determined y-values to p/p_0 .

$$n_m = \frac{1}{a + b} \quad 3.7$$

$$K = \frac{b}{a} + 1 \quad 3.8$$

The mass-specific surface S_m is calculated (Equation 3.9) from the surface of the nitrogen molecule A , the Avogadro constant N_A and the determined monolayer capacity n_m .

$$S_m = n_m \cdot A \cdot N_A \quad 3.9$$

3.2.4.6 Residual moisture determined by infrared scale (IR)

The moisture analyzer (Sartorius MA 45, Sartorius Weighing Technology GmbH, Göttingen, Germany) was used to determine the residual moisture of hydrophilic and hydrophobic APIs. At least 1.8 g (m_{wet}) were weighed onto the measuring pan and dried to a constant mass at 105 °C. Thereafter, the residual moisture was calculated based on the initial mass (Equation 3.10).

$$\text{Residual moisture [\%]} = \frac{m_{wet} - m_{dry}}{m_{dry}} \cdot 100\% \quad 3.10$$

3.2.5 Methods for blend characterization and *in-vitro* deposition behavior

3.2.5.1 Determination of blend homogeneity

Ten randomly taken powder samples (10 mg for each sample) of every blend (powders for inhalation/dissolution testing, Easyhaler[®]) were accurately weighed and solved with 10 ml 9:1 methanol/double distilled water for CS or with ddH₂O for SBS (mean ± sd). 30 mg were weighed for the investigations with the glass beads (HandiHaler[®]/capsule). In each study the sample size corresponded with the size of a single dose [124]. Afterward, the content of API was determined by a validated HPLC analysis. The coefficient of variation (CV) was ≤ 5% for a content uniformity.

3.2.5.2 High performance liquid chromatography (HPLC)

The API content was analyzed by HPLC (Waters[™], Eschborn, Germany) using a LiChro-CART[®] 125-4 LiChrospher[®] 100 RP-18 (5 μm) column with a precolumn (Merck KGaA, Darmstadt, Germany) and a calibration between 1-80 μg (Ph. Eur. 8, 2.2.29). For SBS a wavelength of 220 nm was applied and a mobile phase containing 78% buffering system (heptanesulfonate and potassium dihydrogen phosphate) with a pH adjusted to 3.65 (by orthophosphoric acid 85%) and 22% acetonitrile was utilized. The flow rate was set to 0.8 ml/min and the injection volume was 100 μl. The limit of quantification (LOQ) was 0.1 μg/ml. CS was analyzed at a wavelength of 243 nm. The mobile phase contains 15% ddH₂O and 85% methanol. The flow rate was set to 1.2 ml/min and the injection volume was 100 μl. The LOQ was 0.05 μg/ml.

Both methods for CS and SBS had to be validated in order to demonstrate that the specified requirements are compliant. Especially the storage stability of the samples (up to 5 days) had to be checked due to the transport of samples from Ingelheim to Kiel. The linearity, limit of quantification (LOQ), accuracy, precision and robustness was validated based on the ICH guideline Q2 (R1).

- **Linearity:** The ability to obtain test results which are directly proportional to the concentration. 7 different concentrations were prepared (1-80 µg) and were measured six times by HPLC ($R^2 > 0.99$).
- **Limit of quantification (LOQ):** The lowest amount of analyte which can be quantitatively determined with suitable precision and accuracy. Different dilutions (0.05 µg/ml, 0.08 µg/ml, 0.1 µg/ml, 0.2 µg/ml, 0.5 µg/ml and 1.0 µg/ml) were prepared and measured (Signal to noise ratio > 10:1).
- **Accuracy:** Expresses the closeness of agreement between the value which is accepted either as a conventional true value or an accepted reference value. The same concentration was prepared six times and then measured (recovery: 98-102%).
- **Precision:** Expresses the closeness of agreement between a series of measurements obtained from multiple sampling of the same homogenous sample. One concentration was injected six times and then measured (coefficient of variation < 2.0%).
- **Robustness:** Its capacity to remain unaffected by small, but deliberate variations in method parameters. It provides an indication of its reliability during normal usage. The stability of one concentration (room temperature and daylight) was measured at day 1, day 3 and day 5 (six times injected).

For all samples the average (mean), the standard deviation (sd) and coefficient of variation (CV) was calculated (Appendix 8.3.1).

3.2.5.3 Cascade impactor - Next Generation Impactor (NGI)

The aerodynamic particle size distribution (APSD) of an inhalation powder is determined by impaction analyzes. Thereby, the aerosol is segregated due to differing gravitational forces depending on the particle mass and, thus, can be further classified in aerodynamic particle size fractions. This behavior is comparable to the separation mechanisms of the lungs. In this study, the Next Generation Impactor (NGI) is used for storage stability tests of crystalline and amorphous powder blends regarding its impact on aerodynamic behavior (Ph. Eur. 8, 2.9.18 – Gerät E). This *in-vitro* characterization system is using a specific device design (nozzle size

and nozzle spacing) to classify particles into aerodynamic size ranges (Figure 29). Larger particles impact on initial stages (e.g. size, density and inertial forces) whereas smaller particles can further follow the airflow and impact on final stages [34,125].

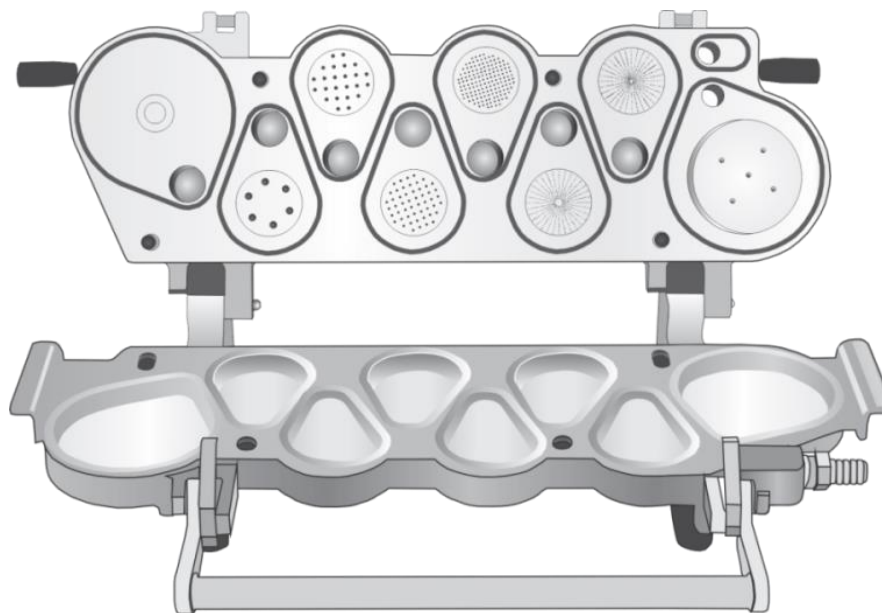


Figure 29: Set-up of an open NGI with collection cups

The aerodynamic particle size distributions (APSD) were determined using the Next Generation Impactor (NGI, Copley Scientific, Nottingham, UK). The throat, the preseparator and the 8 stages were coated with a mixture of Brij[®] 35 (15%), ethanol (51%) and glycerol (34%). Each powder blend (triplicate determination) was filled into the model device Easyhaler[®] and aerodynamically assessed at a flow rate of 50.5 L/min (corresponding to a pressure drop of 4 kPa, 4 l volume). The glass bead blends (30 ± 2 mg) were filled into capsules and tested with the HandiHaler[®] as model device (flow rate of 50.5 L/min, triplicate determination). SBS samples were solved with ddH₂O; CS samples were solved with 9:1 methanol/ddH₂O mixture and analyzed by HPLC analysis. The FPF (% of delivered dose < 5 μ m), FPD (μ g of delivered dose < 5 μ m), MMAD (Mass Median Aerodynamic Diameter, it is defined as the diameter at which 50% of the particles are larger in mass and 50% are smaller) and GSD (Geometric Standard Deviation, it is a measure of the spread of an aerodynamic particle size distribution) were calculated with C.I.T.D.A.S. 3.0 software (Copley Scientific, Nottingham, UK). The FPF is calculated from the delivered dose (DD) and the measured FPD (Equation 3.11).

$$FPF [\%] = \frac{FPD [mg]}{DD [mg]} \cdot 100 \quad 3.11$$

3.2.5.4 Cascade impactor - Andersen Cascade Impactor (ACI)

A modified Andersen Cascade Impactor (ACI) was used to cover a cellulose membrane (pore size 0.45 μm , Whatmann, Dassel, Germany) with fine particles (Figure 30) for dissolution testing (Ph. Eur. 8, 2.9.18 – Gerät D).

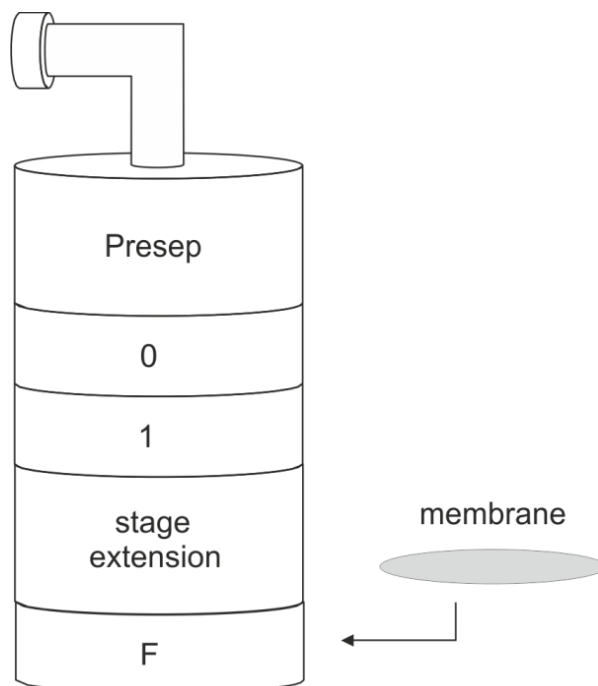


Figure 30: Modified Andersen Cascade Impactor with filter stage for dose collection

Powder blends were filled into the Easyhaler[®] and aerosolized at standard USP airflow conditions (4 kPA pressure drop, 4 l volume). In order to obtain a homogenous particle distribution on the membrane a cylindrical shaped stage extension was inserted between stage 1 and the filter stage (F). After the vacuum pump stopped, the ideal waiting time for the sedimentation was set to 5 minutes [126,127]. Prior of the analysis the preseparator and impact plates (stage 0 and stage 1) were again coated with a mixture of Brij[®] 35 (15%), ethanol (51%) and glycerol (34%).

3.2.6 Methods for dissolution behavior

3.2.6.1 Paddle apparatus with membrane holder (Dissolution testing)

A paddle apparatus (Sotax, Lörrach, Germany) with a membrane holder was used for the dissolution testing (Ph. Eur. 8, 2.9.3 – Apparatus 2). The membrane holder (Copley, Scientific, Nottingham, UK) consists of a watch glass and a plastic mesh. The tests were performed with a stirring speed of 100 rpm at 37 °C in phosphate buffered saline (PBS) buffer at pH 7.4

[126,127]. The samples were taken and filled into vials automatically following a defined time schedule with a simultaneous replacement of the dissolution medium with fresh buffer (Figure 31). The residual amounts of drug on the membrane and the watch glass were determined after the single measurements. The total amount of drug was measured using the maximum of the cumulatively released amounts. All dissolution experiments were performed in a 3-fold determination (average \pm sd).

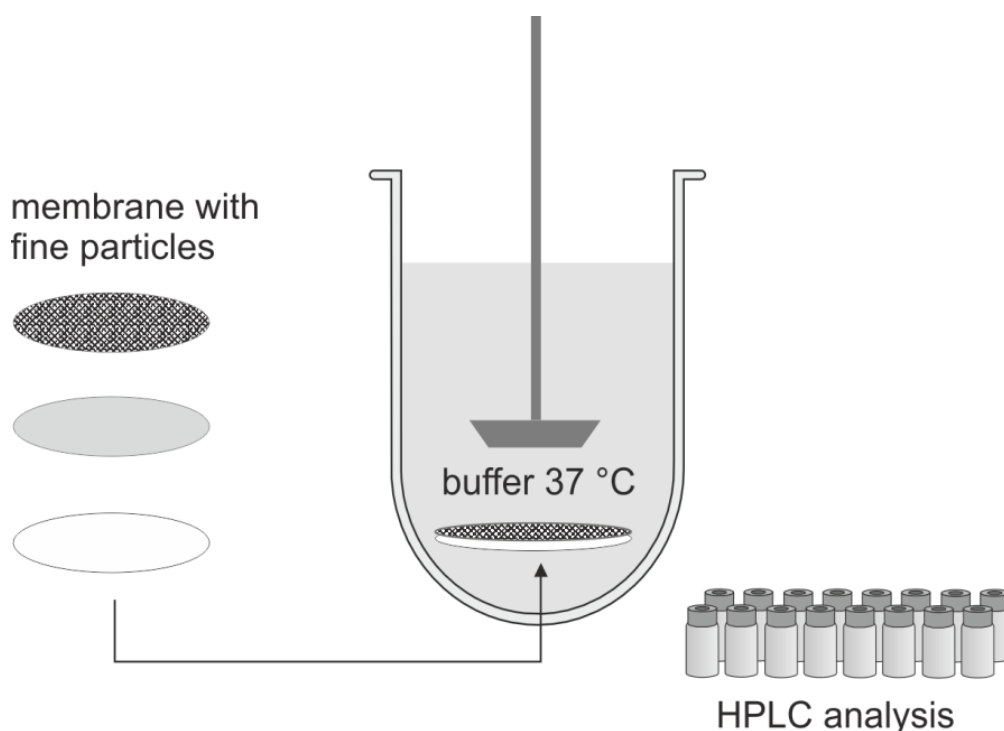


Figure 31: Paddle apparatus with membrane holder

3.2.6.2 Optimization of drug deposition on the filter membrane (ACI)

The drug deposition on the membrane was optimized to reach a higher drug concentration. Different inhaler devices (Easyhaler[®]/HandiHaler[®]), different filter stages and different loads (1-10 actuations, 1-10 capsules) were tested in a single determination. Ultimately, equal amounts of CS and SBS were to be present on the filters.

3.2.6.3 Solubility measurements - Saturation solubility

The dissolution medium (PBS buffer, 100 ml) had to be optimized due to the poor solubility of CS. Saturated solutions (50 mg of CS 1/CS 2/CS 3 blends) were prepared without and with surfactant. Sodium dodecyl sulfate (SDS, 0.05%, 0.1% and 0.5%), Tween[®] 20 (0.5%), Plasdane[®] (0.5%) and a mixture of 9:1 methanol/ddH₂O were used in the solubility test. The solutions were stirred for 48 hours at room temperature and afterward filtered (Minisart

RC 15, Sartorius). All solubility measurements were performed in 3-fold determination and the concentrations were determined with HPLC after dilution (average \pm sd).

3.2.7 Design of Experiments (DoE)

The aim of a statistical experimental design is the efficient consideration of complex processes. Finally, an empirical model is developed in which the tested factors fit well the obtained results [128]. The preparation and the evaluation of the statistical experimental designs were done with Design-Expert[®] 8 (Stat-Ease, Inc., Minneapolis, USA). In this study different important parameters (temperature, solvent vapor, amorphous content and absorption behavior) of dynamic vapor sorption (DVS) measurements were investigated. Table 5 shows important parameter of the implemented analysis of variance (ANOVA).

Table 5: Important parameter of the analysis of variance (ANOVA)

Evaluation	F value	p-value Prob > F	Pred R-squared	Adj R-squared	Adeq Precision
Definition	Random variable which has a F distribution (degrees of freedom)	Tests a statistical hypothesis	Proportion of variance in the design space explained by the model	Explanatory variables are added to the model	Ratio signal/noise
Target value	> 1.0 is desirable	< 0.05 indicate model terms are significant	± 0.2 is in reasonable agreement with Adj R ²	0.7–0.9 is desirable	A ratio > 4 is desirable

4 RESULTS AND DISCUSSION

4.1 Amorphous content and estimation of stability behavior

In the last years the interest in amorphous regions of inhalation dry powder formulations grew more and more. In general, the production techniques, the detection methods, solubility tests and stabilization trials of the amorphous state are in the focus and require greater attention [129–132]. The common active pharmaceutical ingredients (APIs) are synthesized as crystalline solids and subsequently processed by standard pharmaceutical operations such as milling [133], blending [134] and even sieving. These processing steps may lead to structural changes, crystal defects and amorphous regions which may have a huge potential to change during handling and storage and should be limited to a minimum. The conditions and kinetics of such process-induced disorders and changes during storage may affect product stability. In terms of the determination and control of the amorphous content, there is still lack in a reliable method to accurately assess the amorphous content in pharmaceutical powders down to a minimal level (< 1%).

4.1.1 Fully amorphous samples

First of all, suitable and reproducible methods for the production of fully amorphous samples were investigated. The applicability of four different techniques (BM, SD, FD and QC) was evaluated with regard to the varying physico-chemical properties of the APIs (e.g. lipophilicity, solubility and hygroscopicity). The absence of crystalline material in the postulated fully amorphous samples (ITB, FF, SBS, CS, BS and GC) was determined by DSC, TMDSC and XRPD techniques. Hereafter, these amorphous samples were blended with fully crystalline material to produce calibration curves with known amorphous amounts for DVS analytics. The ball-milling process is targeted as the most qualified method for the production of amorphous content because of the high similarity in particle properties (shape/roughness) compared to the investigated micronized powders.

4.1.1.1 Ball-milling process

This complex process incorporates four main variables and therefore is very time-consuming for an optimized production of fully amorphous samples. The interplay between the variables, filling level, grinding time, rotation speed and number of grinding balls is demanding. The main aim is to produce a fully amorphous state and a non-degraded API despite a high ther-

mal stress. Figure 32 visualizes solid bridges between particles of a sintered ball-milled API due to the influence of friction heat and an increase in temperature.

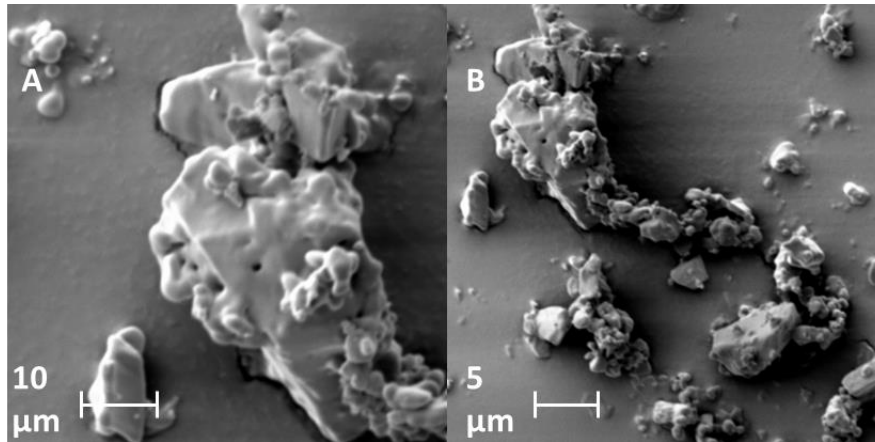


Figure 32: Solid bridges of a sintered ball-milled API

The produced samples are investigated by DSC measurement, whereby the area of the recrystallization event (T_c) is determined. The final powders are supposed to show the largest possible area [mJ] and should be comparable to other fully amorphous powders (such as spray-dried powders). As an additional measurement a XRPD analysis is performed where a broad background signal (“Halo”) is expected. Table 6 gives a generic overview of the optimization process for the determination of the ideal milling parameters to produce fully amorphous BS.

Table 6: Optimized ball-mill parameters for BS

No.	Variable 1 Filling level [g]	Variable 2 Grinding time [h]	Variable 3 Rotation speed [U/min]	Variable 4 Number of grinding balls	Area [mJ] T_c	XRPD sharp peaks?
1	25.0	2 and 6	360	4	-12/-15	Yes
2	25.0	2 and 6	400	4	-15/-16	Yes
3	25.0	6 and 24	420	4	-16/-28	Yes
4	6.8	12	400	6	-31	Yes
5	4.6	28	430	4	-40	Yes
6	3.0	3.5	380	3	-53	Yes
7	2.0	15	345	2	-91	Hardly
8	2.0	20	345	2	-188	No

Hereby, the ratio of the filling level (g) to the weight of grinding ball(s) (one grinding ball = 85 g) plays an important role on the amorphization extent. Over a series of experiments the ratio of the API weight to grinding ball weight was increased from 1:13.6 up to 1:85.0. For BS the T_c was determined at 107.0 ± 3.9 °C associated with a maximal area up to -188 mJ. In general, the ball-milling method was successfully applied to 5 of 6 APIs for the preparation of fully amorphous content (FF, SBS, CS, BS and GC). Table 7 presents the final parameters for each API, respectively.

Table 7: Parameters for all APIs in the ball-milling process for the production of fully amorphous samples

API	Filling level [g]	Grinding time [h]	Rotation speed [U/min]	Number of grinding balls	XRPD sharp peaks?
FF	2.5	16	340	4	No
SBS	25.0	24	450	6	No
CS	25.0	2	350	4	No
BS	2.0	20	345	2	No
GC	2.0	24	240	3	No

The fully amorphous state was further determined with XRPD analysis and compared to the fully crystalline starting material (Appendix 8.3.2). Regarding this analysis all crystalline API starting materials showed sharp peaks in contrast to the amorphous samples, which produce a broad background signal (Figure 33). These results confirmed the absence of crystalline material in the fully amorphous samples and supported the findings from the DSC analytics.

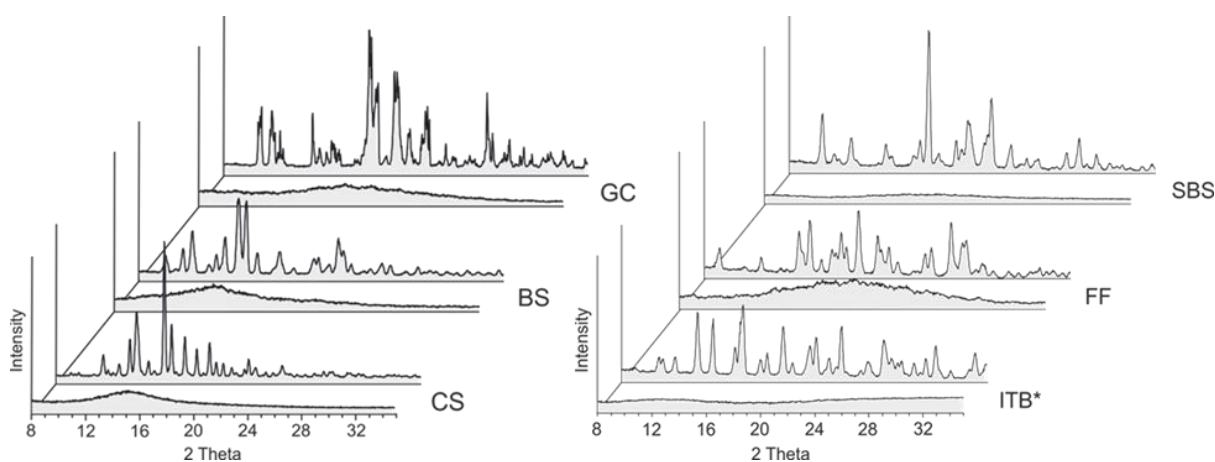


Figure 33: Comparison of fully amorphous and fully crystalline APIs

Regarding the hygroscopic drug ITB the ball-milling process was not suitable. Even after the grinding chamber was fumigated with argon and the starting material was dehydrated (3.7% to 0.4% water content, 2 hours at 150 °C) it was not possible to receive fully amorphous ITB. Therefore other production methods were required such as freeze-drying (freeze-dried ITB*, figure 33).

Furthermore, the influence of an extended grinding time up to 3 days and the thermal resistance was analyzed during ball-milling for CS (Table 8). The particle size is reduced over a longer milling period [135] and this investigation additionally shows a decrease in the melting point (T_m) and the glass transition (T_g). The milled and stressed powders showed a slight yellow coloring (beginning of decomposition) and a trend of a decreasing delta C_p was determined (related to the extent of amorphous content). As a consequence it is recommended to choose the grinding time very carefully.

Table 8: Influence of longer grinding times on CS samples

API	T_m [°C]	Onset T_g [°C]	T_g [°C]	Delta C_p [J/g · °C]
CS starting material	209.4	/	/	/
CS SD	208.7	88.5	97.7	0.318
CS BM 2 h	208.5	88.2	96.4	0.326
CS BM 6 h	207.5	86.9	96.1	0.337
CS BM 24 h	204.3	84.8	94.1	0.311
CS BM 48 h	198.6	80.1	91.1	0.288
CS BM 72 h	192.7	76.9	87.4	0.308

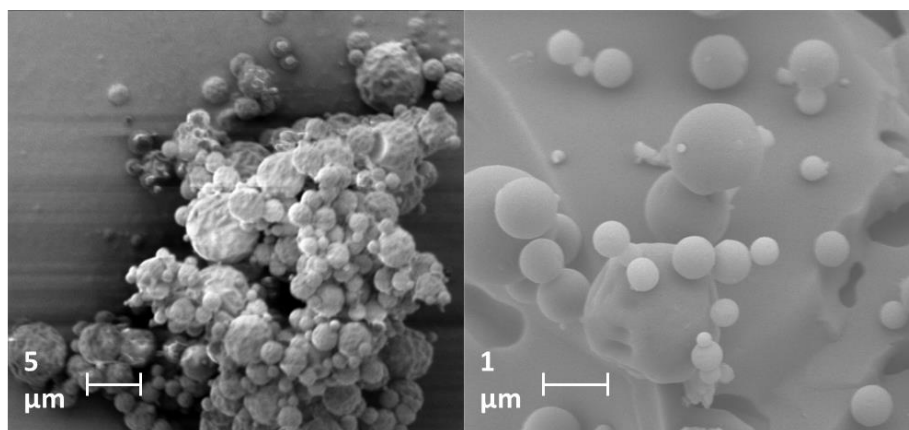
4.1.1.2 Spray-drying process

Firstly, a suitable solvent with a good solubility for the specific API was determined (fits well the requirements of spray-drying apparatus). The spray-drying process was successfully performed for SBS with water, for CS and BS with methylene chloride as the suitable solvent. Table 9 shows the relationship between a low particle size (x_{50}) and an increase in the specific surface (S_v) of the powder samples. All spray-dried APIs are in the range of 0.5 μm and 5.0 μm and might be used in adhesive mixtures for efficient pulmonary drug delivery.

Table 9: Characterization of successful produced fully amorphous spray-dried powders

API	x_{10}	x_{50}	x_{90}	Span	S_v [m^2/cm^3]	T_g [$^{\circ}\text{C}$]
SBS	0.62 ± 0.03	2.20 ± 0.12	5.13 ± 0.16	2.05 ± 0.05	4.26 ± 0.20	116.50 ± 1.35
CS	0.62 ± 0.02	1.26 ± 0.02	2.36 ± 0.05	1.37 ± 0.02	5.53 ± 0.11	96.10 ± 1.04
BS	0.67 ± 0.02	1.77 ± 0.03	4.63 ± 0.07	2.24 ± 0.09	4.44 ± 0.09	77.17 ± 1.11

In general, the inlet temperature and the concentration of the solution have both a fundamental influence on the surface morphology (roughness or smoothness, figure 34) and the particle size of the spheres. A significant influence on the extent of amorphous content was not determined for the various test experiments. ITB with water as a solvent showed a fast recrystallization during spray-drying which led to a crystalline powder [99]. For certain parameters a clear melt was found in the cyclone of the spray-dryer which may be linked to the hygroscopic behavior of the API.

**Figure 34: Difference in surface morphology: Comparison of rough and smooth spheres**

For GC a low solubility was determined for common organic solvents such as methanol, isopropanol and methylene chloride. Spray-drying from a suspension led to crystalline powders without a glass transition. In summary, for both APIs (ITB and GC) other methods were selected for the production of fully amorphous samples.

4.1.1.3 Freeze-drying process

In this investigation the freeze drying process was performed only with the hydrophilic, water-soluble substances, and proved to be the means of choice especially for ITB and SBS. Figure 35 shows the porous amorphous structure of a freeze dried SBS sample. One disadvantage is the wide particle size distribution for future preparations of homogeneous mixtures.

This method was not applied on organic soluble substances due to the incompatibility of the freeze-dryer.

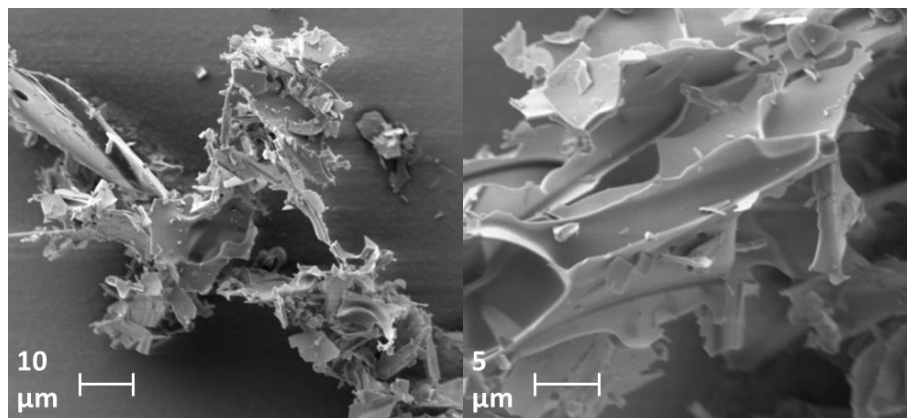


Figure 35: Freeze-dried, porous SBS sample

4.1.1.4 Quench-cooling method

As an alternative method compared to the spray- and freeze-drying process the quench cooling was also used for the preparation of fully amorphous samples. The DSC analytics were used to determine the melting point of the APIs, respectively. ITB and FF showed decompositions near the melting point because of less precise baseline above their T_m (Figure 36). This degeneration of API is impractical for this approach. Table 10 summarizes the specific DSC events. It should be mentioned that the release of hydrate water is not listed (for ITB and FF). The individual measurements are listed in the appendix (8.3.3).

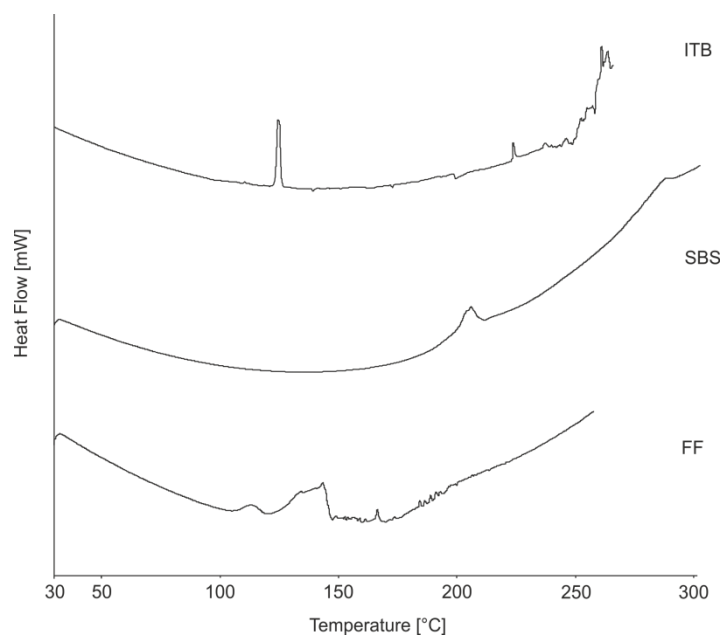


Figure 36: DSC measurement of the hydrophilic APIs

In addition, a degeneration was not determined for GC [117] (Figure 37). The identified temperatures were used as setting parameters for the melting of larger quantities (> 0.5 g) of API on the Kofler heat bench. The melt was successfully transferred into liquid nitrogen. After the amorphization process the particles were sieved to receive a narrow particle size distribution.

Table 10: Overview of the investigated APIs by DSC measurement

API	T_o [°C]	T_m [°C]	Area [mJ]	ΔH [J/g]
ITB	235.68 ± 0.52	237.91 ± 0.36	233.64 ± 15.04	103.21 ± 12.58
FF	138.29 ± 2.54	143.74 ± 1.11	374.26 ± 14.29	84.65 ± 10.11
SBS	192.89 ± 1.32	210.72 ± 0.41	421.06 ± 52.43	161.63 ± 2.91
CS	208.19 ± 0.02	210.38 ± 0.19	414.01 ± 66.46	74.59 ± 11.16
BS	258.09 ± 1.93	260.40 ± 2.09	188.96 ± 33.40	71.10 ± 1.64
GC	169.94 ± 1.20	173.10 ± 1.50	444.19 ± 37.58	83.06 ± 2.43

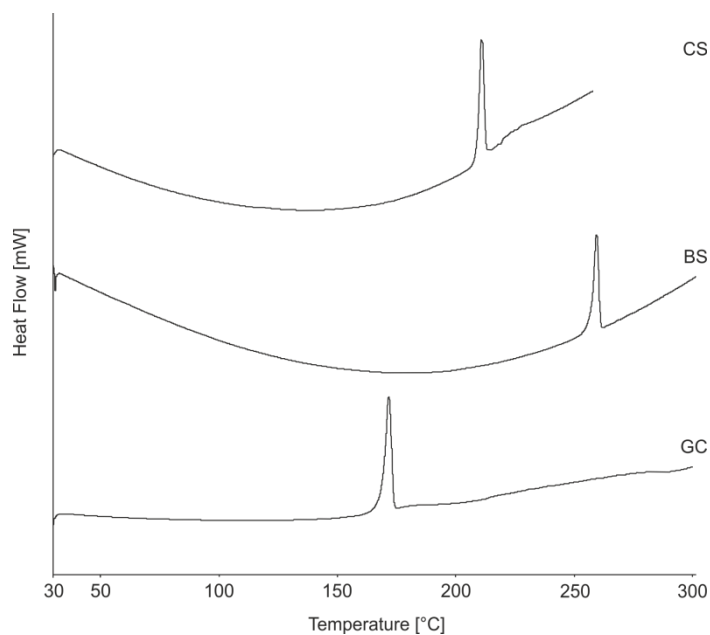


Figure 37: DSC measurement of the hydrophobic APIs

4.1.2 Stability assessment of the amorphous APIs and shelf-life

TMDSC (detection of glass transition), Dynamic vapor sorption (determination of moisture sorption isotherms) and XRPD analytics (determination of pattern) are examined to estimate the stability of the amorphous drugs, respectively.

With the increase of the T_g a slower re-crystallization behavior is expected. It was possible to correlate the glass transition of each fully amorphous API to its molecular weight (Figure 38). The individual T_g measurements are listed in the appendix (8.3.4).

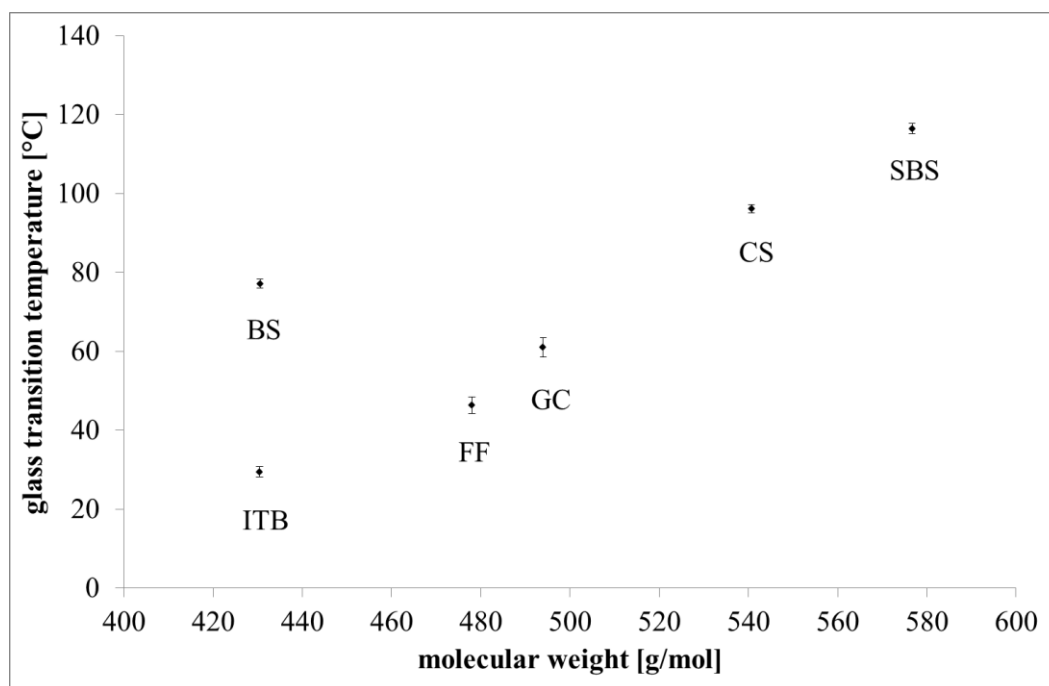


Figure 38: Glass transition of amorphous APIs dependent on molecular weight

As expected, an increase of the glass transition temperature can be linked to an increasing molecular weight. Higher molecular weight leads to lower mobility [136]. In this case the spray-dried Budesonide shows the exception. Significant differences between hydrophilic and hydrophobic samples could not be detected. In general, a higher glass transition is advantageous and contributes to a longer shelf life. It is assumed that ITB, FF and BS show a lower stability of amorphous amounts compared to GC, CS and SBS.

Furthermore, the behavior of these APIs was evaluated in a humidity atmosphere (2 cycles, 0-90% RH, water). Typically, amorphous samples show a significantly higher solvent absorption compared to crystalline materials and the different types of API also differ in their physico-chemical behavior. As expected, the screening vapor sorption measurements (DVS-1) showed different results for the investigated crystalline hydrophilic and hydrophobic APIs (Figure 39).

Moisture sorption isotherms of crystalline ITB showed the highest mass adsorption (increase of 1.1%) at 0.9 p/p_0 for all six investigated APIs. This mass increase of ITB was followed by the crystalline FF (increase of 0.6%) and SBS (increase of 0.4%). These hydrophilic, crystalline materials adsorb water on the surface [137] and show a high affinity to the polar solvent.

In this case the bromide (salt) has the greatest affinity to water vapor compared to fumarate and sulphate [138].

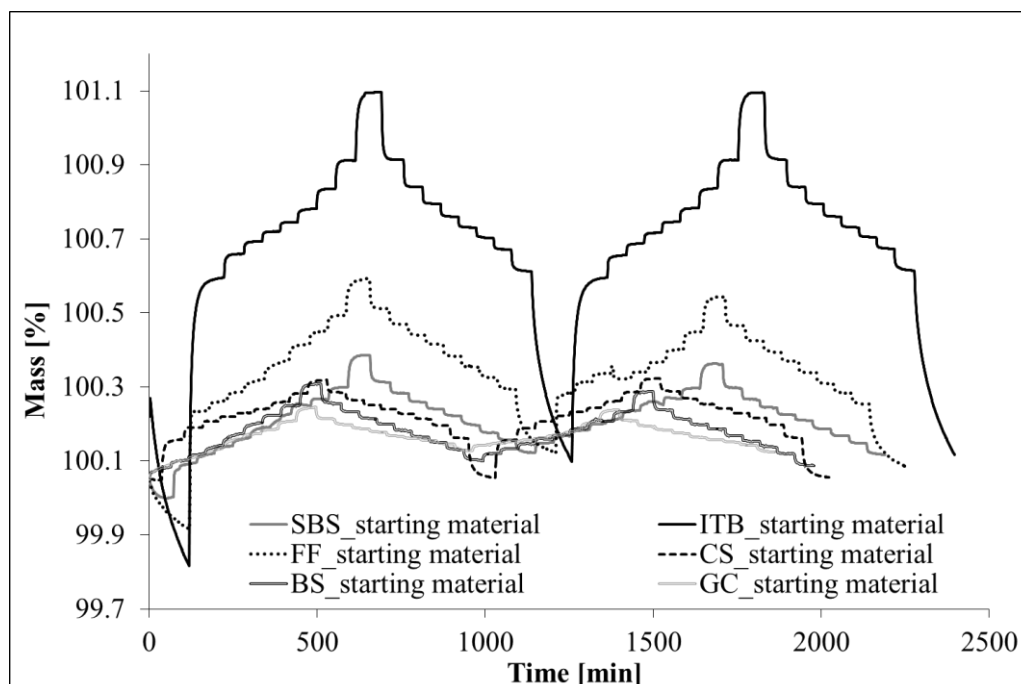


Figure 39: Adsorption behavior of fully crystalline APIs

The hydrophobic APIs showed the lowest adsorption behavior for water vapor (increase of $< 0.3\%$). These APIs were much more inert against the polar component (water vapor). The reason is that the polar solvent only has limited access to the hydrophobic surface and pores [27].

However, it is assumed that the hygroscopic APIs (e.g. ITB) are difficult to examine using DVS-method development because the amorphous amounts might be very unstable due to high water uptake (even at low humidity).

A significantly higher absorption can be detected for the fully amorphous samples applying even the same measurement parameters (2 cycles, 0-90% RH, water). Due to the change in the crystal lattice during the re-crystallization the second cycle shows a different curve progression for ITB, FF and SBS (Figure 40). The ITB sample showed an early re-crystallization ($0.4 p/p_0$, $> 4\%$ change in mass) due to its hygroscopic characteristics. It is presumed that amorphous material absorbs water to its inside which therefore results in a higher water uptake [137]. This process promotes molecular mobility and facilitates the re-crystallization process [139].

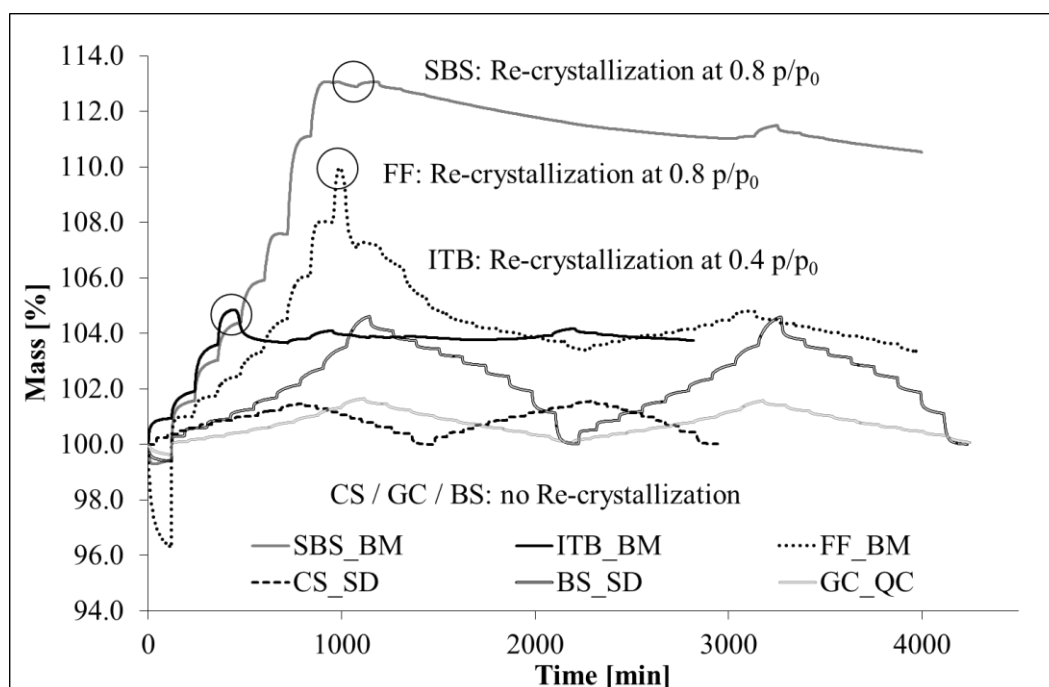


Figure 40: Absorption behavior of fully amorphous APIs

For SBS and FF the re-crystallization events were determined in combination with a very high water uptake at 0.8 p/p_0 (increase of > 10%). Bromide, fumarate and sulphate confirmed their behavior towards absorption (as shown for crystalline starting material) – a higher molecular mobility led to an earlier re-crystallization (ITB > FF > SBS).

Again, the hydrophobic APIs underpin a lower affinity to water vapor (even for fully amorphous samples). Moisture sorption isotherms of CS and GC resulted in the lowest values (increase of < 2%). BS showed a higher affinity to water vapor (increase of < 4.5%) which may also explain the low stability of amorphous amounts. For all hydrophobic APIs neither re-crystallization events, nor sudden losses in mass or different curve progressions for the second cycle were detected for water vapor.

Finally, the absorption values for fully amorphous samples (at level 0.4 p/p_0) demonstrated a trend in terms of the $\text{Log}P$ values (Table 2 and Table 3). APIs with a higher increase of mass are characterized by lower values of $\text{Log}P$.

Also, XRPD investigations were performed to study the stability of fully amorphous ball-milled samples. Especially the influence of temperature (Figure 41) and humidity (Figure 42) was evaluated by X-ray measurements. In each case the temperature or humidity was equilibrated for 1 hour before the XRPD measurement was implemented. The same powder sample was measured again after 1 hour of equilibration at the next temperature or humidity step. The temperature steps were set at 60 °C, 70 °C, 80 °C, 90 °C and 100 °C and the humidity was

raised from 20% RH to 50% RH to 70% RH and again at 70% RH but for 24 hours. Afterward, all diffractograms were compared to fully crystalline samples, respectively.

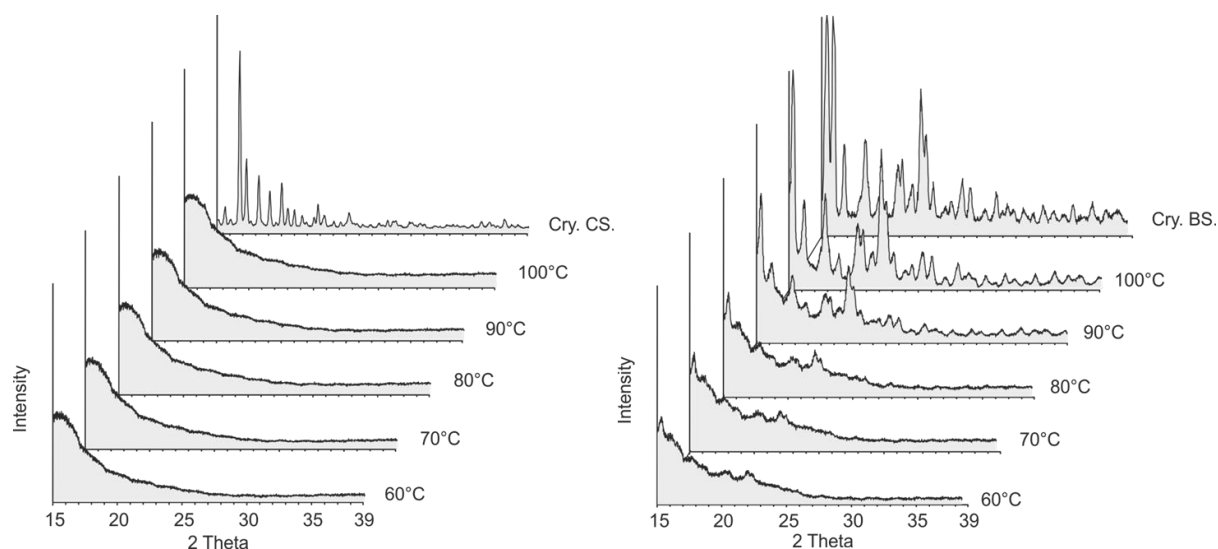


Figure 41: Temperature influence on amorphous ball-milled CS and BS samples

For the hydrophobic samples (CS and BS) significant differences were determined. The amorphous amounts of CS were more stable against the influence of temperature and humidity. After 24 hours at 70% RH CS demonstrated sharp peaks which can be correlated to crystalline parts. At all other temperature and humidity steps CS showed a fully amorphous behavior and a high stability.

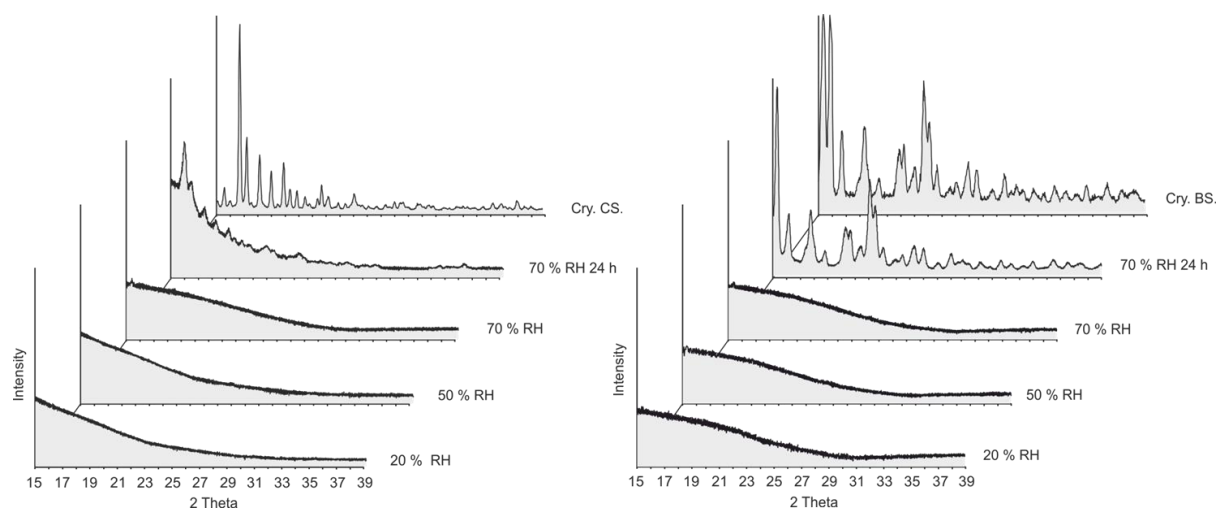


Figure 42: Humidity influence on amorphous ball-milled CS and BS samples

On the contrary, BS showed very low temperature robustness. The re-crystallization process of the ball-milled sample started at a low temperature of 60 °C and the material rebuilt the fully crystal lattice at 100 °C. Also, a humidity of 70% RH (24 hours) led to a fully crystalline

material. These results verify the previous results of TMDSC (lower T_g) and DVS (higher water affinity).

For SBS an influence of moisture on its molecular structure is known, however, the factor temperature is less identified and was also examined by XRPD (Figure 43). Again, the same temperature steps were chosen and the results showed that the amorphous amounts are extremely stable. Finally, the broad background signal was detected up to a temperature of 100 °C after altogether 5 hours of temperature stress. This temperature behavior in the XRPD can be correlated to the TMDSC study and the determination of the glass transition. A high T_g value of the substance demonstrates a less sensitive re-crystallization behavior in this XRPD temperature-study (SBS > CS > BS).

In summary, obvious differences between the APIs were characterized (TMDSC, DVS and XRPD) and indicate a fluctuating stability of the induced amorphous amounts. This post-operational relaxation is fundamentally induced by temperature, humidity and time.

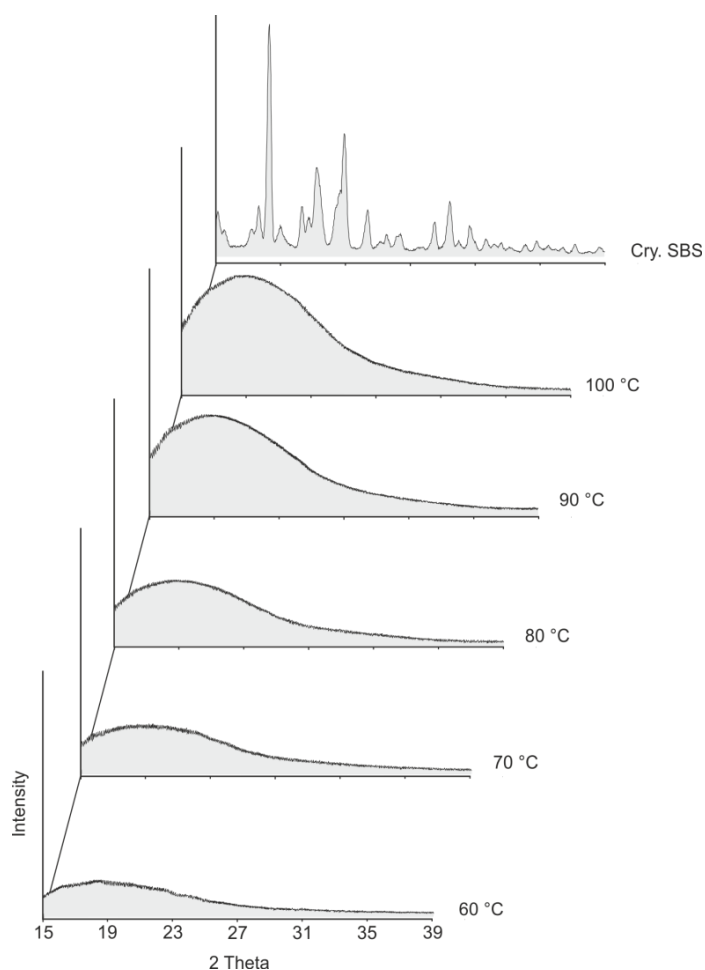


Figure 43: Temperature robustness of an amorphous SBS sample

4.1.3 Semi-crystalline samples

Different methods for the preparation of suitable samples with a low amorphous content are evaluated (< 20% amorphous content). The applicability of two different techniques which are commonly used in the pharmaceutical industry (jet-milling and blending of powders) was investigated. In this study the extent of amorphous amounts in the APIs (ITB, SBS, CS, BS and GC) was determined with individually developed DVS techniques (Chapter 4.3.4).

4.1.3.1 Jet-milling process

The amorphous content of the respective drugs introduced via jet-milling can be correlated to the grinding pressure (1 bar up to 8 bar) and the number of grinding cycles (1-3 Gc). These samples with unknown amorphous amounts served as test substances for DVS analytics. During jet-milling the particle size of the sample was reduced with each grinding cycle at 8 bar (JM1).

Table 11 shows the characteristic particle size distribution for each API and each grinding cycle, respectively. The complete investigation was not performed for the high potent FF due to the hazards of the inhalation at very low concentration (a few μg).

Table 11: Influence of the number of grinding cycles on the particle size distribution

API	x_{10}	x_{50}	x_{90}	Span
ITB starting material	0.70 ± 0.02	1.81 ± 0.01	4.21 ± 0.04	1.95 ± 0.03
ITB JM1 Gc1	0.62 ± 0.00	1.58 ± 0.01	3.87 ± 0.04	2.05 ± 0.03
ITB JM1 Gc2	0.59 ± 0.01	1.53 ± 0.01	3.79 ± 0.06	2.10 ± 0.05
ITB JM1 Gc3	0.58 ± 0.00	1.45 ± 0.01	3.58 ± 0.05	2.07 ± 0.03
SBS starting material	2.03 ± 0.01	9.11 ± 0.07	33.33 ± 1.19	3.44 ± 0.11
SBS JM1 Gc1	0.83 ± 0.01	2.87 ± 0.01	9.87 ± 0.23	3.15 ± 0.08
SBS JM1 Gc2	0.73 ± 0.01	2.07 ± 0.01	5.93 ± 0.01	2.51 ± 0.01
SBS JM1 Gc3	0.71 ± 0.01	1.93 ± 0.01	5.46 ± 0.01	2.47 ± 0.00
CS starting material	4.74 ± 0.05	57.90 ± 2.96	288.91 ± 19.18	4.91 ± 0.16
CS JM1 Gc1	0.67 ± 0.01	2.38 ± 0.10	6.30 ± 0.53	2.36 ± 0.12
CS JM1 Gc2	0.61 ± 0.01	1.94 ± 0.06	5.17 ± 0.29	2.35 ± 0.11
CS JM1 Gc3	0.57 ± 0.01	1.51 ± 0.02	4.52 ± 0.10	2.62 ± 0.05

BS starting material	0.59 ± 0.00	1.66 ± 0.02	4.57 ± 0.10	2.40 ± 0.04
BS JM1 Gc1	0.55 ± 0.01	1.59 ± 0.03	4.40 ± 0.03	2.42 ± 0.03
BS JM1 Gc2	0.54 ± 0.00	1.54 ± 0.04	4.17 ± 0.14	2.36 ± 0.03
BS JM1 Gc3	0.54 ± 0.01	1.51 ± 0.02	3.89 ± 0.06	2.22 ± 0.02
GC starting material	7.31 ± 0.43	34.45 ± 0.39	85.38 ± 0.66	2.27 ± 0.02
GC JM1 Gc1	0.80 ± 0.01	3.45 ± 0.12	11.47 ± 0.76	3.09 ± 0.16
GC JM1 Gc2	0.67 ± 0.00	2.22 ± 0.06	6.25 ± 0.05	2.51 ± 0.04
GC JM1 Gc3	0.64 ± 0.00	1.97 ± 0.06	5.46 ± 0.28	2.45 ± 0.08

SEM pictures confirmed the results as the micronized powder (8 bar, 1 cycle) reveals a smaller particle size distribution compared to the crystalline starting material of SBS (Figure 44). A significant difference of the needle shaped crystals is visible in the length (approximately from 10 μm to 1 μm). These findings can be compared to the other crystal morphologies (significant crushing).

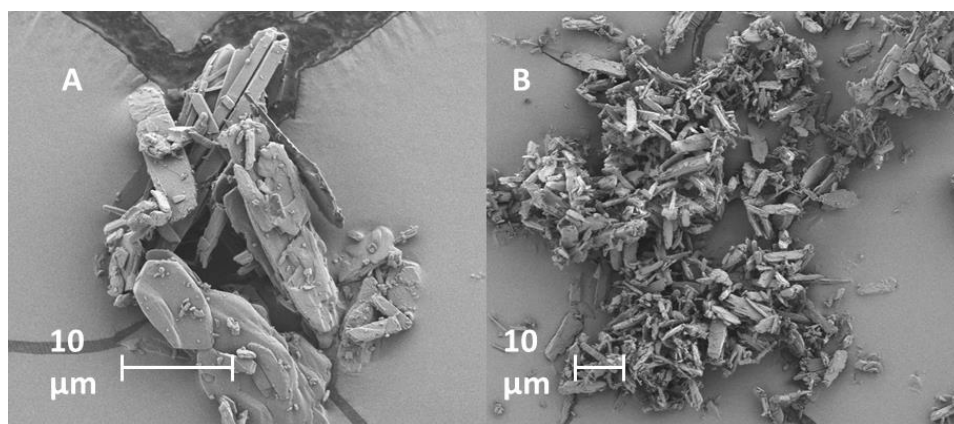


Figure 44: Influence of one grinding cycle on particle size (SBS)

Furthermore, a reduction in the intensity of the sharp peaks (XRPD, figure 45) was determined for the micronized powders (e.g. SBS) in correlation to the number of grinding cycles (1 cycle to 3 cycles). For the fully amorphous sample again no sharp peaks were detected (SBS SD). The same behavior was detected for micronized CS and BS (Appendix 8.3.2).

This behavior indicates a higher amorphous content and was confirmed by a higher absorption behavior by DVS analytics (Chapter 4.3.1.3 and 4.3.4).

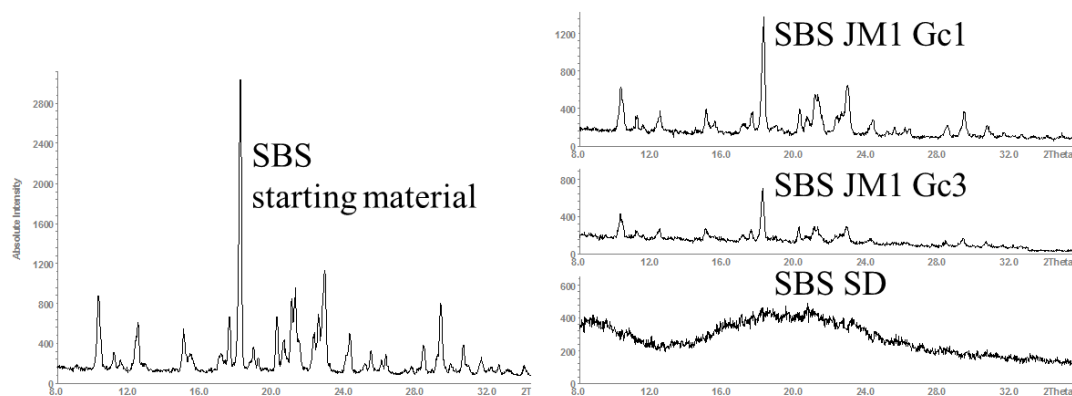


Figure 45: Influence of the number of grinding cycles on the peak intensity in XRPD

4.1.3.2 Mixing tests with glass beads

The quantification of amorphous amounts introduced during the preparation of physical mixtures (carrier and API) proved to be challenging. For this purpose, the initial carrier (e.g. lactose) was replaced by different glass beads (250 μm or 400 μm , figure 46). After a mixing time of 45 minutes (at 42 rpm) these glass beads were removed by an air jet sieve to investigate the pure stressed API. Hereby, the smaller API particles were removed by an air stream and collected by a cyclone.

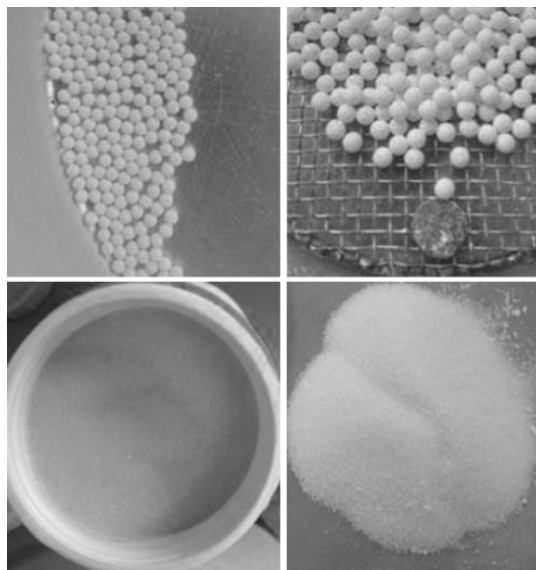


Figure 46: Blends with small and big glass beads

The large-sized glass beads remained on the mesh and were discarded. This process enables to determine the amorphous amounts of the pure API. Blends containing 1.5%, 4.0% and 25% of API (second component: glass bead carrier) were tested to achieve a sufficient amount of API for quantification. High drug loss was determined because of the high press-on forces during mixing leading to a high drug retention on the glass beads. Furthermore the air jet siev-

ing showed a low yield. A blank value was determined for the purely crystalline material during the air jet sieving. Finally, the amorphous amounts generated were determined by DVS analytics (Chapter 4.3.4).

4.2 Additional physico-chemical characterization of the crystalline starting material

The determination of major API properties of the starting material was performed in order to differentiate and compare specific characteristics. Beside the melting points which were determined while investigation for quench cooling (Table 10) and the DVS moisture sorption isotherms which demonstrated initial differences in water uptake for hydrophilic APIs (Figure 39) further characteristics are useful. Additional assessments are necessary for further calculations and experimental procedures with amorphous amounts. Table 12 presents the obtained values of the additional characterization.

Table 12: Physico-chemical characterization of crystalline starting material

API	Density [g/cm ³]	Water content [%]	Mass increase [% at 0.9 p/p_0]	Surface energy [mJ/m ²]	S_v [m ² /cm ³]
ITB	1.4091 ± 0.0042	3.65	1.1	40.04 ± 0.49	4.35 ± 0.06
FF	1.3412 ± 0.0035	2.28	0.6	51.20 ± 1.58	4.74 ± 0.04
SBS	1.3424 ± 0.0044	0.47	0.4	41.11 ± 2.03	1.02 ± 0.01
CS	1.1935 ± 0.0048	0.46	< 0.3	41.01 ± 1.09	0.75 ± 0.01
BS	1.2890 ± 0.0049	0.38	< 0.3	48.40 ± 0.77	4.85 ± 0.02
GC	1.3691 ± 0.0031	0.29	< 0.3	41.70 ± 1.04	0.37 ± 0.02

The true density is required for the investigation and calculation of the common glass transition ($T_{g\text{ mix}}$) of API and solvent (Gordon-Taylor-equation, chapter 4.3.1.2). In general, this model is used to calculate interaction parameters of the API and the plasticizer (solvent) [86].

The initial water content (determined by infrared scale) is used for the additional estimation of the stability of amorphous amounts and furthermore for the optimization of the drying phases (DVS analytic). This residual moisture and the hygroscopic behavior can be linked to the mass increase of crystalline starting material at 0.9 p/p_0 .

The APIs (FF and BS) that were available as micronized starting materials, tend to electrostatic charge. It is assumed that the different adhesion to the inner walls of a mixer lead to a lower homogeneity during the mixing process of calibration curves [140]. Furthermore, the effect of particle shape/size on powder flow and cohesion is well documented in the literature [141].

This presumption can be confirmed by a higher surface energy. Micronized FF showed a surface energy of 51.20 ± 1.58 mJ/m² and BS of 48.40 ± 0.77 mJ/m² compared to the crystalline starting materials with a surface energy of 40.04 mJ/m² to 41.70 mJ/m². Shah et al. postulated that powder cohesion increases in a linear correlation with an increasing surface energy of the API [142]. This observation of micronized powders and high surface energy is supported by an increasing specific surface of the particle compared to crystalline starting material. For FF and BS values of approximately 5 m²/cm³ were measured. The starting materials which were not micronized from the supplier showed values of about 1 m²/cm³.

The values of the volumetric surface (S_v) can be linked to the measured particle size distributions of the crystalline starting materials (Table 11).

Furthermore, XRPD pattern are determined for the crystalline starting materials and show characteristic sharp peaks which is resulted from a high degree of the crystal lattice, respectively. These diagrams of all six active pharmaceutical diagrams are listed in the appendix (8.3.2).

4.3 Development of a one-step Dynamic vapor sorption (DVS) method for the calculation of amorphous amounts

Ciclesonide powder samples (fully crystalline material 0%, blends with an amorphous content of 5%, of 8% and of 15% and the ball-milled sample containing 100% amorphous content) were analyzed to determine the method sensitivity with four different techniques (DSC, TMDSC, Hyper-DSC, XRPD) for low amorphous content (Figure 47).

It turned out that these four different methods were not capable of detecting very small amorphous amounts. Only high amorphous amounts were adequate for the exact determination and showed specific events such as a re-crystallization event (DSC, Hyper-DSC), glass transition event (TMDSC) or a broad background signal (XRPD). Some measurement techniques were able to detect blends with an amorphous content up to 15% (DSC, TMDSC and Hyper-DSC). These results were comparable to the described limit of quantification (LOQ: 5-10%) in the literature for the detection of very low amorphous amounts in powder samples [143].

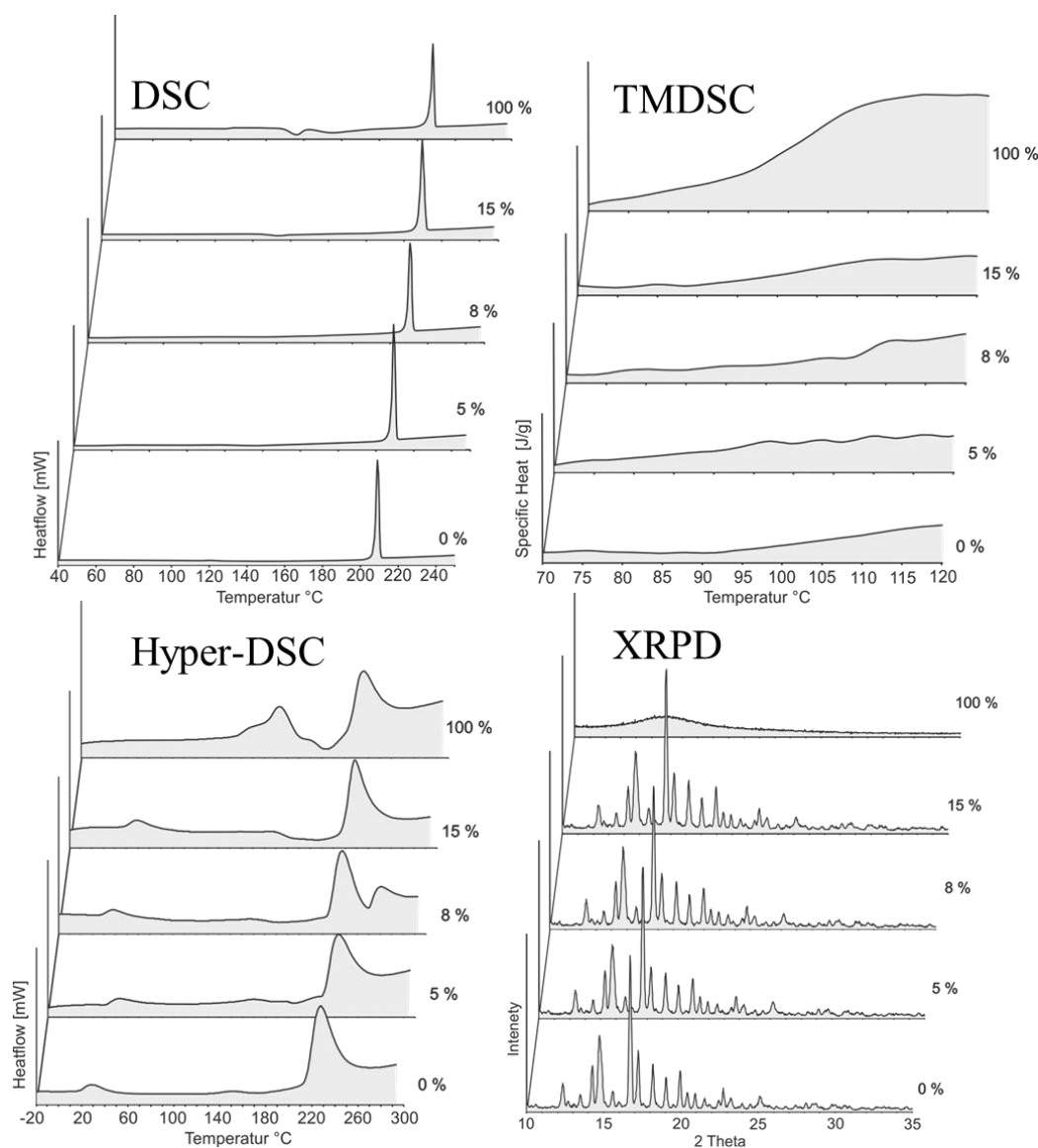


Figure 47: Comparison of different methods to determine amorphous content of CS

Furthermore, these samples (0%, 0.25%, 2%, 5%, 8%, 15% and 100% of amorphous content) were investigated by Dynamic Mechanical Analysis. The powder samples were filled into aluminum pockets and might show a time-dependent deformation (strain) under sinusoidal mechanical stress. Hereby, amorphous amounts are characterized by a viscoelastic behavior compared to an elastic behavior which can be found in crystalline samples.

Nevertheless, small amorphous amounts are again not detectable using this suggested technique. Until 100 °C the loss modulus G'' remains at a low level for the fully amorphous ball-milled sample (CS) in figure 48. This behavior indicates that the powder sample reacts like a solid and the mechanical energy is almost completely stored. Over 100 °C a significant increase of the loss modulus G'' is determined. The sample lost its elastic property and a conversion into heat energy is realized.

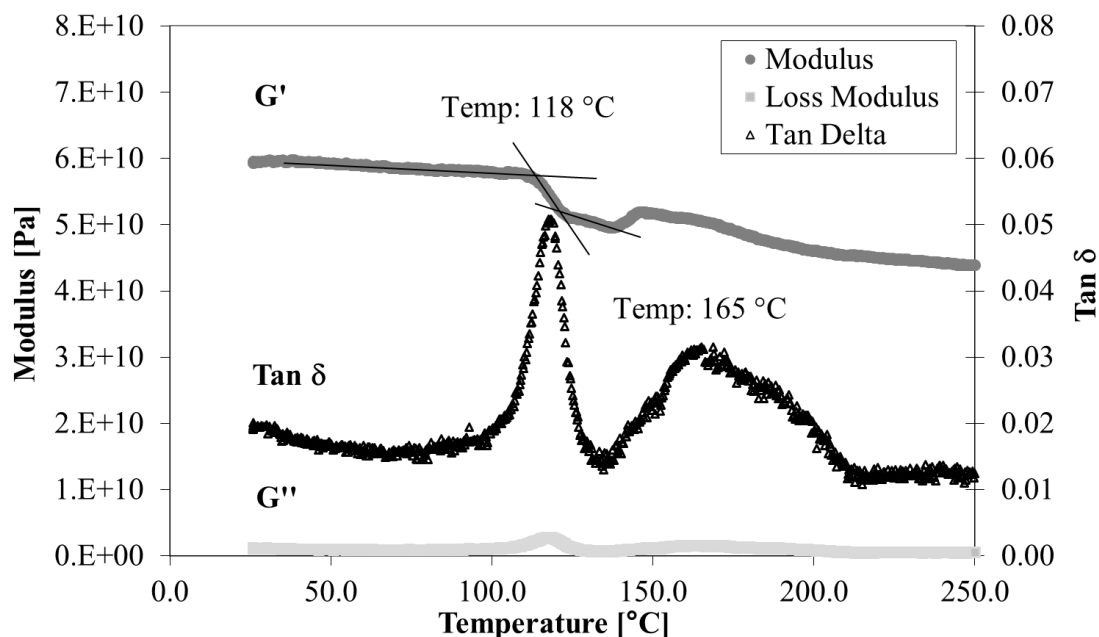


Figure 48: DMA measurement of fully amorphous CS

Another indication is the rapid simultaneous decrease of the storage modulus G' . The maximum is reached at the glass transition of CS (118 °C). Furthermore, a second event (melting temperature) was determined at 165 °C, whereby an increase of the loss modulus G'' and a decrease of the storage modulus G' is determined.

As expected, a glass transition temperature for the crystalline starting material cannot be measured. The melting temperature was detected at 194 °C (data not shown). These thermal events (BM and crystalline starting material) were not comparable to the data measured in the DSC analytics ($T_g = 96.4$ °C and $T_m = 210.4$ °C).

For the blend with an amorphous content of 15% the DMA data showed a different curve progression in comparison to the fully amorphous sample (Figure 49). A decrease in the T_g event and a deviation of the melting point were determined. For the blends of < 5% amorphous content glass transitions were not visible. Finally, this approach was discarded for the accurately determination of very low amorphous amounts.

Finally, the DVS-method was selected at the means of choice for the determination of amorphous content. This analytic tool showed a higher sensitivity for a low amorphous content < 1% and was used as technique of choice [21]. The intention of this proposed work is the establishment and qualification of the DVS sorption method (organic, water) to hydrophilic, lipophilic and hygroscopic drugs, respectively. This reliable method enables the accurate access of the amorphous content in pharmaceutical powders down to a low level.

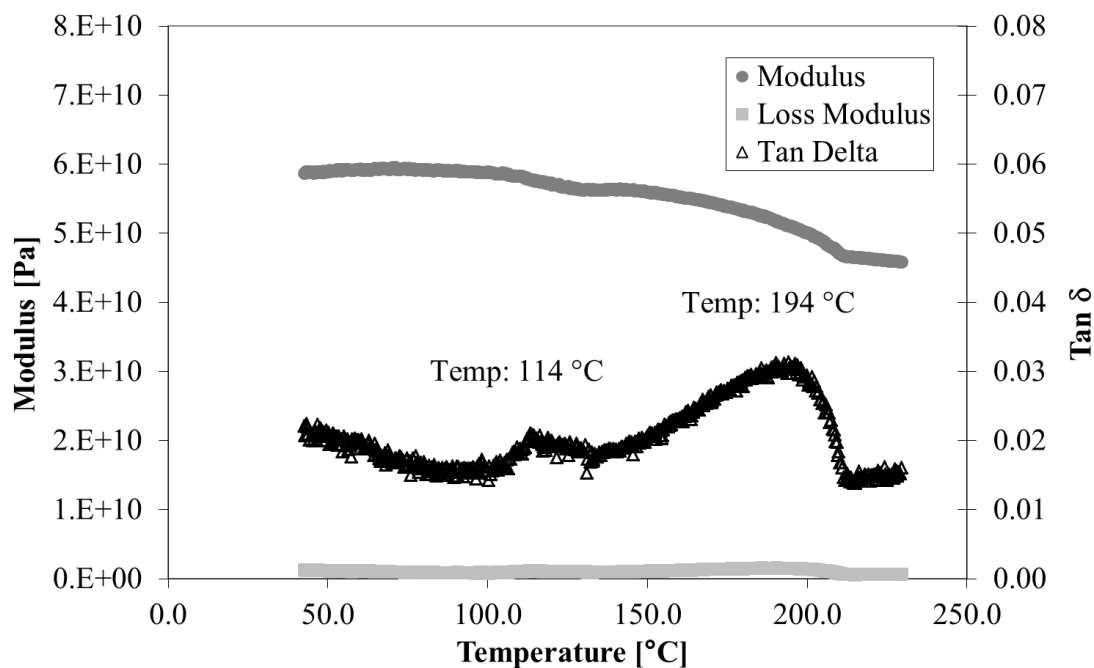


Figure 49: DMA measurement for 15% amorphous content (CS)

4.3.1 Case study of Ciclesonide (CS)

There is lack of qualified/validated DVS methods for the detection of minimal amorphous parts down to a level of 0.5%, especially for hydrophobic APIs. On the other side the quantification of amorphous parts by water moisture sorption isotherms for hydrophilic samples is well documented in the literature [26]. In a review Sheokand et al. divided the DVS-methods for the quantification of amorphous amounts into three main groups [15]. The equilibrium moisture uptake (based on absorption), the water uptake method (based on re-crystallization) and the residual weight (based on solvated solvent) method are discussed. However, for hydrophobic material, which is chemically more stable against water vapor and the change in crystallinity is self-limiting, only a few DVS approaches are available with focus on organic solvents. For example Mackin et al. used acetone as a solvent (for a benzyl ether derivative-type of drug) and Samra et al. used mixtures of ethanol/water and ethanol/n-propanol in their investigations with hydrophobic terfenadine [25,27]. The aim of this study was primarily to find the solvent with the highest affinity to the API, respectively. Finally, the method is simplified as much as possible to shorten measurement procedure resulting in a one-step method (time saving: reduction by 80% over 200 hours). Since the DVS method can easily be adapted to different active pharmaceutical ingredients (adjustment of temperature, vapor p/p_0 and screening of the solvent), this method has a huge advantage compared to the methods mentioned in the previous chapter. At first, this DVS method development based on 'equilibrium moisture uptake' is presented extensively for CS as the hydrophobic model drug. Thereafter,

the applicability of the method to the other five APIs was investigated and adapted according to the case study of CS. A high affinity between API and solvent is targeted to receive a high sensitivity of the method, a higher slope of the calibration curve and to detect minimal differences between powder samples. However, the amorphous content has to be stable for an exact determination. The development can be divided into six main sections (water moisture sorption isotherms, organic solvent screening, optimization of the p/p_0 values, temperature robustness, influence of particle size/surface and validation). Finally, a schematic model for the explanation of the adsorption and absorption theory is introduced [144].

4.3.1.1 Water moisture sorption isotherms - Influence on the absorption behavior and the need for organic solvents

The measurement with water vapor showed differences in the water uptake between the fully amorphous spray-dried and the ball-milled CS (increase of $< 1.0\%$ at $0.4 p/p_0$) and SBS (increase of $> 5.0\%$ at $0.4 p/p_0$) (Figure 50). As expected, the hydrophilic sample (SBS) shows higher water absorption in comparison to the hydrophobic API (CS) which was much more inert against water vapor. The reason is that the polar solvent only has limited access to the hydrophobic surfaces and pores [27]. This finding again demonstrates that the water vapor method is not suitable for hydrophobic powders.

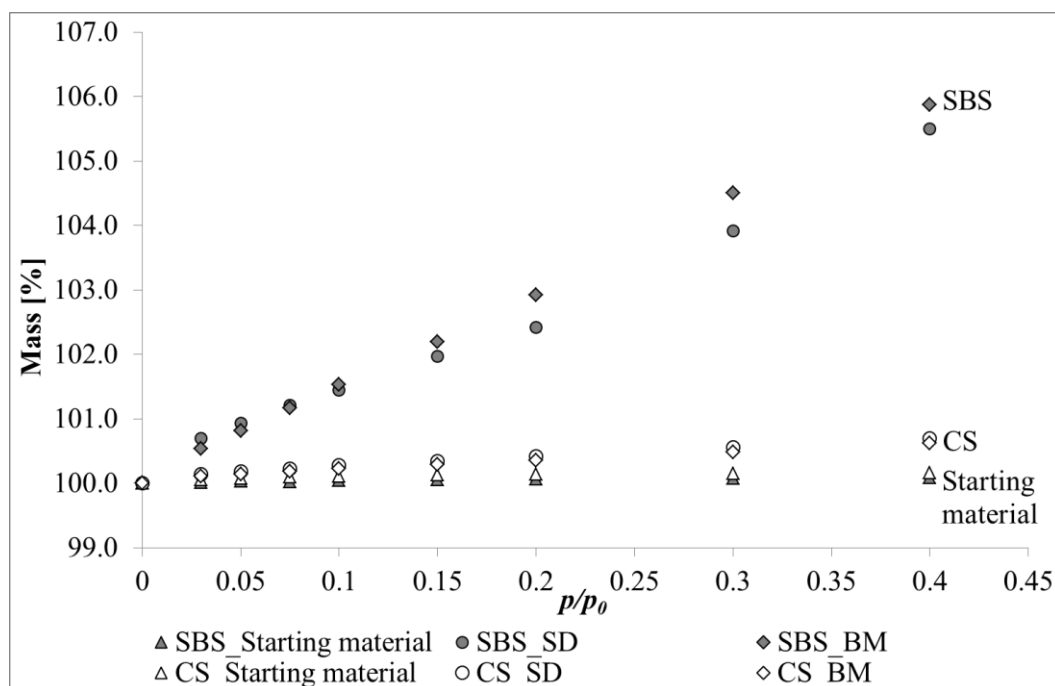


Figure 50: Water moisture sorption isotherms of hydrophilic and hydrophobic samples

With this insensitive analysis low amorphous amounts are not detectable with water vapor because the difference in the absorption behavior between the fully amorphous hydrophobic

powder and the fully crystalline powder is minimal and thus no acceptable precision may be achieved. Further studies with small quantities of hydrophobic API (jet-milled samples) revealed that the water sorption is not suitable to detect small amorphous contents. In this case the crystalline starting material indicates the baseline sorption behavior and the spray-dried and ball-milled powders represent the limit for highest detectable amorphous amounts.

In summary, this measurement clearly shows the maximal sensitivity and the upper limit of detection which is obtained by a high affinity to the solvent (in this case: hydrophilic API to the polar solvent water). This approach will be implemented in the following for a nonpolar solvent and a hydrophobic model drug (CS).

4.3.1.2 Organic solvent screening - Influence on absorption behavior

Based on the results of the water vapor sorption study, a screening with different polar and nonpolar solvents was conducted to receive higher vapor absorption and therefore an increase in the detection limit. Table 13 shows the chemical properties of the used solvents in detail.

Table 13: Physico-chemical characteristics of the polar and nonpolar solvents

Solvent	Water	Methanol	Ethanol	Isopropanol	Ethyl acetate
Chemical formula	H ₂ O	CH ₃ OH	C ₂ H ₅ OH	C ₃ H ₈ O	CH ₃ COOC ₂ H ₅
Molecular weight [g/mol]	18.02	32.04	46.07	60.10	88.11
Boiling point [°C]	99.98	64.70	78.37	82.50	77.10
Density [g/cm ³ , 25 °C]	1.00	0.79	0.79	0.78	0.90
Surface tension [mN/m, 25 °C]	72.75	22.55	22.27	20.77	23.75
Viscosity [10 ⁻³ Pa s, 25 °C]	0.89	0.59	1.19	2.06	0.45
Solubility H ₂ O [25°C]	∞	∞	∞	∞	8.10
Dipole moment [D]	1.85	1.70	1.69	/	1.78
Lipophilicity [miLogP]	-0.29	-0.32	0.06	0.42	0.76

These solvents are comparable to the eluotropic series and exhibit larger differences in the surface tension, viscosity and of course in the lipophilicity. For each solvent the device compatibility (DVS) has to be checked.

The moisture sorption isotherms of crystalline starting material and amorphous samples (BM/SD) were determined (Figure 51). The crystalline sample adsorbed only little vapor of each solvent resulting in a low increase of mass ($< 0.5\%$). In summary, all solvents almost showed the same isotherms for the crystalline powder. This effect indicates the baseline sorption behavior and represents the absence of amorphous material.

The amorphous samples showed a clear increase in the vapor sorption for methanol, ethanol, isopropanol and ethyl acetate compared to water (Appendix 8.3.5). Overall a mass increase of 3.5% to 5.5% at 0.4 p/p_0 was observed. For ethanol (BM material at 0.4 p/p_0 and mass absorption $> 3.5\%$), isopropanol (BM material at 0.4 p/p_0 and mass absorption $> 4.0\%$) and ethyl acetate ((SD material 0.15 p/p_0 and mass absorption $> 3.0\%$)/BM material 0.3 p/p_0 and mass absorption $> 5.0\%$) the point of recrystallization was detected.

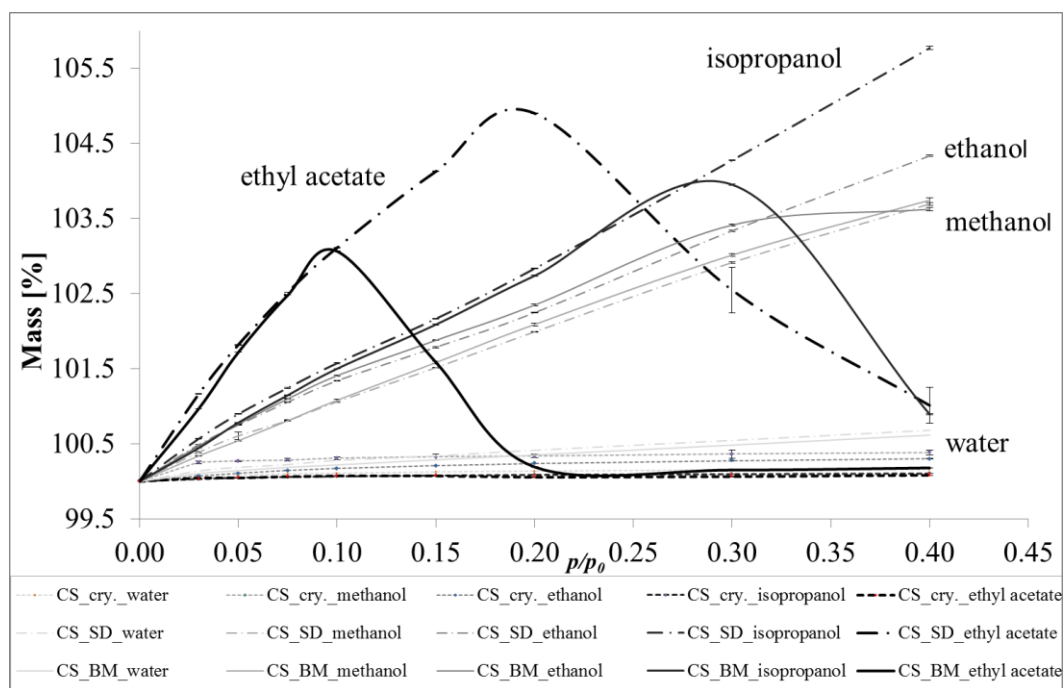


Figure 51: Increase of absorption behavior/re-crystallization to different organic solvents

Isopropanol was found to be the solvent with the highest mass absorption (5.5% at 0.4 p/p_0) and without a re-crystallization below 0.3 p/p_0 for the spray-dried and ball-milled samples (re-crystallization event T_c was measured by DSC, appendix 8.3.3). The BM sample showed a re-crystallization at lower p/p_0 values for each solvent. It is assumed that crystal nuclei were still present in the milled powder and led to a faster re-crystallization compared to the SD sample

(Table 14). The length of experiment is correlated to an increased absorption behavior of these amorphous samples.

Table 14: Experimental observations of the organic solvent screening

Experimental observations	Water	Methanol	Ethanol	Isopropanol	Ethyl acetate
Start of re-crystallization [p/p_0]	/	/	BM: 0.4	BM: 0.4	SD: 0.3 BM: 0.15
Length of experiment [days]	3	10	10	10	9

A further outcome of the initial study is that nonpolar solvents behave like plasticizers and lead to an earlier re-crystallization. Each solvent lowered the glass transition temperature, respectively. Several reasons contributed to this behavior, firstly, solvents with a lower molecular weight have a greater affinity to moisture and interact well with water (methanol, ethanol) and secondly solvents with a larger structure (isopropanol, ethyl acetate) interact well with the hydrophobic Ciclesonide [86]. The calculation of the glass transition temperature (CS SD), using the Gordon-Taylor equation, confirms that ethyl acetate is expected to be the strongest plasticizer (Figure 52). The Gordon-Taylor equation enhances the determination of the glass transition temperature of a mixture ($T_{g\ mix}$ of components), requiring known parameters such as the weight of the single fractions determined by DVS analytics ($w_1 =$ Ciclesonide and $w_2 =$ solvent), the $T_{g\ 1}$ of amorphous Ciclesonide (Table 9), $T_{g\ 2}$ of the solvents (Table 1) and the true density (Table 12, Table 13) of the components. Equation 4.1 and 4.2 shows the calculation for spray-dried CS with ethyl acetate at p/p_0 value of 0.2.

$$K = \frac{1.2143 \text{ g/cm}^3 \cdot 370.7 \text{ K}}{0.90 \text{ g/cm}^3 \cdot 126.0 \text{ K}} = 3.97 \quad 4.1$$

$$T_{g\ mix} = \frac{(95.0999\% \cdot 370.7 \text{ K}) + (3.97 \cdot 4.9001\% \cdot 126.0 \text{ K})}{95.0999\% + (3.97 \cdot 4.9001\%)} = 329.15 \text{ K} = 56.15 \text{ }^\circ\text{C} \quad 4.2$$

In summary, ethyl acetate lowers the glass transition temperature most effectively and therefore, the substance can re-crystallize faster in comparison to the other used solvents. In the case of water, it is first sorbed as a monolayer by the material. At higher p/p_0 values multilayers (adsorption) [80] can be found leading to a very low decrease in the T_g . On the contrary, an absorption into the hydrophobic particle (e.g. fully amorphous BM and SD samples) can be noticed for the organic solvents. As a result of the higher content of solvent the molec-

ular mobility increases (plasticizer) and the glass transition temperature is strongly reduced. This facilitates the spontaneous re-crystallization. The SD and BM samples almost showed the same results.

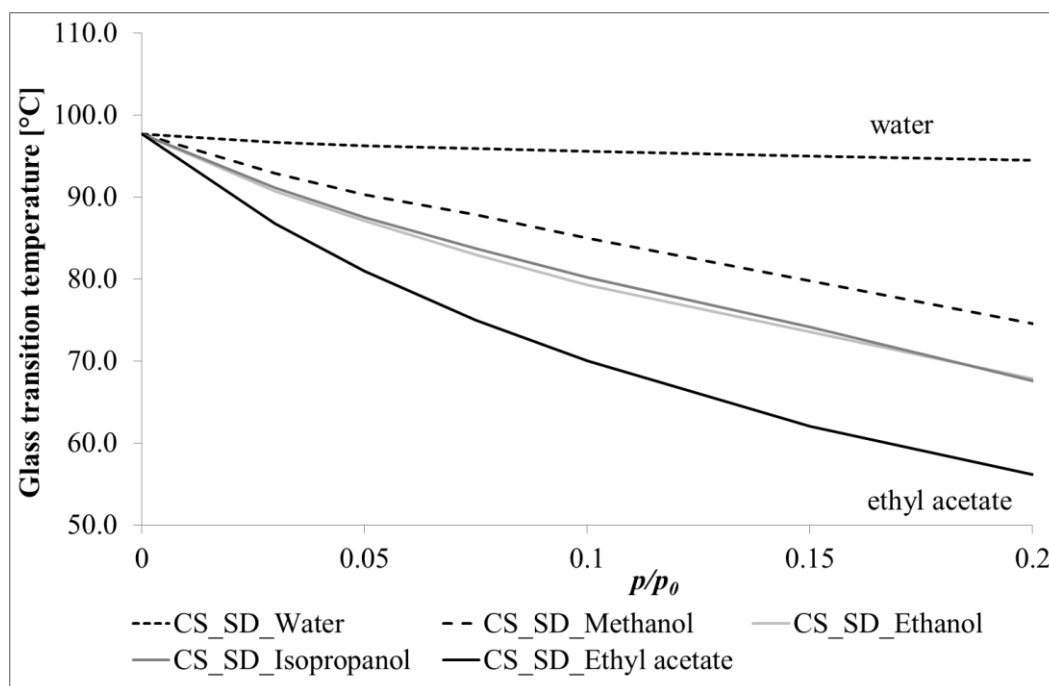


Figure 52: Decrease of glass transition due to solvent type and quantity (Gordon-Taylor)

4.3.1.3 Determination of the optimal vapor (p/p_0) value

Finally, isopropanol (high mass absorption, no early re-crystallization) was used for further single measurements with low amorphous amounts (jet-milled powders) to determine the influence of different vapor pressures in detail. In this test series, 0.10 p/p_0 , 0.15 p/p_0 , 0.20 p/p_0 and 0.30 p/p_0 were analyzed (Figure 53) as a one-step measurement with the objective of saving time (2 days instead of 10 days). This one-step method is designed in a way that the sample is dried for 20 hours and afterward the humidity is adjusted individually for 22 hours. The same micronized powders were used in every measurement. The different amorphous amounts were received by one, two or three grinding cycles (Gc). The lowest humidity (0.10 p/p_0 , Figure 53 A) turned out to be setting of choice, it showed no re-crystallization of the amorphous samples (no loss of weight) and the change in mass was almost in equilibrium over 22 hours; therefore, this p/p_0 value was chosen as the most suitable parameter. Higher humidity levels led to re-crystallization [145] which correlates to a strong and quick loss in mass. Especially for the highest humidity (0.30 p/p_0 , Figure 53 D) this assumption was confirmed. The mass loss (0.15 p/p_0 , 0.20 p/p_0 and 0.30 p/p_0) does not ensure a correct interpretation and therefore is not suitable for the calculation of the amorphous content (comparison of

the equilibrium dried mass and after the equilibrium of solvent absorption). However, significant differences in the absorption behavior were determined by reason of different grinding cycles and small amorphous amounts. The absorption was significantly increased (0.3%) for JM1 Gc3 in comparison to the crystalline starting material at the optimized p/p_0 value of 0.1 (isopropanol).

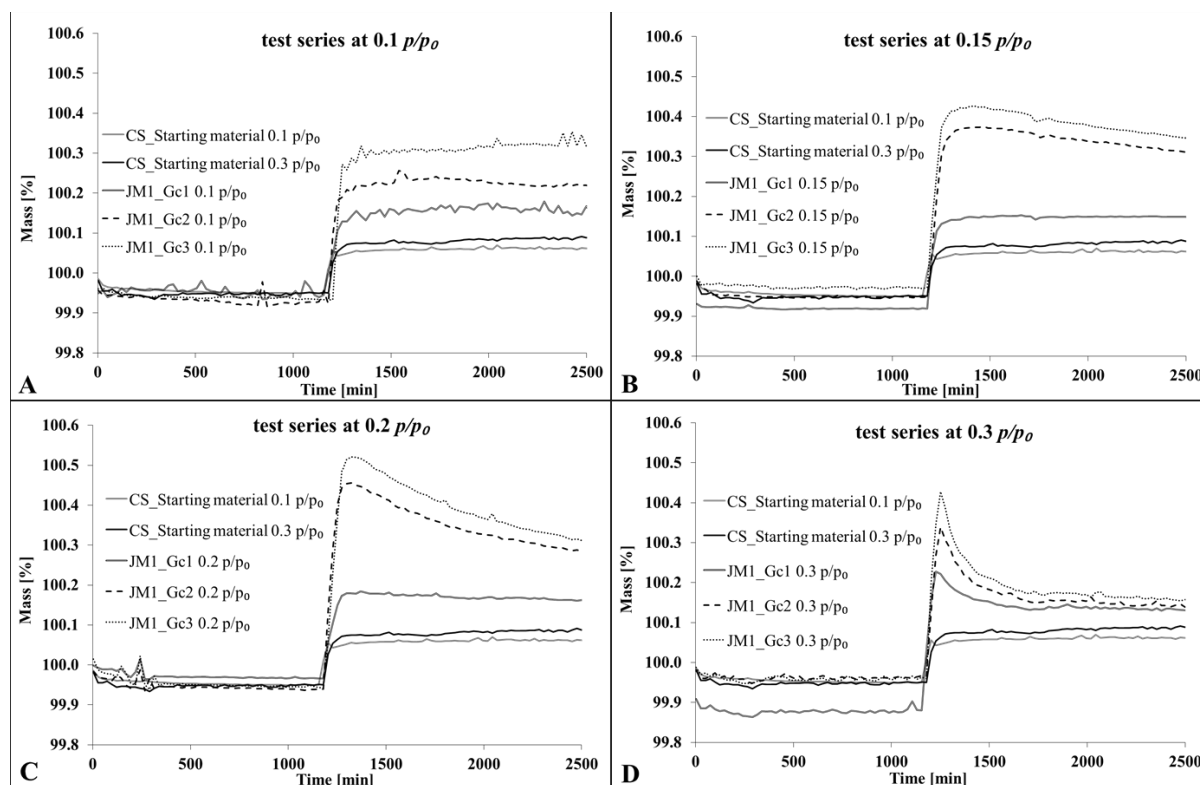


Figure 53: Influence of the p/p_0 value (isopropanol) on the stability of amorphous amounts

4.3.1.4 Temperature robustness - Design of Experiments (DoE)

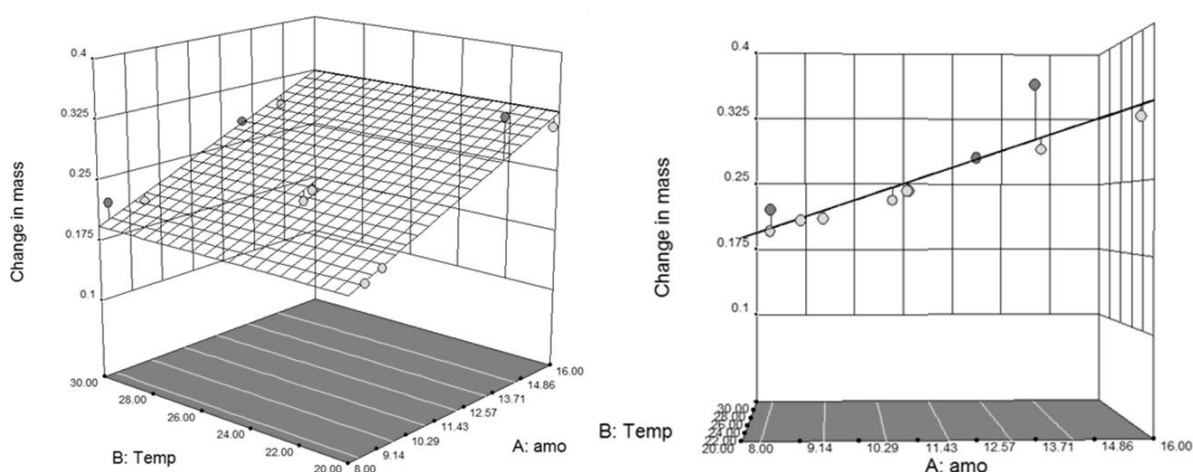
In this study the temperature robustness was evaluated using the software Design-Expert[®]. To estimate the interaction of the parameters (amorphous content and temperature) in this method a factorial plan was used. In general, the factors (p) and a number of levels (n) are varied to measure effects on the target size. The number of experiments is defined by n^p .

From findings of preliminary experiments (3^3 -factorial design, data not shown), the amorphous content of CS (factor 1: 8.33-15.75%) and the temperature (factor 2: 20-30 °C) were chosen as important factors at a fixed value of 0.10 p/p_0 isopropanol. Table 15 shows the used 3^2 -factorial design, whereby the center points are determined in triplication. As a response the change in mass [%] of the samples was determined by DVS analytics influenced by amorphous content and temperature.

Table 15: DoE to investigate the factors amorphous content (1) and temperature (2)

Randomized number	Level	Factor 1	Level	Factor 2	Response [%]
2	0	11.04	0	25	0.23
8	+1	13.68	-1	20	0.34
3	-1	8.56	-1	20	0.20
11	-1	8.33	+1	30	0.22
10	+1	13.12	+1	30	0.28
5	0	11.39	0	25	0.24
7	+1	14.64	+1	30	0.29
9	+1	15.75	-1	20	0.31
1	-1	9.55	+1	30	0.21
4	-1	9.15	-1	20	0.21
6	0	11.35	0	25	0.24

The results did not show that a higher temperature led to higher absorption or to an easier recrystallization of amorphous amounts in the graphical representation. Despite the knowledge of a higher absolute amount of isopropanol in the stream of nitrogen at an increased temperature the findings demonstrate the temperature independence (Figure 54).

**Figure 54: Temperature-robustness of the developed DVS method**

The evaluation of the design (Table 16) showed that the model is significant and factor 1 (A-ammo) is a fundamental model term (F value of 39.32). Factor 2 (B-Temp) is not relevant in

this design space. The Pred R-squared is in a reasonable agreement with the Adj R-squared (± 0.2). The Adeq Precision measures the signal to noise ratio where a ratio greater than 4 is desirable. In summary, well temperature robustness for this DVS method is reached (parallel surface of the model). At 0.10 p/p_0 a temperature of 25 °C was chosen as suitable parameter for a balanced mass absorption without re-crystallization.

Table 16: Evaluation of the DoE - Temperature robustness

Source	p-value Model	p-value Lack of fit	Pred R-squared	Adj R-squared	Adeq Precision
A-amo	< 0.0001	< 0.0001	0.7195	0.7931	13.687

This model can be used to estimate very well effects in the design space. Ultimately, the model proved to be applicable to any other measured absorption of micronized powders (samples of amorphous amounts: 3.81-17.01%). Again, there is no significant influence of temperature (20-30 °C) on the absorption and stability of amorphous amounts in the DVS measurement (Figure 55). Particularly these new samples were integrated that were measured with the one-step DVS method at 25 °C.

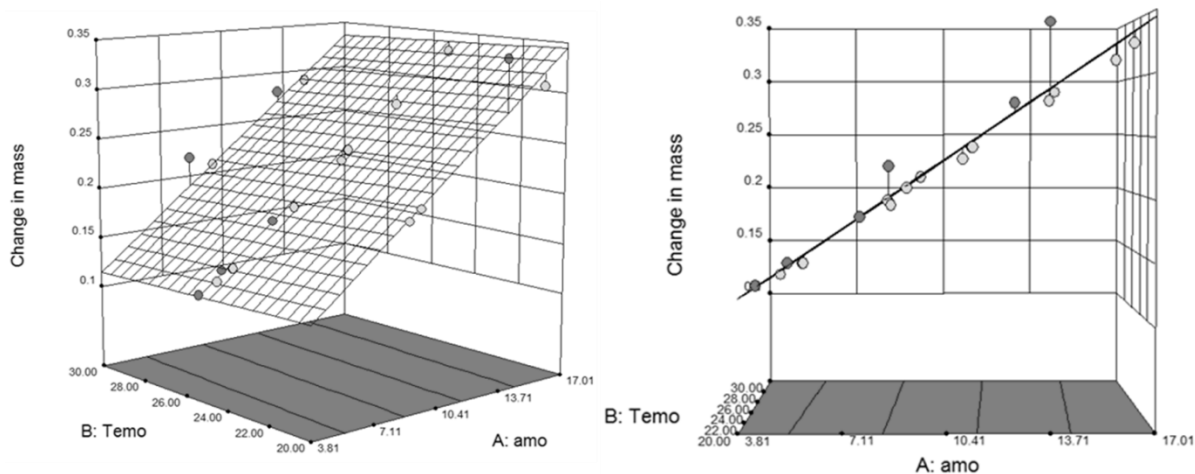


Figure 55: Integration of measured absorption values in the model

4.3.1.5 Influence of particle size/surface on the absorption behavior

Micronized powders (CS) with different particle sizes and amorphous amounts were produced by a jet-mill in dependence on the grinding pressure (2-8 bar) and the number of grinding cycles (1-3 Gc). These powder samples were used to evaluate the influence on the absorption behavior during the DVS measurement. The PSD and the amorphous content were directly characterized after the micronization process. Afterward, all API particles were stored for

2 hours over pure isopropanol (10 ml). This storage guaranteed no major changes in particle size and nearly a complete re-crystallization. Again, the particle size and the amorphous amount were determined directly after the re-crystallization process. The detected ‘amorphous parts’ (%) were correlated to the particle size (x_{50}) (Figure 56).

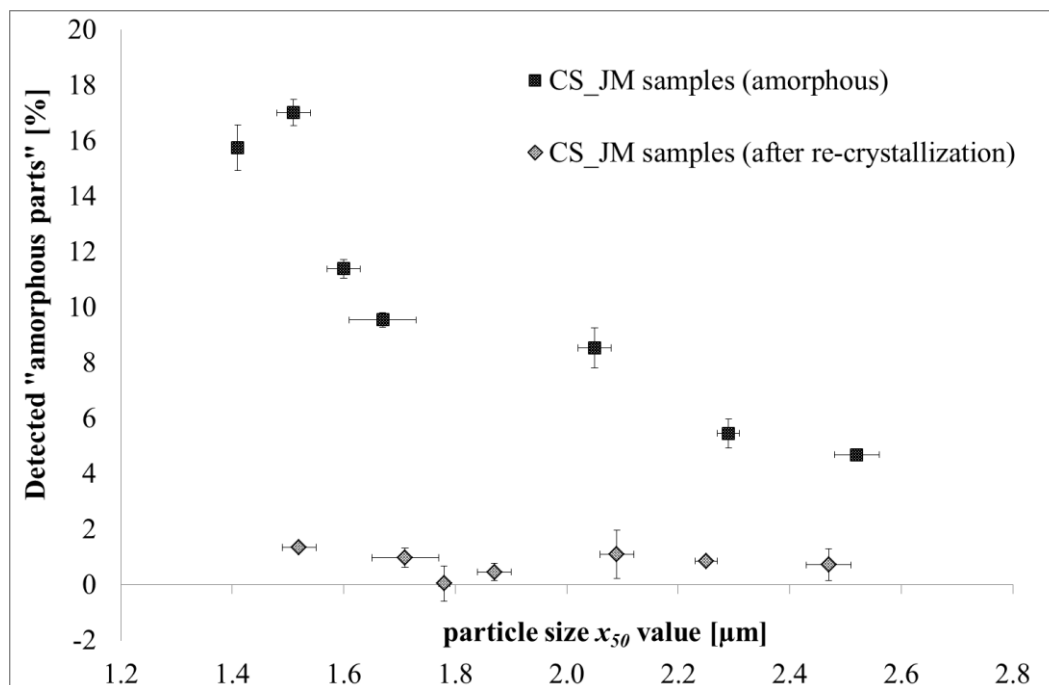


Figure 56: Influence of particle size on the absorption behavior

The DVS-measurement determined about 1% amorphous parts after the re-crystallization process. The diagram shows that particles with a very small particle size lead to a higher vapor sorption directly after their production because of higher amorphous amounts resulting from higher grinding pressures or several grinding cycles (up to nearly 18%). After the re-crystallization process no significant differences in the absorption of isopropanol can be found between smaller and larger particles (1.2 up to 2.8 μm), however, a mass increase of 1% is detected demonstrating that. The isopropanol has access to surface, cracks and pores and therefore is absorbed by particles independent on particle size range tested.

In addition, a calibration curve (0.25-15.0% of fully amorphous ball-milled CS) was blended adding 2% of micronized powder (8 bar, 3 Gc). The amorphous state is localized primarily on the surface of the JM sample but the way of quantification with isopropanol does not differ from the completely amorphous content which is mainly located inside the particle of the BM sample. Figure 57 illustrates the almost parallel shift of the calibration curve with 2% added micronized powder. In conclusion this behavior demonstrates the detection of different amorphous amounts (surface/inside of particles) in the same manner.

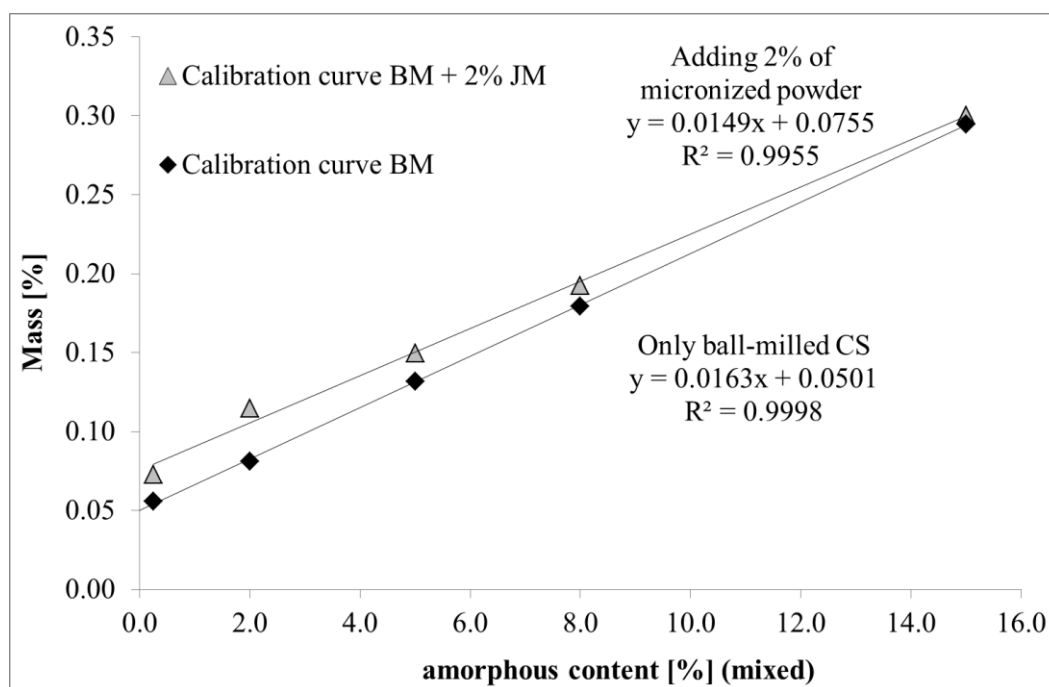


Figure 57: Influence of amorphous state localized on the surface and inside the particle

In general, a linear relationship between increasing amorphous content and the absorption was determined. Looking at the phenomena of absorption the effect of the surface should not be excluded (Figure 58).

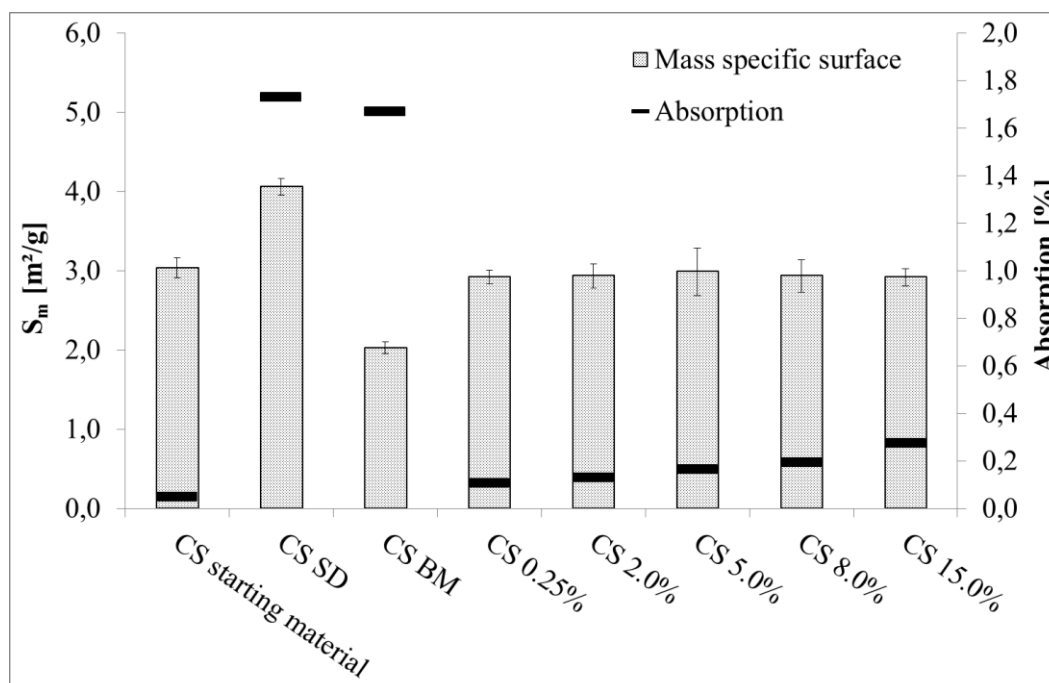


Figure 58: Mass specific surface and absorption behavior of different amorphous samples

Therefore different blends with amorphous amounts were prepared (0.25-15.00%) for the determination of the specific surface by a gas adsorption method. The diagram demonstrates that the absorption values (y-axis 2) of the blends increase due to higher amorphous amounts and

that the specific surface (y-axis 1) is constant for all blended samples. This indicates that the absorption is not significantly influenced by surface effects (Figure 58) in this DVS method and can be correlated to the investigation of the particle size (Figure 56).

Table 17 points out major characteristics of the investigated samples. As expected, a smaller particle size (BM > SD) results in a higher specific surface S_m and S_v . The ratio S_m/S_v should be constant within a substance class (CS powder samples).

Table 17: Powder characterization of investigated samples

Sample	Density [g/cm ³]	S_m [m ² /g]	S_v [m ² /cm ³]	S_m/S_v [cm ³ /g]	Absorption [%]
CS starting material	1.19 ± 0.00	3.04 ± 0.13	3.61 ± 0.16	0.84	0.05
CS SD	1.21 ± 0.01	4.06 ± 0.11	4.92 ± 0.13	0.83	1.73
CS BM	1.20 ± 0.00	2.03 ± 0.08	2.44 ± 0.09	0.83	1.67
CS 0.25%	1.20 ± 0.00	2.92 ± 0.09	3.50 ± 0.11	0.83	0.11
CS 2.0%	1.19 ± 0.00	2.94 ± 0.15	3.49 ± 0.18	0.84	0.13
CS 5.0%	1.19 ± 0.00	2.99 ± 0.30	3.55 ± 0.36	0.84	0.17
CS 8.0%	1.21 ± 0.01	2.94 ± 0.21	3.55 ± 0.25	0.83	0.19
CS 15.0%	1.20 ± 0.00	2.92 ± 0.11	3.50 ± 0.12	0.83	0.28

In addition, two calibration curves, one of fully amorphous ball-milled CS and the other of spray-dried CS were prepared (0.25-15.0%). As shown before these two materials differ in particle shape, surface properties and particle size. Figure 59 shows the almost parallel shift of the calibration curves. This indicates that the particle shape/surface has no effect (parallel displacement of the lines), however, the total amounts of amorphous state in the preparation process (SD/BM) is slightly different.

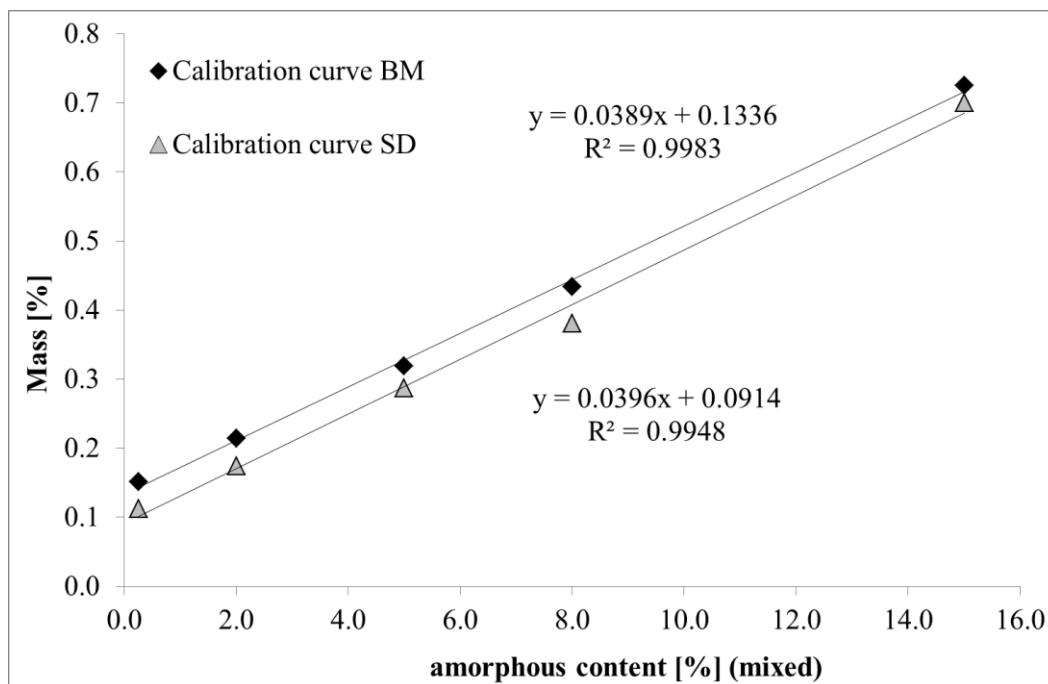


Figure 59: Influence of particle shape on SD and BM samples for CS

Nevertheless, the TMDSC measurement could not show significant differences in the amorphous content of both production methods (Figure 60). The analyses demonstrated approximately the same T_g and a comparable step height (delta C_p). For the crystalline starting material no event was detectable.

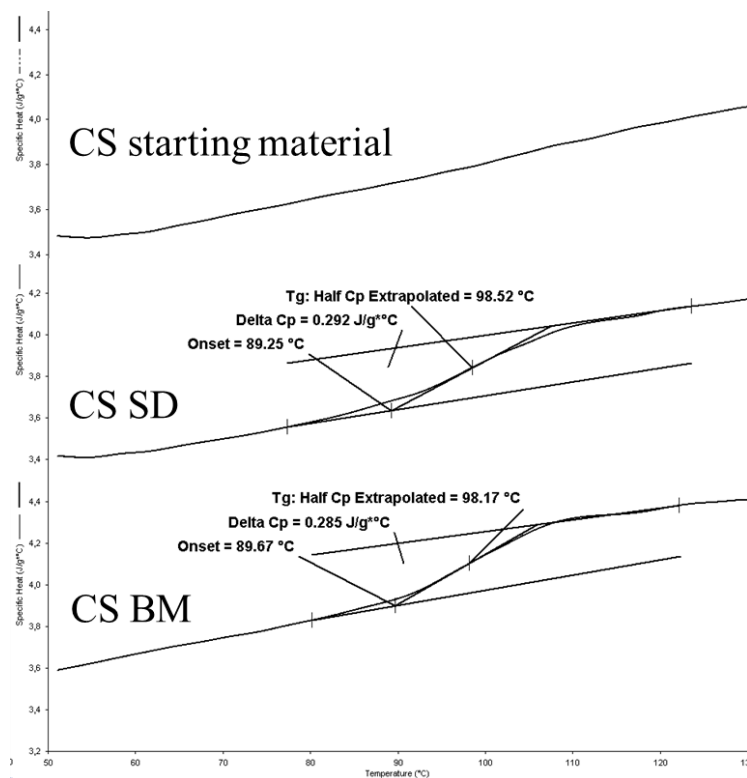


Figure 60: TMDSC measurement of spray-dried and ball-milled CS samples

4.3.1.6 Validation of the organic one-step DVS method based on the ICH Guideline Q2 (R1)

Finally, the one-step DVS method had to be validated in order to demonstrate that the specified requirements are compliant. The linearity, precision/repeatability and the limit of quantification (LOQ) were investigated based on the ICH guideline Q2 (R1).

Accuracy and robustness could not be determined because of a possible instability of amorphous amounts over a few hours.

For all one-step DVS measurements, the mass difference between the weight of the dried powder (0.0 p/p_0 , 20 hours) and the conditioned sample (isopropanol 0.10 p/p_0 , 22 hours) was calculated. For higher amorphous amounts higher mass differences were obtained. After preparing a calibration curve for CS (0.25-15.00% of amorphous content), it was possible to calculate the amorphous amounts in the unknown samples. The coefficient of determination ($R^2 = 0.9996$) shows that there is a very good linearity between mass absorption and amorphous content. All five samples were determined in duplicate in one measurement.

Furthermore, the precision/repeatability for this analytical method were investigated. Therefore one powder sample (micronized powder at 8 bar, 1 Gc) was measured six times. The results show a good system precision in dependence to the measurements (mean = $0.2017\% \pm 0.0031$, CV = 1.51%)

At the end of the method development the limit of quantification (LOQ) was determined by different mixtures with very low amorphous amounts (0.10%, 0.15%, 0.20%, 0.25% and 0.50%). These blends were measured ten times by the one-step DVS method. The results of the LOQ (signal to noise = 10:1) showed that an amorphous content up to 0.5% could be determined with a signal to noise ratio from 10.6:1. For 0.20% the signal to noise ratio was 7.5:1. For the mixture 0.15% and 0.10% the signal to noise ratio was smaller than 5:1 because of a smaller change in mass due to its higher crystalline proportion.

Figure 61 shows the increase of the absorption values of the crystalline starting material and blends with very low amorphous amounts at a noise value of 0.005% (mean value). In this case the absorption of the sample has to be twice as large for a LOQ of 10:1. That implies for fully crystalline material with the baseline absorption of 0.044% at least an amorphous content of 0.5%. However, if the noise value might be reduced only smaller differences in terms of the individual signals of crystalline starting material and sample are required. In addition, with increased noise value an extrapolation of the curves might be informative for the assessment of the LOQ.

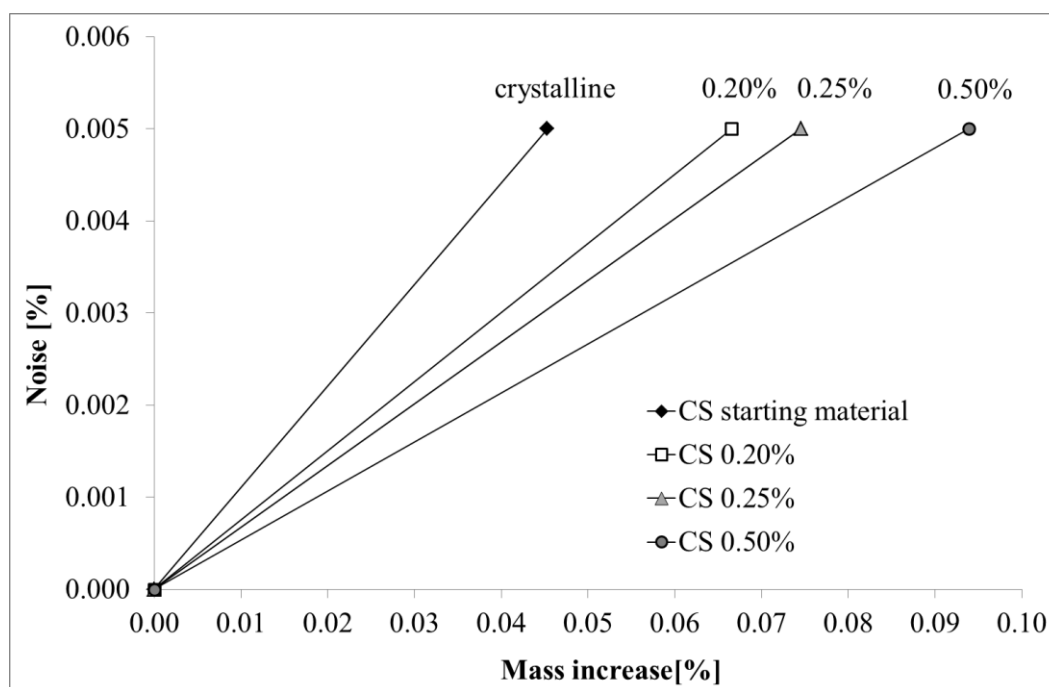


Figure 61: Estimation of LOQ based on baseline absorption of crystalline material for CS

Figure 62 shows the new evaluated method in detail. Because of diverse mass adsorptions it is possible to calculate different amorphous amounts. Isopropanol (0.10 p/p_0 , 25 °C) which was found to be the most suitable solvent allows to analyze a minimal amorphous content and to discriminate between different hydrophobic powder samples (CS).

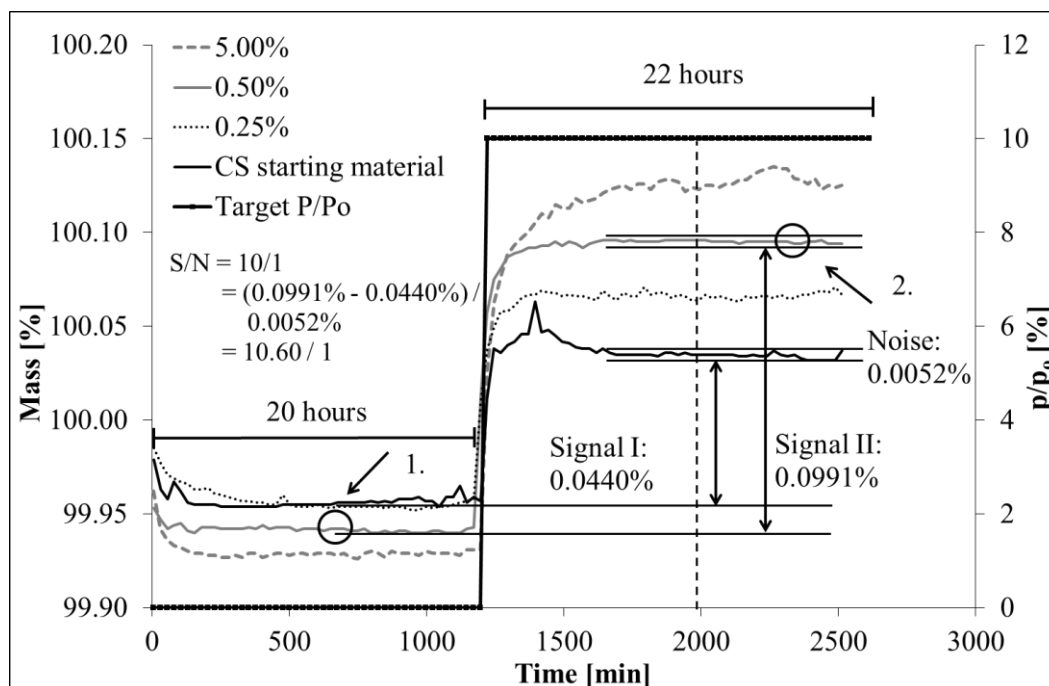


Figure 62: One-step DVS method for CS in detail

This figure shows the exact calculation of the LOQ (10.6:1). Hereby, the signal I (baseline absorption of fully crystalline material) is subtracted from the signal II (absorption of the

blend with 0.5% amorphous content). Finally, the absolute value is divided by the mean of the noise value.

4.3.1.7 Schematic absorption behavior of hydrophilic and hydrophobic samples with polar and nonpolar solvents

Water as polar solvent has a high affinity to hydrophilic powder samples. This behavior can be enhanced when transforming the crystalline lattice which consists of a higher order degree to an amorphous state (Figure 63).

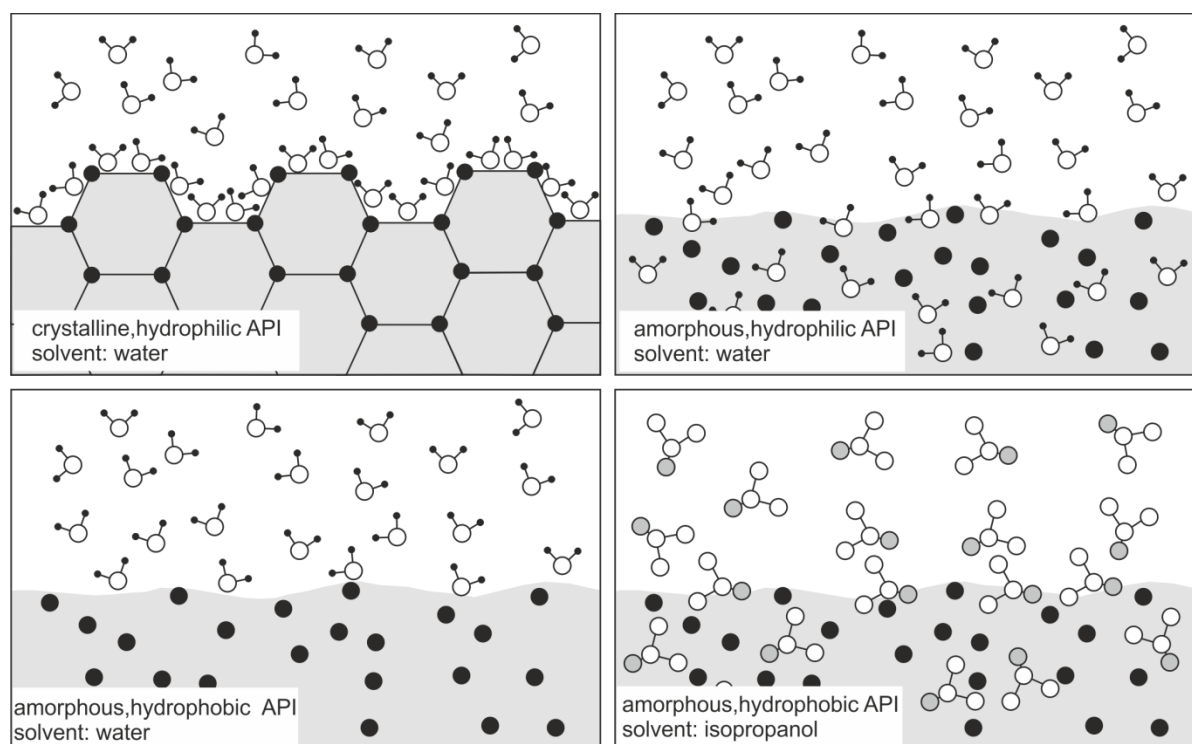


Figure 63: Schematic absorption behavior modified from Weiler et al., 2008

Thereby, the adsorption on the surface is reinforced by the absorption effects into the particles. This phenomenon results in a significantly higher mass increase in comparison to simple adsorption (monolayer/multilayer at the surface).

In an exchange of the amorphous powder state from a hydrophilic to a hydrophobic sample, the material again sorbs less water due to the good chemical stability and inertness against water vapor which characterizes the hydrophobic material. The absorption into the particles can be forced by changing the solvent from polar to nonpolar. In this case isopropanol shows a high affinity to the CS powder samples. This mechanism might declare the principle of the developed organic dynamic sorption vapor method.

4.3.2 Applicability to other model APIs

In chapter 4.3.1 it was shown that low amounts of amorphous content (LOQ of 0.5%) in a hydrophobic model API (Ciclesonide) can be measured with a simple one-step dynamic organic vapor sorption method. This gravimetric method quantifies exactly the amorphous content once a suitable solvent, the correct p/p_0 value and the exact temperature have been found. After the sample undergoes a drying phase, the moisture is adjusted with the particular solvent (one-step). As soon as the equilibration of mass with a definite humidity is balanced, different amorphous amounts can be calculated on the basis of different absorption. Generally, the background absorption of the crystalline starting material and the blends with known content (between 0.25% up to 15.0%) of amorphous amounts are determined, respectively. Following this, the amorphous amounts of unidentified samples are measured and calculated using the calibration curve.

In this part the applicability of the method is tested on various APIs which differ in lipophilicity (poor water solubility) and hygroscopicity (high absorption of water). The focus is set on BS and GC representing hydrophobic samples and on ITB, SBS and FF representing hydrophilic samples. In particular, the screening process of hydrophobic substances is difficult and time consuming. Thereby, it is necessary that the parameters are selected individually for each API (Figure 64).

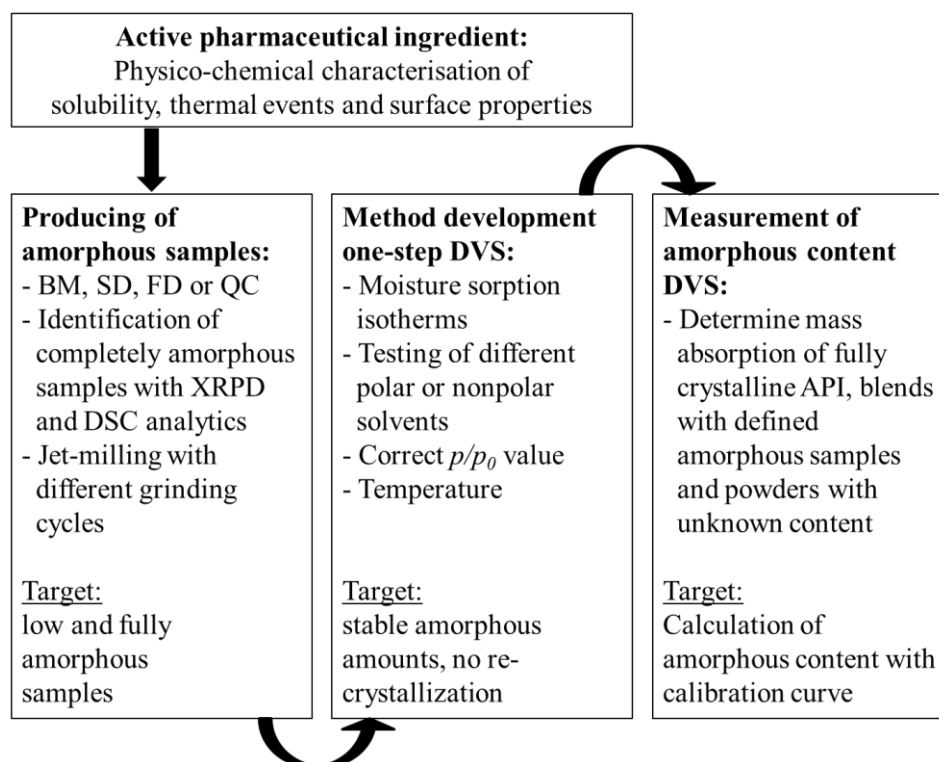


Figure 64: Overview of the DVS-method development: Production, test measurement and calculation

It must be kept in mind that the use of only certain solvents (toxicity in terms of personal safety, as well as device compatibility) is possible. This work is intended to show a possible approach on the procedure of adapting and refining the method for new APIs in the future. The primary objective is to develop a fast (less than 2 days) and accurate method with high selectivity. A general guidance for the adaptation of the method to other drugs is established. Figure 64 shows a flow diagram for method development including the production of amorphous parts, test measurements and the calculation of the one-step DVS-method.

4.3.2.1 Adaption for hydrophobic model drugs (BS/GC)

Due to low water absorption in hydrophobic substances (Figure 39) a change from a polar to a nonpolar solvent was necessary. Isopropanol showed the best characteristics for CS powder samples where a high mass absorption without an early re-crystallization was found compared to methanol, ethanol and ethyl acetate (Figure 51). Different organic solvents were tested for BS and GC in order to receive a higher affinity, selectivity and higher slope of the calibration curve. Screening measurements were conducted with water, methanol, isopropanol and methylene chloride. As requirement a balanced mass absorption is again necessary and different grinding cycles of each API may lead to different mass absorption.

Even at low humidity levels ($0.05 p/p_0$) very nonpolar solvents (e.g. isopropanol and methylene chloride) led to a fast re-crystallization (Figure 65).

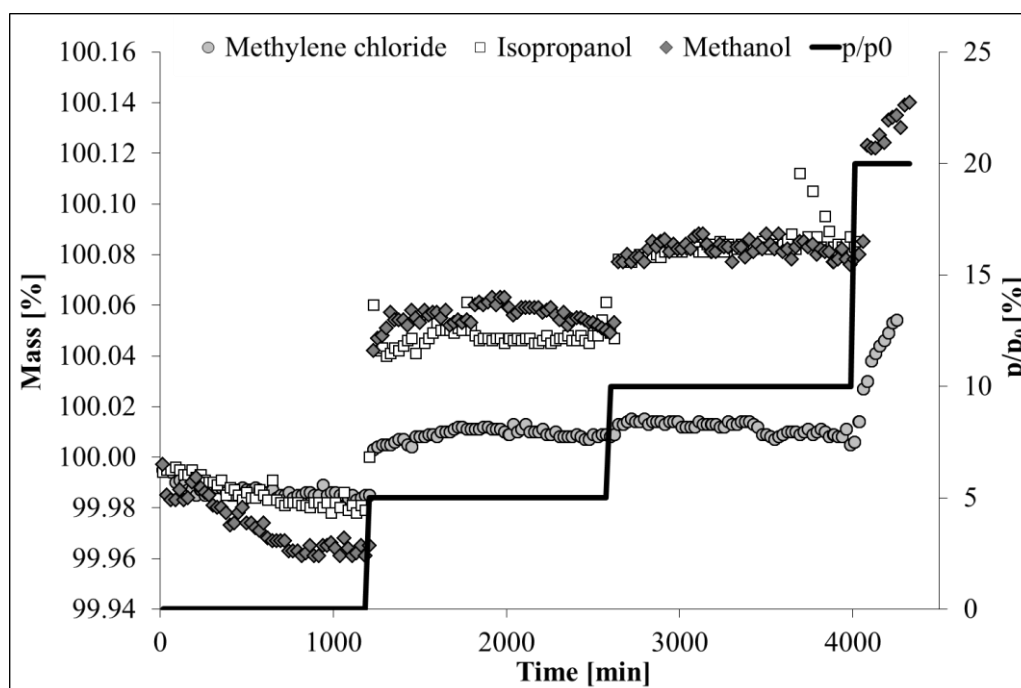


Figure 65: Organic solvent screening for BS (JM1 Gc3)

The low absorption was comparable to the crystalline starting material and indicates an unstable amorphous BS sample (micronized powder 8 bar, 3 Gc). Especially the increase in mass was very low and demonstrated a minor affinity for methylene chloride. Methanol was determined as the most appropriate solvent with an increased, stable mass absorption and the highest affinity to this hydrophobic powder (methanol > isopropanol > methylene chloride). Optimized vapor for methanol was a p/p_0 with the value of 0.05; higher p/p_0 values of 0.2 to 0.3 can initialize a re-crystallization for all tested solvents. These results were confirmed by further test measurements with blends that contained defined amorphous amounts of 0.25% up to 15.0% (Figure 66).

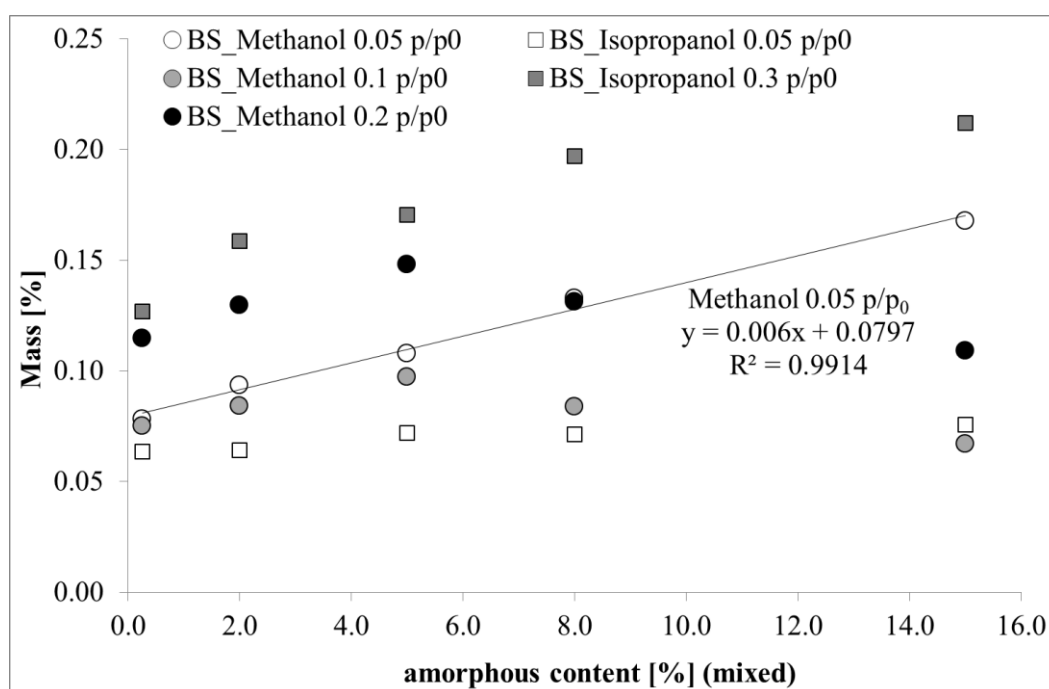


Figure 66: BS calibration curves measured with different solvent types and intensity levels

Hereby, the nonpolar isopropanol led to re-crystallization at low humidity levels (0.05 p/p_0 and 0.3 p/p_0). Also higher amorphous blends (8.0% and 15.0%) were re-crystallized by higher methanol vapors. The calibration curves of BS showed a decreasing mass especially for 0.1 and 0.2 p/p_0 . For 0.05 p/p_0 a good linearity was shown between the increasing amorphous content and absorption ($R^2 = 0.9914$). This behavior indicates a stable amorphous state and enables the entire determination.

For GC all solvents led to a balanced mass increase at 0.05 p/p_0 , however, significant difference in mass absorption (maximal 0.03%) was not detectable due to the low affinity to all solvents (Figure 67). The absorption behavior was hardly increased in relation to the more nonpolar solvents (water < methanol < isopropanol < methylene chloride). However, a re-

crystallization of the amorphous amounts is initiated by a prolonged moisture-level time of methylene chloride (quick mass loss). At higher p/p_0 values of 0.1 to 0.2 a balanced mass adsorption was not measured for methanol and isopropanol. At these humidity levels amorphous amounts were not stable. Finally, isopropanol and methylene chloride showed a lower mass adsorption ($0.05 p/p_0$) compared to water ($0.5 p/p_0$) due to the poor solubility of GC. The solvents demonstrated significant differences in the absorption behavior when changing the humidity level (10 times higher).

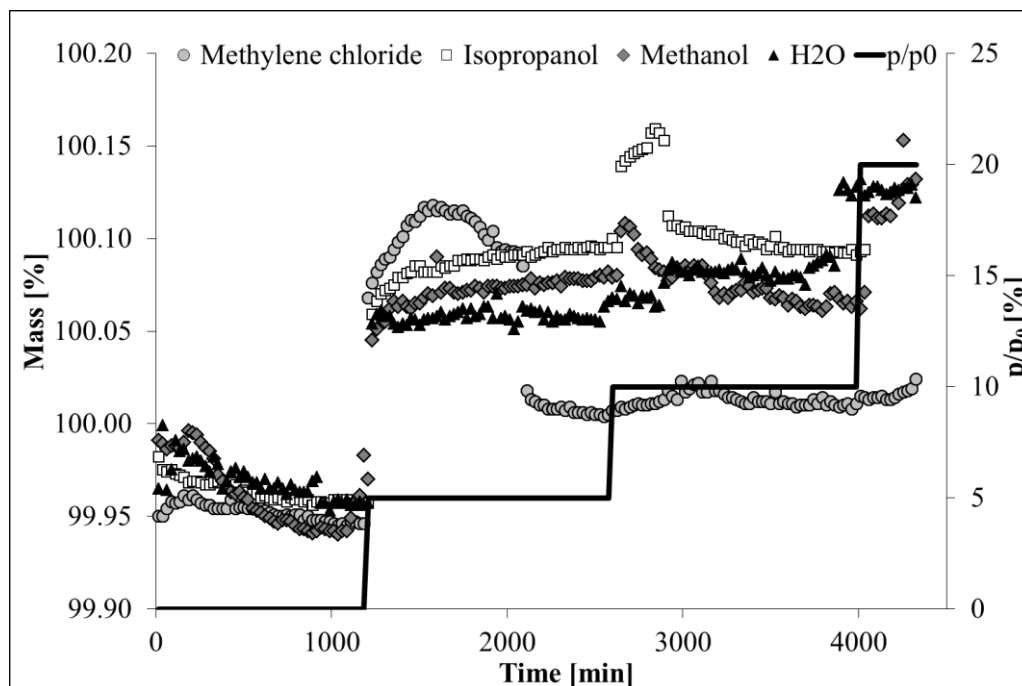


Figure 67: Organic solvent screening for GC (JM1 Gc3)

For water a good linearity was shown between an increasing amorphous content and the absorption at $0.5 p/p_0$ ($R^2 = 0.9949$) (Figure 68). As mentioned in the literature benzyl alcohol and dimethyl sulfoxide should increase the solubility, but cannot be used because of their toxicity in terms of personal safety, as well as device compatibility.

It is recommended to measure at higher levels of water vapor ($0.5 p/p_0$) since none of the solvents show a high affinity/solubility to the hydrophobic GC. As a consequence the raising of the humidity level led to an extreme increase in mass and allowed a more precise determination of the amorphous content.

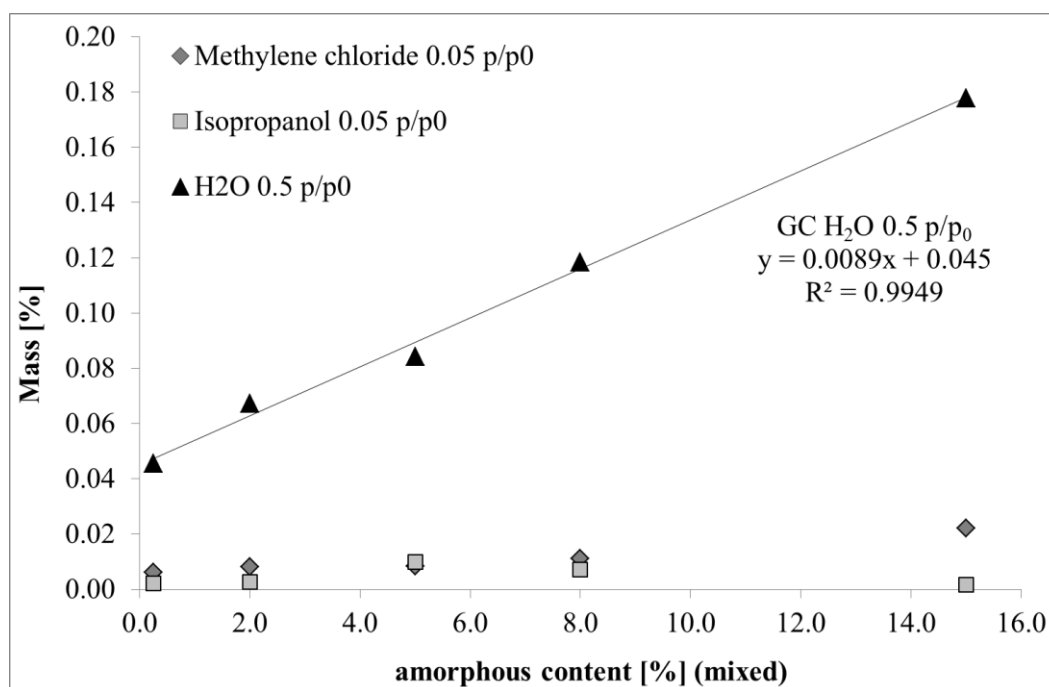


Figure 68: GC calibration curves measured with different solvent types

Figure 69 shows the one-step measurement and corresponding sorption behavior of the hydrophobic samples (CS, BS and GC). The amorphous amounts of the GC and CS samples were more stable in comparison to the BS samples during the screening process.

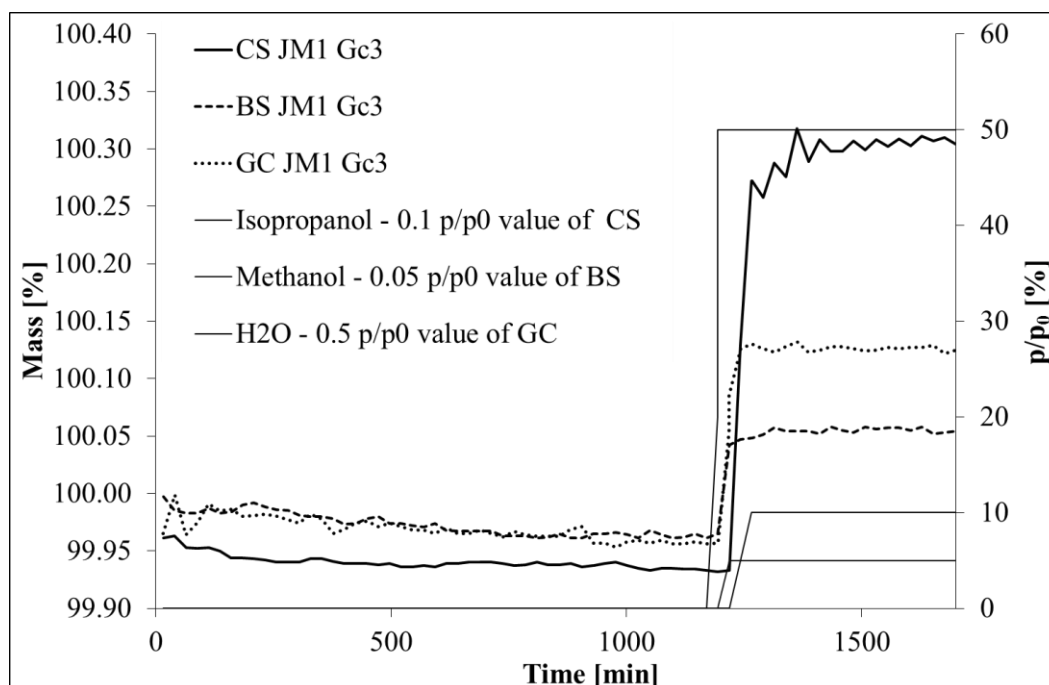


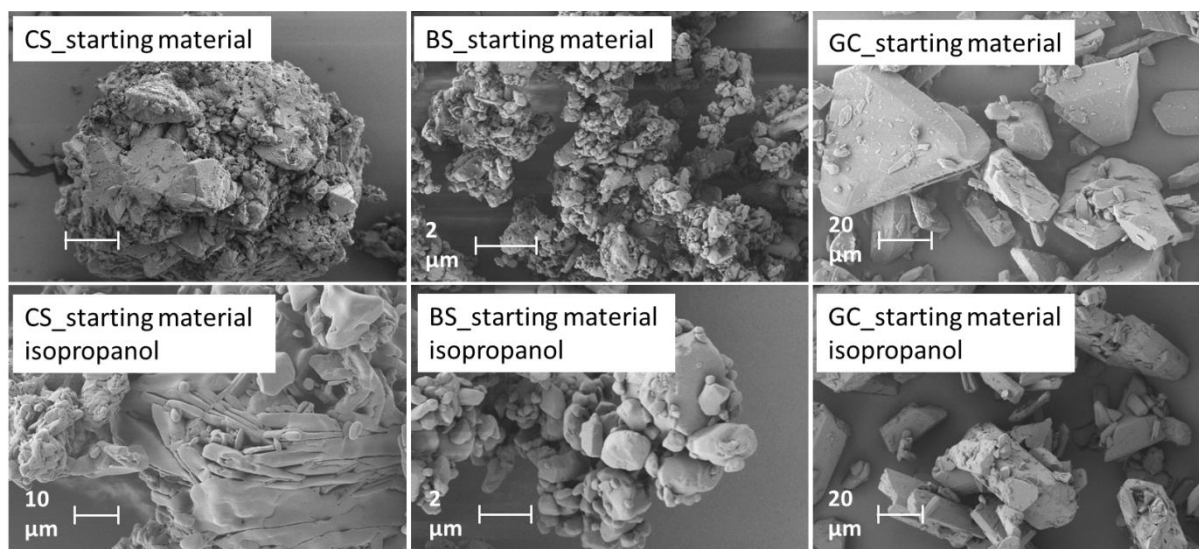
Figure 69: Optimized one-step DVS method for the calculation of amorphous parts (CS, BS and GC)

A total gas flow of 200 sccm and a temperature of 25 °C were used for all organic solvents. Table 18 summarizes the final parameters which were used for the determination of the amorphous contents in these powder samples.

Table 18: Final parameters for all hydrophobic APIs for the determination of amorphous content by DVS

API	Solvent	Drying time [min]	p/p_0 value	Temperature [°C]	Total gas flow [sccm]
CS	Isopropanol	1200	0.1	25	200
BS	Methanol	1200	0.05	25	200
GC	ddH ₂ O	1200	0.5	25	400

In conclusion, optical investigations were conducted to find significant differences in particle morphologies of these hydrophobic powders. These pictures may clarify important interactions with the organic solvents and explain mechanisms of the one-step DVS method. The storage was carried out in a desiccator (2.4 l, room temperature) for 2 hours with the organic solvent, respectively. Hereby, no significant changes in PSDs were determined. In this study the respective solvents from the organic solvent screening of the DVS measurements were used again. SEM photographs of crystalline and micronized APIs (CS, BS and GC) are investigated and compared to the conditioned samples (organic solvents: methanol, isopropanol and methylene chloride). Figure 70 demonstrates the influence of isopropanol on the starting materials of the hydrophobic samples.

**Figure 70: Hydrophobic starting material and the conditioned samples with isopropanol**

It can be seen that isopropanol seems to have a high affinity to the CS sample because the surface structures look slightly melted and very smooth (CS > BS > GC). This phenomenon was reinforced with amorphous content in micronized powders (Figure 71).

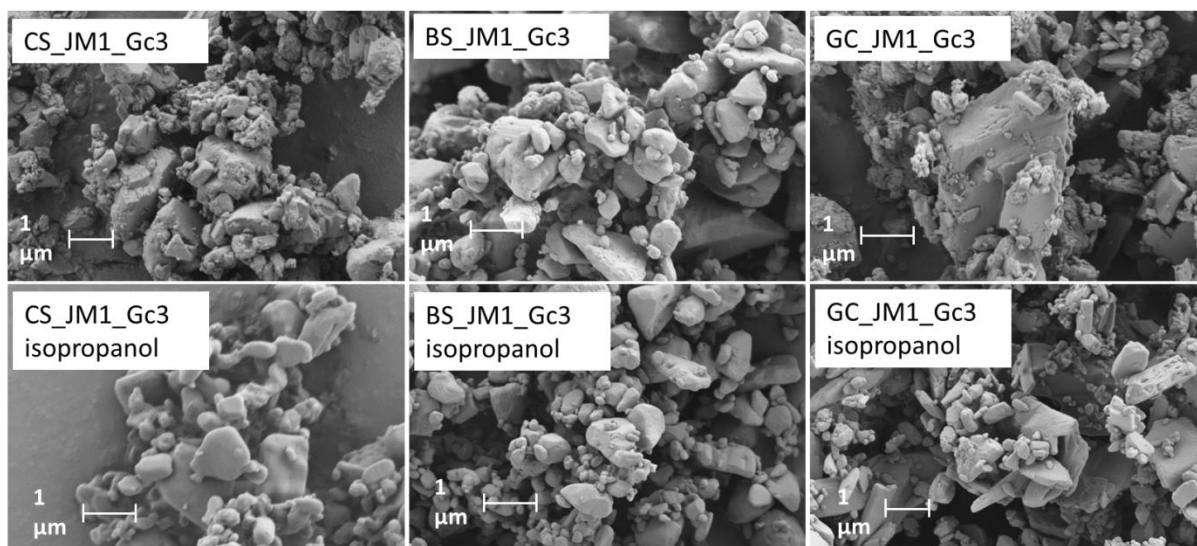


Figure 71: Micronized powders compared to conditioned samples with isopropanol

Again, a very smooth surface was determined which is an indication of the high affinity. Particle corners are rounded and touching particles are melted together (coalesce). This behavior might prove to be advantageous for higher absorption and enable a precise detection of amorphous content. For the other hydrophobic samples (BS and GC) no optical changes were observed when storing over isopropanol for 2 hours.

This changing of appearance was also determined when storing BS over appropriate solvent. In this case the starting material and the micronized powder were stored over methanol for 2 hours.

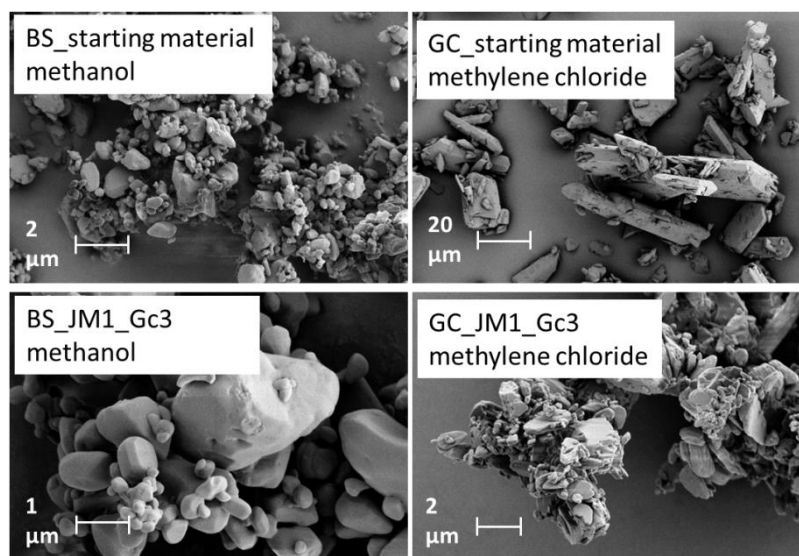


Figure 72: Further organic solvent storages for BS and GC

The SEM pictures (Figure 72) showed a very smooth surface as well which is in correspondence to a high solvent affinity. GC visualized a low affinity to methylene chloride which re-

flects a comparable situation looking at the isopropanol storage. These results can explain the findings from the screening enabling a suitable solvent for GC. The problem of low affinity leading to low absorption was solved by a significant higher water vapor (10 times) in the DVS method.

4.3.2.2 Adaption for hydrophilic model drugs (ITB/FF/SBS)

The results of moisture sorption isotherms (Figure 39 and Figure 40) can provide an indication which can be used for further measurement parameters. The investigated humidity levels provide a first overview of the stability of amorphous amounts in these hydrophilic samples and furthermore help to receive p/p_0 values in order to gain a balanced equilibration of mass. Especially the re-crystallization events for ITB, FF and SBS are helpful in the development of the one-step DVS-HT method. After the drying phase of the sample the amorphous amounts have to stay stable without a re-crystallization during the measurement.

For the hydrophilic APIs, all further screening measurements (DVS-HT) were conducted with water as the solvent. Humidity levels were chosen below the determined re-crystallization events. For SBS and FF p/p_0 values between 0.3 p/p_0 and 0.4 p/p_0 were tested (re-crystallization 0.8 p/p_0) and for ITB p/p_0 values between 0.1 p/p_0 and 0.2 p/p_0 were tested (re-crystallization 0.4 p/p_0). Test series were performed with micronized powders (JM1, Gc 1 to Gc 3) of each API, a number of higher grinding cycles led to higher amorphous amounts and therefore to higher absorption values.

Especially the drying time had to be adapted and was increased for these hygroscopic APIs (FF: 30 hours and ITB: 36 hours). The increase of 10 hours/16 hours enables a balanced drying phase. Because of the risk of an easy re-crystallization an optimized p/p_0 value of 0.1 was chosen for ITB despite the equilibrium for both vapor values. For SBS and FF a higher p/p_0 value of 0.4 was chosen on the basis of the re-crystallization point at a higher humidity. A total gas flow of 400 sccm and a temperature of 25 °C were chosen for all measurements.

Figure 73 gives an overview of the optimized parameters for all investigated hydrophilic APIs and the corresponding sorption behavior. At the time of moisture increase, a sudden increase in mass (Y-axis 1) is visible and over the entire period an equilibrium mass was maintained. This indicates a stable and calculable amorphous content for all three samples. Y-axis 2 shows the used p/p_0 value (water) of the method for all three hydrophilic drugs.

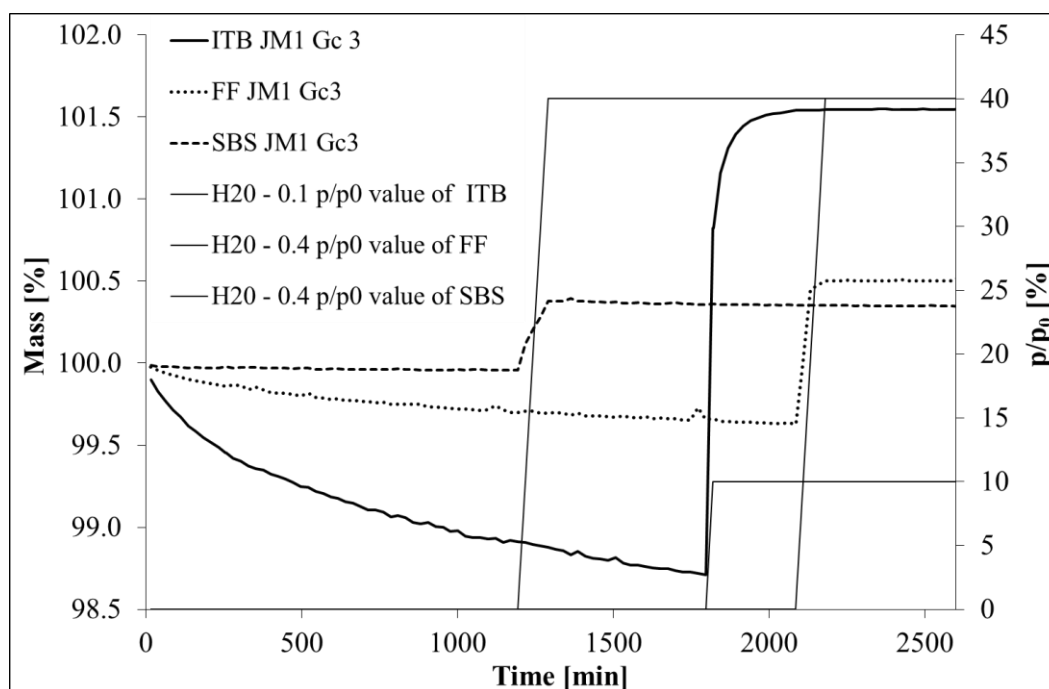


Figure 73: Optimized one-step DVS method for the calculation of amorphous parts (ITB, FF and SBS)

Table 19 shows the final parameters which were used for the determination of the amorphous content in these powder samples. In the screening process amorphous samples of ITB showed the lowest stability compared to FF and SBS.

Table 19: Final parameters for all hydrophilic APIs for the determination of amorphous content

API	Solvent	Drying time [min]	p/p_0 value	Temperature [°C]	Total gas flow [scm]
ITB	ddH ₂ O	1800	0.1	25	400
FF	ddH ₂ O	2160	0.4	25	400
SBS	ddH ₂ O	1200	0.4	25	400

4.3.3 Conclusion I

This DVS study demonstrates with a high accuracy how amorphous regions are specifically detectable as “reactive spots” [15] to vapor. The amorphous content is the critical outstanding factor and becomes the deciding part of nearly the total signal [23] distinguished to various analytical techniques (e.g. DSC and XRPD measurements). It was shown that different APIs behave individually; in this case hygroscopicity and lipophilic behavior play an important role. Since hydrophilic APIs show a high initial water content (> 2.0 % for crystalline material, table 12), these APIs (ITB and FF) interact well with vapor. This phenomenon resulted in a longer drying phase for the measurement (over 30 hours). ITB samples were quantified at low

water vapor ($0.1 p/p_0$) because of a facilitated re-crystallization at higher humidities. Amorphous samples of SBS were more stable and consequently measured with an increased humidity-level ($0.4 p/p_0$). CS as a hydrophobic model drug was measured with isopropanol ($0.1 p/p_0$) after an implemented organic solvent screening. Also, BS had to be measured with an organic solvent (in this case: methanol) and at a low humidity ($0.05 p/p_0$). GC showed a low solubility for all usable solvents therefore the measurement was performed with water ($0.5 p/p_0$) and an enormously raised humidity level (10 times higher, without re-crystallization).

4.3.4 Usability of the one-step method on selected powder samples

After the measurement of the respective mixtures (0.25-15.0% of amorphous content) it was possible to calculate the amorphous amounts in the unknown samples (e.g. jet-milled powders). Figure 74 shows an overview of the calibration curves for all APIs. The coefficient of determination shows that there is a very good linearity between mass absorption and mixed amorphous content for almost all APIs ($R^2 > 0.99$). These results confirm that amorphous amounts are detectable with these methods and amorphous amounts remain stable during the measurement, respectively.

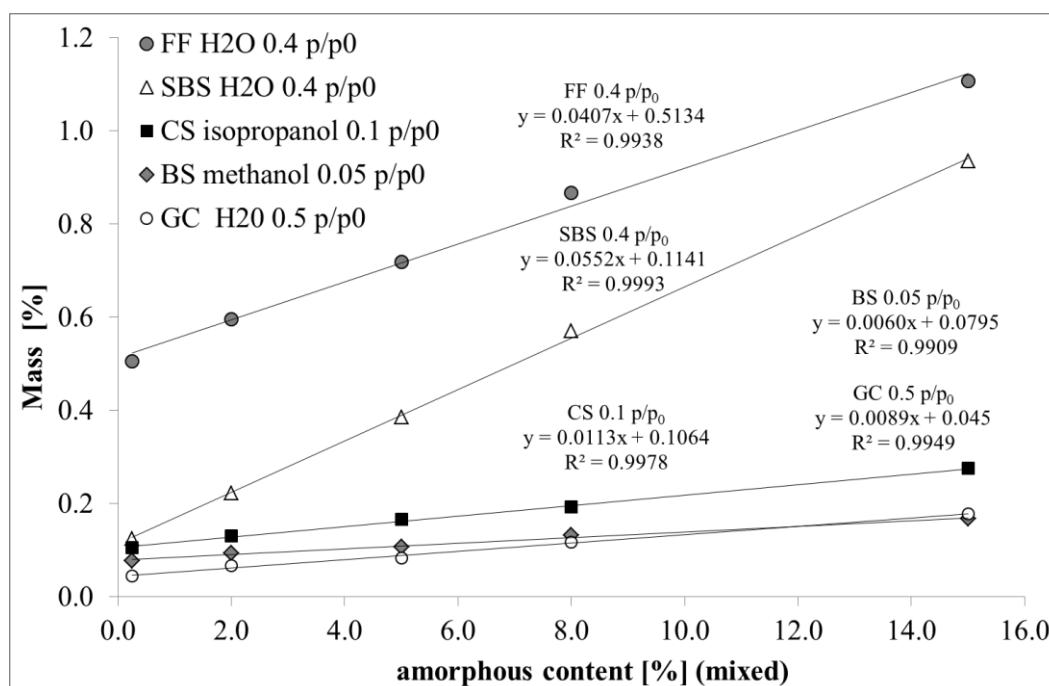


Figure 74: Calibration curves of all investigated APIs for the calculation of amorphous amounts

Only the hygroscopic ITB showed a low stability of its amorphous parts (data not shown), which was not induced by the measuring method. The mixture of the amorphous freeze-dried component absorbed moisture coming from the crystalline sample ($> 3.7\%$ water content).

This led to the re-crystallization process and resulted in a decreasing mass absorption. In this case a calibration is not possible and practicable. For FF the highest baseline sorption behavior was determined compared to the other APIs.

Furthermore, the process standard deviation (S_{x0}) and the process coefficient of variation (V_{x0}) of these calibration curves were calculated (Table 21). The performance of the measurement method is reflected in the process standard deviation (S_{x0}) (Equation 4.3). Hereby, the calculation of the spread of the measured values of the calibration curve (RSD) and the slope of curve (b), which represents the precision and the sensitivity, were used for this further calculation.

The determined value is corresponding to a process coefficient of variation (V_{x0}) (Equation 4.4). This parameter describes the relative measure of the precision including the process standard deviation (S_{x0}) and the mean of the amorphous amounts (x-axis) [146]. The content of unknown samples was determined by using the created linear equation, respectively.

$$S_{x0} = \frac{RSD}{b} \quad 4.3$$

$$V_{x0} = \frac{S_{x0}}{\bar{x}} \cdot 100\% \quad 4.4$$

Table 20: Process standard deviation and process coefficient of variation of the calibration curves of the developed DVS methods

Sample	RSD [%]	S_{x0} [%]	V_{x0} [%]
FF	0.0216	0.5297	8.7557
SBS	0.0099	0.1799	2.9741
CS	0.0036	0.3145	5.1981
BS	0.0039	0.6459	10.6762
GC	0.0042	0.4766	7.8774

For these DVS methods a respectable precision was reached. Nearly all APIs showed a low coefficient of variation for this new introduced method. Nevertheless, FF and BS demonstrated an increased value.

Table 21 shows the significant mass increase of the single CS blends with varying amorphous content in detail. These mixtures were compared to fully crystalline material at $0.1 p/p_0$ and $0.3 p/p_0$.

Table 21: Absorption values of different amorphous blends at $0.1 p/p_0$ and $0.3 p/p_0$

Amorphous content [%]	Mass increase [%], $0.1 p/p_0$	Mass increase [%], $0.3 p/p_0$
0.0	0.0440	0.1022
0.25	0.0556	0.1516
2.0	0.0811	0.2145
5.0	0.1317	0.3193
8.0	0.1792	0.4334
15.0	0.2945	0.7249

The following chart shows an obvious enhancement of the curves from $m_{15\%} > m_{8\%} > m_{5\%} > m_{2\%} > m_{0.25\%} > m_{\text{cryst}}$. (Figure 75). On the x-axis the ratio of the increase in mass and the ratio of the change in humidity of fully crystalline material are given whereas the change in mass and the ratio of humidity of the respective samples are fixed at the y-axis.

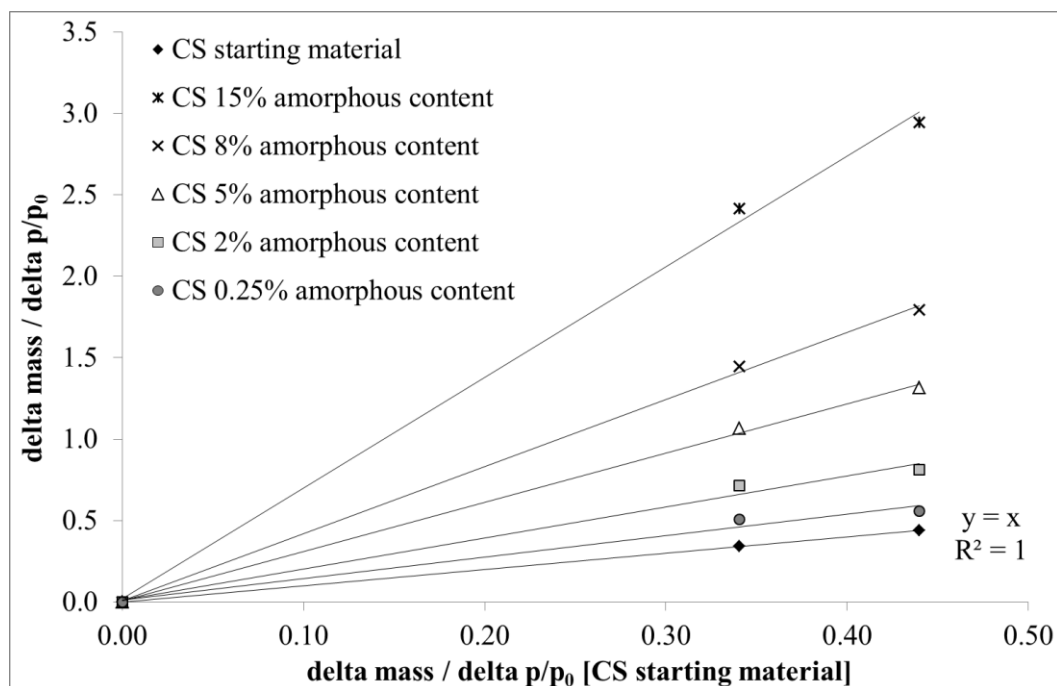


Figure 75: Increase of mass absorption of the single blends of CS in dependence to the vapor value

In this case $Y = X$ applies for the fully crystalline material. For all other amorphous blends $Y > X$ is given resulting from higher absorption values.

Furthermore, an alternative method for the blending process was tested avoiding the long mixing time and sample preparation of 5 hours (nearly 1 hour preparation time for 1 blend). For this investigation the Turbula mixer was replaced by a Vortex mixer (SBS). Thereby, the mixing time was reduced to 2 minutes for each blend. Figure 76 shows the two calibration curves and a consensus of the gradient. The coefficient of determination was only slightly decreased ($R^2 = 0.9993$ to $R^2 = 0.9967$). However, these findings could not be confirmed with a repeated experiment with FF. A ball-like formation of particles was determined because of higher residual moisture in the starting material.

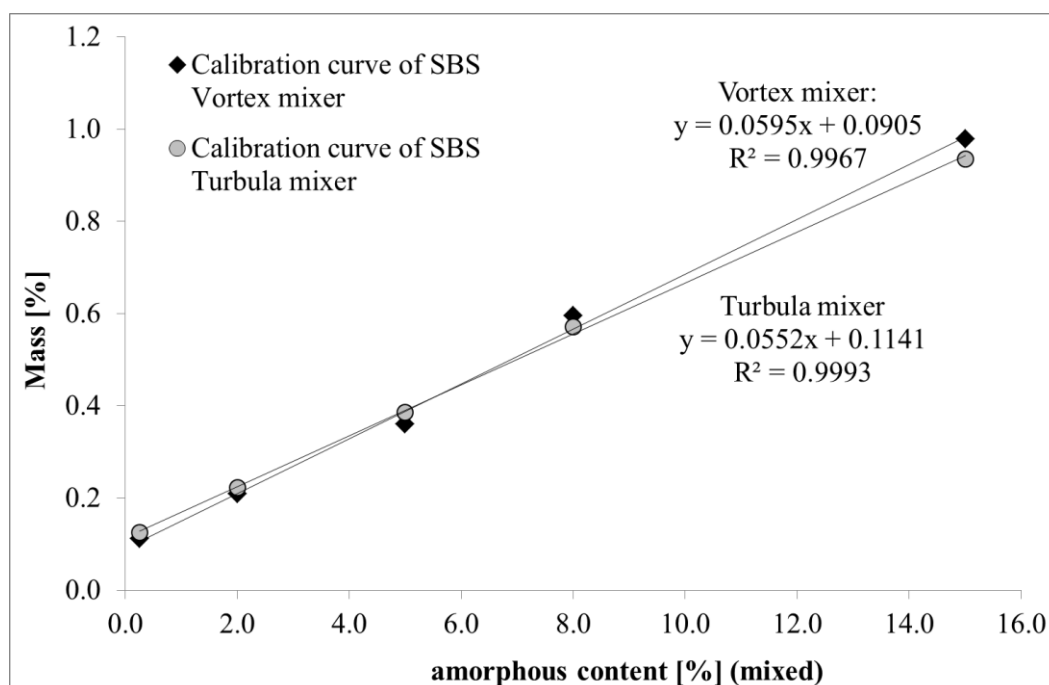


Figure 76: Alternative method for the preparation of homogenous mixtures of amorphous amounts

The absorption behavior of jet-milled powders (8 bar, 1 grinding cycle up to 3 grinding cycles) were measured using the individual methods and finally the amorphous content was calculated (Table 22).

The hydrophilic APIs almost showed no amorphous amounts ($< 0.25\%$) for FF, however, amorphous amounts were measured from 1.5%, 4.2% and 5.1% for SBS. The amorphous amounts for hydrophobic APIs resulted in 5.5%, 14.0% and 17.0% for CS, almost no amorphous content ($< 0.25\%$) for BS and finally 5.7%, 7.7% and 8.5% of amorphous content for GC. In summary, FF and BS tend to re-crystallize very fast. GC and CS demonstrate a high stability of amorphous amounts because these hydrophobic materials are much more inert

against water vapor. For SBS a lower affinity to water was measured which results in more stable powders.

Table 22: Determination of the amorphous content of micronized powders

API	Suitable method?	Possible calibration?	Amorphous content?
ITB	yes	No, blends are not stable	No calculation possible
FF	yes	yes	< 0.25%
SBS	yes	yes	1.5% up to 5.1%
CS	yes	yes	5.5% up to 17.0%
BS	yes	yes	< 0.25%
GC	yes	yes	5.7% up to 8.5%

Furthermore, powder samples from the mixing tests with glass beads (stress of crystal lattice) were investigated and compared to micronized powders (for SBS and CS). These DVS measurements are intended to give a short overview of how the amorphous content alters depending on production and processing. All measurements were accomplished with the introduced one-step DVS method for both APIs.

The water vapor method for SBS ($0.4 p/p_0$) shows the difference in water uptake between fully amorphous spray-dried and ball-milled SBS ($> 5.0\%$ at $0.4 p/p_0$) and semi-crystalline SBS (micronization and blending; $< 0.4\%$ at $0.4 p/p_0$) in figure 77. The fully crystalline starting material results in a baseline sorption of 0.09% at $0.4 p/p_0$. Small differences were determined for the blending and micronization process compared to this crystalline starting material. The micronized powder showed the highest mass adsorption (0.39% at $0.4 p/p_0$) at 8 bar grinding pressure and 3 grinding cycles which is due to the highest amorphous amounts except for SD- and BM-samples. It is assumed that the number of grinding cycles increases the amorphous amount as mentioned. The mixing tests with small (0.15% at $0.4 p/p_0$) and big (0.12% at $0.4 p/p_0$) glass beads showed a lower absorption than the micronization process at 8 bar grinding pressure and 1 grinding cycle (0.20% at $0.4 p/p_0$). The value ‘cyclone’ is the fully crystalline material which was sieved with the air jet sieve for the simulation of the separation process of the glass beads. In summary, there is a significant higher absorption for all performed micronization tests, ball-milled and spray-dried samples.

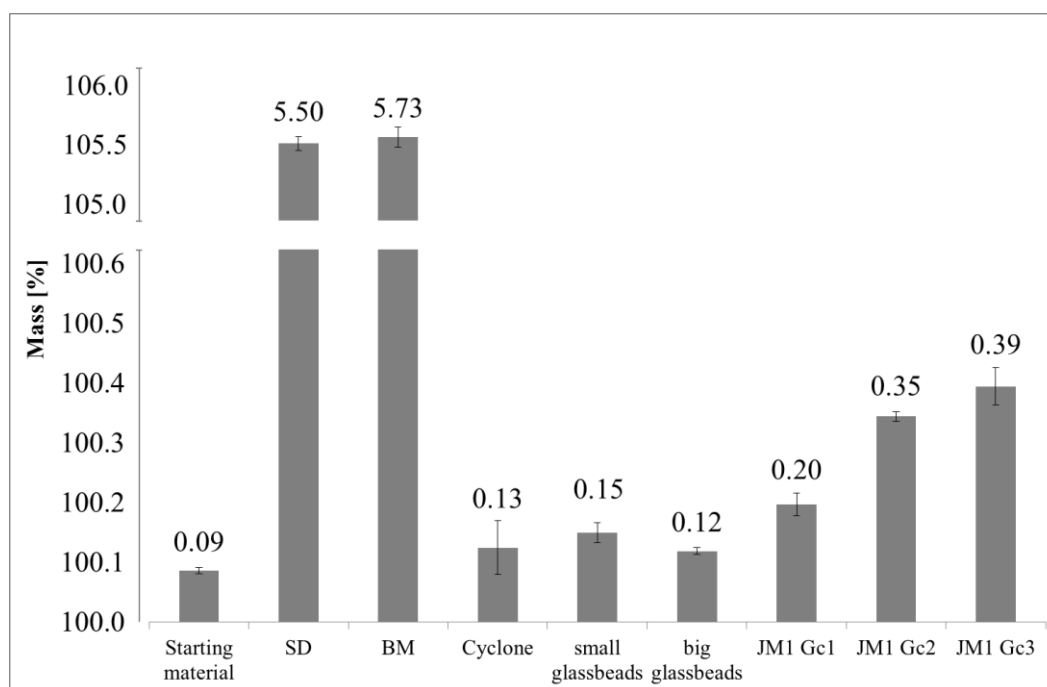


Figure 77: Overview of the absorption behavior of SBS samples

Similarly, high vapor sorption for the fully amorphous SD and BM samples ($> 1.6\%$ at $0.1 p/p_0$) and low vapor sorption ($< 0.35\%$ at $0.1 p/p_0$) for the semi-crystalline starting material were detected using the isopropanol-based measurement ($0.10 p/p_0$) for CS (Figure 78). The fully crystalline starting material results in a baseline sorption of 0.05% at $0.1 p/p_0$. After blending with the big glass beads (0.17% at $0.1 p/p_0$) a slightly higher vapor sorption was observed than after the micronization of Ciclesonide at 8 bar grinding pressure and 1 grinding cycle (0.14% at $0.1 p/p_0$). Again, with a higher number of grinding cycles (Gc2 and Gc3) significant differences were detectable. Beside the fully amorphous samples, Gc3 showed the highest absorption (0.33% at $0.1 p/p_0$) due to the highest amorphous amounts.

Comparing the results from both APIs, a different behavior is observed when looking at the mixing tests with big glass beads and micronization using one grinding cycle. It is assumed that the particle shape (SBS: needle crystals and CS: angular crystals) may also have an influence on amorphous parts which are localized on the surface. The calculation of the amorphous parts showed that the high values are maintained when stored over P_2O_5 in a desiccator especially for micronized powders with a higher number of grinding cycles (JM1 Gc3). The CS powder showed a significant higher amount of amorphous parts compared to the hydrophilic SBS. Some SBS samples (e.g. big glass beads, cyclone) show highly crystalline properties and they cannot be distinguished from the baseline sorption of the fully crystalline starting material.

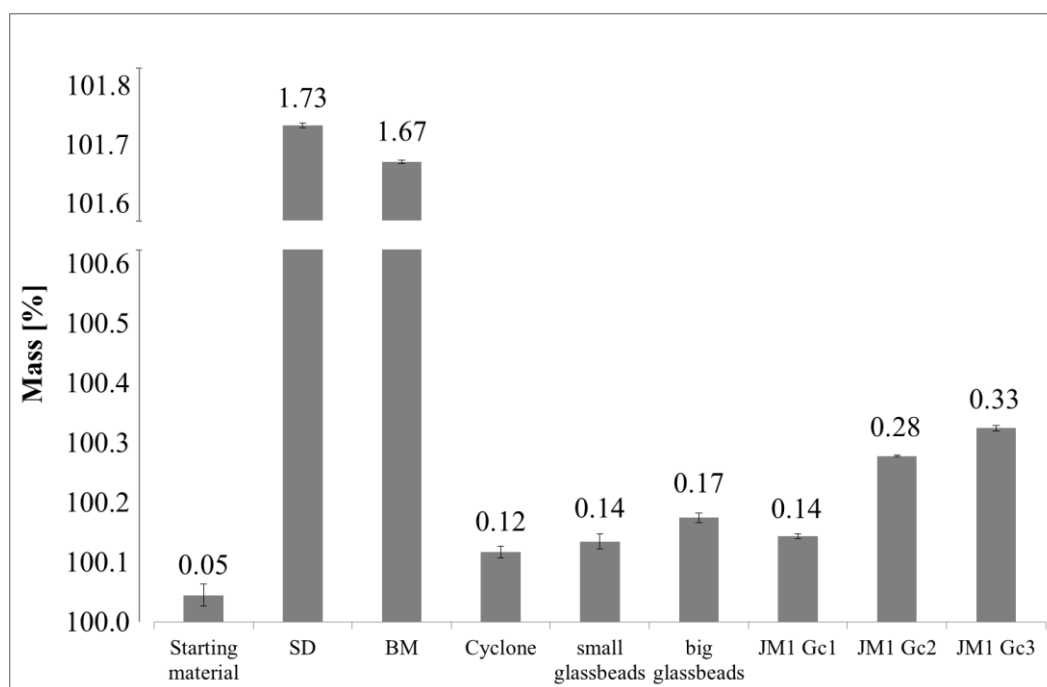


Figure 78: Overview of the absorption behavior of CS samples

4.3.5 Conclusion II

In summary, FF showed unstable amorphous amounts due to its hygroscopic behavior (< 0.25%). Furthermore no stability (fast re-crystallization) of the amorphous amounts (calibration curve) was determined for ITB blends. In comparison SBS showed significant stable amorphous amounts (up to 5.1%). CS as a hydrophobic drug showed the most stable amorphous content (up to 17.0%). The investigated amorphous parts for GC (up to 8.5%) are also stable against water vapor and thereby not likely to switch to their crystalline counterparts. Also, BS showed minimal and less stable amorphous amounts (< 0.25%). In general, all micronized starting materials (FF and BS) have to be treated with an electrostatic discharge stick to achieve blend homogeneity for the calibration of this DVS-method. These micronized starting materials showed a high surface energy (increased by > 6.5 mJ/m²).

However, it is assumed that these stable amorphous amounts can influence drug delivery and product stability. The amorphous content might have a huge influence on the FPFs of inhalable mixtures (Chapter 4.4.1 and 4.4.2) as well as on the dissolution behavior (Chapter 4.5). The hydrophilic APIs might show a high trend for re-crystallization over the storage time. Thereby, a change in the surface morphology is assumed. These modifications could be reinforced by a hydrophilic carrier (e.g. lactose). Hydrophobic APIs might interact less with vapor and therefore show an increased stability of the amorphous amounts.

A general estimation for the stability of further inhalation grade APIs seems to be possible based on the conducted measurements for the different types of APIs. In general, hydrophilic APIs (e.g. Tiotropium bromide) might interact well with water vapor and could show a low stability of amorphous amounts (hours, days or weeks) compared to other hydrophobic APIs (e.g. Salmeterol xinafoate) (up to several months). In summary, it is necessary that amorphous parts are determined and re-crystallized after the production process under controlled conditions. This approach of the one-step DVS method may facilitate the specifications for in-process controls in the pharmaceutical industry.

4.4 Aerodynamic investigations: Influence of different amorphous amounts on the de-agglomeration and deposition behavior

Methods such as spray-drying, grinding, jet milling and liquid-liquid antisolvents [147] are used for the micronization of the drug (particle size < 5 μm). These operations used in the pharmaceutical industry lead to structural changes (for example amorphous regions, chapter 4.3.4) and thus could alter the surface properties. This involuntarily produced metastable state may change during handling, over storage time or by changes in humidity and/or temperature (Chapter 4.1.2). It is well documented that it could induce re-crystallization of amorphous regions and particle size changes post-production [95].

In order to investigate the impact of these amorphous amounts, inhalable homogenous powder mixtures with very high/low amorphous content and a defined particle size were prepared with a Turbula blender for each API (SBS/CS), respectively. These amorphous amounts are calculated on the basis of the approved one-step dynamic vapor sorption method (DVS). A hydrophilic lactose carrier was chosen which could absorb moisture during storage time in the study 1. In addition, blends with an inert carrier (glass beads) instead of the hydrophilic lactose were prepared for the study 2. Thereby, a lower affinity to water vapor and a higher stability of the amorphous amounts are expected. All blends were stored (6 months, 45% RH, room temperature) to evaluate the influence of storage on amorphous amounts. The fine particle fraction (FPF: % of delivered dose < 5 μm) was determined at defined time points (1 day, 1 week, 2 weeks, 1 month, 3 months and 6 months) using the Next Generation Impactor.

In general, the de-agglomeration behavior and the aerodynamic deposition are characterized by a complex interplay of many different mechanisms. Primarily the reduction as well as the increase of cohesion or adhesion forces (drug-to-drug or drug-to-carrier) depend on macroscopic properties of the particles [84]. Important parameters that have an influence on the aerosolization behavior, which may change during re-crystallization, are mainly the particle size

of API and the carrier [56], but also the particle shape [70] and surface rugosity [148]. During milling and blending electrostatic charging [65] may occur causing new contact areas on particles. In the course of use, whenever a higher relative humidity is reached and more water molecules are present a thin film layer is formed which induces higher capillary forces [149]. Furthermore, regarding the flow properties a change in physico-chemical properties may influence important parameters such as binding energy and binding forces (e.g., van der Waals forces) between the detaching drug and the lactose carrier during dispersion [150].

4.4.1 Study 1: Lactose, SBS, CS and the Easyhaler®

In this investigation the same α -lactose-monohydrate was used as a carrier for all four blends (Table 4). Only the type of API (hydrophilic or hydrophobic) and the extent of amorphous content (high or low) were varied (Figure 79).

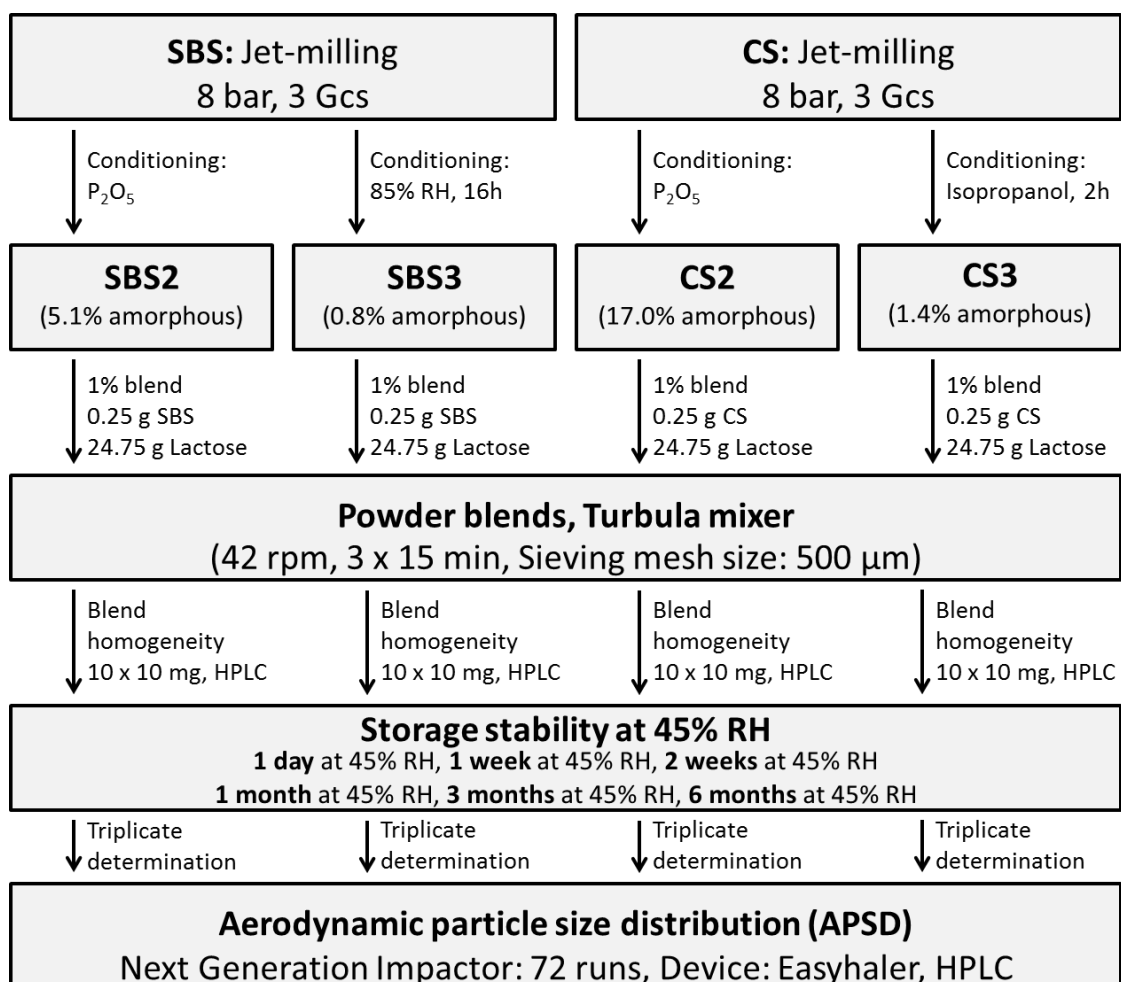


Figure 79: Design of Study 1: Investigation of the influence of different amorphous amounts in hydrophilic and hydrophobic APIs on the de-agglomeration and aerodynamic deposition behavior

In both designs of storage stability processing parameters such as the micronization or the blending (grinding pressure, grinding cycles, type of mixer [151], mixing speed [152], mixing time [153] and batch size), the drug content [154] (drug-to-carrier ratio of 1:100), the carrier/drug properties (particle size, roughness [155]) and the storage conditions (6 months, 45% RH, room temperature) are identical. All these parameters can lead to changes in the FPF and are well-documented in the literature.

To re-crystallize parts of the amorphous amounts of both APIs (type SBS 2 und CS 2), a conditioning time was chosen which did not lead to changes in particle size (type SBS 3 und CS 3). Although both APIs still had a small detectable residue of amorphous parts the same desired particle size distribution was maintained. Furthermore, the blend homogeneity was determined by validated HPLC analytics.

In initial experiments an in-house constructed model inhalation device was used to apply these powder blends to the NGI. But a low FPF and thus no possibility of discrimination between different powders (data not shown) resulted in the decision to change the device to the Easyhaler[®]. Due to a better de-agglomeration, higher values in the FPF and an improved discrimination were obtained. This change in the device might demonstrate trends for the FPF to higher and also lower values.

4.4.1.1 Bulk powder and blend characterization

The PSD shows that the micronized powder particles of both APIs are significantly reduced in size (x_{50}) compared to the crystalline starting material (Table 23).

Table 23: PSD and amorphous content of the conditioned SBS and CS samples - Study 1

Sample	x_{50}	Span	Amorphous content [%]
Respirose SV003	57.92 ± 0.15	0.99 ± 0.02	/
SBS starting material	9.11 ± 0.07	3.44 ± 0.11	/
SBS 2	1.94 ± 0.01	2.43 ± 0.01	5.09 ± 0.56
SBS 3	1.96 ± 0.01	2.40 ± 0.02	0.76 ± 0.34
CS starting material	57.90 ± 2.96	4.91 ± 0.16	/
CS 2	1.51 ± 0.02	2.62 ± 0.05	17.01 ± 0.47
CS 3	1.52 ± 0.03	2.63 ± 0.06	1.35 ± 0.09

In addition, SBS and CS both show no significant change in particle size (x_{50}) after the temporary conditioning (SBS: 16 hours at 85% RH, CS: 2 hours over 10 ml isopropanol). These significant changes in the particle size when jet-milling the SBS samples can be seen looking at the overview of the cumulative distribution (Q_3) (Figure 80). Again, three grinding cycles (SBS 2) led to smaller particle sizes than one grinding cycle (SBS 1). No significant change was determined in the conditioning process. The re-crystallized sample SBS 3 is in line with the unconditioned sample SBS 2 (white squares are on top of the black circles).

Because of the similar particle size distribution these micronized powders can be used in the storage stability test over half a year. Furthermore, the evaluation of the influence of the amorphous content on the de-agglomeration behavior is achieved for this study 1.

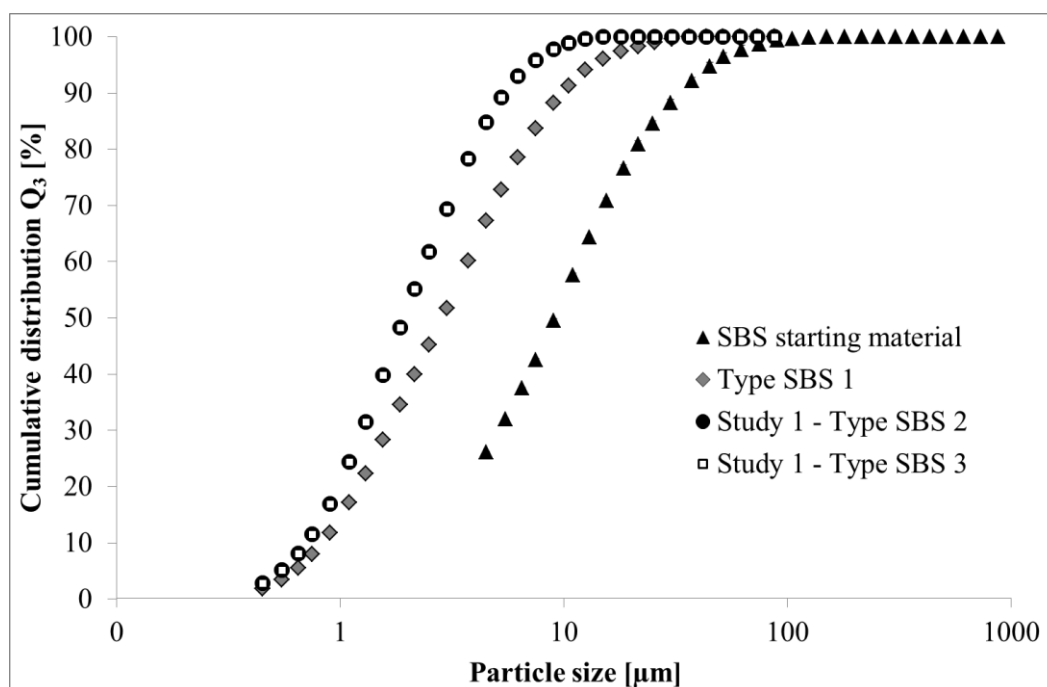


Figure 80: Relation of the cumulative distribution of SBS particles - Study 1

These findings were equal for the CS samples (Figure 81). Nevertheless, the particle size of the starting material was of a larger size compared to the SBS starting material.

The detection of the amorphous parts (Table 23) showed that the high values are maintained when storing over P_2O_5 in a desiccator especially for micronized powders with a higher number of grinding cycles (JM1 Gc3, SBS 2/CS 2). In general, the CS powder samples showed significantly higher amorphous amounts compared to the hydrophilic SBS samples. The re-crystallized samples (SBS 0.8% of amorphous parts at 85% RH and CS 1.4% of amorphous parts at isopropanol for 2 hours) showed profound crystalline properties. Both APIs and their

induced amorphous amounts provide ideal conditions for the storage stability tests and analysis with the Next Generation Impactor.

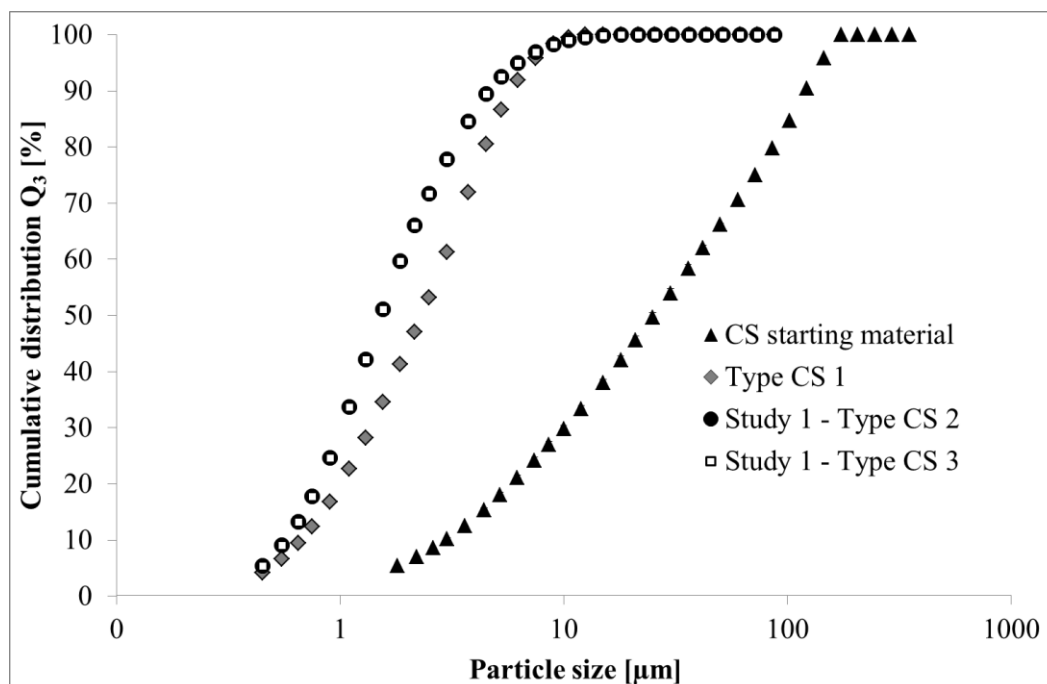


Figure 81: Relation of the cumulative distribution of CS particles - Study 1

The coefficient of variation for the homogenous mixtures was below 5% for all formulations which indicates a suitable mixing time (3×15 minutes) and mixing speed (42 rpm). Table 24 shows the characteristic parameters of the 1.0% API blends.

Table 24: Content uniformity of the blended inhalable mixtures - Study 1

Blend	Content [%]	sd	CV [%]	Recovery [%]
SBS 2	0.9749	0.0091	0.9377	97.5767
SBS 3	0.9750	0.0485	4.9698	97.4581
CS 2	1.0045	0.0113	1.1266	100.0597
CS 3	1.0165	0.0235	2.3169	101.4477

A striking aspect is that the re-crystallized APIs (SBS 3/CS 3) led to less homogenous mixtures (higher values of the coefficient of variation). It is assumed that small agglomerates (API-to-API) are easily formed due to the higher moisture content in the bulk powder prior to the mixing process [156]. These capillary forces might impede the uniform distribution of

lactose and the API. A significant drug loss for both types of blends was not determined (< 2.6%).

The scanning electron microscopy (Figure 82) showed the typical needle shaped SBS crystals. The micronized powder (SBS 2) exhibits very small and rough particles (2 μm) compared to the crystalline starting material (10 μm). These particle sizes can be linked to the PSD determined by laser diffraction analysis. Furthermore, the re-crystallized powder (SBS 3) showed no significant change in surface morphology and particle size (2 μm). An increased particle agglomeration as mentioned above was not visible on various magnifications for SBS 3.

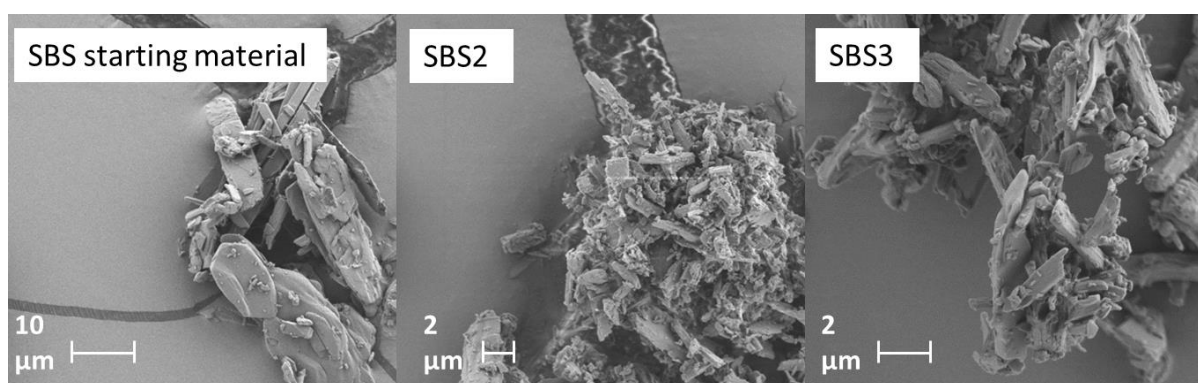


Figure 82: SEM pictures of the conditioned SBS samples - Study 1

Looking at the CS samples a more angular particle shape can be seen (Figure 83). Again, the micronized powder (CS 2) showed a smaller particle size (2 μm).

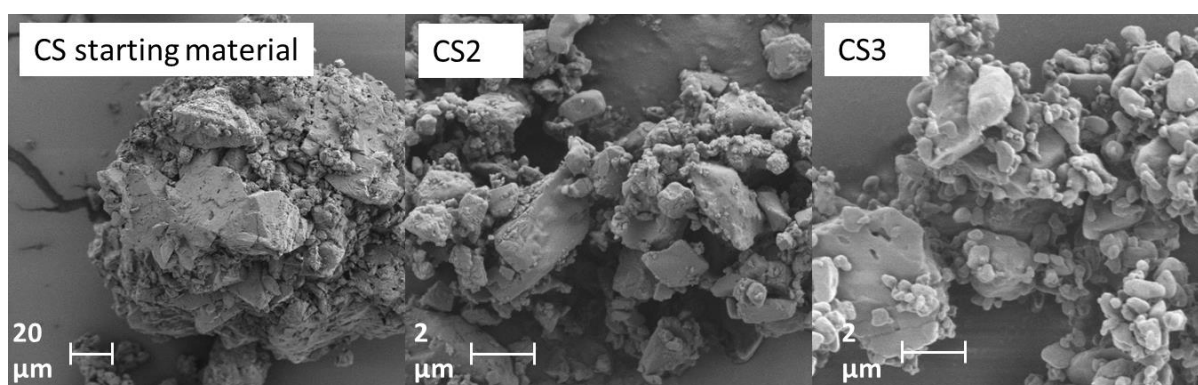


Figure 83: SEM pictures of the conditioned CS samples - Study 1

A change in the surface morphology was not visible for this sample. However, a smoother surface was visible for the re-crystallized sample (CS 3) (2 h, over isopropanol). This result can be compared to other re-crystallized CS samples with isopropanol (Chapter 4.3.2.1). In general, an increase of smoothness was achieved by a higher grinding pressure or a higher number of grinding cycles.

4.4.1.2 Impaction analysis

Over the storage of 6 months both APIs showed opposing aerodynamic particle size distributions in the deposition behavior determined by impaction analysis. Larger particles impact on initial stages whereas smaller particles are able to further follow the airflow and impact on the final stages (Stage 4 - Stage 8). Primarily, the particle size, density and induced inertial forces are responsible for the deposition behavior [38].

The SBS blends led to a significantly higher deposition on the final stages (stage 3, 4, 5, 6 and 7) compared to the CS blends after 1 day (Figure 84). However, the amorphous amounts of both blends resulted in an increased aerodynamic deposition behavior compared to the recrystallized blends. The major part of the API was quantified in the induction port and the preseparator. It is assumed that these API particles did not de-agglomerate from the large-sized carrier particles or remained stable as larger aggregates.

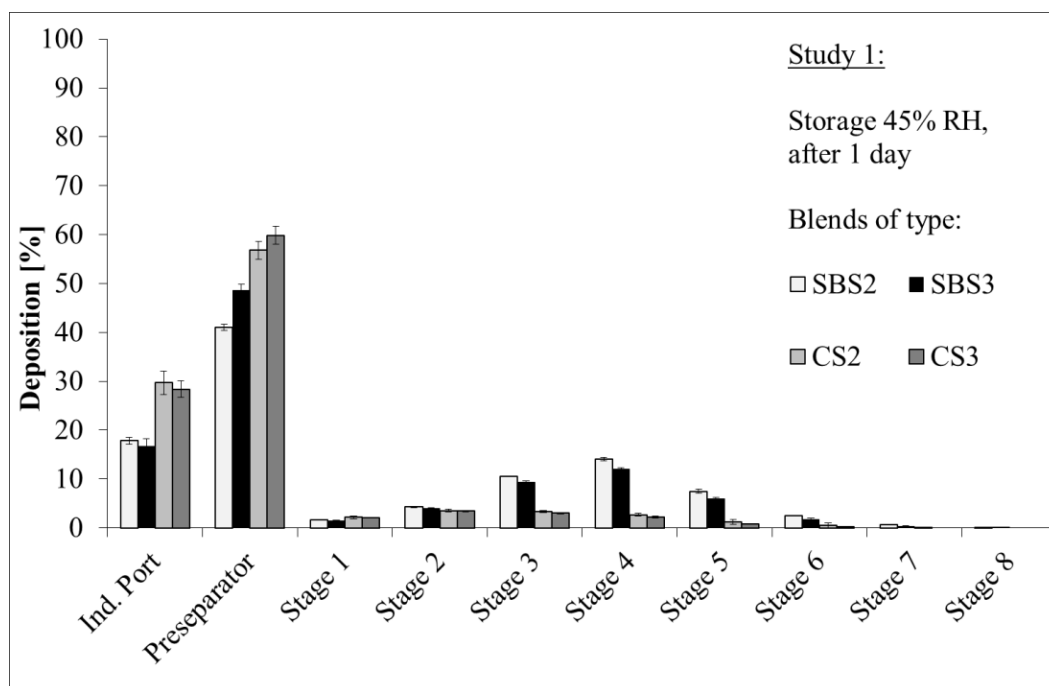


Figure 84: Deposition behavior of SBS and CS blends with different amorphous amounts after 1 day of storage at 45% RH - Study 1

A change in the deposition behavior was determined after 180 days of storage (Figure 85). The amorphous SBS 2 showed an increased impact on initial stages matching SBS 3. For recrystallized SBS 3 no significant changes were visible. On the contrary, both CS blends led to higher depositions on the final stages.

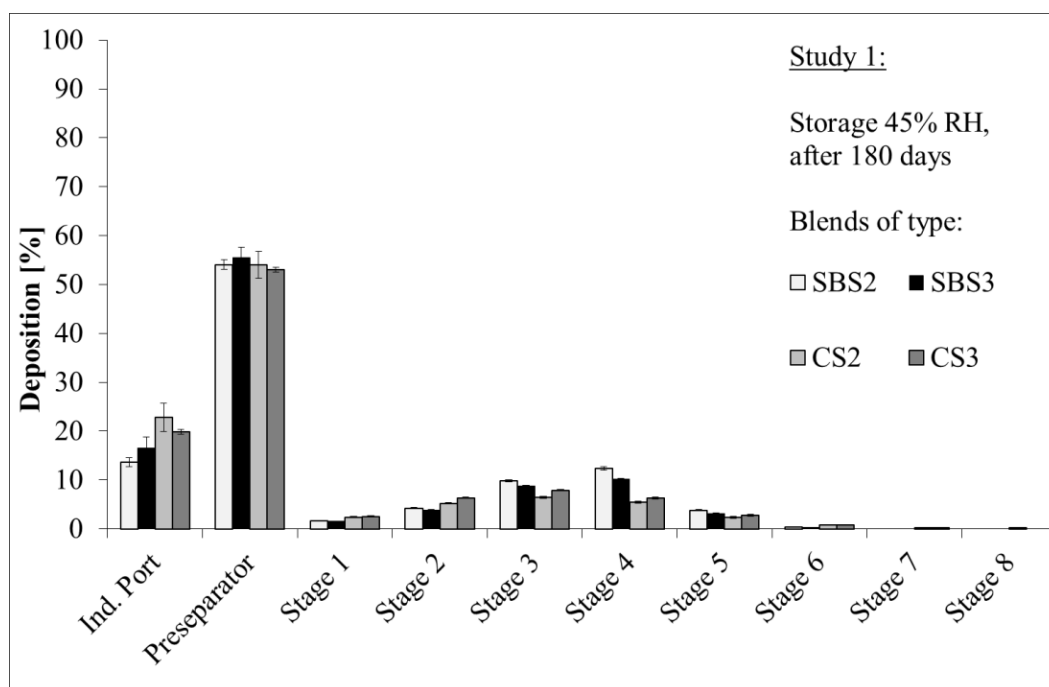


Figure 85: Deposition behavior of SBS and CS blends with different amorphous amounts after 180 days of storage at 45% RH - Study 1

For an accurate assessment the calculated fine particle fraction (% of delivered dose < 5 μm) from measurements at different time points (1 day, 1 week, 2 weeks, 1 month, 3 months and 6 months) was compared. Furthermore, possible interactions between the hydrophilic carrier, the respective API and the humidity (H_2O) were discussed.

The hydrophilic SBS blends showed a significantly higher FPF (> 29%) after 1 day (Figure 86). Samples that initially contained 5.1% amorphous content showed a FPF of 36% at the beginning which decreased constantly over the storage time (Storage: 45% RH, room temperature) to about 27%. The initially re-crystallized sample achieved a comparable constant level of about 25%. In addition, significant changes in surface morphology cannot be observed in SEM analysis after the conditioning process (Figure 82). Young and Price have made similar observations with amorphous SBS blends which showed decreasing FPFs over storage time [157].

It can be assumed that the amorphous blend (SBS 2) re-crystallizes over storage time (6 months) to an extent that can be compared to the initially conditioned sample (SBS 3). The reduction of the FPF could be explained by an increase in particle size due to a) stronger inter-particle forces (capillary forces) at the higher humidity [158] and b) solid material bridges that were formed during re-crystallization between the particles [159].

It is expected that the water molecules interact with the hydrophilic API and hydrophilic excipient leading to a re-crystallization of the remaining amorphous amounts of both mixtures over the period of storage.

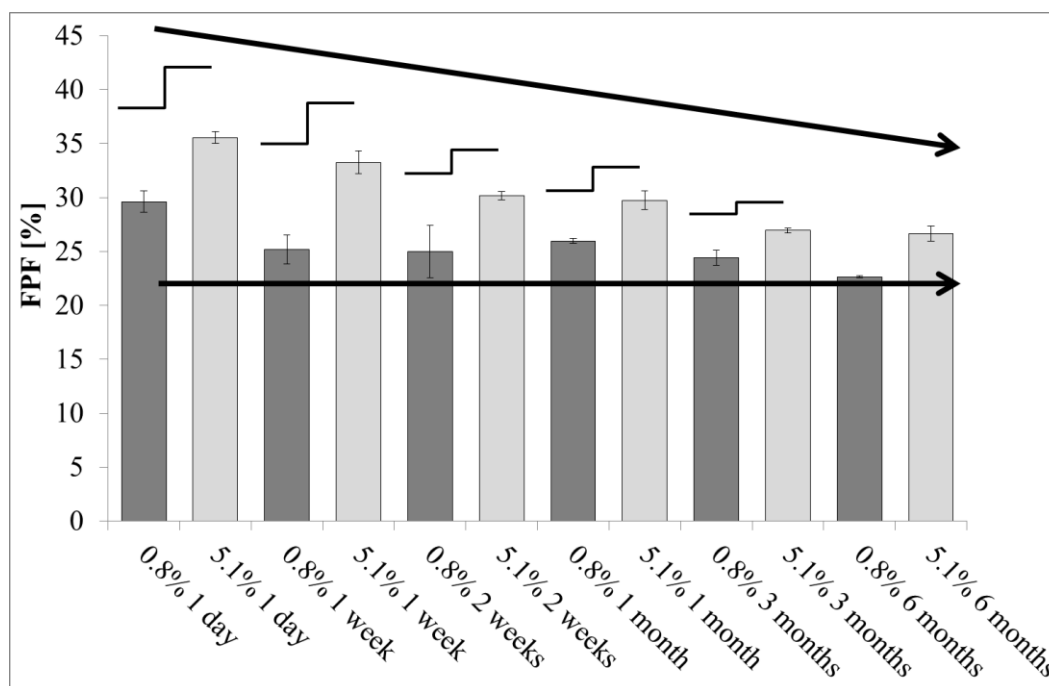


Figure 86: Change of fine particle fraction for amorphous SBS blends (storage over 6 months at 45% RH and RT) - Study 1

Table 25 summarizes the SBS study 1. Thereby, FPF, MMAD, GSD and FPD are listed corresponding to each time point. Mechanisms such as inter-particle forces, material bridges, changes of particle shape/size or degradation of hydrogen bonds have a strong influence on these FPF/FPD values.

The MMAD values demonstrate a minor increase over the storage time. It is assumed that the particle size changed due to higher moisture content in the powder [160]. The GSD seems to be less affected and remained constant at one level over six months. The DVS measurements showed a decrease of the amorphous amounts for pure SBS powder samples over several weeks.

The delivered doses of SBS depending on the storage time (1 day, 1 week, 2 weeks, 1 month, 3 months and 6 months) are listed in the appendix (8.3.6).

Table 25: NGI results of both SBS blends with lactose - Study 1

Sample	SBS_5.1%	SBS_0.8%	SBS_5.1%	SBS_0.8%	SBS_5.1%	SBS_0.8%
	1 day	1 day	1 week	1 week	2 weeks	2 weeks
FPF (% < 5 μm)	35.56 \pm 0.56	29.62 \pm 0.98	33.26 \pm 1.04	25.18 \pm 1.33	30.16 \pm 0.37	25.00 \pm 2.45
MMAD [μm]	2.64 \pm 0.02	2.76 \pm 0.04	2.70 \pm 0.02	2.85 \pm 0.02	2.80 \pm 0.02	2.84 \pm 0.04
GSD	1.78 \pm 0.02	1.76 \pm 0.03	1.73 \pm 0.05	1.73 \pm 0.04	1.77 \pm 0.02	1.79 \pm 0.02
FPD (μg < 5 μm)	35.10 \pm 3.42	25.79 \pm 1.34	30.82 \pm 6.98	19.60 \pm 1.05	24.60 \pm 0.21	21.56 \pm 1.23
	SBS_5.1%	SBS_0.8%	SBS_5.1%	SBS_0.8%	SBS_5.1%	SBS_0.8%
	1 month	1 month	3 months	3 months	6 months	6 months
FPF (% < 5 μm)	29.74 \pm 0.87	25.98 \pm 0.23	26.95 \pm 0.22	24.43 \pm 0.72	26.66 \pm 0.73	22.65 \pm 0.08
MMAD [μm]	2.86 \pm 0.06	2.96 \pm 0.03	2.96 \pm 0.04	2.94 \pm 0.04	3.03 \pm 0.02	3.11 \pm 0.04
GSD	1.74 \pm 0.02	1.74 \pm 0.02	1.73 \pm 0.03	1.76 \pm 0.03	1.73 \pm 0.00	1.77 \pm 0.01
FPD (μg < 5 μm)	27.66 \pm 2.88	22.14 \pm 1.30	22.41 \pm 0.46	21.84 \pm 0.60	22.62 \pm 1.63	18.77 \pm 0.80

The hydrophobic CS showed a relatively low FPF (< 10%) directly after production (1 day) which is presented in figure 87. The constantly increasing FPF (> 15%) during the 3 months of storage (Storage: 45% RH, room temperature) in both types of blends (with and without conditioning) can be explained by a) a reduction in surface electrostatics in presence of humidity [158] and b) a reduction of inter-particle forces (weak hydrogen bridge bonds) by water up-take from the surface of lactose particles [161]. Similar results were determined for hydrophobic Budesonide by Harjunen et al [158]. At all points of time, except for day 1, the powder with the actively re-crystallized amorphous amounts (1.4%, CS 3) tends to a higher FPF. It even shows a FPF 3% higher than the samples which initially contained more amorphous parts (17.0%, CS 2).

From SEM analysis (Figure 83) a significant change in morphology can be observed for the samples conditioned over isopropanol for 2 hours. The shape of these particles turned from an angular shape to a more spherical shape. This induced smooth surface may reduce inter-particle contacts and therefore could lead to the higher FPF values. It is assumed that the nonpolar API does not interact with 45% RH and that the amorphous parts have barely changed over storage time (6 months).

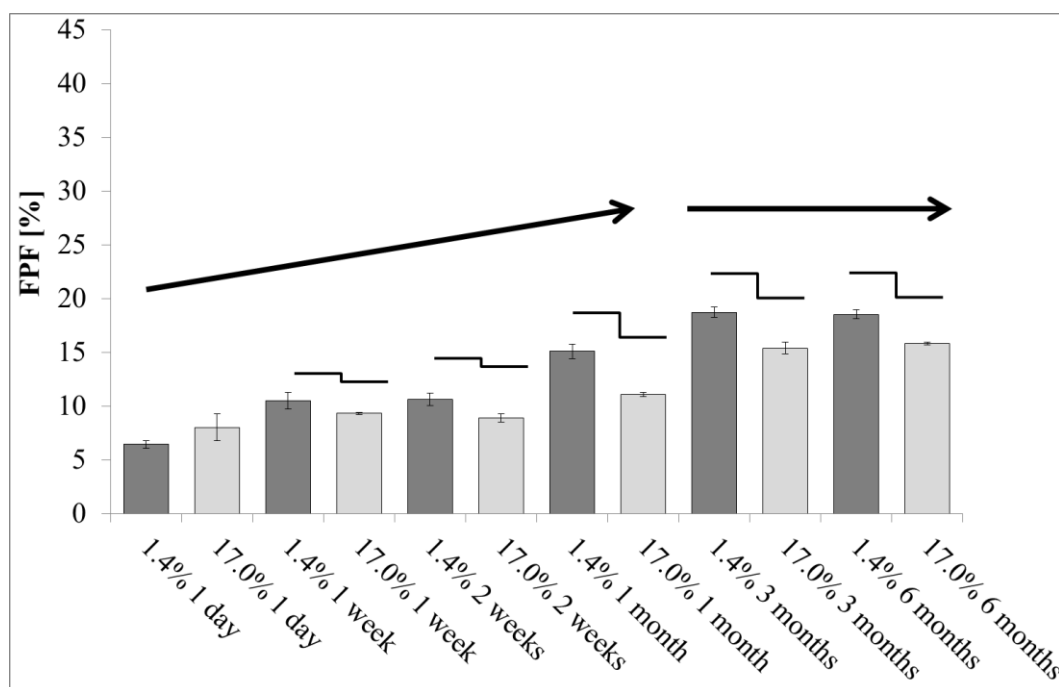


Figure 87: Change of fine particle fraction for amorphous CS blends (storage over 6 months at 45% RH and RT) - Study 1

Table 26 summarizes all relevant data of the CS study 1. Surface electrostatics and the decrease of inter-particle forces (weak hydrogen bridge bonds) might be involved in the increase of the FPFs. Differences in FPFs of both blends are caused by the surface modification of the API particles during the initially executed conditioning process (smoothness).

Table 26: NGI results of both CS blends with lactose - Study 1

Sample	CS_17.0%	CS_1.4%	CS_17.0%	CS_1.4%	CS_17.0%	CS_1.4%
	1 day	1 day	1 week	1 week	2 weeks	2 weeks
FPF (% < 5 μm)	8.01 \pm 1.24	6.43 \pm 0.35	9.30 \pm 0.12	10.47 \pm 0.79	8.91 \pm 0.39	10.60 \pm 0.57
MMAD [μm]	4.23 \pm 0.36	4.61 \pm 0.08	4.11 \pm 0.05	3.92 \pm 0.13	4.07 \pm 0.15	3.88 \pm 0.11
GSD	2.14 \pm 0.21	2.01 \pm 0.03	2.07 \pm 0.01	2.11 \pm 0.03	2.16 \pm 0.06	2.13 \pm 0.03
FPD (μg < 5 μm)	7.20 \pm 1.84	6.11 \pm 0.33	8.13 \pm 0.31	9.84 \pm 1.57	9.54 \pm 0.87	11.11 \pm 0.57
Sample	CS_17.0%	CS_1.4%	CS_17.0%	CS_1.4%	CS_17.0%	CS_1.4%
	1 month	1 month	3 months	3 months	6 months	6 months
FPF (% < 5 μm)	11.04 \pm 0.20	15.07 \pm 0.68	15.36 \pm 0.54	18.72 \pm 0.51	15.80 \pm 0.15	18.52 \pm 0.40
MMAD [μm]	3.84 \pm 0.05	3.62 \pm 0.06	3.38 \pm 0.13	3.45 \pm 0.04	3.67 \pm 0.07	3.72 \pm 0.07
GSD	2.13 \pm 0.03	2.07 \pm 0.02	2.16 \pm 0.02	2.01 \pm 0.03	2.00 \pm 0.01	1.92 \pm 0.00
FPD (μg < 5 μm)	11.77 \pm 0.46	16.19 \pm 1.68	19.75 \pm 2.08	20.65 \pm 3.25	13.59 \pm 0.26	16.45 \pm 1.34

A decreasing trend was determined for the MMAD and GSD values. These findings can be explained by an easier de-agglomeration caused by high moisture content over storage time. The delivered doses of CS depending on the storage time (1 day, 1 week, 2 weeks, 1 month, 3 months and 6 months) are listed in the appendix (8.3.6).

The optical SEM analysis was again performed at the end of the 6 months storage at 45% RH. The pictures showed API needles which might be of the same particle size for both SBS blends (Figure 88 A and B). These needles are marked with white circles. Also, for the CS blends no differences were optically visible (data not shown). In conclusion a precise statement about the particle size (particle growth) is difficult because the distinction between small carrier particles and API particles with this SEM technique is problematic.

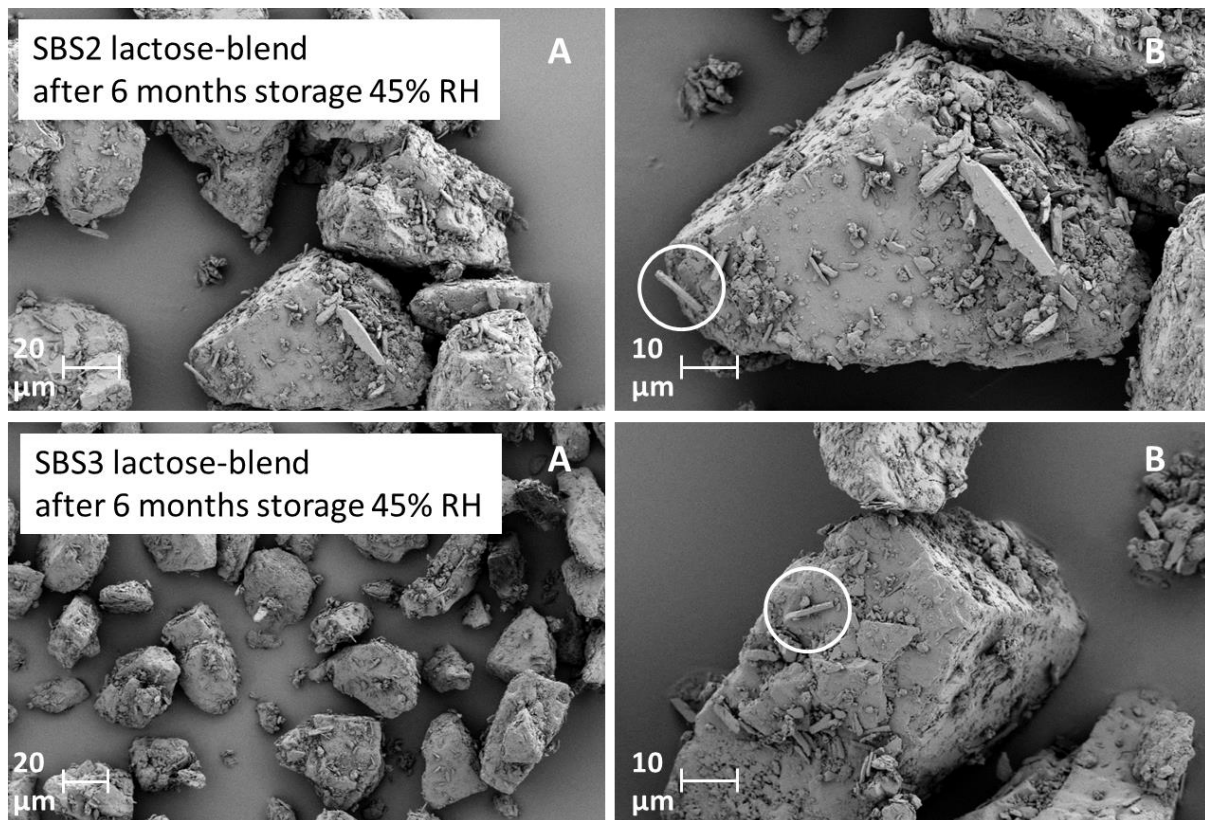


Figure 88: Blends of SBS 2 and SBS 3 after storage at 45% RH for 6 months (A) overview and (B) magnification - Study 1

4.4.1.3 Schematic model based on NGI results - Influence on FPF (Study 1)

The FPFs constantly decreased (9%) in relation to the amorphous parts in the case of SBS during storage time. Figure 89 A shows a possible mechanism of the de-agglomeration at the beginning of the stability study (dry powder state). Hereby, the small API particles are easily de-agglomerated from the lactose carrier which results in high FPFs during the inhalation process.

This situation may change during storage at 45% RH over a few weeks (Figure 89, B). Higher humidity and a higher water content in the powder blend led to a particle growth of the micronized and amorphous SBS. For this study, it is assumed that the particle size, particle shape and surface rugosity of the API changes over storage time. In addition, an increasing of the inter-particle forces (e.g. capillary forces) might occur. Also, the building of solid material bridges between particles is induced. The described phenomena take place during the re-crystallization process of the blend which contains a higher amorphous amount. In conclusion these modifications lead to decreasing FPFs. In the case of the initially re-crystallized API blend a comparable constant level was achieved.

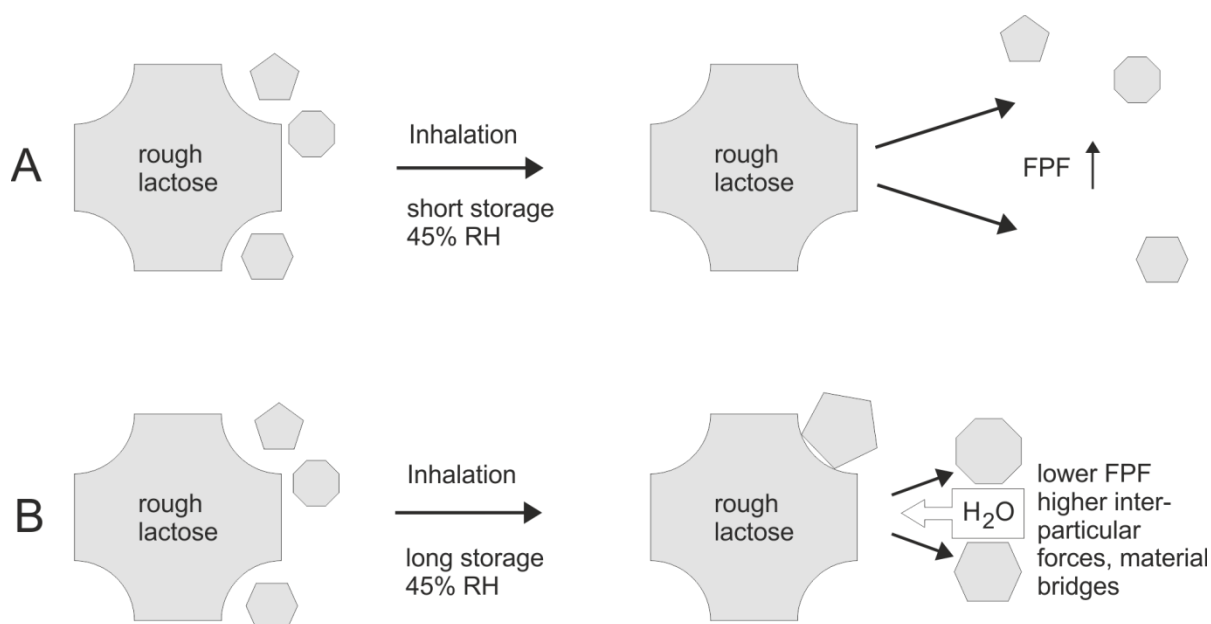


Figure 89: De-agglomeration model of SBS (A) at the beginning of storage (B) during storage at 45% RH

Strong hydrogen bridge bonds are built between the hydrophilic lactose and the SBS molecule (Figure 90). The degradation process of these bonds plays a minor role in comparison to the high binding forces which are present during complete storage time. In general, three double-hydrogen bridge bonds can be established assuming the three polarized hydroxyl-groups of the molecule (show strong electronegative properties). An increase of the water content might be necessary to solve these bonds between both types of molecules (lactose and SBS). The water molecules have to be present in overage and are indicated by many H₂O molecules. In this study the degradation of hydrogen bonds might not be the primary factor for this hydrophilic API; the de-agglomeration rather is influenced by the other described phenomena.

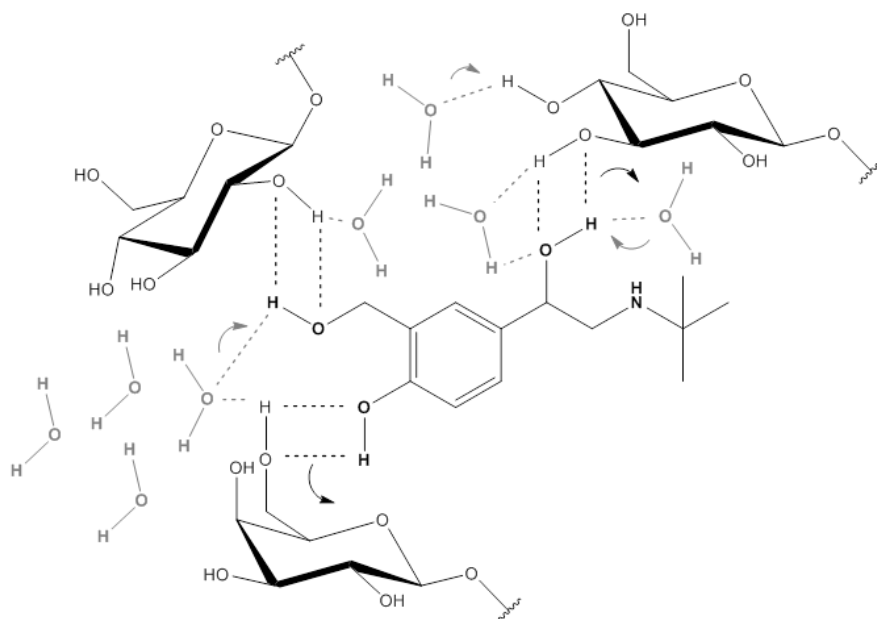


Figure 90: Degradation of strong hydrogen bridge bonds (SBS) during storage at 45%

The results for CS showed that the re-crystallized API achieves higher FPFs (3%) due to its smoother surface. A lower interaction took place on the relatively rough surface of lactose particles at every storage time point, after day 1 (Figure 91, A). This phenomenon led to higher FPFs. The smooth surface that was induced by isopropanol did probably not convert because of the constant 3% difference in FPF over the 6 months of storage time.

In case of the un-conditioned amorphous CS particles that show a rougher surface (Figure 83), more mechanical interlocking can be expected [162]. The formation of agglomerates and a poor detachment led to lower FPFs (Figure 91, B). It is assumed that the particle size of CS, the particle shape and the surface rugosity were not significantly altered by water vapor at 45% RH (from SEM analysis no significant changes are optically visible) during the storage stability test over a six month period. For the hydrophobic CS it may only be possible with organic solvents. The increase of the FPFs for both mixtures (with and without conditioning) can be explained by a reduction in surface electrostatics in the presence of humidity and the degradation of weak hydrogen bridge bonds during storage time.

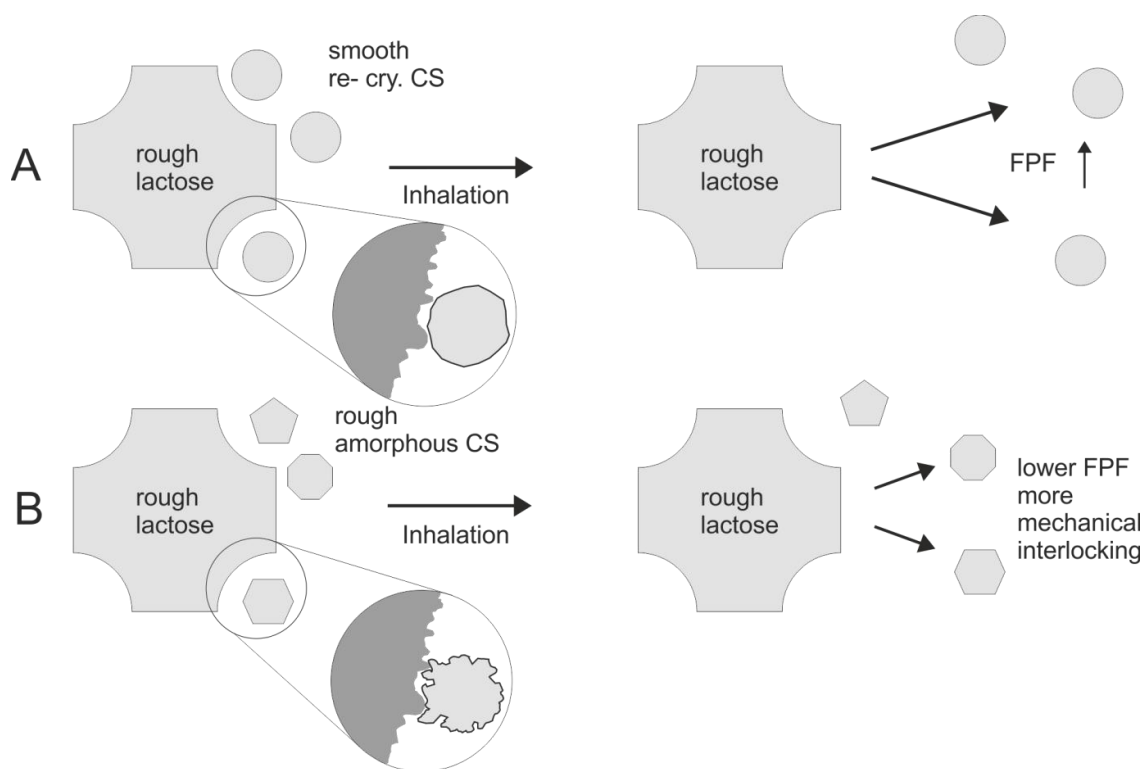


Figure 91: De-agglomeration model during inhalation for CS (A) smooth and (B) rough API particle surface

Hydrogen bridge bonds between the disaccharide lactose (condensation of D-galactose and D-glucose) can only be formed with one hydroxyl-group (more electronegative) and two carbonyl-groups (also hydrogen-bond acceptor) in the CS molecule (Figure 92).

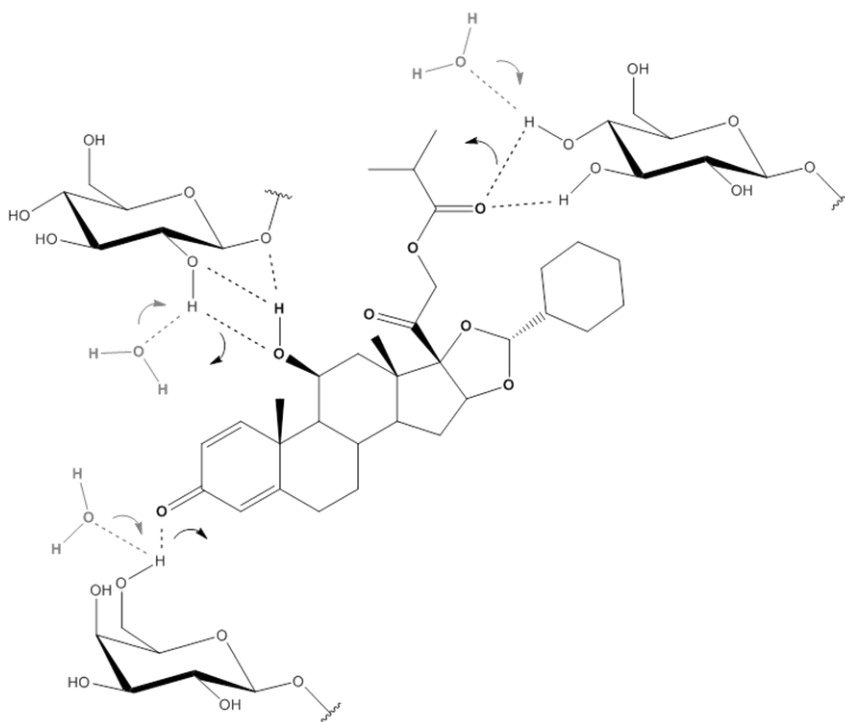


Figure 92: Degradation of weak hydrogen bridge bonds (CS) during storage at 45% RH

These bonds can be affected by the presence of water resulting in the reduction of hydrogen bonds between CS and lactose molecules. This phenomenon may also explain the increase in the FPFs.

4.4.2 Study 2: Glass beads, SBS, CS and HandiHaler®

In a second investigation the α -lactose-monohydrate carrier was replaced by glass beads (250 μm). This type of carrier might be inert against water vapor (45% RH) which leads to the expectation of a change in the de-agglomeration behavior of the API. The aim of the aerodynamic characterization is to determine a higher influence of amorphous amounts over the storage for 6 months compared to study 1. A strong re-crystallization process is excluded for both types of API on the basis of lower moisture content in the blends (Figure 93).

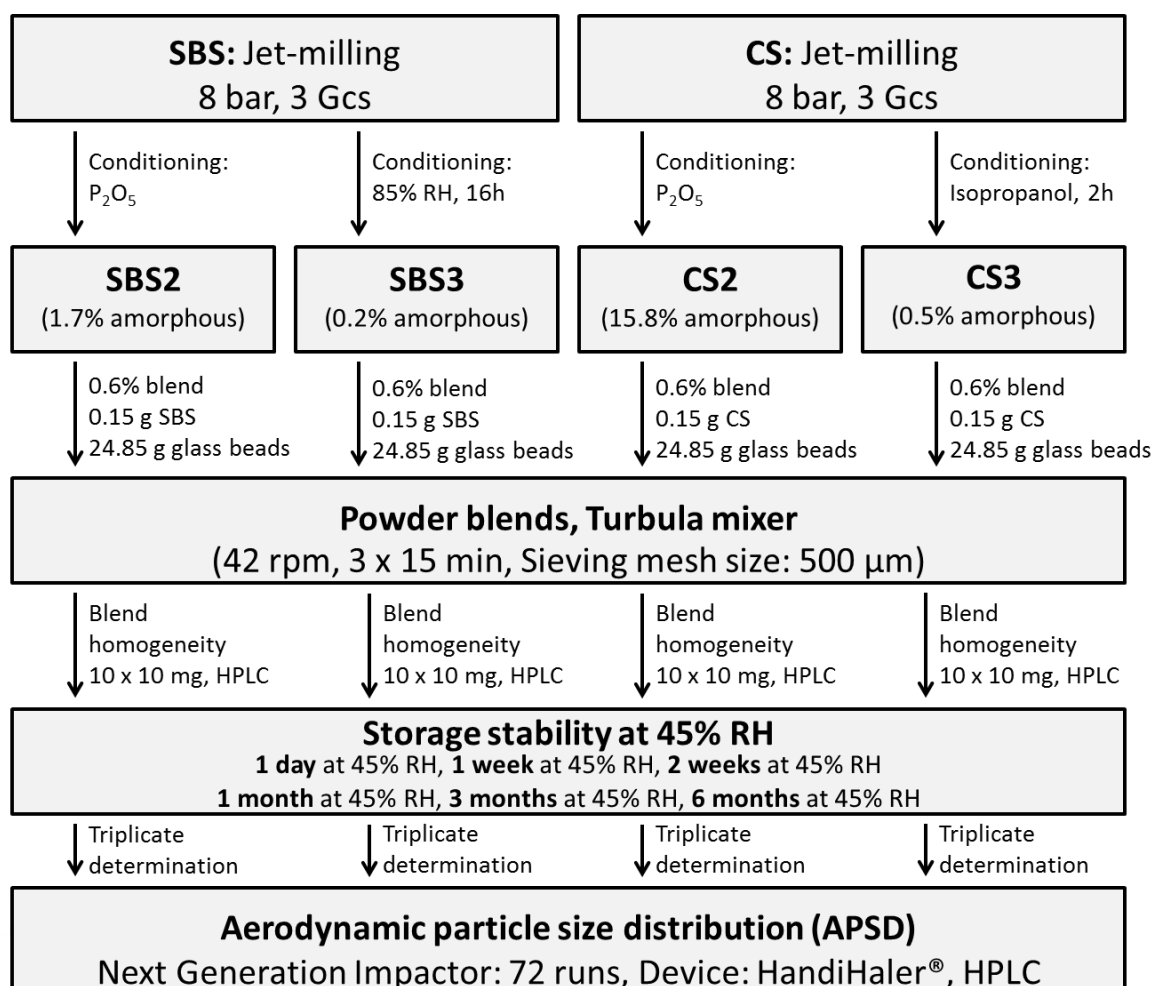


Figure 93: Design of Study 2: Investigation of the influence of different amorphous amounts in hydrophilic and hydrophobic APIs on the de-agglomeration and aerodynamic deposition behavior

Again, four blends were prepared, whereby the type of API (hydrophilic or hydrophobic) and the extent of amorphous content (high or low) were changed, respectively. In both designs of

storage stability processing parameters such as the micronization or the blending (grinding pressure, grinding cycles, type of mixer, mixing speed, mixing time and batch size), the drug content (drug-to-carrier ratio of 1:166.7), the drug properties (particle size) and the storage conditions (6 months, 45% RH, room temperature) were identical.

A change in the inhalation device from the Easyhaler[®] to the HandiHaler[®] was necessary due to serious dosing issues using glass beads. The single dose was therefore filled into capsules and subsequently aerodynamically assessed to the NGI (Figure 94).



Figure 94: Formulated glass beads with a concentration of 0.6% API

To re-crystallize parts of the amorphous content in both APIs (type SBS2 und CS2), a conditioning time was chosen which did not lead to changes in particle size (type SBS3 und CS3). This conditioning process was similar to study 1 with the lactose carrier. Therefore, both APIs still had a measurable residue of amorphous parts but the same desired particle size distribution. Finally the blend homogeneity was determined by validated HPLC analytics.

4.4.2.1 Bulk powder and blend characterization

Again, SBS and CS showed no significant change in particle size (x_{50}) after temporary conditioning (SBS: 16 h at 85% RH, CS: 2 h over 10 ml isopropanol). Because of the same particle size distribution (Table 27) these micronized powders can be used for the storage stability test over half a year. Thereby, a precise evaluation of the influence of the amorphous content can be done. The glass beads exhibit a larger PSD compared to the lactose carrier. Nevertheless,

the spherical and smooth surface led to a lower drug-to-carrier ratio. Thus, the API concentration was reduced from 1.0% to 0.6% for both, SBS and CS.

Table 27: PSD and amorphous content of the conditioned SBS and CS samples - Study 2

Sample	x_{50}	Span	Amorphous content [%]
Glass beads	343.70 ± 6.13	0.40 ± 0.01	/
SBS starting material	9.11 ± 0.07	3.44 ± 0.11	/
SBS 2	1.60 ± 0.02	2.24 ± 0.05	1.69 ± 0.31
SBS 3	1.68 ± 0.01	2.26 ± 0.06	0.18 ± 0.14
CS starting material	57.90 ± 2.96	4.91 ± 0.16	/
CS 2	1.67 ± 0.02	2.43 ± 0.05	15.75 ± 0.82
CS 3	1.71 ± 0.06	2.23 ± 0.06	0.45 ± 0.28

The detection of the amorphous parts (Table 27) showed that the high values are maintained over the storage time in a desiccator over P_2O_5 especially for micronized powders with a higher number of grinding cycles (JM1 Gc3, SBS 2/CS 2). The CS powder samples showed significantly higher amorphous amounts compared to the hydrophilic SBS samples. The recrystallized samples (SBS 0.2% of amorphous parts at 85% RH and CS 0.5% of amorphous parts at isopropanol for 2 hours) showed highly crystalline properties. Ideal conditions are provided by both APIs and their induced amorphous amounts to perform the storage stability tests with the Next Generation Impactor.

Table 28 shows characteristic parameters for the content uniformity of the 0.6% API-glass beads-blends. The coefficient of variation is significantly increased for all formulations containing glass beads. This result is an indication for a poor homogenous mixture.

Table 28: Content uniformity of the blended inhalable mixtures - Study 2

Blend	Content [%]	sd	CV [%]	Recovery [%]
SBS 2	0.5139	0.0461	5.3684	89.9743
SBS 3	0.4877	0.0286	2.2643	84.0538
CS 2	0.5668	0.0104	1.8393	94.2814
CS 3	0.5351	0.0606	5.2860	94.8720

The spherical and smooth surface of the glass bead led to a lower loading ratio for the API (Figure 95 A). It is assumed that API-API agglomerates are present in the mixtures despite the reduction of the API concentration (1.0% to 0.6%). This phenomenon might also explain a lower recovery for both types of blends.

Figure 95 B demonstrates an API-glass beads-blend with an excess of API which is localized between two glass beads (white circle). An easily performed detachment of these API-API agglomerates can be an indicator for a higher drug loss. In the second study the re-crystallized APIs (SBS 3/CS 3) did not lead to less homogenous mixtures compared to study 1 with the lactose. The SEM pictures that show the pure unconditioned and conditioned APIs are not presented because of the similarity in the results for SBS and CS compared to study 1 (Chapter 4.4.1.1).

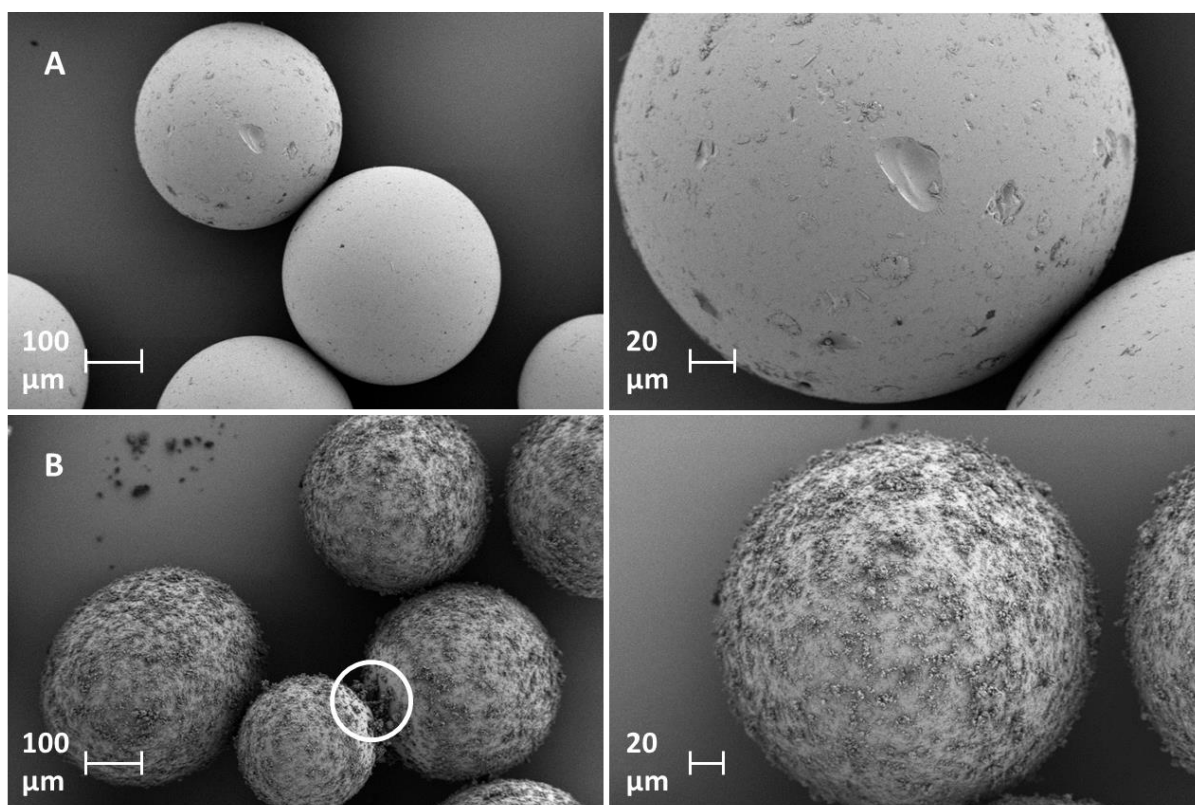


Figure 95: SEM pictures of glass beads without (A) and with API (B)

4.4.2.2 Impaction analysis

Both APIs showed nearly the same aerodynamic particle size distribution which was determined by an impaction analysis. Larger particles impact on the initial stages (on the basis of size, density and induced inertial forces) whereas smaller particles can follow the airflow further and impact on the final stages (Stage 4 - Stage 8). In this investigation the SBS blends did

not lead to a significantly higher deposition on the final stages (stage 3, 4, 5 and 6) at day 1 compared to the CS blends (Figure 96).

In addition, the amorphous amounts of both blends did not result in an increased aerodynamic deposition behavior compared to the re-crystallized blends after 1 day. The major part of the API was again quantified in the induction port and the preseparator.

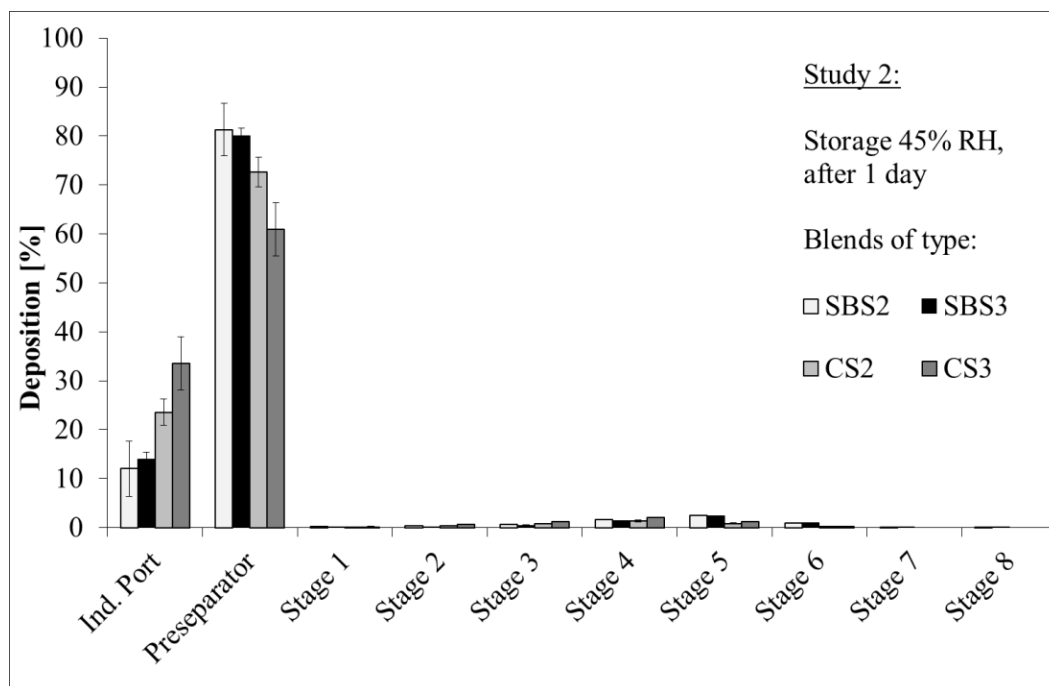


Figure 96: Deposition behavior of SBS and CS blends with different amorphous amounts after 1 day of storage at 45% RH - Study 2

The value at the induction port was even higher for the CS blends. It is assumed that these API particles were not de-agglomerated from the glass beads because of high press-on forces during the blending process resulting in earlier deposition [163].

After 180 days of storage no significant change in the deposition behavior was determined (Figure 97). The amorphous and re-crystallized blends showed a nearly similar and low impact on the final stages.

Finally the fine particle fractions (% of delivered dose < 5 μm) were compared at single time points (1 day, 1 week, 2 weeks, 1 month, 3 months and 6 months). Furthermore, possible interactions between the inert glass bead carrier, the respective API and the humidity (H_2O) were discussed.

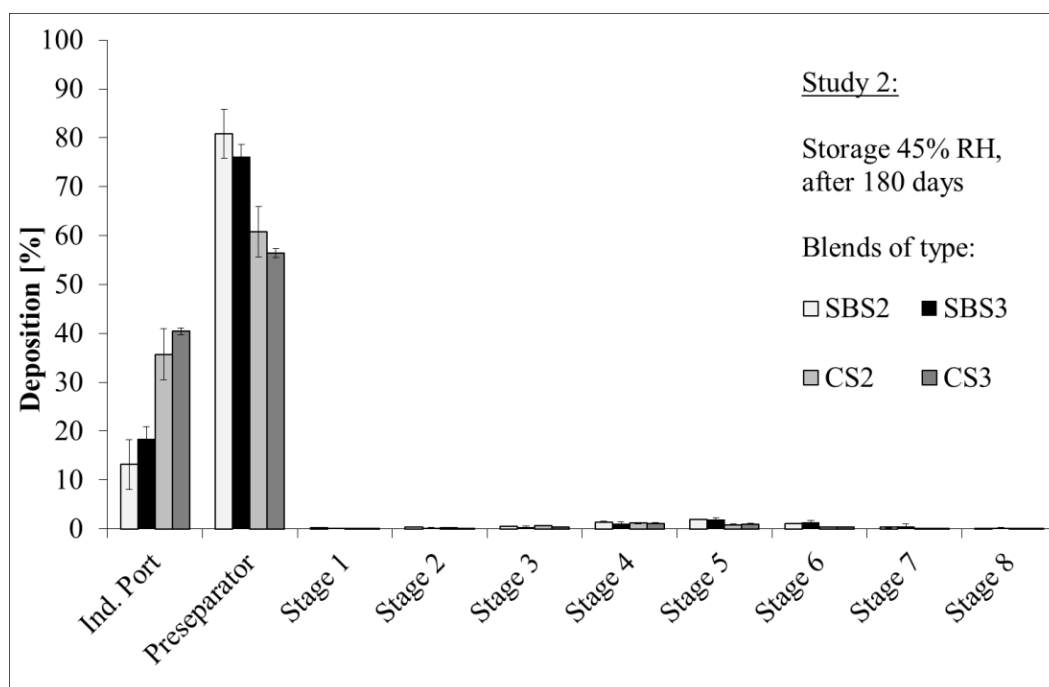


Figure 97: Deposition behavior of SBS and CS blends with different amorphous amounts after 180 days of storage at 45% RH - Study 2

The hydrophilic SBS blends showed significantly lower FPFs compared to the blends containing the lactose carrier. The value was reduced by 30%. Study 1 is indicated by the arrows in the diagram of study 2 (Figure 98).

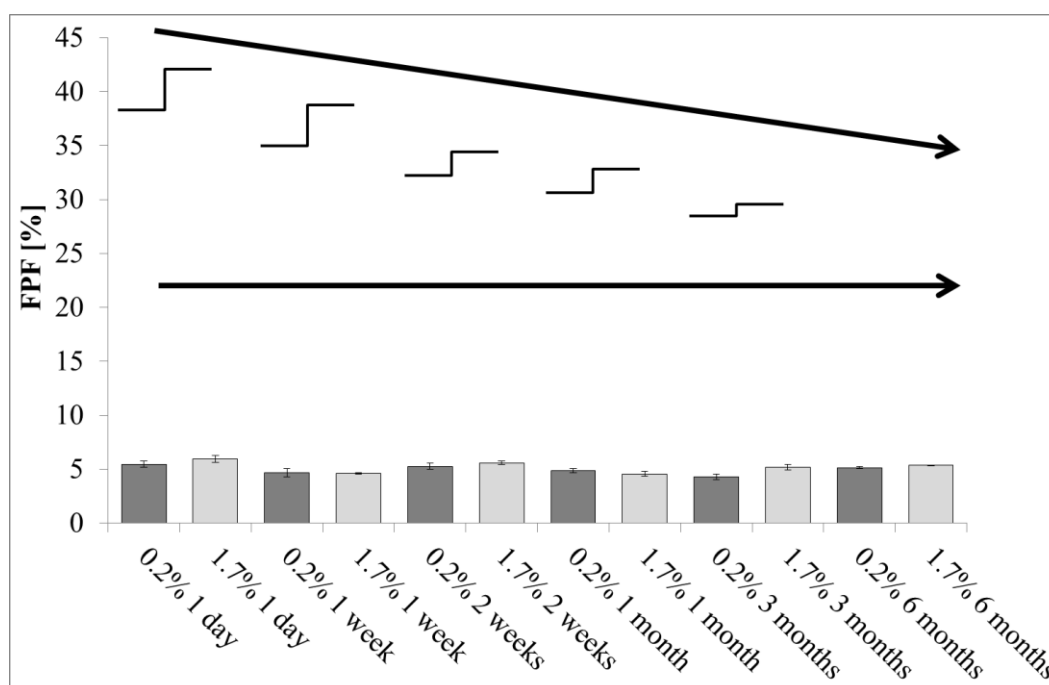


Figure 98: Change of fine particle fraction for amorphous SBS blends (storage over 6 months at 45% RH and RT) - Study 2 in comparison to study 1

Samples that initially contained 1.7% amorphous content showed an FPF of about 6% at the beginning which did not decrease constantly (approximately 5% FPF) over storage time (Storage: 45% RH, room temperature) as it was determined in study 1.

On the contrary, the initially re-crystallized sample (0.2% amorphous content) achieved a comparable constant level of about 5% FPF. Significant changes in surface morphology for SBS cannot be observed after the conditioning process by SEM analysis (data not shown). It can be assumed that the carrier material plays a major role on the de-agglomeration behavior. Especially the extent of the surface area and its roughness might influence the loading ratio [164], the type of interaction and the intensity of binding forces. In this study the inert glass beads demonstrated a low affinity to water vapor (45% RH). Nevertheless, a high stability of amorphous amounts for hydrophilic SBS is not realistic during six months. It is presumed that API-API interactions are more present in these blends because of the high press on forces during the mixing process [57]. An API coating (film) and an incomplete de-agglomeration of these stabile agglomerates are assumed (Figure 95) and could lead to low FPFs and high deposition on the preseparator.

Table 29 summarizes the SBS study 2. Thereby, FPF, MMAD, GSD and FPD are listed corresponding to each time point for each of the SBS blends.

Table 29: NGI results of both SBS blends with glass beads - Study 2

Sample	SBS_1.7%	SBS_0.2%	SBS_1.7%	SBS_0.2%	SBS_1.7%	SBS_0.2%
	1 day	1 day	1 week	1 week	2 weeks	2 weeks
FPF (% < 5 μm)	5.95 \pm 0.32	5.47 \pm 0.28	4.62 \pm 0.08	4.68 \pm 0.37	5.58 \pm 0.16	5.28 \pm 0.30
MMAD [μm]	1.68 \pm 0.03	1.55 \pm 0.03	1.75 \pm 0.02	1.62 \pm 0.02	1.68 \pm 0.02	1.54 \pm 0.06
GSD	2.19 \pm 0.06	1.87 \pm 0.04	2.21 \pm 0.04	1.95 \pm 0.03	2.09 \pm 0.07	1.82 \pm 0.06
FPD (μg < 5 μm)	7.46 \pm 0.40	6.02 \pm 0.44	5.21 \pm 0.16	5.07 \pm 0.59	6.40 \pm 0.47	5.40 \pm 0.32
	SBS_1.7%	SBS_0.2%	SBS_1.7%	SBS_0.2%	SBS_1.7%	SBS_0.2%
	1 month	1 month	3 months	3 months	6 months	6 months
FPF (% < 5 μm)	4.56 \pm 0.22	4.87 \pm 0.19	5.19 \pm 0.24	4.31 \pm 0.25	5.36 \pm 0.02	5.15 \pm 0.07
MMAD [μm]	1.72 \pm 0.04	1.56 \pm 0.06	1.67 \pm 0.03	1.61 \pm 0.04	1.58 \pm 0.07	1.32 \pm 0.36
GSD	2.24 \pm 0.16	1.82 \pm 0.10	2.08 \pm 0.09	1.88 \pm 0.06	2.21 \pm 0.03	2.08 \pm 0.22
FPD (μg < 5 μm)	5.10 \pm 0.28	4.95 \pm 0.50	5.82 \pm 0.22	4.56 \pm 0.21	5.59 \pm 0.14	5.24 \pm 0.45

A strong influence on FPF/FPD values was not recognized. Also, the MMAD/GSD values demonstrated no significant changes in six months.

Directly after production (1 day) relatively low FPFs (< 5%) were obtained for the hydrophobic CS in figure 99. The values for both blends were only lowered by 2-3% in their FPF compared to the lactose carrier blends (study 1). A constantly increasing FPF was not determined for both types of blends over storage time (45% RH, room temperature). Again, study 1 is indicated by the arrows in the diagram. After 6 months a change in the FPF was not recognized similar to SBS.

Once more it was shown that the carrier material plays a major role on the de-agglomeration behavior. The surface area and its roughness influences the loading ratio [164], the type of interaction and the binding forces. In conclusion the inert glass beads demonstrated a low affinity to water vapor (45% RH). It is presumed that the amorphous amounts are stable in the case of hydrophobic CS over six months.

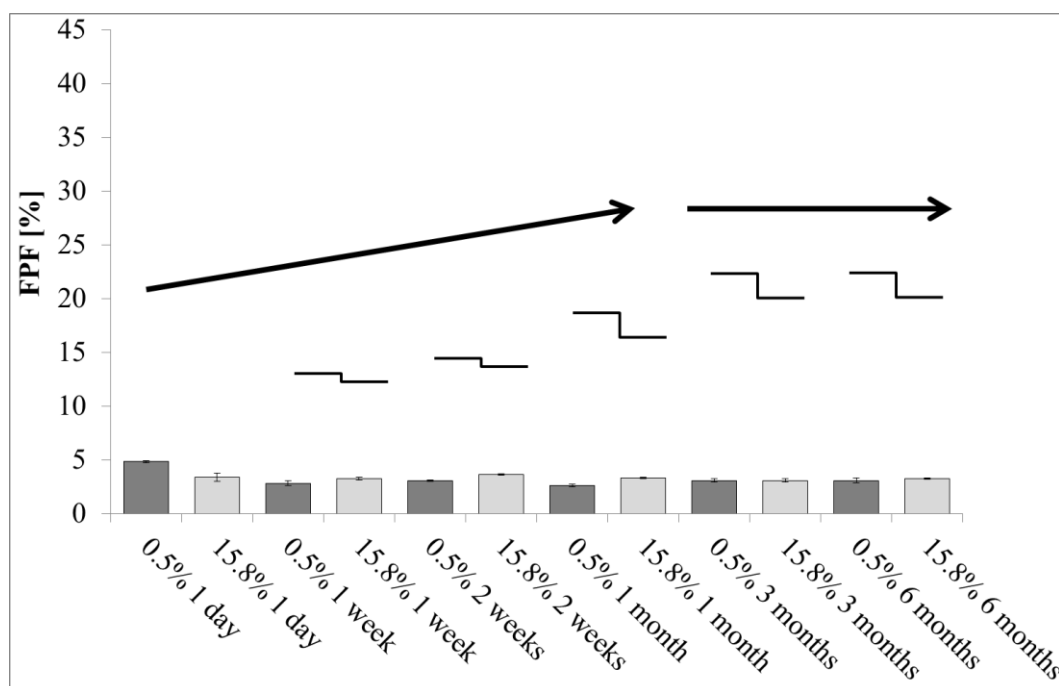


Figure 99: Change of fine particle fraction for amorphous CS blends (storage over 6 months at 45% RH and RT) - Study 2 in comparison to study 1

Table 30 shows a summary of the CS study 2. The values of FPF, MMAD, GSD and FPD are listed corresponding to each time point for both CS blends. In addition, a strong influence on FPF/FPD values was not recognized. The MMAD/GSD values again demonstrated no significant changes over 6 months.

Table 30: NGI results of both CS blends with glass beads - Study 2

Sample	CS_15.8%	CS_0.5%	CS_15.8%	CS_0.5%	CS_15.8%	CS_0.5%
	1 day	1 day	1 week	1 week	2 weeks	2 weeks
FPF (% < 5 μm)	3.38 \pm 0.39	4.81 \pm 0.09	3.22 \pm 0.12	2.80 \pm 0.22	3.60 \pm 0.07	3.03 \pm 0.08
MMAD [μm]	2.40 \pm 0.08	2.52 \pm 0.05	2.36 \pm 0.04	2.13 \pm 0.05	2.29 \pm 0.05	2.08 \pm 0.01
GSD	1.81 \pm 0.06	1.82 \pm 0.06	1.82 \pm 0.06	1.75 \pm 0.06	1.82 \pm 0.05	1.77 \pm 0.01
FPD (μg < 5 μm)	5.57 \pm 0.15	6.38 \pm 0.16	4.85 \pm 0.28	3.39 \pm 0.18	5.23 \pm 0.20	4.30 \pm 0.16
	CS_15.8%	CS_0.5%	CS_15.8%	CS_0.5%	CS_15.8%	CS_0.5%
	1 month	1 month	3 months	3 months	6 months	6 months
FPF (% < 5 μm)	3.30 \pm 0.07	2.60 \pm 0.10	3.09 \pm 0.15	3.06 \pm 0.16	3.24 \pm 0.05	3.07 \pm 0.24
MMAD [μm]	2.35 \pm 0.01	2.11 \pm 0.02	2.29 \pm 0.03	2.05 \pm 0.01	2.09 \pm 0.13	1.83 \pm 0.03
GSD	1.69 \pm 0.02	1.57 \pm 0.01	1.66 \pm 0.02	1.63 \pm 0.02	1.84 \pm 0.09	1.69 \pm 0.03
FPD (μg < 5 μm)	4.35 \pm 0.28	3.78 \pm 0.21	4.36 \pm 0.16	4.70 \pm 0.26	4.90 \pm 0.02	5.04 \pm 0.51

A significant change in morphology (for pure CS) can be again observed by SEM analysis for the samples conditioned with isopropanol for 2 hours. The shape of these particles turned once more from an angular shape to a more spherical shape and a smooth surface which may reduce inter-particle contacts.

However, a change in surface morphology of the APIs was determined after the blending process with the glass beads by SEM. The pictures demonstrate that the spherical shape/surface of the glass beads are coated by the API particles (Figure 100).

Almost a thin and continuous film appeared on the surface. These API crystals are solidified during the mixing time (film formation). A change in particle shape is the logical consequence (particle fusion). Significant differences in particle size and shape were not determined for SBS (A) and CS (B) in figure 100. These findings might explain a similar low FPF for both types of API.

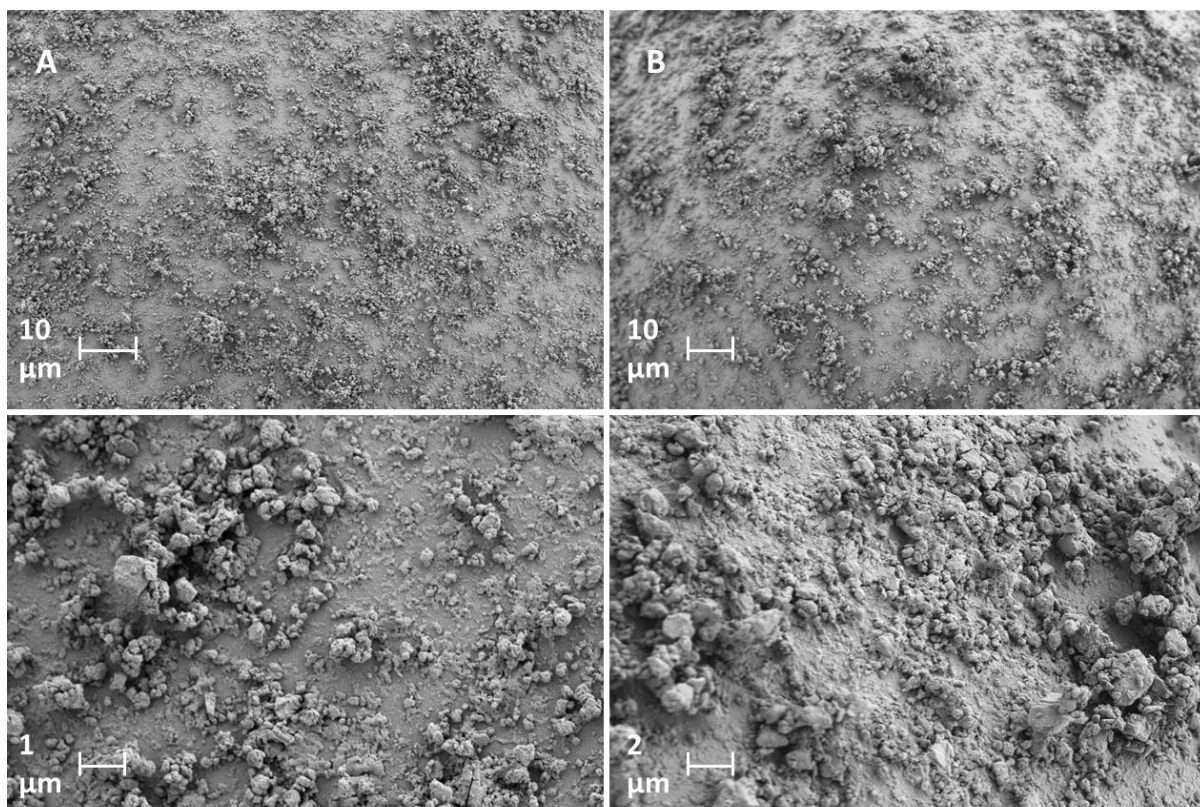


Figure 100: SEM pictures of the thin API-film on the surface of glass beads formulation with (A) SBS and (B) CS

4.4.2.3 Schematic model based on NGI results (Study 2)

The type of carrier has a fundamental influence on the API particles. Especially, the particle size and shape is modified during the mixing procedure. Similar results were received when mixing for 15 to 45 minutes. Higher centrifugal forces were achieved which originated from the increased weight of the glass beads compared to the lactose carrier. This behavior led to a crushing of the crystal shape and solidified a thin film on the surface (Figure 101).

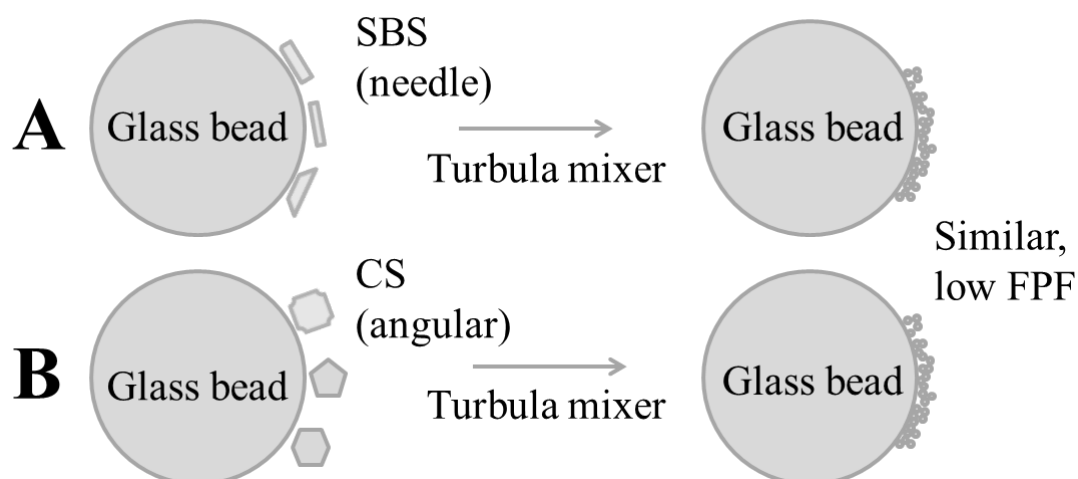


Figure 101: Change of crystal shape during the mixing process

Finally for both APIs a low and comparable FPFs were determined that did not change during the storage at 45% RH over 6 months.

4.4.3 Conclusion III

The aerodynamic investigations demonstrated that the amorphous content has a huge influence on the FPFs. The hydrophilic SBS showed a high trend for re-crystallization over the storage time. Thereby, a change in the surface morphology is assumed. These modifications are reinforced by a hydrophilic carrier (e.g. lactose). Finally, capillary forces and solid material bridges complicate the detaching of API particles. After 6 months both types of blends showed almost similar FPFs.

The hydrophobic API seems to be less affected by water vapor (45%). Electrostatic charges and a reduction of hydrogen bonds lead to higher FPFs over storage time. A significant difference was detected for both blends in the smooth surface of the initially re-crystallized API (isopropanol). This re-crystallized blend showed an increase in FPFs over the whole storage time.

Low FPFs were determined for both blends with glass beads. An increase in the press-on forces led to a thin API film on the surface of the beads. Figure 102 shows a possible mechanism; hereby the structure of the glass beads surface enables a higher compaction of the API crystals during the collision over the mixing time. The resulted binding forces cause a low de-agglomeration behavior.

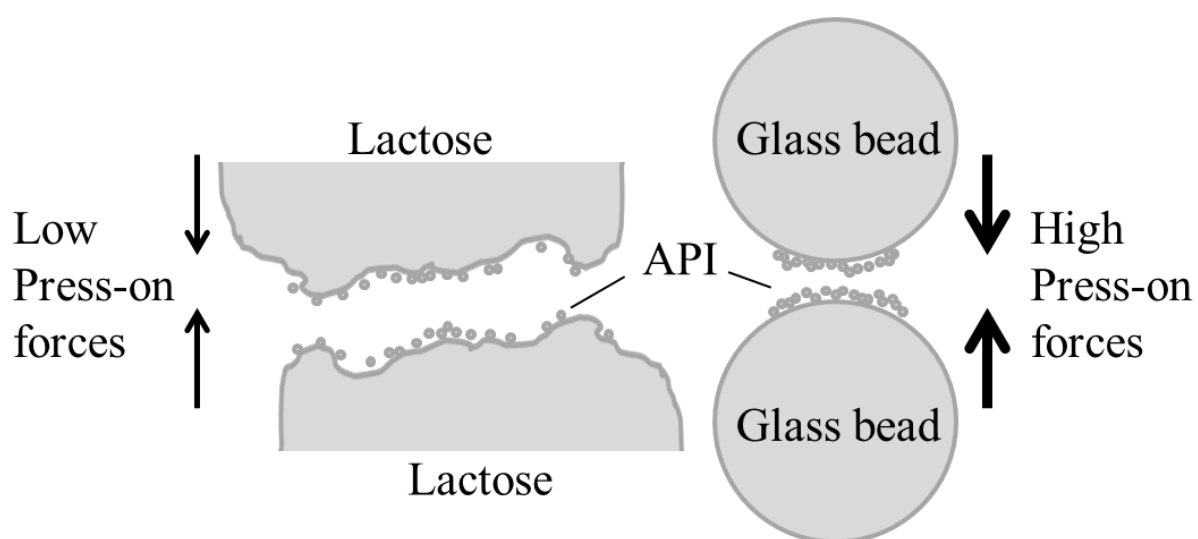


Figure 102: Press-on forces on different types of carrier (lactose/glass bead) modified from de Boer et al., 2006

On the contrary, API particles which were agglomerated on a rough and heterogenic lactose surface were less compacted. An increased binding capacity and a higher degree of saturation of the active lactose carrier sites (g/m^2) were determined [165].

In summary, it is necessary that amorphous amounts are determined and further re-crystallized under controlled conditions. Otherwise the product stability is not guaranteed because of the possibility of a re-crystallization and a change in the particle size (crystal growth) [166]. Ultimately, an impact on the dissolution characteristics or drug delivery cannot be ruled out.

4.5 Dissolution testing

The dissolution testing is an extremely well established and standardized method in all Pharmacopoeias for evaluating solid and semi-solid dosage forms [167]. It is defined as the process by which a solid substance enters into a solvent to yield a solution. This solubility is controlled by the affinity between the solid substance and the solvent [168]. Furthermore, it allows the investigation of the dissolution behavior *in-vitro* to provide some predictions of the dissolution behavior *in-vivo* [169]. These release methods are routinely used in the quality control/R&D sector and enable the specification of batch-to-batch consistency and the estimations of stability issues. However, several factors can influence the dissolution process, such as the particle size and surface, the wettability of the materials, the temperature, pH value, the stirring speed and the surrounding concentration of already dissolved substance in the medium [170].

Up to this date there is no compendial dissolution method for testing aerosols compared to standardized dissolution test methods for solid dosage forms such as tablets and capsules. Unfortunately, it is not an easy task to truthfully model the lung and simulate small amounts of aqueous fluids and the lung surfactant [171]. Furthermore, the dose collection of the API is challenging because of very fine and electrostatic powder characteristics [172]. For example, the deposition can be determined using initially impactor systems (e.g. Andersen Cascade Impactor). Afterward, the solubility of these particles (less than $5\ \mu\text{m}$) can be characterized by different dissolution techniques. May et al. compared the flow through cell, Franz diffusion cell and paddle apparatus 2 and studied their ability to differentiate between various formulations [173]. Basically the dissolution process is characterized by the dissolution rate, the dose-to-solubility ratio and the permeation rate [174] and is poorly indicated for hydrophobic substances. The biopharmaceutical classification system (BCS) was introduced and hydrophilic and hydrophobic drugs were categorized based on their aqueous solubility and intestinal per-

meability into four different classes. Hereby, low dose-to-solubility ratio/high permeability (as class I), high dose-to-solubility ratio/high permeability (as class II), low dose-to-solubility ratio/low permeability (as class III) and high dose-to-solubility ratio/low permeability (as class IV) are defined [175].

In this part of the study the applicability of the introduced dissolution testing system (ACI and USP paddle apparatus 2) is investigated for SBS and CS (Figure 103).

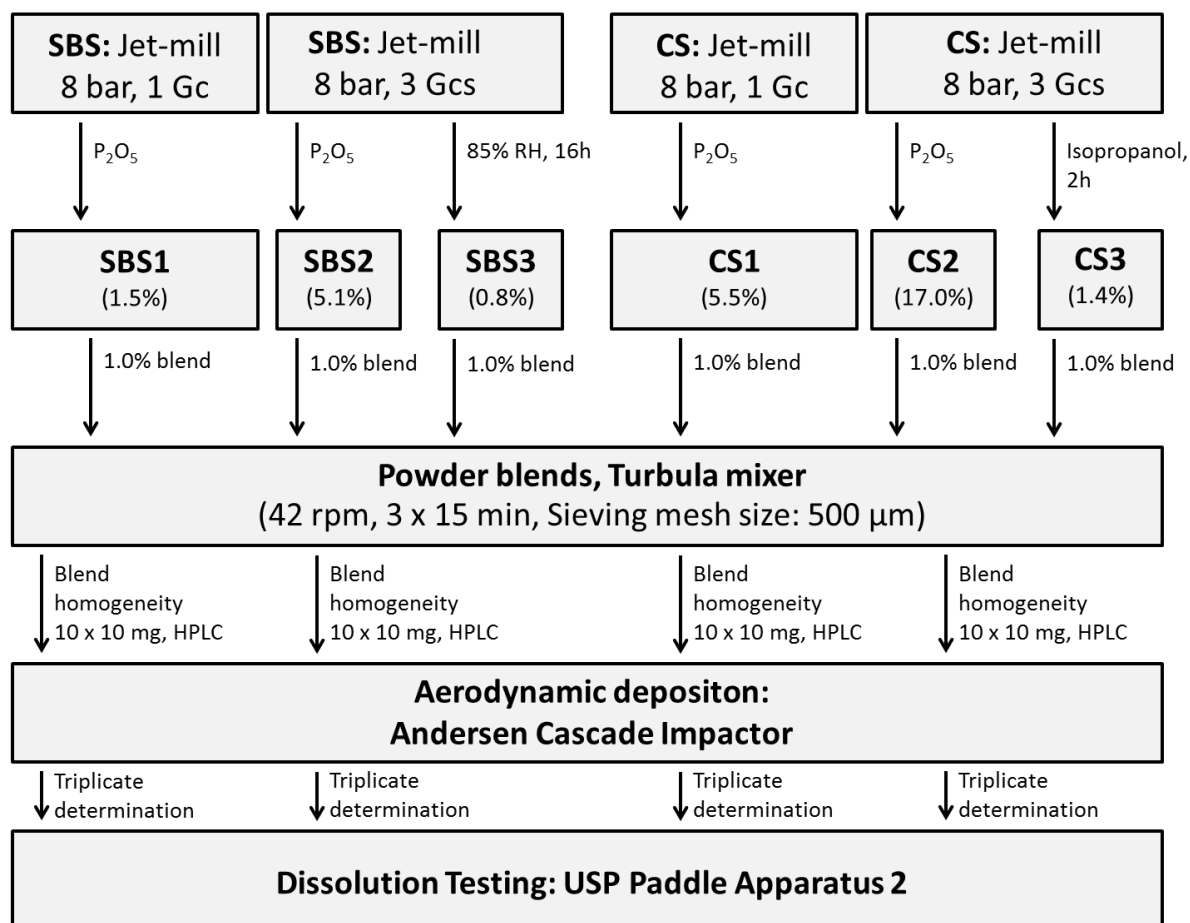


Figure 103: Overview of the dissolution testing

The objective is to evaluate the influence of different amorphous amounts in inhalation powders on the dissolution rate. Three different blends with low, middle and high amorphous amounts were prepared. These amounts were achieved by different jet-milling parameters and varied storage conditions. In addition, hydrophilic and hydrophobic characteristics were studied with the attention on SBS and CS. The blends with lactose as a carrier were prepared and tested for a homogenous distribution. Finally, the ACI (Device: Easyhaler[®]) with modified filter stage (better sedimentation) was utilized to collect a defined amount of fine powder on a membrane (dose collection) [126,127]. In the last step the API that was impacted on the membrane was released in triplicate determination by a USP paddle apparatus 2.

4.5.1 Bulk powder and blend characterization

It should be mentioned that the same bulk powders (type 2 and 3 for both APIs) were prepared in the same week for the production of the blends for study 1 (aerodynamic deposition) and for the dissolution testing (Table 23). Only the PSD of the micronized powder with one grinding cycle (SBS 1 and CS 1) is presented at this point and is as well strongly reduced in size compared to the crystalline starting material (Table 31).

Table 31: PSD and amorphous content of the conditioned SBS and CS samples for the dissolution testing

Sample	x_{50}	Span	Amorphous content [%]
Respitose SV003	57.92 ± 0.15	0.99 ± 0.02	/
SBS starting material	9.11 ± 0.07	3.44 ± 0.11	/
SBS 1	2.87 ± 0.01	3.15 ± 0.08	1.51 ± 0.34
CS starting material	57.90 ± 2.96	4.91 ± 0.16	/
CS 1	2.38 ± 0.10	2.36 ± 0.12	5.48 ± 0.22

The API bulk powder SBS 1 and CS 1 showed a larger particle size because of the one grinding cycle that was conducted compared to the SBS 2 and CS 2 (3 Gc). Furthermore, an increase of the amorphous amount was induced by a higher number of grinding cycles for these powders. The particle size distribution and the amorphous content are API properties that might significantly influence the dissolution profile.

Table 32 shows the characteristic parameters of the homogenous 1.0% API blends.

Table 32: Content uniformity of the blended inhalable mixtures for the dissolution testing

Blend	Content [%]	sd	CV [%]	Recovery [%]
SBS 1	1.0255	0.0436	4.2559	101.2405
SBS 2	0.9884	0.0192	1.9435	98.8812
SBS 3	1.0105	0.0363	3.5880	101.1005
CS 1	1.0047	0.0287	2.8581	100.4317
CS 2	1.0490	0.1018	3.9217	101.8788
CS 3	0.9966	0.0672	1.7043	97.5235

The coefficient of variation for these homogenous mixtures was below 5% for all formulations. This result indicates a suitable mixing time (3×15 minutes) and mixing speed (42 rpm). A trend in the re-crystallized APIs (SBS 3/CS 3) to result in a less homogenous mixture was not detectable. Also, a significant drug loss for both types of blends was not determined ($\pm 2.0\%$).

The scanning electron microscopy again demonstrated typical needle shaped crystals for the SBS samples. Very small particles ($2 \mu\text{m}$) with a rougher surface were visible for all micronized powders. Larger particles were determined for SBS 1 (1 Gc) compared to SBS 2 and SBS 3 (Figure 104). These results can be correlated to the PSDs determined by laser diffraction analysis. Furthermore, the re-crystallized powder (SBS 3) did not show a significant change in surface morphology and particle size ($2 \mu\text{m}$). An intensified particle agglomeration because of a higher humidity (85% RH) was not visible on various magnifications for SBS 3 compared to SBS 2.

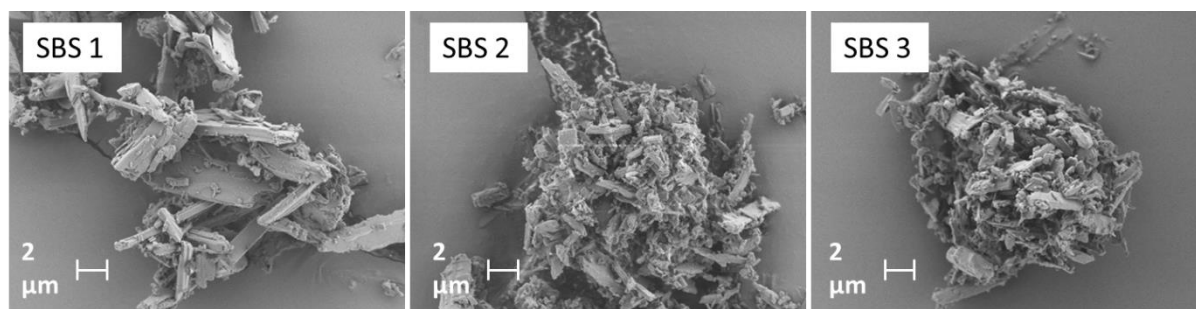


Figure 104: SEM pictures of the bulk powders for SBS

In contrary, the CS samples showed a more angular particle shape (Figure 105). For all micronized powders a small particle size distribution was determined (approximately $2 \mu\text{m}$). In addition, larger particles were visualized for CS 1 (1 Gc).

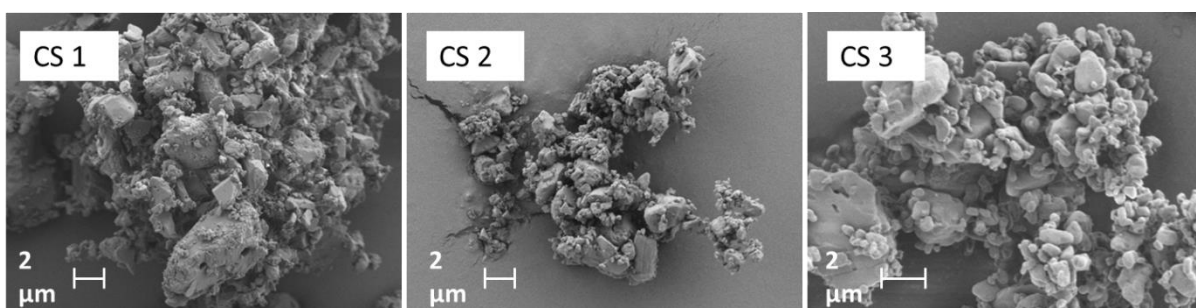


Figure 105: SEM pictures of the bulk powders for CS

A change in the surface morphology was visible for CS 3. The smooth surface is a characteristic for the re-crystallized sample (2 h, over isopropanol). The result was comparable to other re-crystallized CS samples with isopropanol (Chapter 4.3.2.1).

4.5.2 Optimization of the phosphate buffer as dissolution media for CS

In general, solubility is defined as the degree to which a hydrophilic or hydrophobic substance dissolves in any solvent to reach a homogenous solution. As mentioned the solubility of substances differs and is strongly dependent on the chemical properties of the API and the solvent. Particle properties (such as particle size, morphology and amorphous content) are predefined by the production method (jet-milling) and the conditioning process, respectively. These API properties should eventually enable a determination of different dissolution profiles of the prepared inhalable blends possible. During the release investigation a constant temperature and pH value of the dissolution media should allow comparable and reproducible process parameters.

In consequence to the poor solubility behavior of CS only the dissolution media can be optimized by adding different and various amounts of surfactants. Sodium dodecyl sulfate (SDS), Tween[®] 20 and Plasdone[®] were screened in a preliminary test (Figure 106).

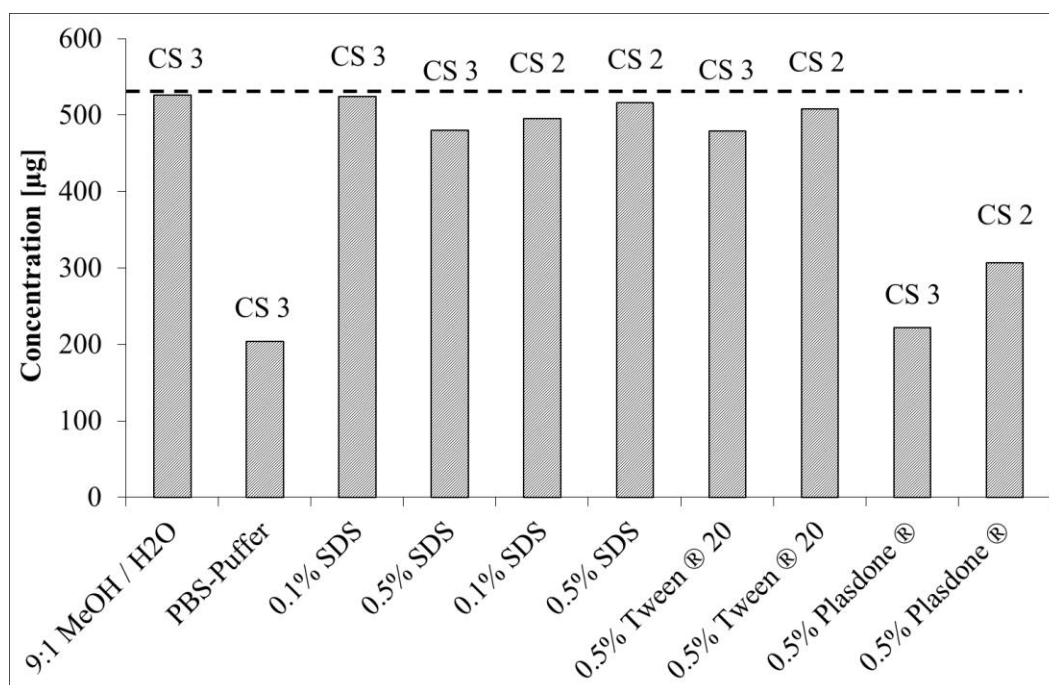


Figure 106: Solubility test of CS by adding different and various amounts of surfactants

First, a mixture of methanol and water (9:1) was prepared to determine the maximal solubility of the hydrophobic CS (100% of recovery). Pure phosphate buffered saline (PBS, pH 7.4) was

used to access the poor solubility of CS (minimal concentration). The API recovery rate was determined at 41.6% without surfactant (Table 33). Afterward, defined amounts of SDS (0.1% and 0.5%), Tween[®] 20 (0.5%) and Plasdane[®] (0.5%) were added to 100 ml of PBS buffer and used for the solubility test with high (CS 2) and low (CS 3) amorphous amounts in a beaker. For almost all surfactants the recovery was significantly increased. Especially SDS and Tween[®] 20 led to a recovery rate of almost 100%. Unfortunately, this data cannot give an indication of the influence of the amorphous amounts on the dissolution rate for further conducted dissolution tests.

It is assumed that the blends may show higher dissolution rates/permeation rates when containing an increased amorphous amount which is the case for CS 2 (17.0%). An increase of the solubility (4.2%) compared to pure PBS buffer and an increase of the solubility rate with regard to the amorphous amounts (13.0%) was realized only with the surfactant Plasdane[®].

Table 33: Screening for an optimized solubility of CS powder samples

Solution	Sample	Concentration [μg]	Recovery [%]
9:1 MeOH/H ₂ O	CS 3	526.42	101.63
PBS-Puffer	CS 3	203.68	41.57
0.1% SDS	CS 3	524.12	102.17
0.5% SDS	CS 3	480.00	98.77
0.1% SDS	CS 2	495.36	96.19
0.5% SDS	CS 2	516.25	98.33
0.5% Tween [®] 20	CS 3	479.28	97.81
0.5% Tween [®] 20	CS 2	508.10	96.41
0.5% Plasdane [®]	CS 3	221.82	45.74
0.5% Plasdane [®]	CS 2	306.69	58.75

Further solubility tests showed that a significantly higher amount of the hydrophobic CS is soluble (Figure 107). Nearly 25% of this poor soluble API can be solved when enhanced by the surfactant Plasdane[®]. Normally it is used to manufacture wet granulates, dry granulates or to facilitate the direct compression whereas in this approach it is used to increase the viscosity/solubility of the dissolution media. A significant improvement in the solubility was recog-

nized for CS 2 compared to CS 1. The higher amorphous amount can cause this effect. Nevertheless, this trend was not visible for CS 3 (re-crystallized with isopropanol). It is assumed that residual solvent molecules can facilitate the drug wetting and thereby result in a higher soluble API amount.

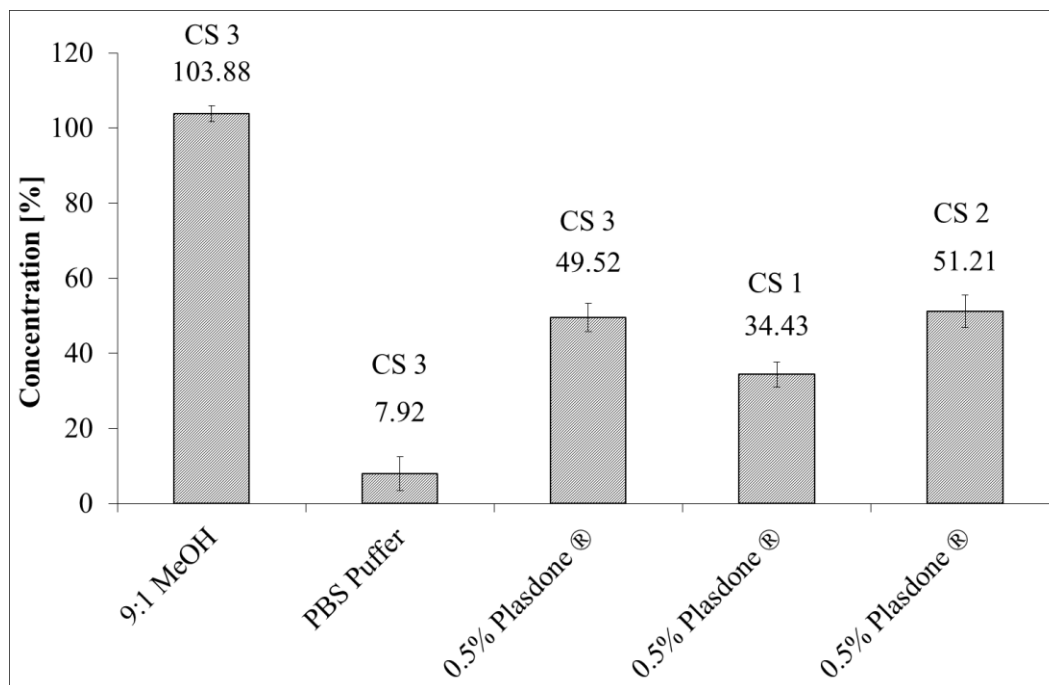


Figure 107: Adding of 0.5% Plasdone® for higher solubility of CS samples

Furthermore, adding very low concentrations of SDS (0.05%) to improve the solubility of hydrophobic CS were investigated (Figure 108). In the first screening tests concentrations of 0.1% and 0.5% led to completely solved API amount. Blends containing higher amorphous amounts may improve the solubility of CS and can be compared to the results achieved with Plasdone®. The soluble amount of the re-crystallized sample (CS 3) was greater than CS 1 (amorphous content of 5.5%). Nevertheless, all samples showed an increase in the solubility when adding 0.05% SDS although the total amount was significantly lower than with the surfactant Plasdone®. As a result to these findings 0.5% of Plasdone® was added to the dissolution media for the quantification of the poorly soluble CS powder samples in the dissolution tests. This type of surfactant might allow the discrimination between the dissolution rates/total amounts of blends containing varying amorphous amounts.

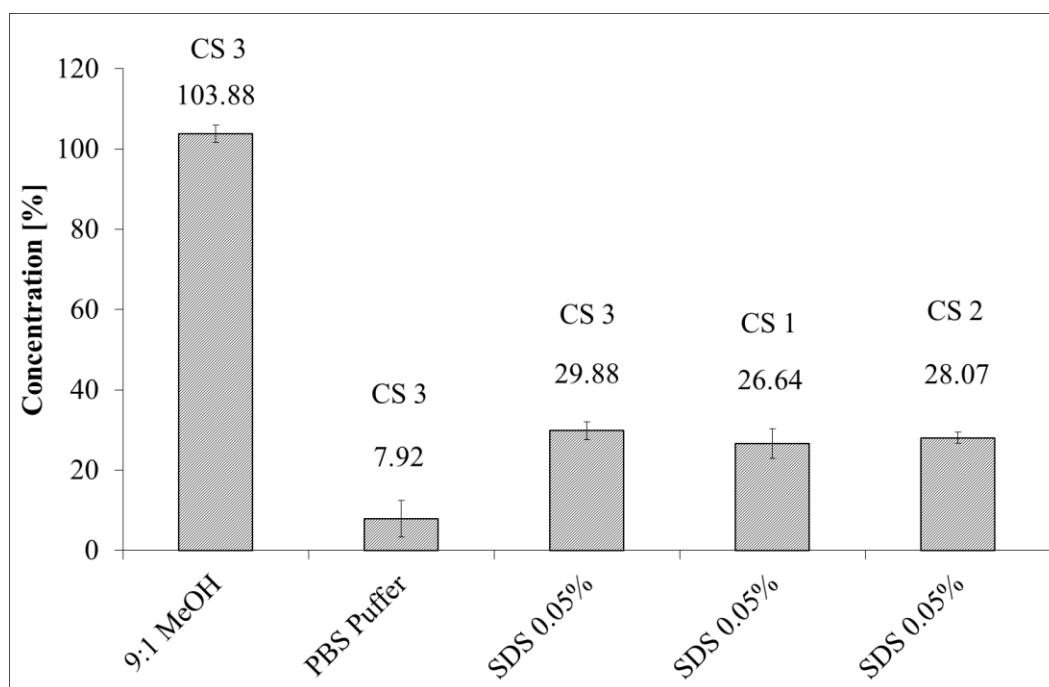


Figure 108: Adding of 0.05% SDS for higher solubility of CS samples

4.5.3 Optimization of the dose collection for SBS and CS with the Andersen Cascade Impactor (ACI)

Upon the optimization of the dissolution media the dose collection had to be adapted for SBS and CS. The aim was to define equal doses of both APIs on the membrane. Therefore, the Andersen Cascade Impactor and two types of filter stages were used. The first filter stage consists of a high number of little cavities and the second one persists of three large openings (highlighted with O in each figure). On top of these stages a regenerated cellulose membrane filter was placed to collect the amount of the fine particle doses (FPDs). Afterward, the concentration of the API was determined by the validated HPLC analytic. The deposition experiments were conducted with the HandiHaler[®] where the produced API blends were filled into capsules, respectively. After each inhalation (capsule) the sedimentation time was set to 5 minutes to ensure the complete impaction of the powder on the membrane. Figure 109 shows the deposition of each SBS blend. A significant trend was visible with regard to the number of capsules. As expected the API concentration was increased with the usage of more and more capsules for all three blends. No differences in the deposition behavior for SBS 1, SBS 2 and SBS 3 were detectable. The second type of filter stage (O) led to very low concentrations despite a high number of used capsules.

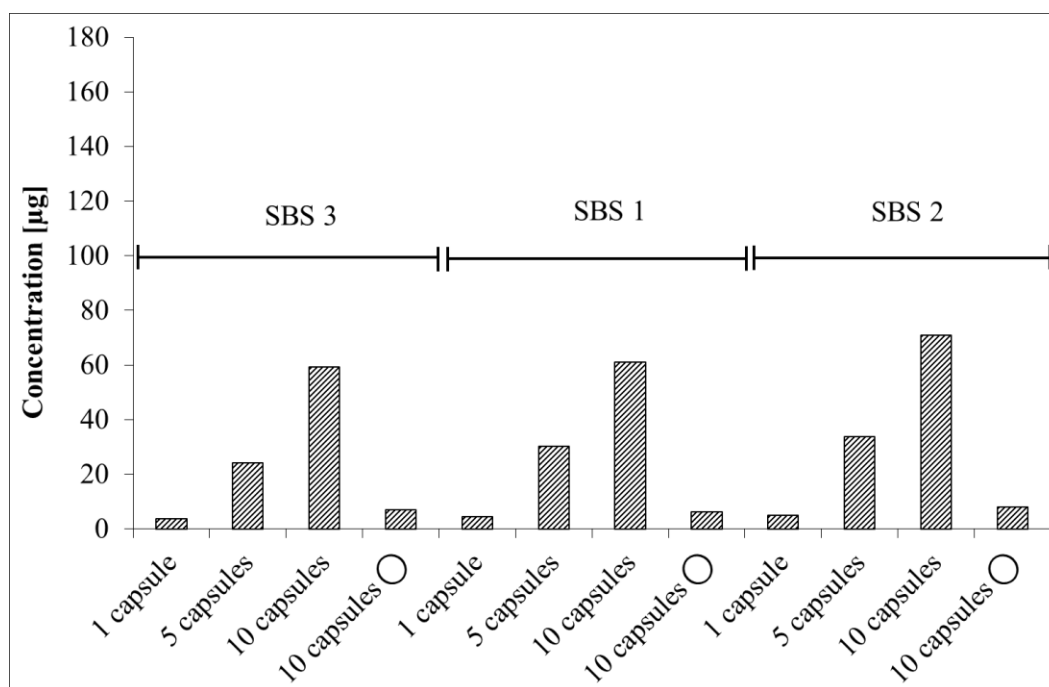


Figure 109: Impaction of SBS blends in dependence to multi dosing (HandiHaler®)

On the contrary, lower concentrations were reached for CS (Figure 110). It is assumed that the particle shape has an enormous influence on the deposition behavior. The crystal needles of SBS might reach the final stages of the Andersen Cascade Impactor easier.

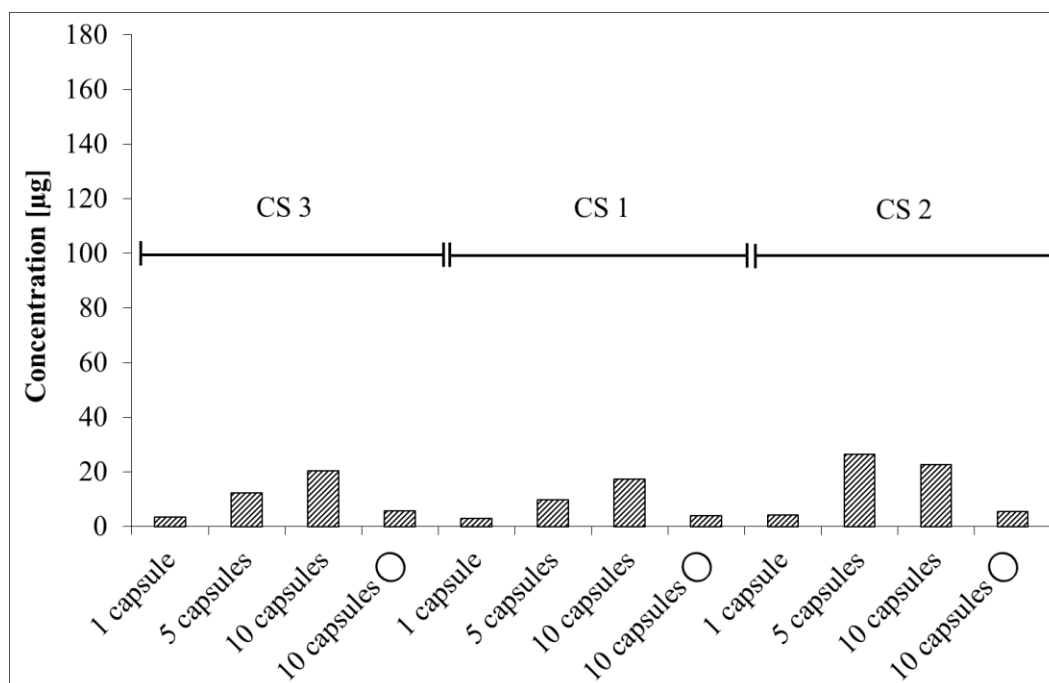


Figure 110: Impaction of CS blends in dependence to multi dosing (HandiHaler®)

Nevertheless, an increase of the API deposition was determined with regard to a higher number of capsules used. An exception is blend CS 2. Again, lower depositions were detected for the second type of filter stage (O). In summary, the amount of CS is not sufficient for a suitable

ble dissolution testing therefore another type of device (Easyhaler[®]) was investigated where an increase in FPD should be found.

Figure 111 shows the deposition behavior of each SBS blend that was applied to the Andersen Cascade Impactor with the Easyhaler[®]. Fortunately, a higher amount of API was determined compared to the HandiHaler[®] (nearly double quantity). Again, a significant trend was visible with regard to the number of actuations which resulted in an increase of the API concentration on the membrane.

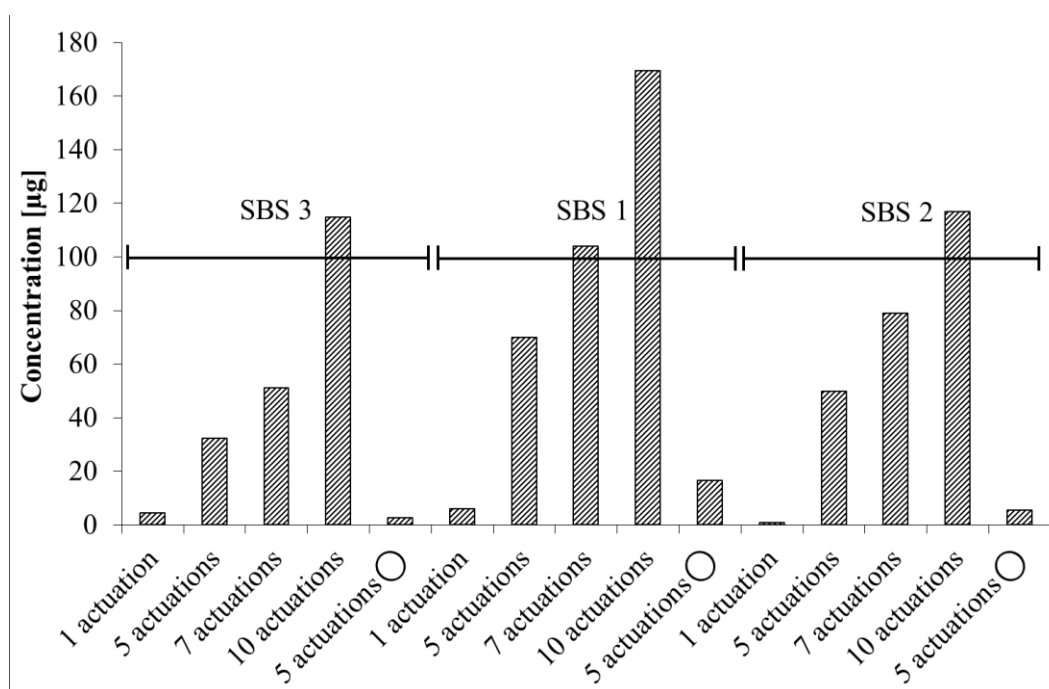


Figure 111: Impaction of SBS blends in dependence to multi dosing (Easyhaler[®])

In general, the blend SBS 1 showed the highest amounts despite the largest measured x_{50} value. These findings were not manifested in the first impaction analysis with the HandiHaler[®]. As sedimentation is one of the assumed mechanisms it appears reasonable. The second type of filter stage (O) again led to very low concentration despite 5 actuations.

An increase in the concentration was also well determined for the hydrophobic CS (at least a third of the amount impacted with the HandiHaler[®]). In addition, an increase of the API deposition was determined due to a higher number of actuations (Figure 112). But in comparison to the SBS blends only a half of the quantity was impacted on the membrane.

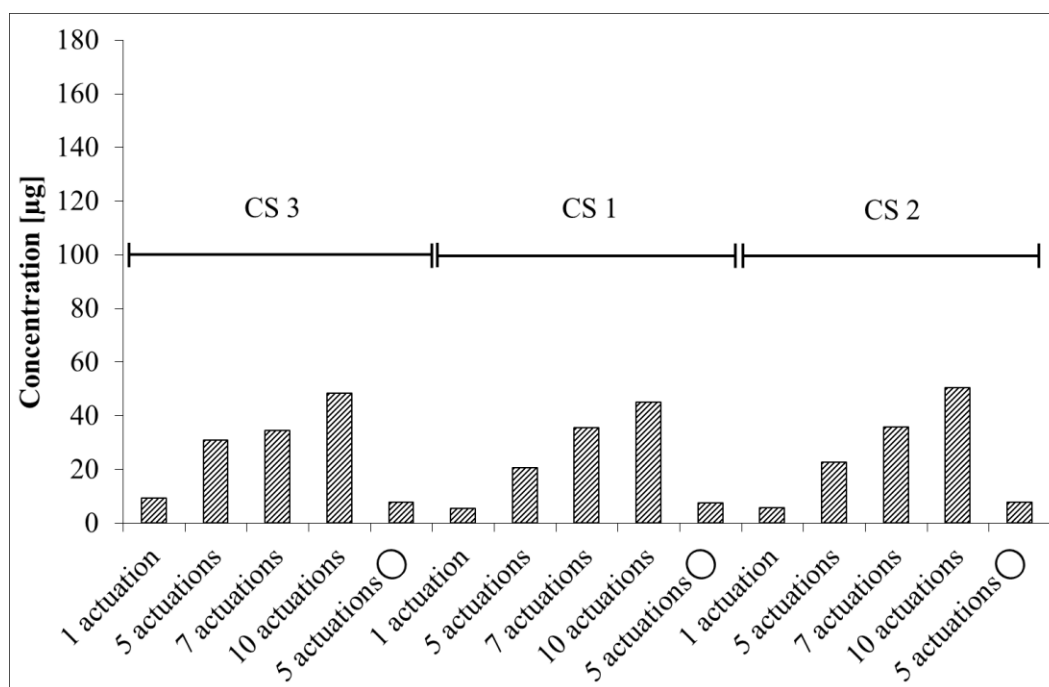


Figure 112: Impaction of CS blends in dependence to multi dosing (Easyhaler®)

As a final conclusion the Easyhaler® was selected to apply the powder blends to the impactor in the following dissolution testing. Finally, the number of actuations was determined which facilitates the impaction of similar amounts of APIs on the membrane. Therefore it is necessary that higher actuations are conducted in case of the hydrophobic CS blends compared to the hydrophilic SBS blends.

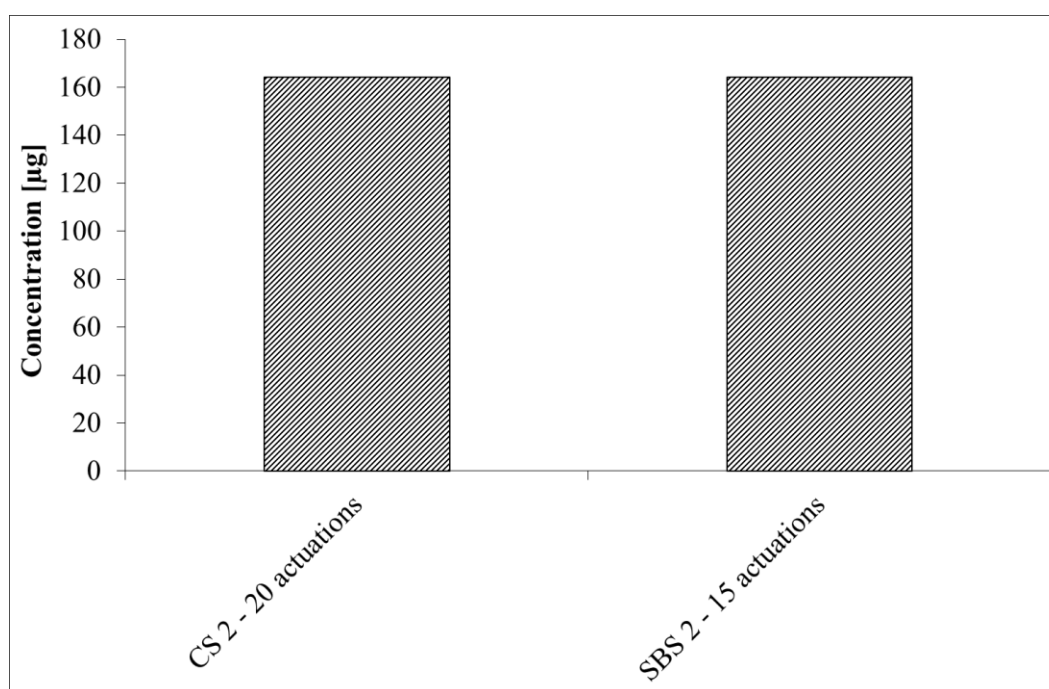


Figure 113: Equal doses of both blends because of different actuations applied with the Easyhaler®

The final investigation led to the conclusion that 20 actuations are needed for CS using the Easyhaler[®] compared to only 15 actuations for SBS to impact equal FPDs (160 µg) on the membrane, respectively (Figure 113).

4.5.4 Burst release and poor solubility

Using the Easyhaler[®] (15 actuations) and ACI a final dose collection was conducted for SBS on the membrane. Afterward, a watch glass and a plastic mesh were used to fix the membrane (standard membrane holder). Finally, the dissolution testing was performed with a stirring speed of 100 rpm at 37 °C in PBS buffer pH 7.4 in the paddle apparatus 2. The dissolution media was optimized with 0.5% of Plasdone[®] for the hydrophobic samples.

Figure 114 shows the concentrations of each SBS blend in the paddle apparatus with the membrane holder over the time of 248 minutes. Despite the 15 equal actuations it can be seen that different API amounts were solved. Especially, the concentration of SBS 1 was significantly increased (middle amorphous content and largest particle size). This result can be correlated to figure 111 where it was noticed that SBS 1 led to the highest deposition amounts on the membrane. SBS 2 and SBS 3 demonstrated a similar release and thus the discrimination between the dissolution profiles/rates could not be achieved.

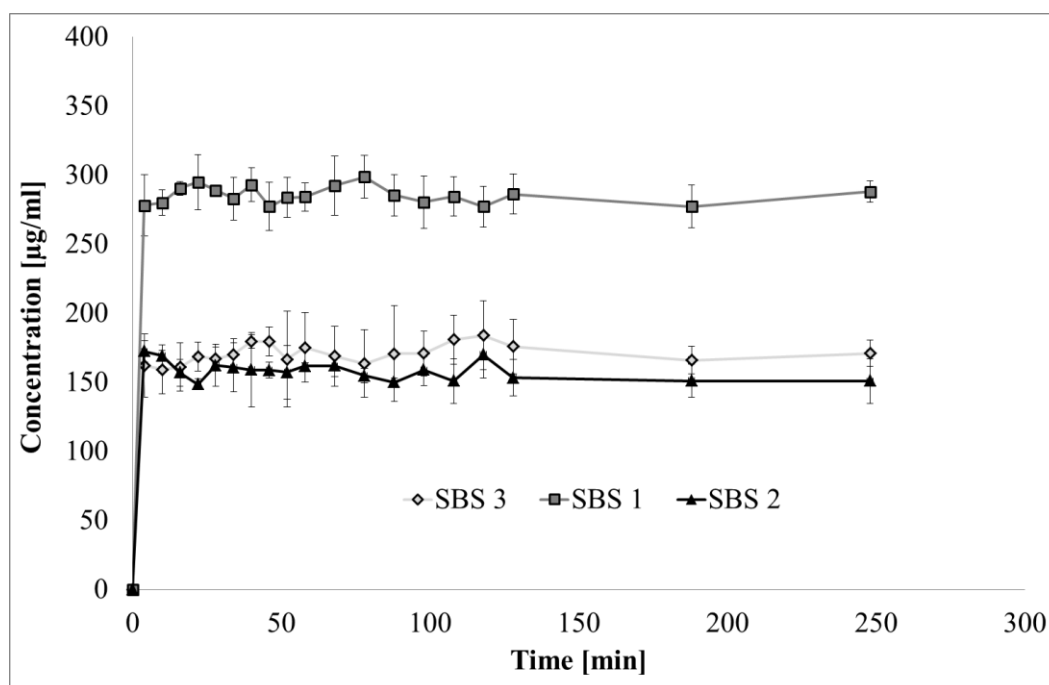


Figure 114: Absolute amount of each SBS blend dissolved over 4 hours

It can be assumed that the blend containing the highest amorphous amount (SBS 2) led to a re-crystallization during the handling and afterward was comparable to the initially re-

crystallized (SBS 3). The amorphous SBS 2 demonstrates an increased affinity to water vapor. In contrast the SBS 1 blend which contains a lower amorphous content might be more stable over handling.

After the dissolution testing the residual amounts of API on the membrane and on the watch glass were determined by washing both parts (Figure 115). For all SBS samples very low residual concentrations were detected on the membrane and on the watch glass. A significant difference between SBS 1, SBS 2 and SBS 3 was not detected.

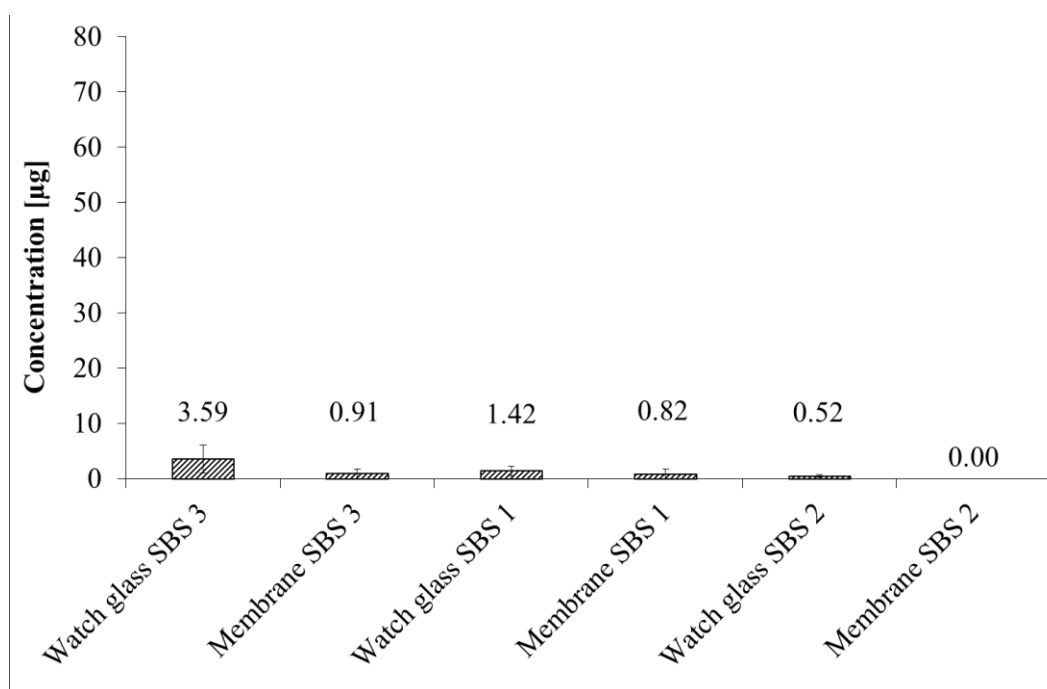


Figure 115: Residual amounts of each SBS blend on the watch glass and on the membrane

In addition, the concentration on the watch glass was increased compared to the cellulose membrane. In conclusion, it is supposed that nearly the entire amount of hydrophilic API was solved in the dissolution testing over 4 hours.

The total amount of drug that was initially loaded on the membrane was determined using the maximum of the cumulatively released amounts and adding the remaining quantity on the membrane determined at the end of each experiment. The fraction of released drug was calculated by dividing the amount of drug released with the initial drug mass loaded on the membrane.

Figure 116 demonstrates the calculated dissolved amount of each SBS blend. The sampling was automated according to a defined time schedule. For all hydrophilic blends a high solubility was detected (nearly 100%). Unfortunately, the whole amount of API impacted on the

membrane was released after 4 minutes and the concentration barley changed over 248 minutes. Only at the first sampling the released amount of drug can be correlated to the amorphous content (SBS 3 < SBS 1 < SBS 2). However, this burst release did not enable the discrimination between the single dissolution profiles. An influence of the amorphous content was not demonstrated because of the hydrophilic characteristics and the thereby resulted fast release (high dissolution rate and high permeation rate). This release behavior can also be linked to the processing conditions, surface characteristics and particle morphology of the hydrophilic fine particles [176].

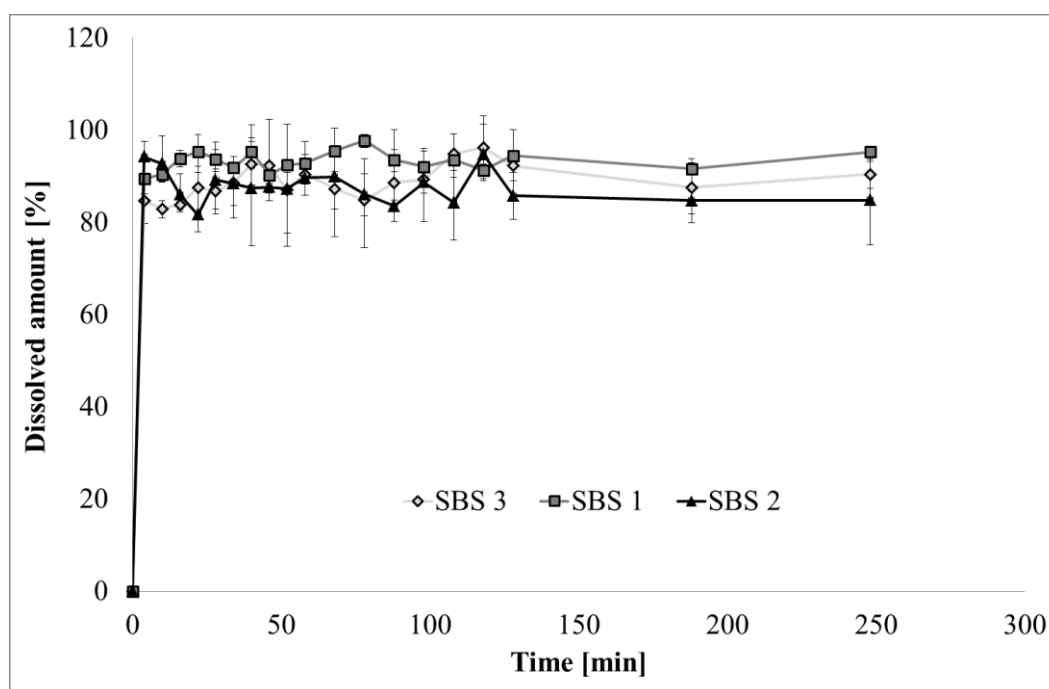


Figure 116: Release profiles of the SBS blends with different amorphous amounts

In summary, these profiles might explain the quick stimulation of the β_2 -adrenergic receptors and the induced bronchodilating effect in reversible, obstructive airway diseases such as bronchial asthma. Following the oral administration this effect might occur within 2 to 3 hours [177]. In addition, due to its high solubility and permeability, SBS is considered a class I drug by the Biopharmaceutics Classification System (BCS). As an amphoteric compound with an acidic phenolic group and a basic secondary amine group it has two ionization constants ($pK_{a1} = 9.07$ and $pK_{a2} = 10.37$). At the used physiological pH its solubility is not expected to be affected by its ionization [178].

On the contrary, the dissolution experiment of each CS blend did not show a measureable concentration in the paddle apparatus with membrane holder (Figure 117). It was not possible to solve even minimal concentrations despite the optimized 20 actuations (increase of FPD)

and the optimization of the dissolution media which contains an additional of surfactant (0.5% Plasdone[®]). Even for the blends containing higher amorphous amounts (CS 1 and CS 2) a release from API of the standard membrane holder was not possible.

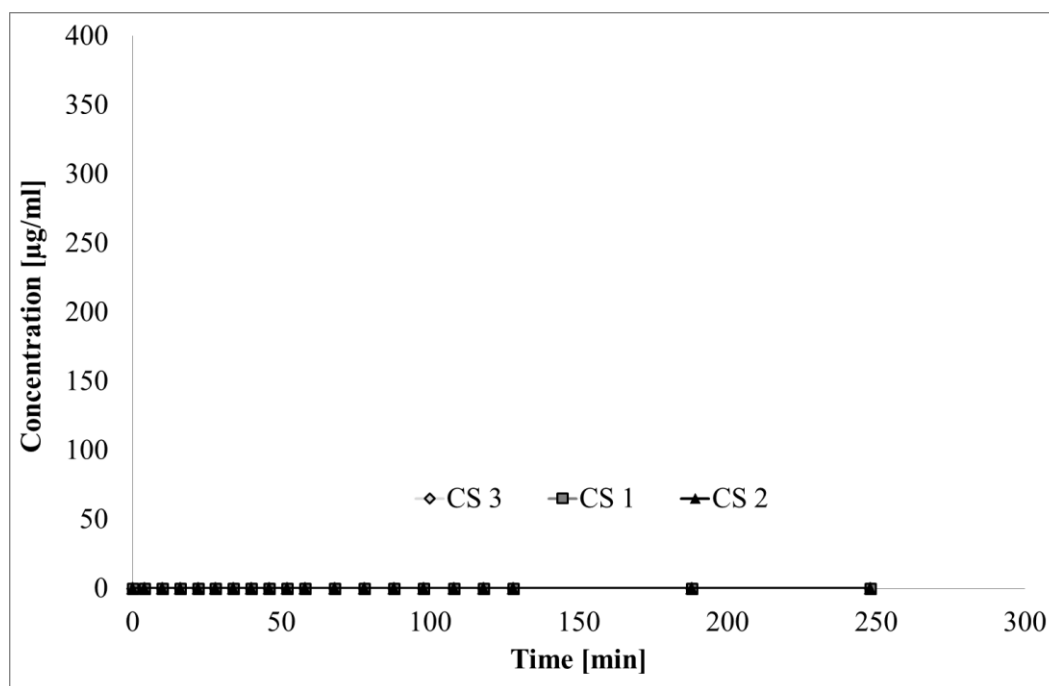


Figure 117: Absolute amount of the CS blends dissolved after 4 hours

It is assumed that the very hydrophobic API is more inert against the hydrophilic dissolution media and therefore poorly soluble. Maybe the type of dissolution apparatus is not suitable or the release of the standard membrane holder is not adequate. In the solubility experiments conducted in a beaker it was shown that this poor soluble API might solve when enhanced by the surfactant Plasdone[®] (Chapter 4.5.2). These findings were not confirmed when transferring them to the USP apparatus 2. Furthermore, a higher affinity to the membrane could be one reason for a poor solubility. Probably high hydrophobic binding forces led to strong interactions [179]. The adhesion forces might be reinforced by cohesive properties between individual CS particles. In summary, it is surprising that no release was detectable despite a small particle size ($< 5 \mu\text{m}$) and the resulting increase of the surface area for all CS blends.

The residual amounts of CS were determined by washing the cellulose membrane and the watch glass (Figure 118). As expected, high concentrations were detected on these membranes for all CS blends. The concentration on the watch glass was rather little. A significant trend was determined for the blends of CS 3, CS 1 and CS 2. The decrease of the concentration on the membrane was visible with regard to higher amorphous amounts. In conclusion, it is supposed that nearly the entire amount of hydrophobic API was not solved in the dissolu-

tion testing over 4 hours. A reason could be a low wettability because of the highly hydrophobic properties.

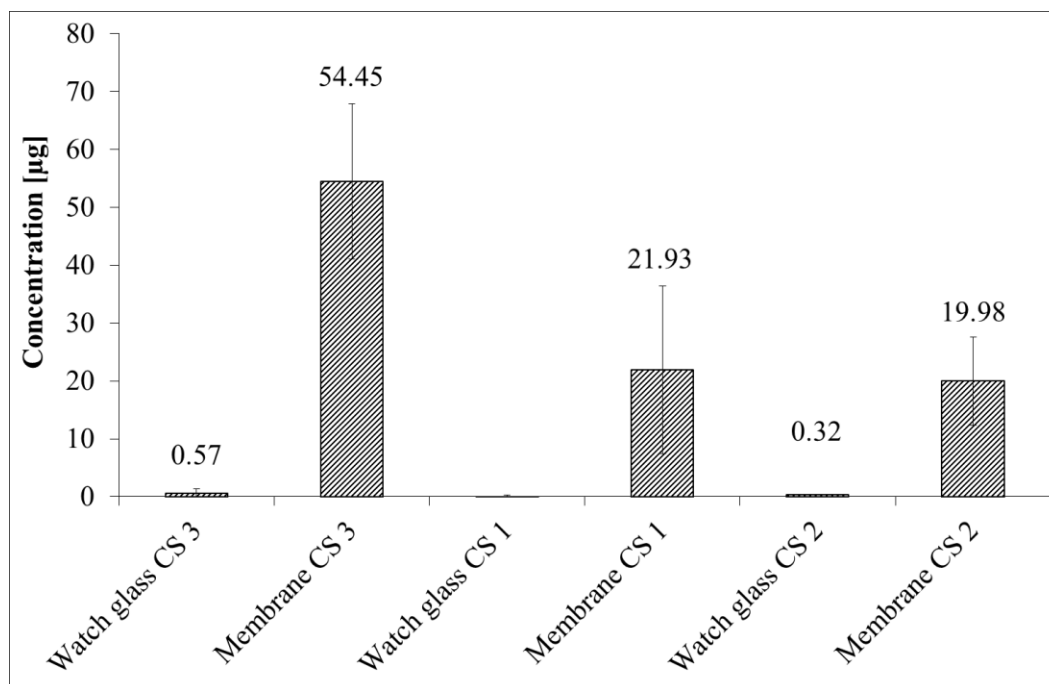


Figure 118: Residual amounts of each CS blend on the watch glass and membrane

4.5.5 Conclusion IV

The dissolution testing demonstrated a diverse behavior for both types of APIs. Dissolution profiles were obtained after the optimization of the dose collection (ACI + Easyhaler[®]) for hydrophilic SBS samples. The improvement of the solubility of the dissolution media (Plasdone[®]) for the hydrophobic substance (CS) did not lead to dissolution profiles.

The hydrophilic blends demonstrated a fast release through the membrane. A difference in the release speed corresponding to the amorphous amounts (low to high) was not recognized. All blends nearly showed a complete dissolving after a few minutes (burst release). Figure 119 might explain a feasible mechanism of these findings. The hydrophilic SBS offers a high wettability and therefore a good solubility in this dissolution media. The diffusion layer (liquid layer) adheres easily to the solid surface of this hydrophilic drug.

Furthermore, the thickness of liquid layer is influenced by the particle size distribution (μm) [180] and the paddle speed (rpm) [181] but should be almost similar for both investigated APIs. In addition, a time independent diffusion layer with a constant diameter is described during particle shrinking [182]. It is assumed that this phenomenon occurs when testing the dissolution behavior of the hydrophilic SBS blends.

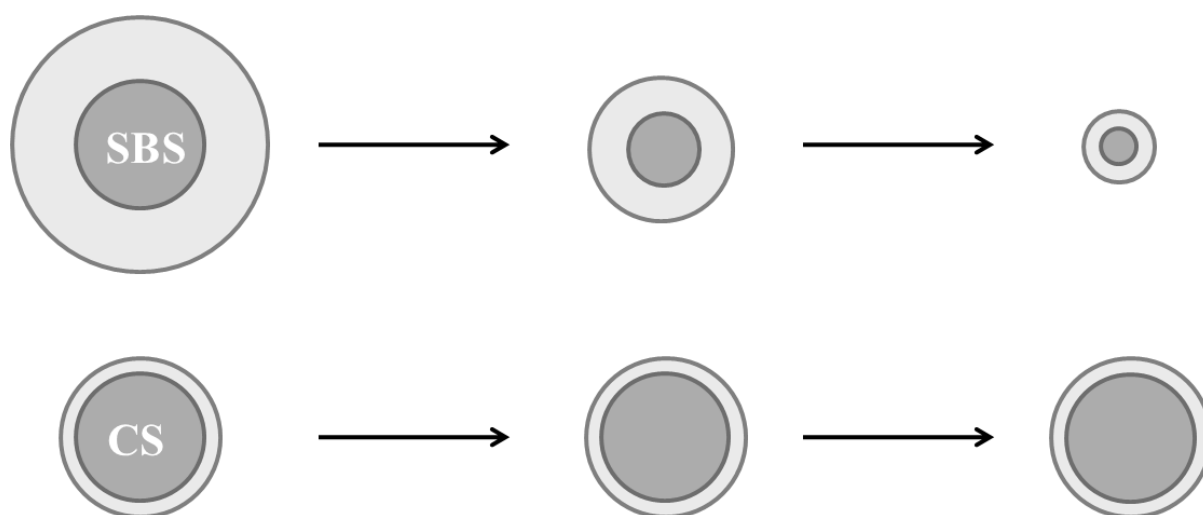


Figure 119: Time-dependent diffusion layer of SBS and CS

In contrast the hydrophobic CS showed a poor solubility and dissolution profiles could not be determined. An increased concentration of API was detected on the cellulose membranes after the dissolution testing (4 hours). Also a change in the dissolution rate/permeation rate was not visible for amorphous amounts (up to 17.0%). It is assumed that the wettability is very low and a diffusion layer is formed to a lesser extent on the hydrophobic surface. This behavior might explain a low to almost no release of API through the membrane.

5 OVERALL CONCLUSION AND FUTURE PERSPECTIVES

The presented work highlights that standard pharmaceutical unit operations can lead to batch variations due to induced structural changes (amorphous parts). These variations could affect performance and stability characteristics of dry powder inhaler (DPI) products. It is shown that dynamic vapor sorption techniques can be used for an accurate assessment of the amorphous content in pharmaceutical powders down to a level of $< 0.5\%$. The developed one-step DVS method helps to gain an understanding of induced amorphous amounts in hydrophilic and hydrophobic powders.

The first part clearly demonstrates that structural and thermal properties as well as characteristics may differ slightly once different preparation techniques are used. The imitation of process-induced disorders (semi-crystalline) can be accomplished by the introduced jet-milling process and the mixing tests with glass beads. Ball-milling, spray-drying, freeze-drying and quench-cooling may be used for the production of the fully amorphous state depending on the type of API.

Secondly, after evaluating different methods (DSC, TMDSC, XRPD and DMA) the practical applicability of the dynamic vapor sorption techniques is demonstrated. The developed one-step DVS method which is based on ‘equilibrium moisture uptake’ is adaptable for hydrophilic and also hydrophobic APIs. This highly accurate DVS study demonstrates how amorphous regions are specifically detectable as “reactive spots” to vapor. A high affinity of the API to the solvent was targeted to receive a high sensitivity of the method, a higher slope of the calibration curve and to detect minimal differences between powder samples. However, the amorphous content had to be stable for an exact determination. The development considered different factors influencing the sensitivity of the assay (water moisture sorption isotherms, organic solvent screening, optimization of the p/p_0 values, temperature robustness, influence of particle size/surface and validation) and based on the results, a schematic model for the explanation of the adsorption and absorption theory was illustrated. This approach may facilitate the specifications for in-process controls in the pharmaceutical industry.

In the third part aerodynamic investigations demonstrated that the amorphous content has a great influence on the fine particle fractions. The hydrophilic SBS showed a high trend for recrystallization over the storage time (six months). Thereby, a change in the surface morphology is assumed. These modifications are reinforced by a hydrophilic carrier (e.g. lactose) compared to the inert glass beads. Finally, capillary forces and solid material bridges complicate the detaching of API particles. After 6 months storage-time both types of blends showed al-

most similar FPFs. The hydrophobic API seemed to be less affected by water vapor (45%). Electrostatic charges and a reduction of hydrogen bonds can lead to higher FPFs over storage time. A significant difference in the smooth surface of the initially re-crystallized API (isopropanol) was detected for both blends. Low FPFs were determined for both blends with glass beads. An increase in the press-on forces led to a thin API film on the surface of the beads. Hereby, the structure of the glass beads' surface enables a higher compaction of the API crystals during the collision over the mixing time. The resulted binding forces induced a low deagglomeration behavior. In summary, it is necessary that amorphous amounts are determined (e.g. one-step DVS method) and further re-crystallized under controlled conditions. Otherwise the product stability is not guaranteed because of a possible re-crystallization and a change in the particle size (crystal growth).

In the attempt to investigate the effect of amorphous contents in powders on the dissolution of APIs, the used dissolution testing system (Andersen Cascade Impactor and USP paddle apparatus 2) was found to be unsuitable despite the continuous optimization for SBS and CS. The influence of different amorphous amounts in inhalation powders on the dissolution rate could not be determined. The hydrophilic API showed a burst release and the hydrophobic one showed only low solubility. Up to this date there is no applicable method available for testing aerosols whereas standardized dissolution test methods for solid dosage forms such as tablets and capsules are specifically defined.

6 SUMMARY

The efficient delivery of active pharmaceutical ingredients (APIs) to the lung by inhalation products depends on several parameters which include the formulation, the inhaler device, and the patient's inhalation technique. APIs which exhibit larger sized particles ($> 5 \mu\text{m}$) might impact in upper airways and thus boost side effects.

In general, the common active pharmaceutical ingredients (APIs) are synthesized as crystalline solids and subsequently processed by standard pharmaceutical operations such as milling, blending and even sieving. These processing steps can lead to structural changes, crystal defects and amorphous regions which may have an enormous potential to change during handling and storage and should be limited to a minimum. The conditions and kinetics of such process-induced disorders and changes during storage may affect product stability. In terms of the determination and control of the amorphous content, there is still lack in reliable methods that accurately assess the amorphous content in pharmaceutical powders down to a minimal level ($< 1\%$).

Therefore, this thesis focuses on the impact of amorphous parts of inhalation APIs, the improvement of their production techniques and detection methods for quantifying minimal amorphous amounts as well as the understanding of their influence on inhalation powder formulations. In a first step the preparation techniques of semi-crystalline/fully amorphous samples were investigated by using different technologies and process conditions. The focus was set on ball-milling, spray-drying, freeze-drying and quench cooling for the establishment of purely amorphous material. On the contrary, jet-milling and intensive blending (simulation with glass beads) led to the generation of partially amorphous APIs (up to 17%) mainly localized on the surface of the particles. Furthermore, the influence of these process-induced disorders on the stability and shelf-life was investigated (humidity/temperature/time).

The accurate assessment of the amorphous content down to a level $< 0.5\%$ in pharmaceutical powders was demonstrated by a developed one-step DVS method which is based on 'equilibrium moisture uptake'. The applicability was tested for various hydrophilic and hydrophobic powders and their induced amorphous amounts. This highly accurate DVS study demonstrates how amorphous regions are specifically detectable as "reactive spots" to polar or nonpolar vapors. A high affinity of the API to the solvent was targeted to receive a high sensitivity of the method, a higher slope of the calibration curve and to detect minimal differences between powder samples. The development was divided into six main sections (water moisture sorption isotherms, organic solvent screening, optimization of the p/p_0 values, temperature robust-

ness, influence of particle size/surface and validation). Finally, a schematic model for the explanation of the adsorption and absorption theory was illustrated. This approach may facilitate the specifications for in-process controls in the pharmaceutical industry.

Additionally performed aerodynamic investigations demonstrated that the amorphous content has a huge influence on the fine particle fraction (% of delivered dose < 5 μm). Especially the hydrophilic sample showed a high trend for a re-crystallization over the storage time of six months and showed decreasing values for the FPFs (9%). This behavior is a proof for insufficient product stability. In summary, it is necessary to determine amorphous amounts (e.g. one-step DVS method) and further to ensure complete re-crystallization under controlled conditions. Otherwise the product stability is not guaranteed because of a possible re-crystallization with consequences such as solid bridging and changes in the particle size (crystal growth).

7 SUMMARY (GERMAN)

Die effiziente Applikation von Arzneistoffen in der Lunge hängt von vielen Parametern ab, wie zum Beispiel der Arzneiformulierung, dem Inhalationssystem und der Inhalationstechnik des Patienten. In der Regel scheiden sich Arzneistoffpartikel, die größer als 5 μm sind, in den oberen Atemwegen ab und können deshalb zu Nebenwirkungen führen.

Im Allgemeinen werden heutzutage die Arzneistoffe als kristalline Feststoffe synthetisiert und danach durch verschiedene pharmazeutische Techniken wie die Mikronisation, Mischvorgänge und Siebungen prozessiert. Bei diesen Verarbeitungsschritten kann es jedoch zu strukturellen Veränderungen, Kristalldefekten oder amorphen Regionen kommen, welche dann wiederum eine hohe Tendenz zur Umwandlung während der weiteren Verarbeitung und Lagerung zeigen. Deshalb sollten besonders amorphe Anteile auf ein Minimum reduziert werden, da dieser metastabiler Zustand die Produktstabilität des Endprodukts stark beeinflussen kann. Im Hinblick auf die Detektion und Kontrolle dieser amorphen Regionen mangelt es an vernünftigen Methoden zur Charakterisierung minimaler Anteile in pharmazeutischen genutzten Pulvern (< 1 %).

Aufgrund dessen beschäftigt sich diese Arbeit explizit mit dem Thema der amorphen Anteile, um ein besseres Verständnis über Herstelltechniken, der Bestimmung und Quantifizierung von minimalen Anteilen und den Einfluss auf inhalative, speziell in hydrophoben Arzneistoffpulvern zu erhalten. Im ersten Teil wurden dabei Herstellmethoden für geringe und vollständig amorphe Pulver mittels verschiedener Technologien und Prozessbedingungen untersucht. Der Schwerpunkt für die Etablierung von stark amorphen Substanzen lag dabei auf der Mahlung mittels Kugelmühle, der Sprühtrocknung, Gefriertrocknung und dem Quench cooling. Im Folgenden wurde gezeigt, wie mittels Luftstrahlmahlung und Intensivmischung (Simulierung mit Glass beads) geringe amorphe Bereiche speziell auf der Partikeloberfläche erzeugt wurden (bis zu 17 %). Des Weiteren wurde der Einfluss dieser prozessinduzierten Kristallstrukturveränderungen in Hinblick auf die Stabilität und Haltbarkeit untersucht (Feuchtigkeit/Temperatur/Zeit).

Die exakte Bestimmung des amorphen Anteils bis zu einem Level von 0.5 % wurde durch eine selbst entwickelte 1-Schritt DVS-Methode, die auf der Grundlage der Gleichgewichtsabsorption basiert, gewährleistet. Die Anwendbarkeit wurde dabei für hydrophile und besonders auch für hydrophobe Pulver mit organischen Lösungsmitteln, im Hinblick auf die Detektion minimal amorphe Mengen, getestet. Diese DVS-Methode konnte zeigen, dass amorphe Regionen als ‚reaktive Spots‘ mit Hilfe von polaren oder organischen Lösungsmitteln mit einer

hohen Genauigkeit sehr gut zu quantifizieren waren. In der Regel musste eine hohe Affinität zwischen dem Arzneistoff und dem Messlösungsmittel erreicht werden, um letztendlich eine hohe Sensitivität der Methode und eine entsprechende Steigung der Kalibriergerade zur Bestimmung geringster Mengen zu garantieren. Im Allgemeinen ließ sich dieser Entwicklungsprozess in 6 Hauptschritte (Wasserdampfabsorptions Isotherme, Organisches Lösungsmittelscreening, Optimierung der Feuchtigkeit, Belegung der Temperaturstabilität, Möglicher Einfluss auf Partikelgröße/Partikeloberfläche und Validierung) unterteilen. Im Anschluss daran konnten schematische Modelle für Adsorptions- und Absorptionstheorien erstellt werden. Zusammenfassend kann dieser Ansatz mittels der entwickelten 1-Schritt DVS-Methode die Bestimmung und Einhaltung von bestimmten Spezifikationen für amorphe Anteile in der Pharmazeutischen Industrie erleichtern.

Im weiteren Verlauf der Arbeit zeigten aerodynamische Bestimmungen, dass auch bei diesen der amorphe Anteil in inhalativen Pulvermischungen einen großen Einfluss auf die lungengängige Feinpartikelfraktion hat (% der Dosis, die $< 5 \mu\text{m}$ ist). Besonders hydrophile Arzneistoffe zeigten dabei einen großen Trend zur Rekristallisation und damit verbundenen Abnahme der FPF (9 %) über eine Lagerzeit von 6 Monaten. Dieses Verhalten deutet auf eine nicht ausreichende Produktstabilität hin und kann mit den induzierten amorphen Regionen in Zusammenhang gebracht werden. Zusammenfassend lässt sich festhalten, dass es absolut notwendig ist, amorphe Regionen zu quantifizieren (z.B. mit der vorgestellten 1-Schritt DVS-Methode) und diese danach unter kontrollierten Bedingungen zur Rekristallisation zu bringen. Andernfalls kann eine Produktstabilität nicht garantiert werden, da es speziell bei Inhalativa zu gravierenden Partikelgrößenveränderungen (Kristallwachstum des Arzneistoffs) kommen kann.

8 APPENDIX

8.1 Methods

8.1.1 Quantification of API content - HPLC

A Waters HPLC system (Waters Corp. Milford, USA) was used for the quantification of the sample contents of SBS and CS. The obtained data was evaluated with Empower[®] Pro2 software (Waters Corp. Milford, USA).

8.1.1.1 Salbutamol sulphate

Mobile phase: 78% buffering system (containing 2.87 g/l sodium heptanesulfonate and 2.5 g/l KH_2PO_4 (0.2 mmol); pH adjusted to 3.65 with ortho-phosphoric acid 85%)

22% acetonitrile

Flow rate: 0.8 ml/min

Stationary phase: LiChroCART[®] 125-4,
LiChrospher[®] 100 RP-18 (5 μm) with precolumn

Wavelength: 220 nm

Retention time: 4 min

Calibration: 1-80 $\mu\text{g/ml}$

Injection volume: 100 μl

Oven temperature: 25 °C

Samples were dissolved in 100% ddH₂O.

8.1.1.2 Ciclesonide

Mobile phase: 85% methanol

15% ddH₂O

Flow rate: 1.2 ml/min

Stationary phase: LiChroCART[®] 125-4,

LiChrospher[®] 100 RP-18 (5 μm) with precolumn

Wavelength: 243 nm

Retention time: 8 min

Calibration: 1-80 μg/ml

Injection volume: 100 μl

Oven temperature: 25 °C

Samples were dissolved in 9:1 methanol/ddH₂O.

8.2 Materials

Acetone	SIGMA-ALDRICH, Inc., St. Louis, USA
Acetonitrile	SIGMA-ALDRICH, Inc., St. Louis, USA
Brij [®] 35	ICI Specialty, Essen, Germany
Cellulose membrane	Whatmann, Dassel, Germany
ddH ₂ O	freshly produced with Finn Aqua 75, San-Asalo Sohlberg Corp., Helsinki, Finland
Decane	SIGMA-ALDRICH, Inc., St. Louis, USA
Ethanol	Merck KGaA, Darmstadt, Germany
Ethyl acetate	Merck KGaA, Darmstadt, Germany
Glass beads Ø 0.25 mm	Carl Roth GmbH & Co. KG, Karlsruhe, Germany
Glass beads Ø 4.0 mm	Carl Roth GmbH & Co. KG, Karlsruhe, Germany
Glycerol	Merck KGaA, Darmstadt, Germany
Helium 5.0	Air Liquide, Paris, France
Heptane	Merck KGaA, Darmstadt, Germany
HPMC capsules	Qualicaps Europe S.A., Madrid, Spain
Hydrogen 5.0	Air Liquide, Paris, France
Isopropanol	AppliChem GmbH, Darmstadt, Germany
Methanol	J.T. Baker, Deventer, The Netherlands
Methylene chloride	LGC Standards GmbH, Wesel, Germany
Nitrogen 5.0	Air Liquide, Paris, France
Nonane	SIGMA-ALDRICH, Inc., St. Louis, USA
Octane	SIGMA-ALDRICH, Inc., St. Louis, USA
o-phosphoric acid 85%	Merck KGaA, Darmstadt, Germany

Phosphate buffered saline	SIGMA-ALDRICH, Inc., St. Louis, USA
Plasdone [®]	Ashland Industries GmbH, Schaffhausen, Switzerland
Potassium dihydrogen phosphate	FAGRON, Barsbüttel, Germany
Respitose SV003	DFE pharma, Goch, Germany
Sodium dodecyl sulfate	Merck KGaA, Darmstadt, Germany
Sodium heptanesulfonate	SIGMA-ALDRICH, Inc., St. Louis USA
Syringe top filter, Minisart RC 15	Sartorius AG, Göttingen, Germany
Tween [®] 20	Croda Europe Ltd., Yorkshire, UK

8.3 Raw data

8.3.1 Validation of High Performance Liquid Chromatography (HPLC) methods for SBS and CS

A coefficient of determination of $R^2 > 0.999$ was determined for both calibration curves of SBS and CS in the linearity test series. Seven different concentrations showed a linear relation to the area under the curve (AUC) of the detected signal, respectively. Table 34 demonstrates this directly proportional behavior. Each concentration was measured six times for both APIs. The performance of the measurement method is reflected in the process standard deviation (S_{x0}) which was of 0.113 μg for SBS and 0.313 μg for CS. The determined value is corresponding to a process coefficient of variation (V_{x0}) of 0.442% for SBS and 1.242% for CS.

Table 34: HPLC linearity of different SBS and CS amounts

Amount [$\mu\text{g/ml}$]		AUC (mean)		sd		CV [%]	
SBS	CS	SBS	CS	SBS	CS	SBS	CS
82.56	81.64	15058165	10810575	21214	7445	0.14	0.07
51.60	51.03	9467013	6844578	30956	13458	0.33	0.20
20.64	20.41	3774338	2657125	5063	5209	0.13	0.20
10.32	10.21	1891951	1339451	5991	1821	0.32	0.14
8.26	8.16	1518202	1073440	17088	712	1.13	0.07
4.13	4.08	751936	547551	2760	1278	0.37	0.23
1.03	1.02	191843	136592	1808	648	0.94	0.47

The limit of quantification (LOQ) was determined using dilutions of 1.0 $\mu\text{g/ml}$, 0.5 $\mu\text{g/ml}$, 0.2 $\mu\text{g/ml}$, 0.1 $\mu\text{g/ml}$, 0.08 $\mu\text{g/ml}$ and 0.05 $\mu\text{g/ml}$ for each API. An aimed ratio of a signal-to-noise value of 10:1 was reached with the amount of 0.1 $\mu\text{g/ml}$ for SBS and 0.05 $\mu\text{g/ml}$ for CS. Figure 120 visualizes the described ratio 10:1 of signal/noise for SBS (4.05 minutes) and for CS (8.30 minutes), respectively.

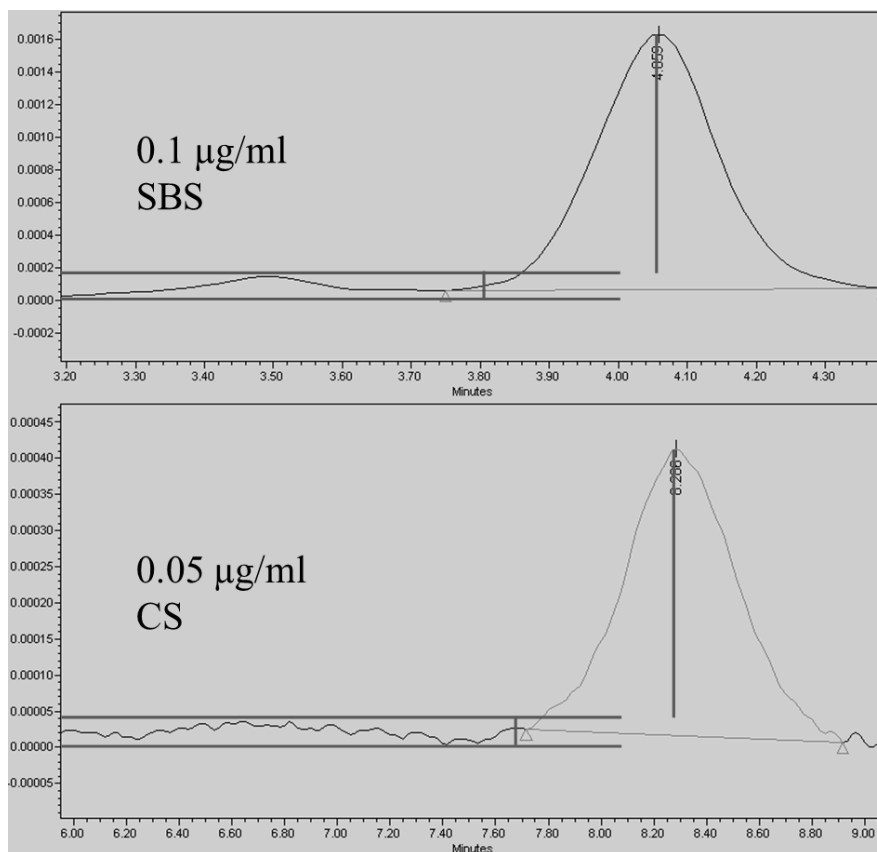


Figure 120: HPLC signal/noise ratio of both APIs

Furthermore, the same concentrations were produced six times for both APIs. The accuracy was determined by the closeness of the agreement between the value which is accepted either as a conventional true value and the value found. Hereby, respectable recovery rates between 98-102% were found for both APIs. Table 35 shows the recovery rates [%] of the six samples with the same concentration for SBS and CS.

Table 35: HPLC recovery rates of both APIs in the accuracy test series

AUC (mean)		True value [$\mu\text{g/ml}$]		Value found [$\mu\text{g/ml}$]		Recovery [%]	
SBS	CS	SBS	CS	SBS	CS	SBS	CS
13818473	8817162	75.12	65.43	75.05	65.16	99.91	99.60
13897434	8969742	75.12	65.43	75.48	66.29	100.48	101.32
13913146	8932953	75.12	65.43	75.56	66.02	100.59	100.91
13915229	8734967	75.12	65.43	75.57	64.55	100.61	98.67
13834715	8745134	75.12	65.43	75.14	64.63	100.02	98.78
13887777	8691927	75.12	65.43	75.43	64.24	100.41	98.18

The closeness of the agreement between a series of measurements (6 times) obtained from multiple sampling of the same homogenous sample was determined for evaluation of the precision. A coefficient of variation of < 2.0% is target and was defined for both APIs. Table 36 shows the precision values for SBS and CS, respectively.

Table 36: Closeness of agreement between a series of measurements for the precision

Injection	AUC	
	SBS	CS
1	202652	130192
2	203394	130634
3	203392	130730
4	202516	131696
5	201565	130763
6	202091	129688
mean	202602	130617
sd	721	670
CV [%]	0.36	0.51

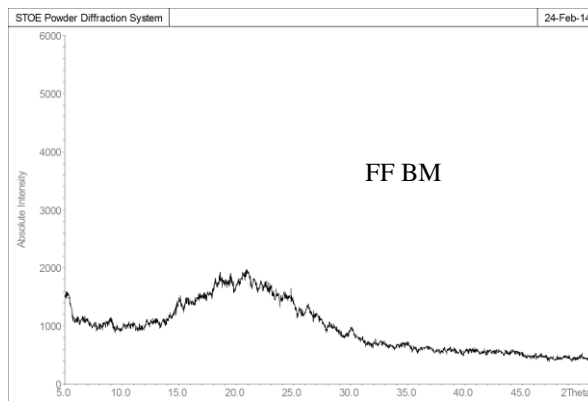
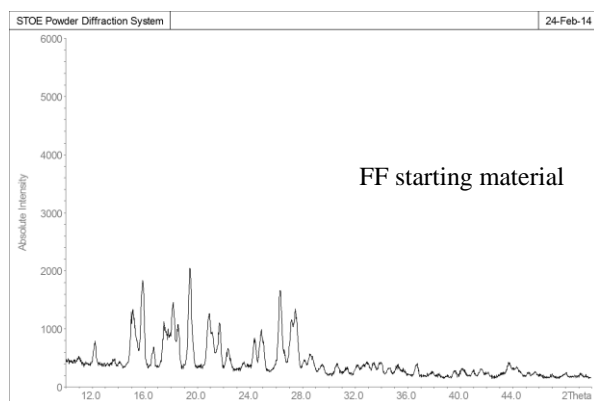
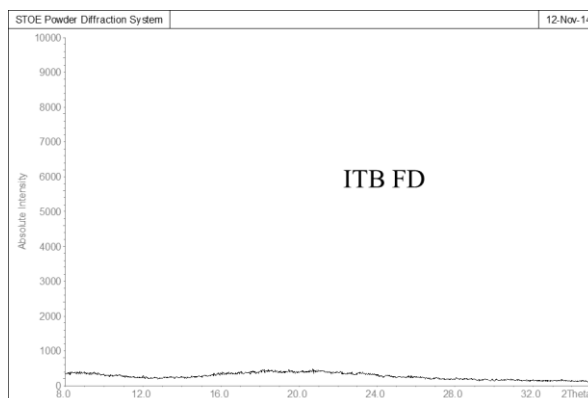
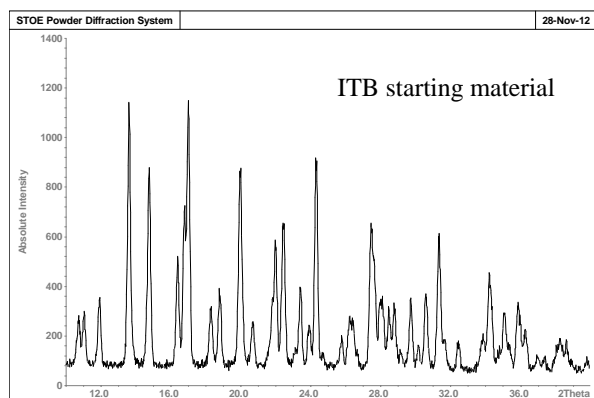
Concerning the stability testing (robustness) of one concentration over 1 day, 3 days and 5 days, SBS and CS showed constant and precise results when stored at room temperature and daylight. The robustness of this analytical procedure showed its high capacity to detect significant results unaffected by small variations (Table 37). It is an indication of the reliability during normal usage.

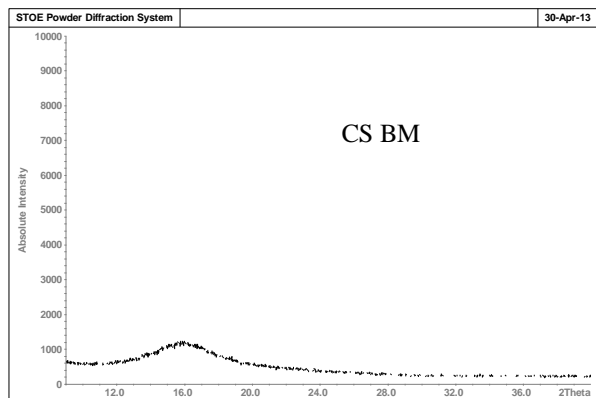
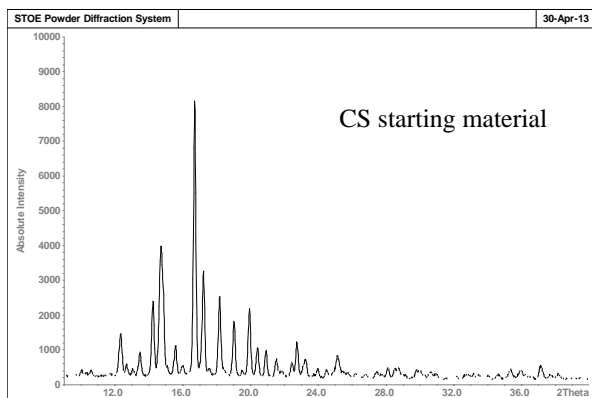
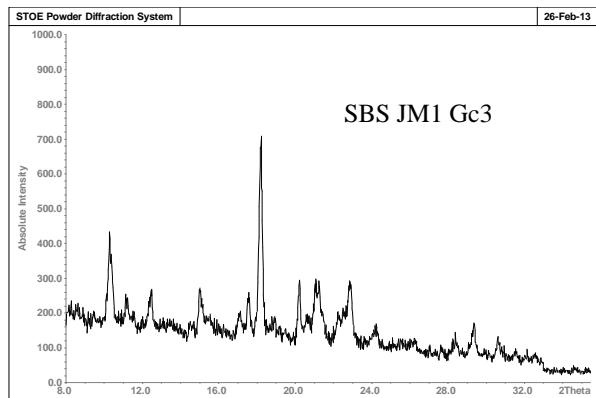
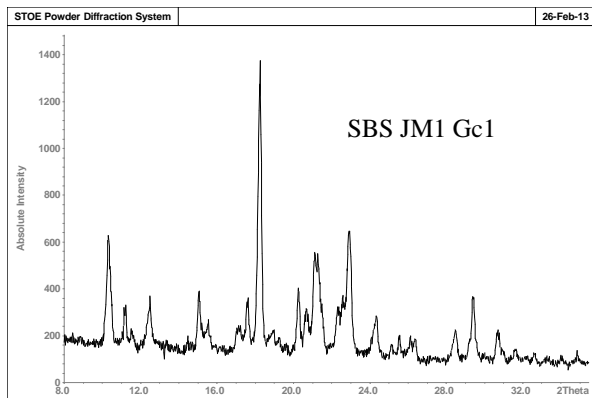
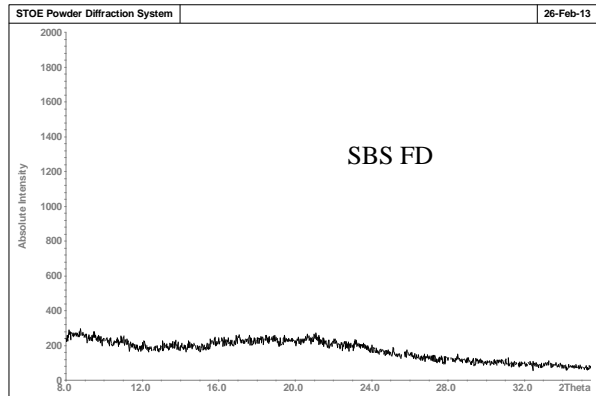
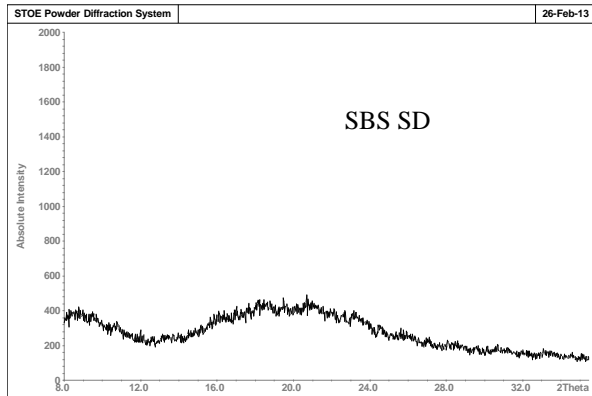
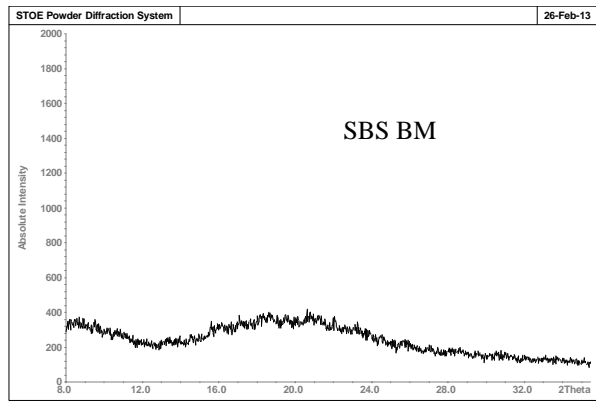
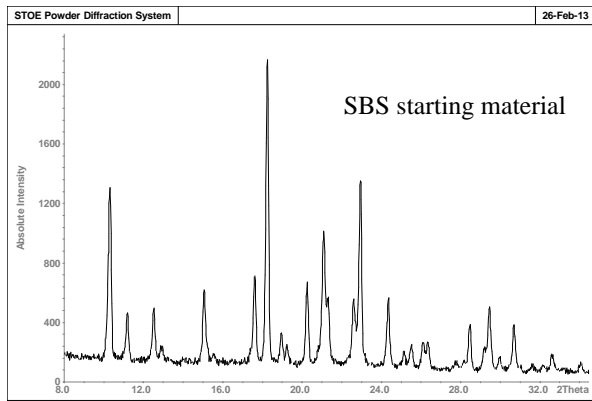
In summary, the objective of validating this HPLC analytical procedure was to demonstrate the suitability for the individual measurement of SBS and CS. Typical validation characteristics such as linearity, limit of quantification (LOQ), accuracy, precision and robustness were determined and are within its specified range, respectively. These findings enable a specific quantification of the API for the investigations with the impactors and dissolution experiments.

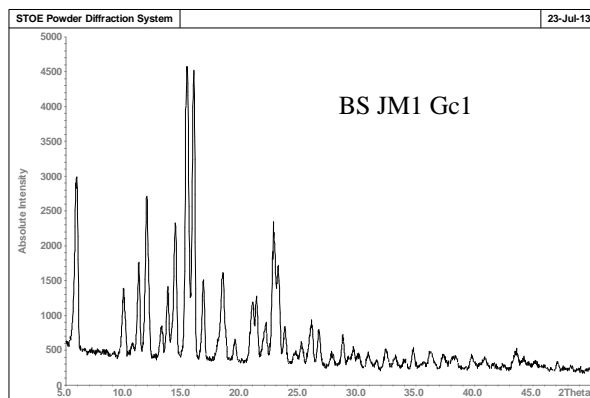
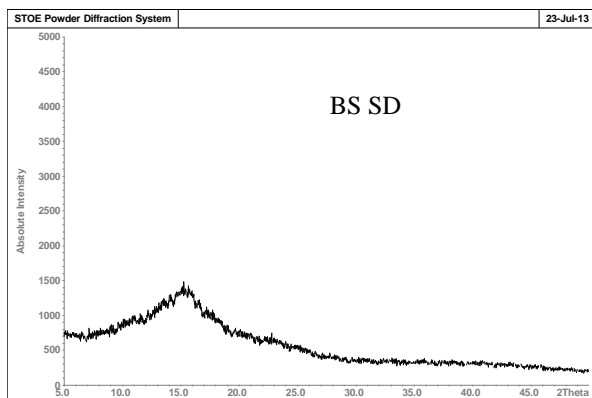
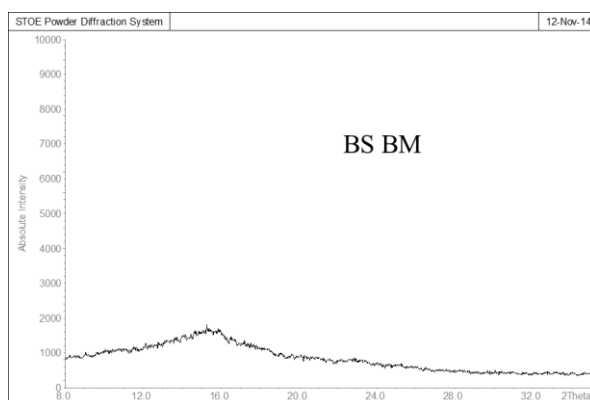
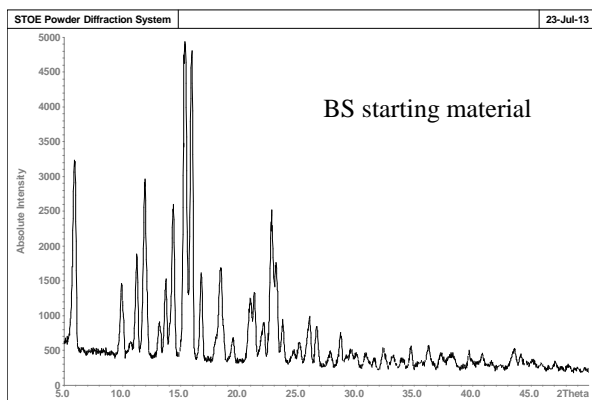
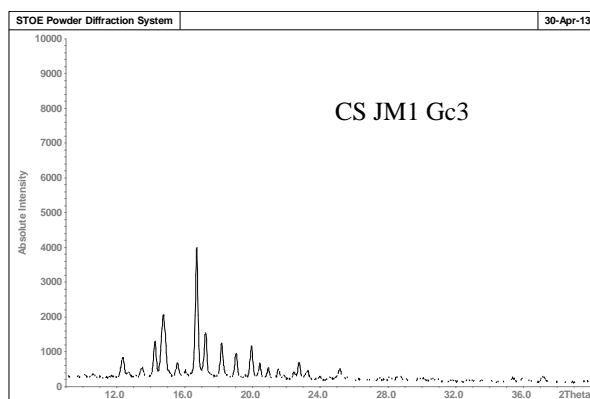
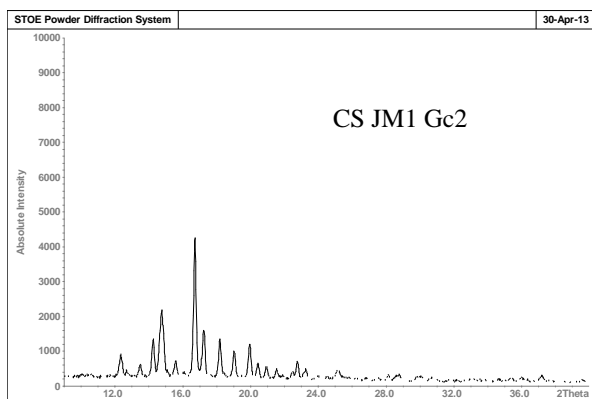
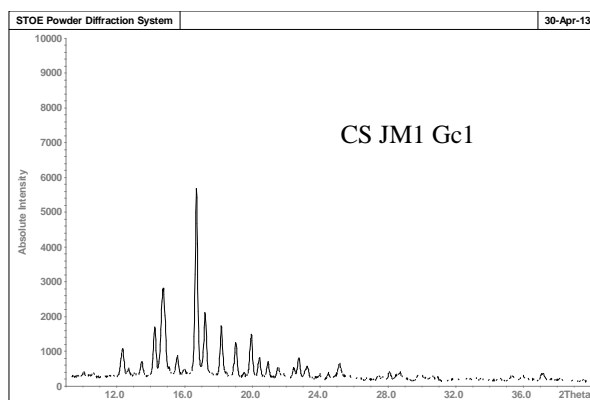
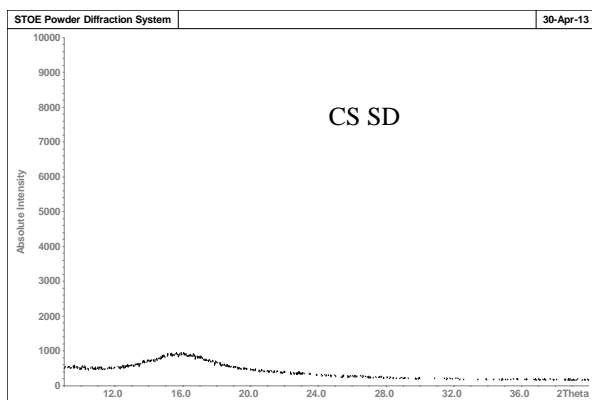
Table 37: Robustness of SBS and CS HPLC analytics up to 5 days

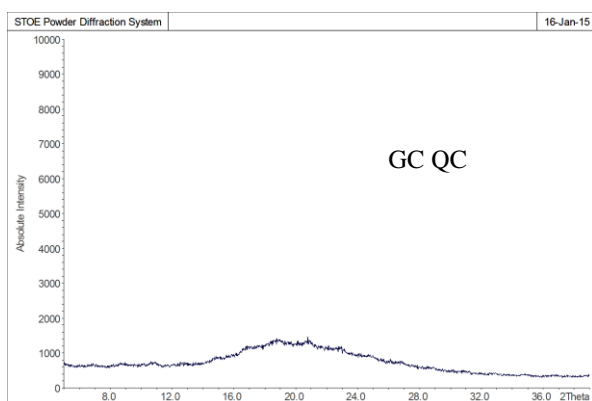
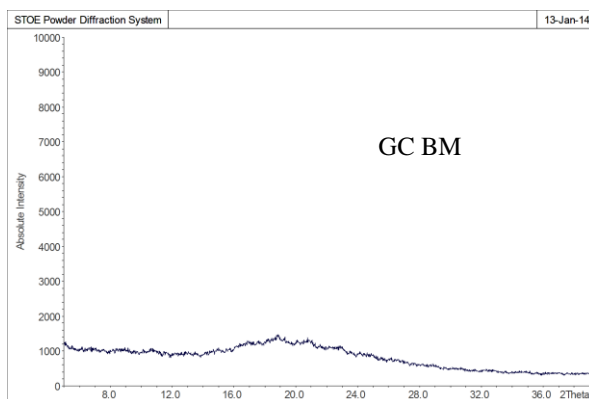
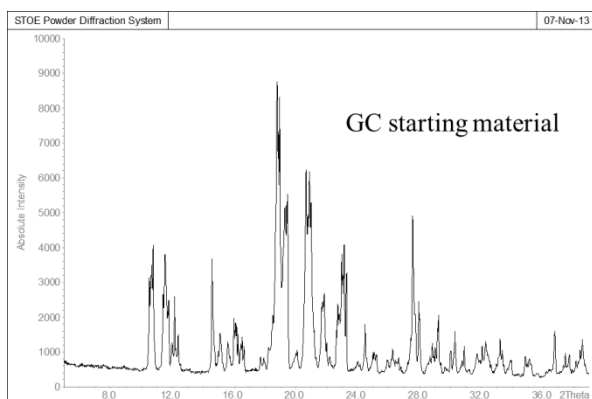
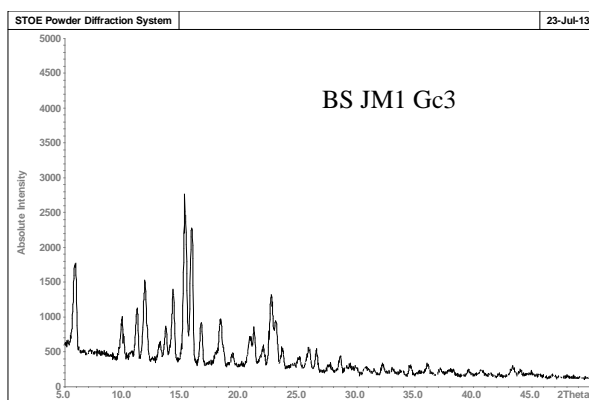
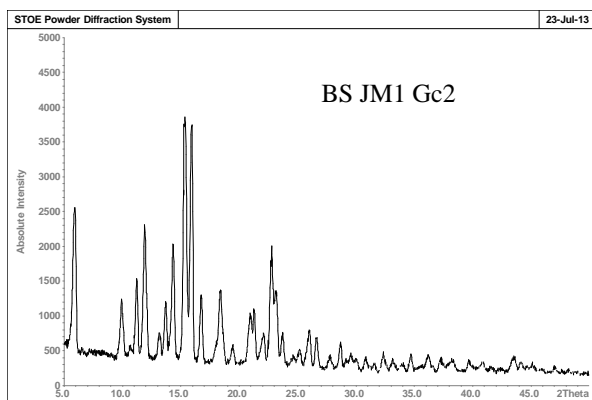
Injection	Amount [$\mu\text{g/ml}$] 1 day		Amount [$\mu\text{g/ml}$] 3 days		Amount [$\mu\text{g/ml}$] 5 days	
	SBS	CS	SBS	CS	SBS	CS
1	1.05	1.39	1.06	1.40	1.07	1.40
2	1.04	1.38	1.04	1.41	1.06	1.41
3	1.05	1.39	1.06	1.40	1.07	1.39
4	1.04	1.39	1.04	1.40	1.06	1.42
5	1.04	1.40	1.06	1.54	1.05	1.43
6	1.04	1.40	1.06	1.55	1.06	1.40
mean	1.04	1.39	1.05	1.45	1.06	1.41
sd	0.00	0.01	0.01	0.07	0.01	0.01
CV [%]	0.47	0.50	0.81	5.03	0.70	0.90

8.3.2 Selected XRPD diagrams

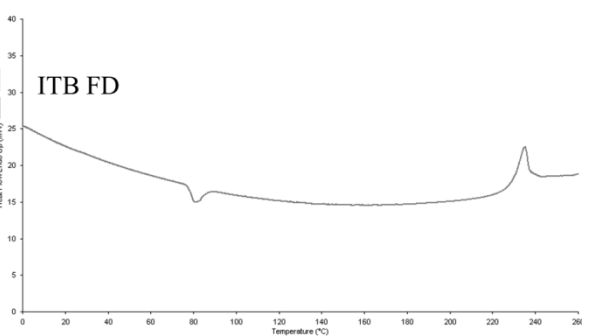
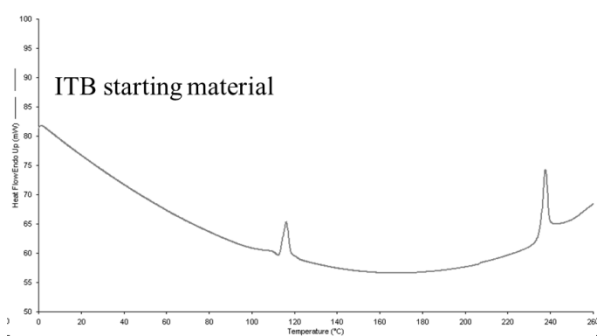


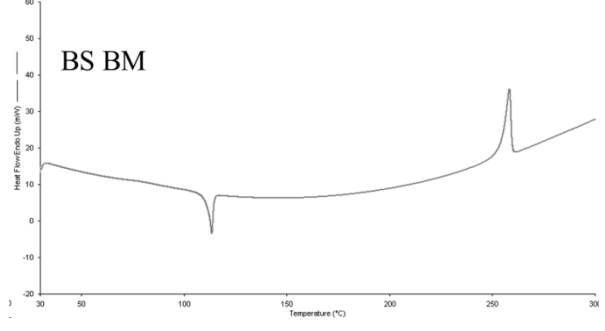
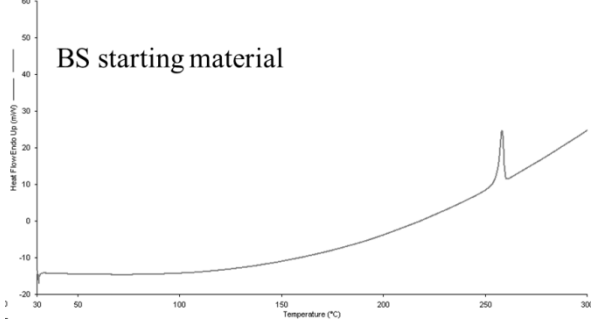
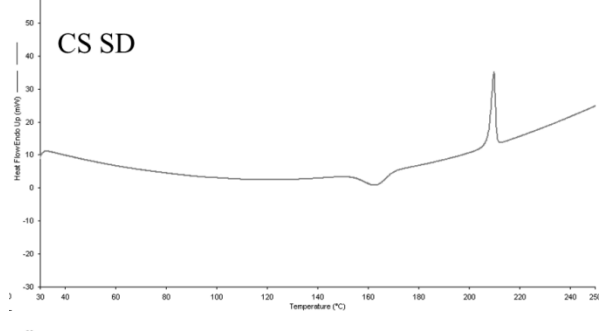
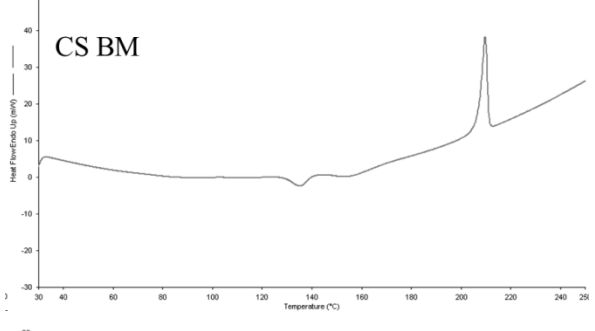
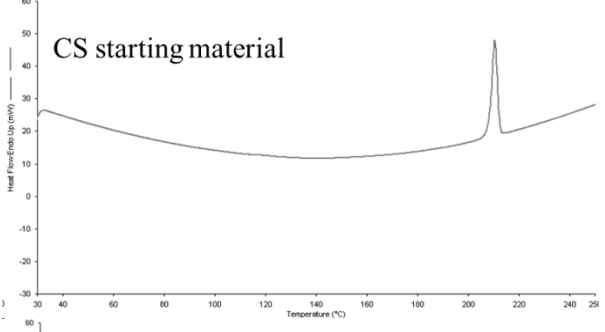
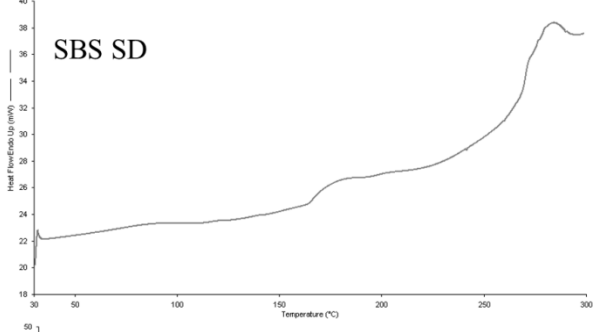
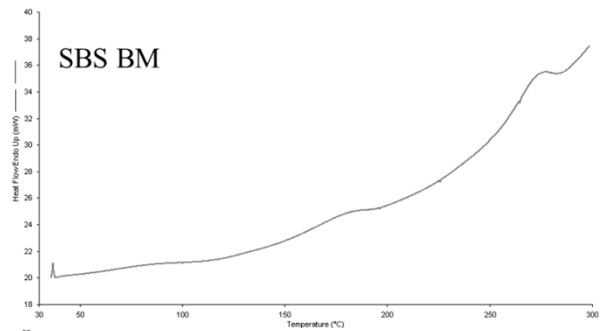
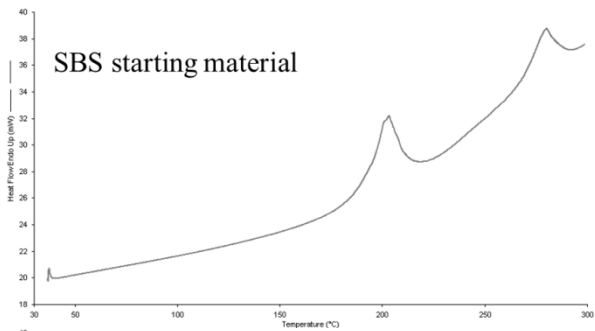
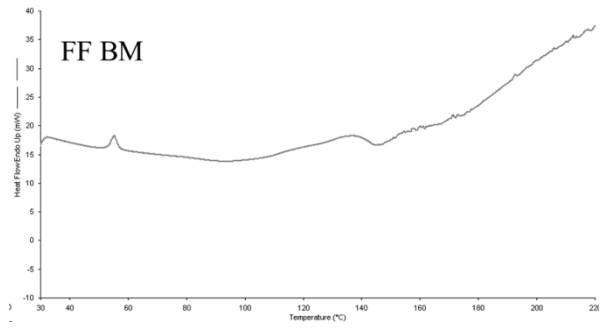
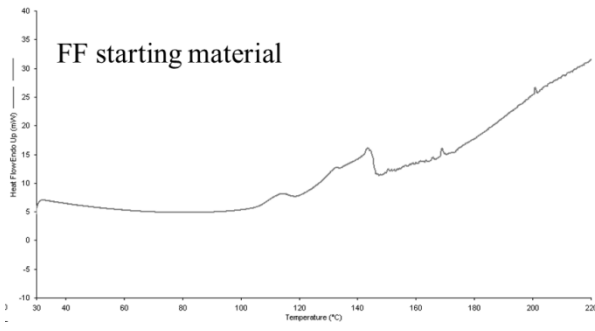


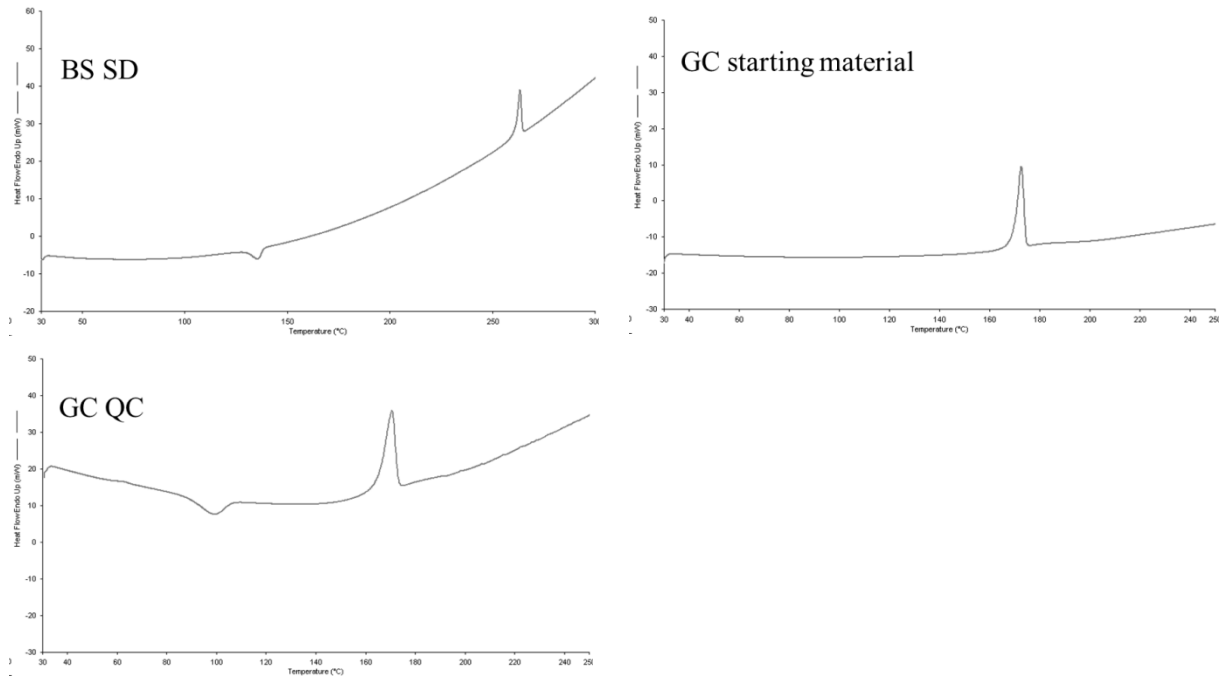




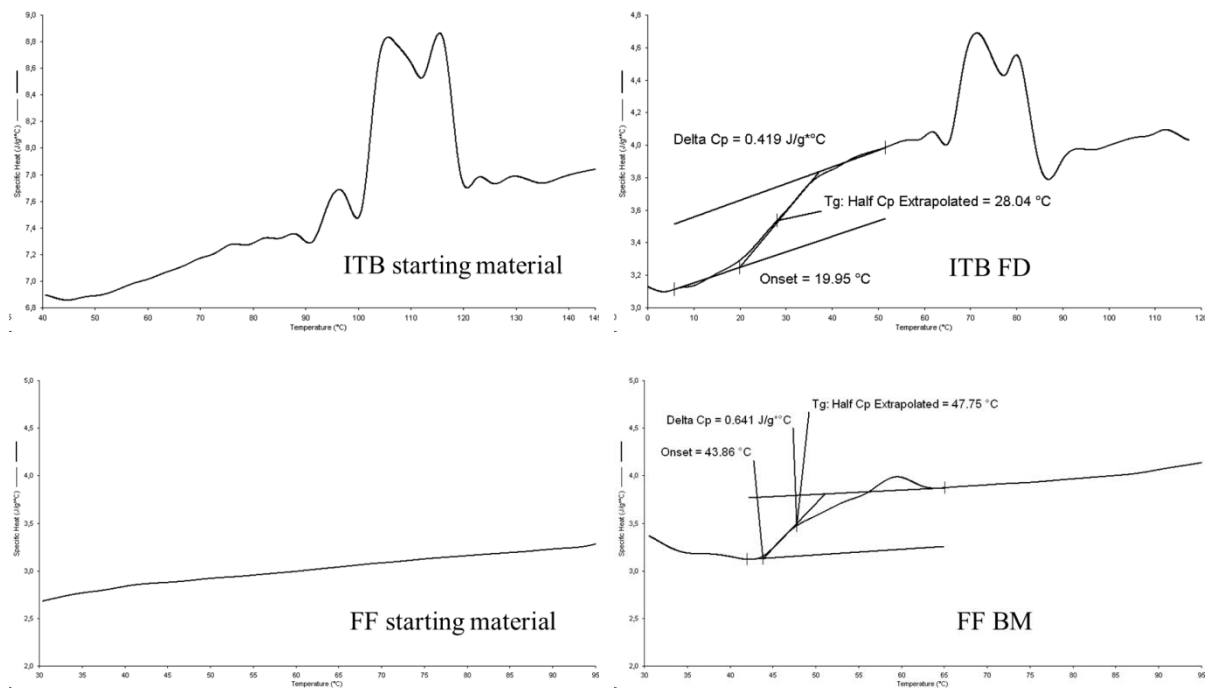
8.3.3 Selected DSC diagrams

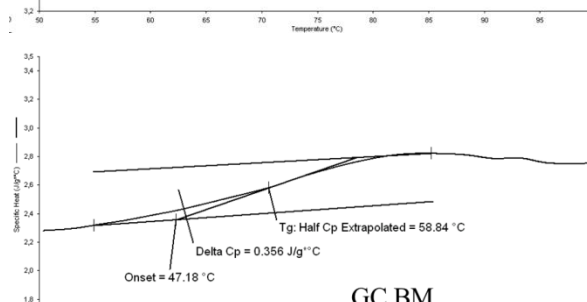
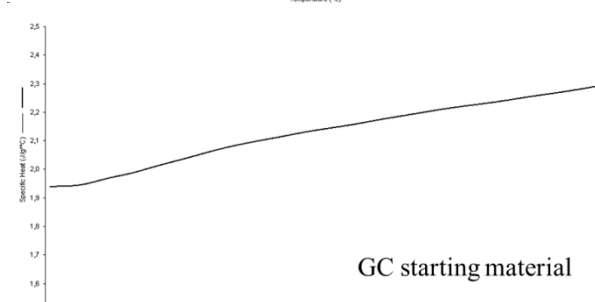
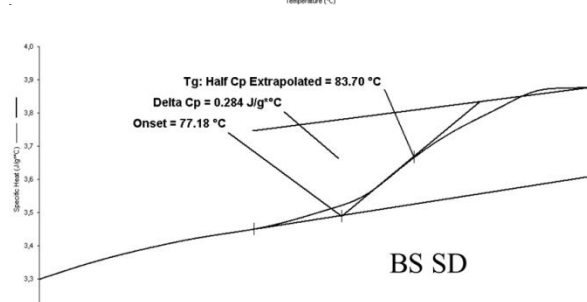
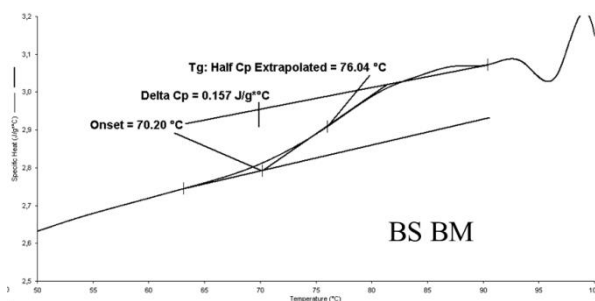
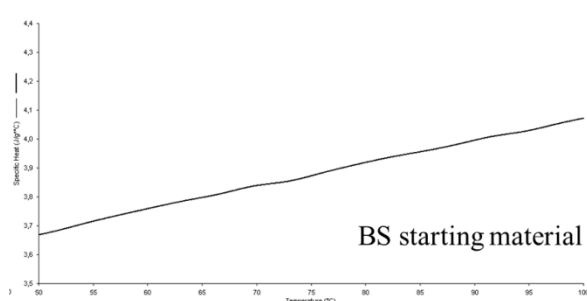
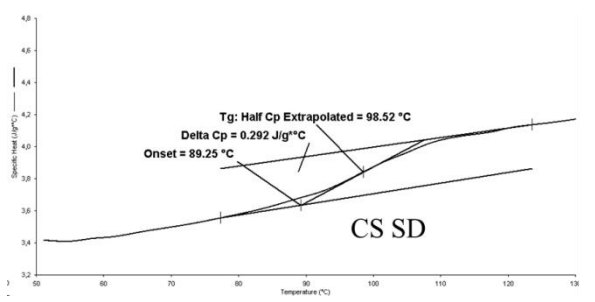
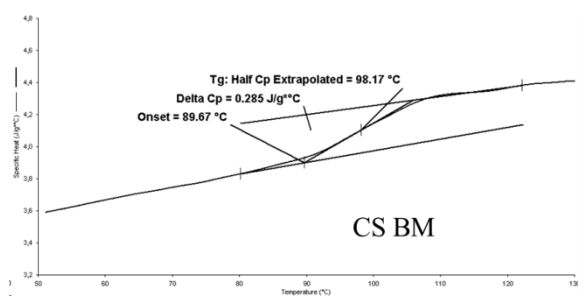
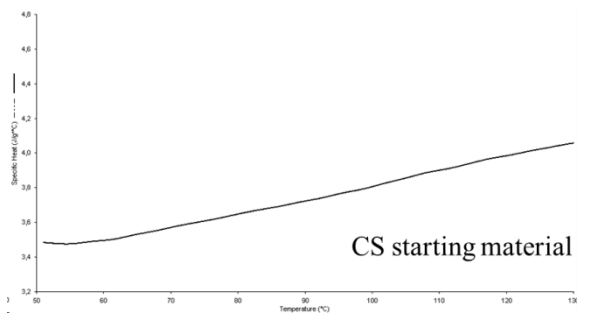
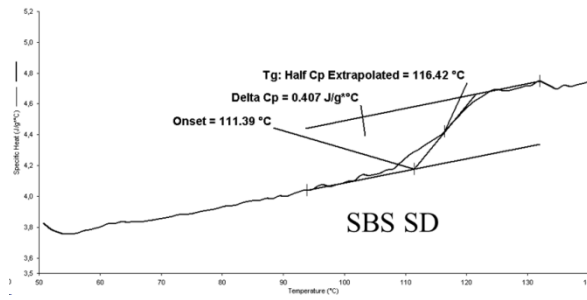
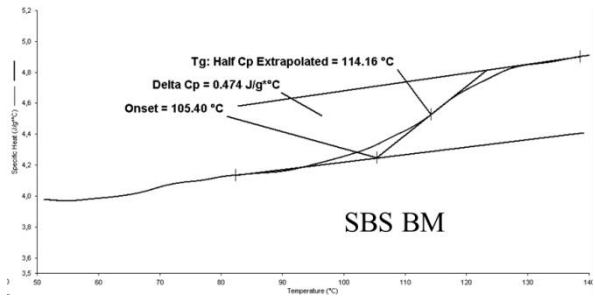
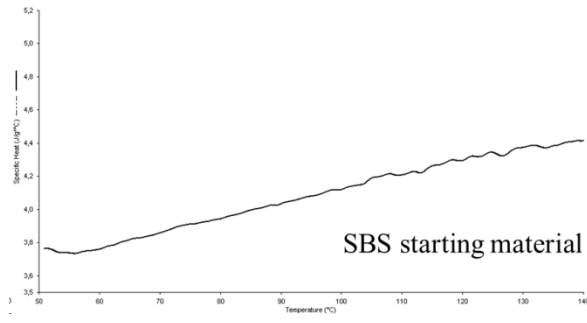




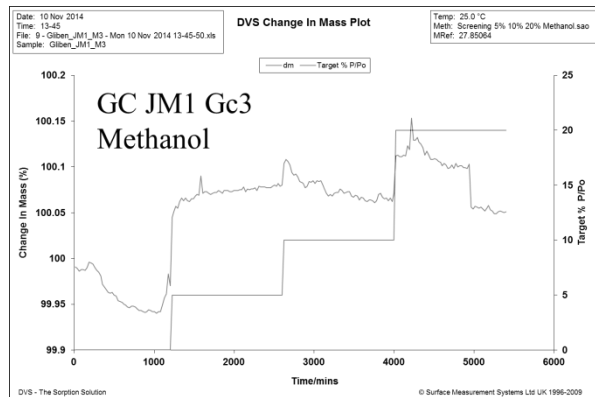
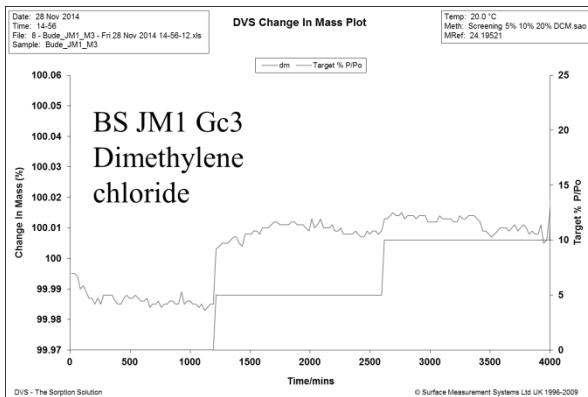
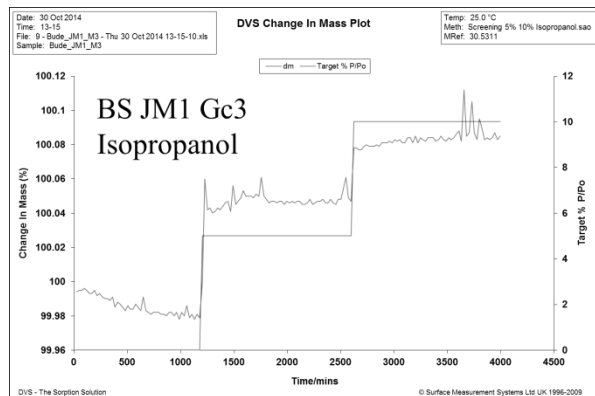
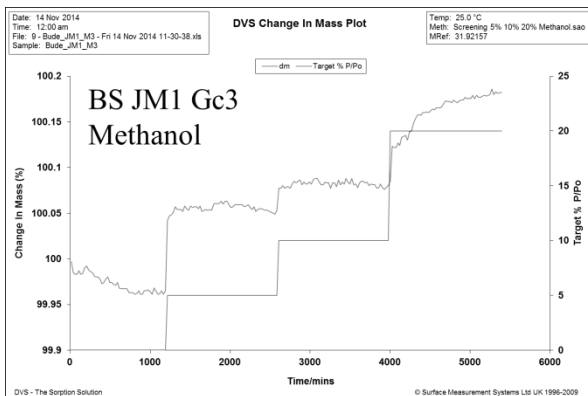
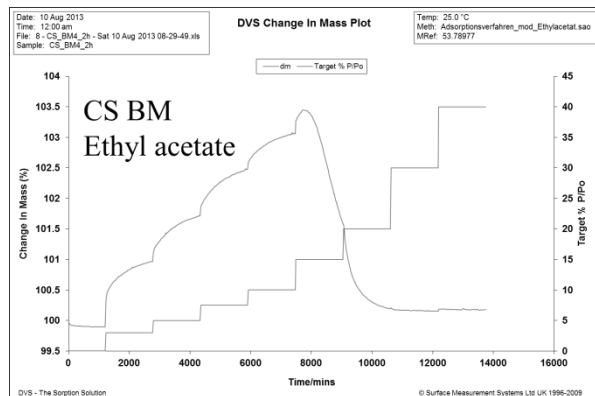
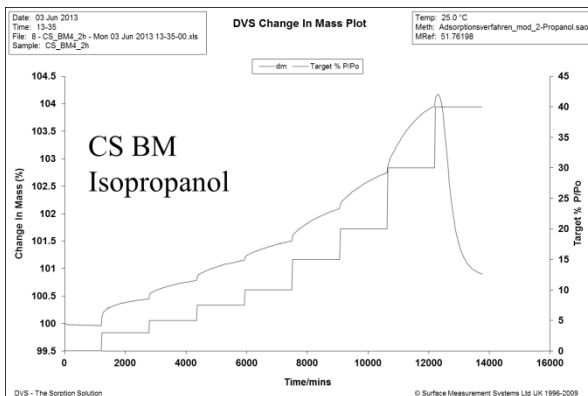
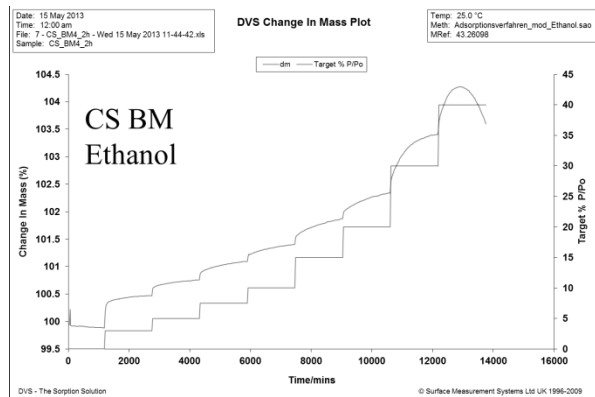
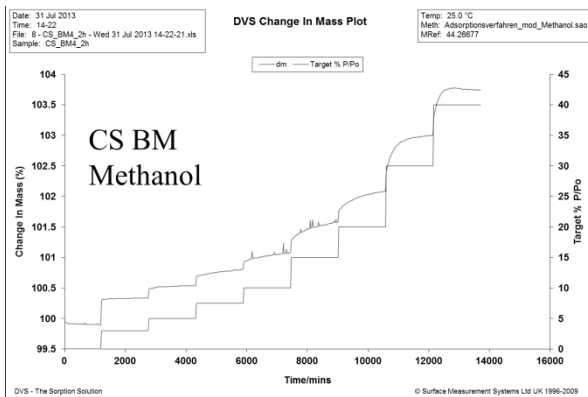


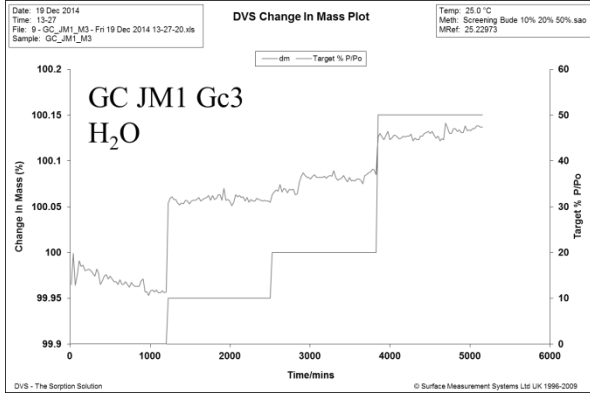
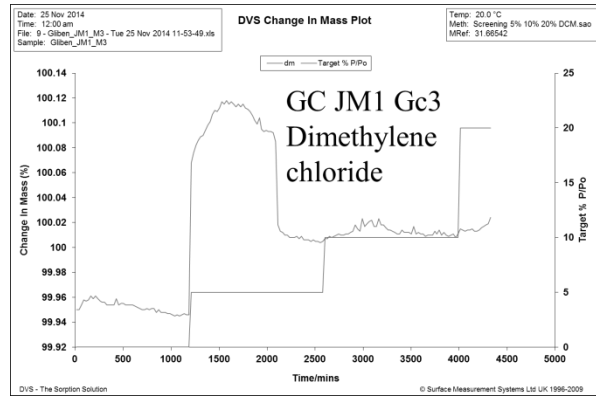
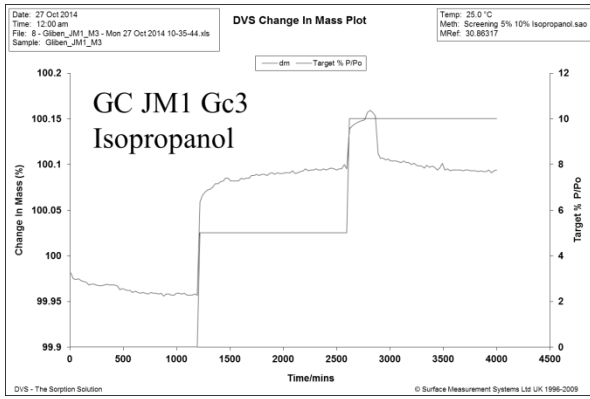
8.3.4 Selected TMDSC diagrams



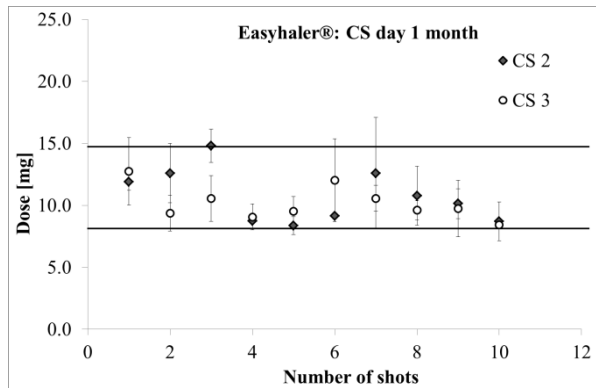
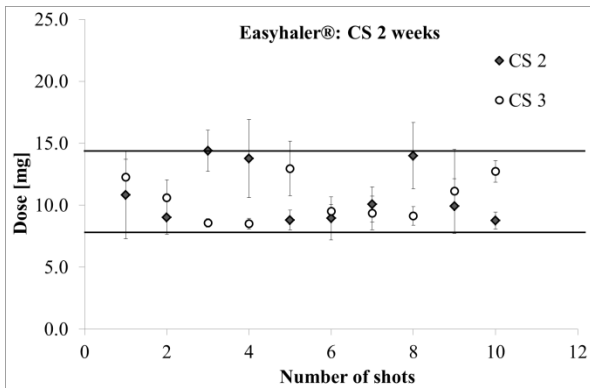
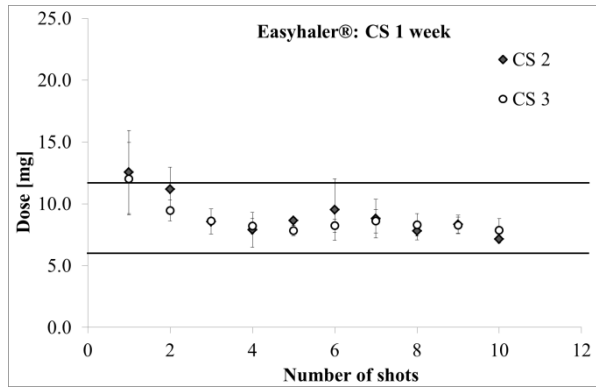
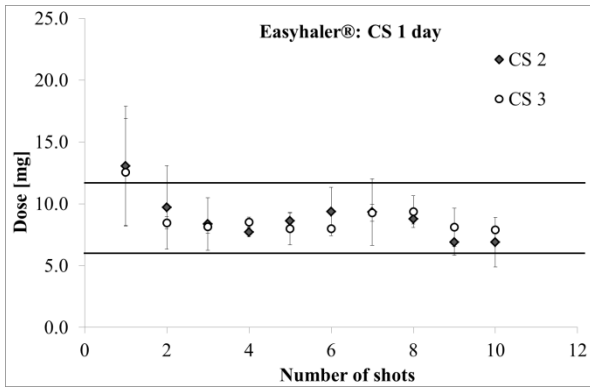


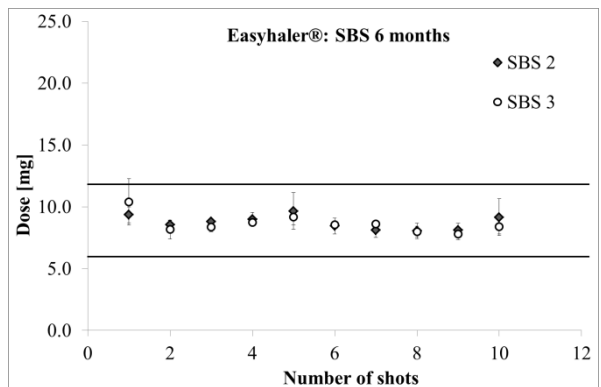
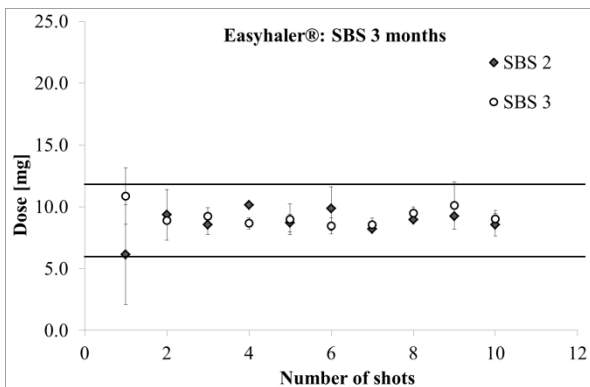
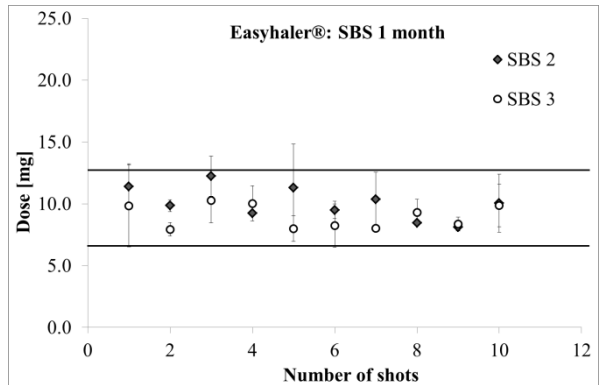
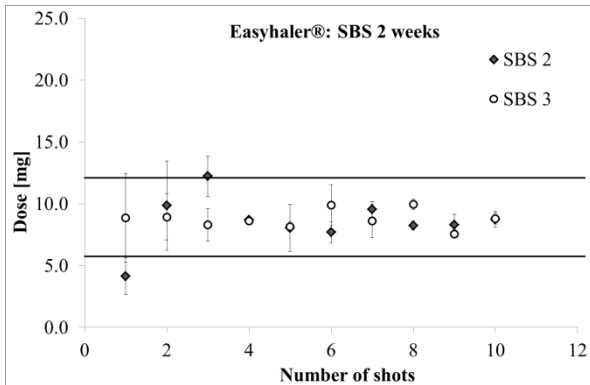
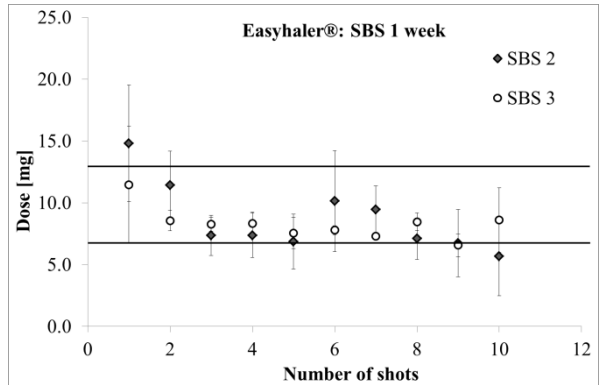
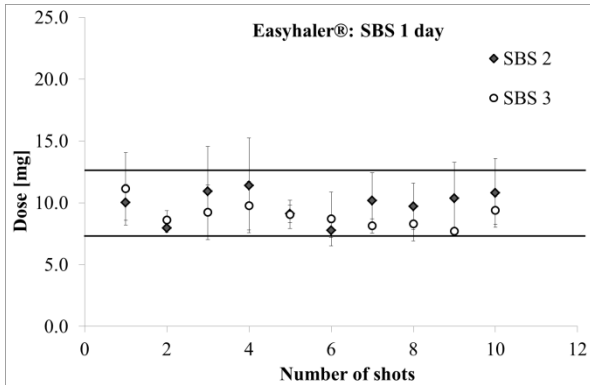
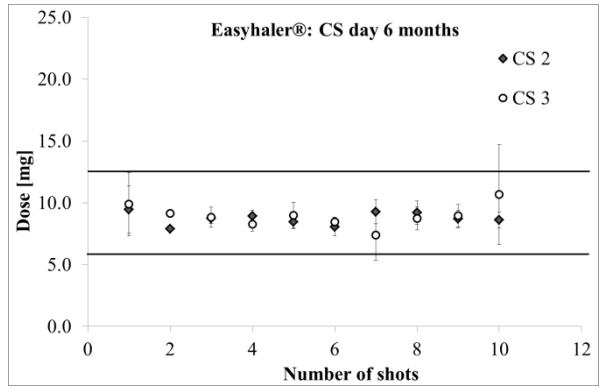
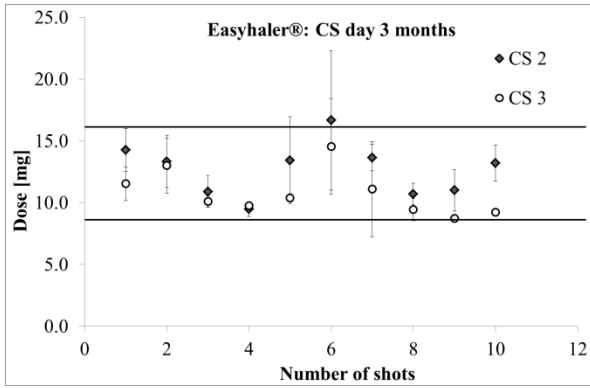
8.3.5 Selected organic moisture sorption isotherms by DVS





8.3.6 Delivered dose (Easyhaler®) of the NGI Study 1





9 REFERENCES

- [1] Stegemann S, Kopp S, Borchard G, Shah VP, Senel S, Dubey R, Urbanetz N et al. Developing and advancing dry powder inhalation towards enhanced therapeutics. *European Journal of Pharmaceutical Sciences* 2013;48:181–94.
- [2] Bousquet J, Dahl R, Khaltaev N. Global Alliance against Chronic Respiratory Diseases. *The European respiratory journal* 2007;29:233–9.
- [3] Arora P, Kumar L, Vohra V, Sarin R, Jaiswal A, Puri MM, Rathee D et al. Evaluating the technique of using inhalation device in COPD and Bronchial Asthma patients. *Respiratory Medicine* 2014;108:992–8.
- [4] Mentz RJ, Fiuzat M, Kraft M, Lindenfeld J, O'Connor CM. Bronchodilators in Heart Failure Patients With COPD: Is It Time for a Clinical Trial? *Journal of Cardiac Failure* 2012;18:413–22.
- [5] Mueannoorn W, Srisongphan A, Taylor KMG, Hauschild S, Gaisford S. Thermal ink-jet spray freeze-drying for preparation of excipient-free salbutamol sulphate for inhalation. *European Journal of Pharmaceutics and Biopharmaceutics* 2012;80:149–55.
- [6] Claus S, Weiler C, Schiewe J, Friess W. How can we bring high drug doses to the lung? *European Journal of Pharmaceutics and Biopharmaceutics* 2014;86:1–6.
- [7] Le VNP, Hoang Thi, T. H., Robins E, Flament MP. In vitro evaluation of powders for inhalation: The effect of drug concentration on particle detachment. *International Journal of Pharmaceutics* 2012;424:44–9.
- [8] Geller DE, Weers J, Heuerding S. Development of an inhaled dry-powder formulation of tobramycin using PulmoSphere™ technology. *Journal of aerosol medicine and pulmonary drug delivery* 2011;24:175–82.
- [9] Prime D, Atkins PJ, Slater A, Sumbly B. Review of dry powder inhalers. *Dry Powder Formulations for Inhalation* 1997;26:51–8.
- [10] Ivey JW, Lewis D, Church T, Finlay WH, Vehring R. A correlation equation for the mass median aerodynamic diameter of the aerosol emitted by solution metered dose inhalers. *International Journal of Pharmaceutics* 2014;465:18–24.
- [11] Nolan LM, Li J, Tajber L, Corrigan OI, Healy AM. Particle engineering of materials for oral inhalation by dry powder inhalers. II—Sodium cromoglicate. *International Journal of Pharmaceutics* 2011;405:36–46.
- [12] Xu K, Zheng S, Zhai Y, Guo L, Tang P, Yan J, Di Wu et al. Two solid forms of tauroursodeoxycholic acid and the effects of milling and storage temperature on solid-state transformations. *International Journal of Pharmaceutics* 2015;486:185–94.

- [13] Wang MH, Onai Y, Hoshi Y, Lei H, Kondo T, Uchida T, Singkarat S et al. Thermal change of amorphous indium tin oxide films sputter-deposited in water vapor atmosphere. 5th International Symposium on Transparent Oxide Thin Films for Electronics and Optics 2008;516:5809–13.
- [14] Ruiz-Cabrera MA, Schmidt SJ. Determination of glass transition temperatures during cooling and heating of low-moisture amorphous sugar mixtures. *Journal of Food Engineering* 2015;146:36–43.
- [15] Sheokand S, Modi SR, Bansal AK. Dynamic vapor sorption as a tool for characterization and quantification of amorphous content in predominantly crystalline materials. *Journal of pharmaceutical sciences* 2014;103:3364–76.
- [16] Stubberud L, Forbes RT. The use of gravimetry for the study of the effect of additives on the moisture-induced recrystallisation of amorphous lactose. *International Journal of Pharmaceutics* 1998;163:145–56.
- [17] Kawashima Y, Serigano T, Hino T, Yamamoto H, Takeuchi H. Effect of surface morphology of carrier lactose on dry powder inhalation property of pranlukast hydrate. *International Journal of Pharmaceutics* 1998;172:179–88.
- [18] Nielsen LH, Gordon S, Holm R, Selen A, Rades T, Müllertz A. Preparation of an amorphous sodium furosemide salt improves solubility and dissolution rate and leads to a faster Tmax after oral dosing to rats. *European Journal of Pharmaceutics and Biopharmaceutics* 2013;85:942–51.
- [19] Wlodarski K, Sawicki W, Paluch KJ, Tajber L, Grembecka M, Hawelek L, Wojnarowska Z et al. The influence of amorphization methods on the apparent solubility and dissolution rate of tadalafil. *European Journal of Pharmaceutical Sciences* 2014;62:132–40.
- [20] Karmwar P, Graeser K, Gordon KC, Strachan CJ, Rades T. Effect of different preparation methods on the dissolution behaviour of amorphous indomethacin. *European Journal of Pharmaceutics and Biopharmaceutics* 2012;80:459–64.
- [21] Saleki-Gerhardt A, Ahlneck C, Zografi G. Assessment of disorder in crystalline solids. *International Journal of Pharmaceutics* 1994;101:237–47.
- [22] Lane RA, Buckton G. The novel combination of dynamic vapour sorption gravimetric analysis and near infra-red spectroscopy as a hyphenated technique. *International Journal of Pharmaceutics* 2000;207:49–56.

- [23] Buckton G, Darcy P. Assessment of disorder in crystalline powders—a review of analytical techniques and their application. *International Journal of Pharmaceutics* 1999;179:141–58.
- [24] Briggner L, Buckton G, Bystrom K, Darcy P. The use of isothermal microcalorimetry in the study of changes in crystallinity induced during the processing of powders. *International Journal of Pharmaceutics* 1994;105:125–35.
- [25] Mackin L, Zanon R, Park JM, Foster K, Opalenik H, Demonte M. Quantification of low levels (<10%) of amorphous content in micronised active batches using dynamic vapour sorption and isothermal microcalorimetry. *International Journal of Pharmaceutics* 2002;231:227–36.
- [26] Hunter NE, Frampton CS, Craig DQM, Belton PS. The use of dynamic vapour sorption methods for the characterisation of water uptake in amorphous trehalose. *Carbohydrate Research* 2010;345:1938–44.
- [27] Samra RM, Buckton G. The crystallisation of a model hydrophobic drug (terfenadine) following exposure to humidity and organic vapours. *International Journal of Pharmaceutics* 2004;284:53–60.
- [28] Hakim A, Usmani OS. Structure of the Lower Respiratory Tract. In: Reference Module in Biomedical Sciences: Elsevier; 2014.
- [29] Mutschler E. Mutschler Arzneimittelwirkungen: Lehrbuch der Pharmakologie und Toxikologie. 9th ed.: Wissenschaftliche Verlagsgesellschaft mbH Stuttgart; 2008.
- [30] Daniher DI, Zhu J. Dry powder platform for pulmonary drug delivery. *Particuology* 2008;6:225–38.
- [31] Schlesinger RB, Gardner DE. Respiratory Tract Toxicology. In: Wexler P, editor. *Encyclopedia of Toxicology (Third Edition)*. Oxford: Academic Press; 2014. p. 103–125.
- [32] Healy AM, Amaro MI, Paluch KJ, Tajber L. Dry powders for oral inhalation free of lactose carrier particles. Improving the efficacy of inhaled drugs for severe lung diseases: emerging pulmonary delivery strategies 2014;75:32–52.
- [33] Duret C, Wauthoz N, Sebti T, Vanderbist F, Amighi K. Solid dispersions of itraconazole for inhalation with enhanced dissolution, solubility and dispersion properties. *International Journal of Pharmaceutics* 2012;428:103–13.
- [34] de Boer, A. H, Gjaltema D, Hagedoorn P, Frijlink HW. Characterization of inhalation aerosols: a critical evaluation of cascade impactor analysis and laser diffraction technique. *International Journal of Pharmaceutics* 2002;249:219–31.

- [35] Pilcer G, Amighi K. Formulation strategy and use of excipients in pulmonary drug delivery. *International Journal of Pharmaceutics* 2010;392:1–19.
- [36] Patil-Gadhe A, Kyadarkunte A, Patole M, Pokharkar V. Montelukast-loaded nanostructured lipid carriers: Part II Pulmonary drug delivery and in vitro–in vivo aerosol performance. *European Journal of Pharmaceutics and Biopharmaceutics* 2014;88:169–77.
- [37] Yang MY, Chan, John Gar Yan, Chan H. Pulmonary drug delivery by powder aerosols. *Drug Delivery Research in Asia and the Pacific Region* 2014;193:228–40.
- [38] Copley Scientific. *Quality Solution for Inhaler Testing* 2012.
- [39] Alhaider SA, Alshehri HA, Al-Eid K. Replacing nebulizers by MDI-spacers for bronchodilator and inhaled corticosteroid administration: Impact on the utilization of hospital resources. *International Journal of Pediatrics and Adolescent Medicine* 2014;1:26–30.
- [40] Kwok, Philip Chi Lip, Chan H. Delivery of inhalation drugs to children for asthma and other respiratory diseases. *Drug delivery and the paediatric population: where are we at?* 2014;73:83–8.
- [41] Steckel H, Eskandar F. Factors affecting aerosol performance during nebulization with jet and ultrasonic nebulizers. *European Journal of Pharmaceutical Sciences* 2003;19:443–55.
- [42] Sheth P, Stein SW, Myrdal PB. The influence of initial atomized droplet size on residual particle size from pressurized metered dose inhalers. *International Journal of Pharmaceutics* 2013;455:57–65.
- [43] Poochikian. *MDI and DPI Drug Products*. Food and Drug Administration 1998.
- [44] Otto-Knapp R, Conrad F, Hösch S, Metzenauer P, Maus J, Noga O, Petzold U et al. Efficacy and safety of formoterol delivered through the Novolizer®, a novel dry powder inhaler (DPI) compared with a standard DPI in patients with moderate to severe asthma. *Pulmonary Pharmacology & Therapeutics* 2008;21:47–53.
- [45] D'Sa D, Chan H, Chrzanowski W. Predicting physical stability in pressurized metered dose inhalers via dwell and instantaneous force colloidal probe microscopy. *European Journal of Pharmaceutics and Biopharmaceutics* 2014;88:129–35.
- [46] Suwandecha T, Wongpoowarak W, Maliwan K, Srichana T. Effect of turbulent kinetic energy on dry powder inhaler performance. *Powder Technology* 2014;267:381–91.
- [47] Dolovich MB, Dhand R. Aerosol drug delivery: developments in device design and clinical use. *The Lancet* 19;377:1032–45.

- [48] Stoklosa AM, Lipasek RA, Taylor LS, Mauer LJ. Effects of storage conditions, formulation, and particle size on moisture sorption and flowability of powders: A study of deliquescent ingredient blends. *Food Research International* 2012;49:783–91.
- [49] Ghorl MU, Šupuk E, Conway BR. Tribo-electric charging and adhesion of cellulose ethers and their mixtures with flurbiprofen. *European Journal of Pharmaceutical Sciences* 2014;65:1–8.
- [50] Kaialy W, Nokhodchi A. Dry powder inhalers: Physicochemical and aerosolization properties of several size-fractions of a promising alternative carrier, freeze-dried mannitol. *European Journal of Pharmaceutical Sciences* 2015;68:56–67.
- [51] Markert M, Klumpp A, Trautmann T, Guth B. A novel propellant-free inhalation drug delivery system for cardiovascular drug safety evaluation in conscious dogs. *Journal of Pharmacological and Toxicological Methods* 2004;50:109–19.
- [52] Kuhli M, Weiss M, Steckel H. A new approach to characterise pharmaceutical aerosols: Measurement of aerosol from a single dose aqueous inhaler with an optical particle counter. *European Journal of Pharmaceutical Sciences* 2010;39:45–52.
- [53] Zhou Q, Morton, David A. V. Drug–lactose binding aspects in adhesive mixtures: Controlling performance in dry powder inhaler formulations by altering lactose carrier surfaces. *Lactose as a carrier for inhalation products* 2012;64:275–84.
- [54] Behara, Srinivas Ravindra Babu, Kippax P, McIntosh MP, Morton, David A. V., Larson I, Stewart P. Structural influence of cohesive mixtures of salbutamol sulphate and lactose on aerosolisation and de-agglomeration behaviour under dynamic conditions. *European Journal of Pharmaceutical Sciences* 2011;42:210–9.
- [55] Zeng XM, Martin GP, Tee S, Ghoush AA, Marriott C. Effects of particle size and adding sequence of fine lactose on the deposition of salbutamol sulphate from a dry powder formulation. *International Journal of Pharmaceutics* 1999;182:133–44.
- [56] Zeng XM, Martin GP, Tee S, Marriott C. The role of fine particle lactose on the dispersion and deaggregation of salbutamol sulphate in an air stream in vitro. *International Journal of Pharmaceutics* 1998;176:99–110.
- [57] Dickhoff, B. H. J., de Boer, A. H., Lambregts D, Frijlink HW. The effect of carrier surface treatment on drug particle detachment from crystalline carriers in adhesive mixtures for inhalation. *International Journal of Pharmaceutics* 2006;327:17–25.
- [58] Grasmeijer F, Lexmond AJ, van den Noort M, Hagedoorn P, Hickey AJ, Frijlink HW, Boer, Anne H. de. New mechanisms to explain the effects of added lactose fines on the dispersion performance of adhesive mixtures for inhalation. *PLoS ONE* 2014;9:e87825.

- [59] Pilcer G, Wauthoz N, Amighi K. Lactose characteristics and the generation of the aerosol. Lactose as a carrier for inhalation products 2012;64:233–56.
- [60] Schubert H. Grundlagen des Agglomerierens. Chem. Ing. Techn. 1979;266–77.
- [61] Bauer / Frömmig / Führer. Pharmazeutische Technologie: Mit Einführung in die Biopharmazie. 9th ed. Stuttgart: Wissenschaftliche Verlagsgesellschaft; 2012.
- [62] Butt H, Kappl M. Normal capillary forces. Advances in Colloid and Interface Science 2009;146:48–60.
- [63] Müller A. Untersuchungen zur fließregulierenden Eigenschaft hochdispenser Fällungskieselsäuren; 2008.
- [64] Knoll J, Nirschl H. Influence of the magnetic force on the van der Waals force of superparamagnetic composite particles. Powder Technology 2014;259:30–6.
- [65] Bailey AG. Charging of Solids and Powders. Journal of Electrostatics 1993;30:167–80.
- [66] Matsusaka S, Maruyama H, Matsuyama T, Ghadiri M. Triboelectric charging of powders: A review. Chemical Engineering Science 2010;65:5781–807.
- [67] Ouyang Q, Ishida K, Okada K. Investigation of micro-adhesion by atomic force microscopy. Applied Surface Science 2001;169–170:644–8.
- [68] Atkins PW, Paula J de. Kurzlehrbuch Physikalische Chemie. 4th ed.: WILEY-VCH Verlag GmbH & Co. KGaA; 2008.
- [69] Zijlstra GS, Hinrichs, Wouter L. J., Boer, Anne H. de, Frijlink HW. The role of particle engineering in relation to formulation and de-agglomeration principle in the development of a dry powder formulation for inhalation of cetorelix. European Journal of Pharmaceutical Sciences 2004;23:139–49.
- [70] Zeng XM, Martin GP, Marriott C, Pritchard J. The influence of carrier morphology on drug delivery by dry powder inhalers. International Journal of Pharmaceutics 2000;200:93–106.
- [71] de Boer, A. H., Hagedoorn P, Gjaltema D, Goede J, Kussendrager KD, Frijlink HW. Air classifier technology (ACT) in dry powder inhalation Part 2. The effect of lactose carrier surface properties on the drug-to-carrier interaction in adhesive mixtures for inhalation. International Journal of Pharmaceutics 2003;260:201–16.
- [72] Zeng X, MacRitchie HB, Marriott C, Martin GP. Humidity-induced changes of the aerodynamic properties of dry powder aerosol formulations containing different carriers. International Journal of Pharmaceutics 2007;333:45–55.

- [73] Niedballa S. Dispergierung von feinen Partikelfractionen in Gasströmungen - Einfluss von Dispergierbeanspruchung und oberflächenmodifizierenden Zusätzen; 1999.
- [74] Hofmann W. Modelling inhaled particle deposition in the human lung—A review. *Journal of Aerosol Science* 2011;42:693–724.
- [75] Fernández Tena A, Casan Clarà P. Deposition of Inhaled Particles in the Lungs. *Archivos de Bronconeumología (English Edition)* 2012;48:240–6.
- [76] Lee WL, Jayathilake PG, Tan Z, Le DV, Lee HP, Khoo BC. Muco-ciliary transport: Effect of mucus viscosity, cilia beat frequency and cilia density. *Computers & Fluids* 2011;49:214–21.
- [77] Carvalho TC, Peters JI, Williams III, Robert O. Influence of particle size on regional lung deposition – What evidence is there? *International Journal of Pharmaceutics* 2011;406:1–10.
- [78] Zeng XM, Martin G, Marriott C. *Particulate Interactions in Dry Powder Formulations* for. London: Informa Healthcare; 2000.
- [79] Caron V, Willart J, Lefort R, Derollez P, Danède F, Descamps M. Solid state amorphization kinetic of alpha lactose upon mechanical milling. *Carbohydrate Research* 2011;346:2622–8.
- [80] Vollenbroek J, Hebbink GA, Ziffels S, Steckel H. Determination of low levels of amorphous content in inhalation grade lactose by moisture sorption isotherms. *International Journal of Pharmaceutics* 2010;395:62–70.
- [81] Cheng SZ. *Phase Transitions in Polymers: The Role of Metastables State*: Elsevier; 2008.
- [82] Kauzmann W. *The Nature of the Glassy State and the Behavior of Liquids at low Temperatures* 1948.
- [83] Hancock BC, Shamblin SL. Molecular mobility of amorphous pharmaceuticals determined using differential scanning calorimetry. *New Advances in Pharmaceutical Thermal Analysis* 2001;380:95–107.
- [84] Price R, Young PM, Edge S, Staniforth JN. The influence of relative humidity on particulate interactions in carrier-based dry powder inhaler formulations. *International Journal of Pharmaceutics* 2002;246:47–59.
- [85] Monkos K. Determination of the glass-transition temperature of proteins from a viscometric approach. *International Journal of Biological Macromolecules* 2015;74:1–4.

- [86] Chaudhary DS, Adhikari BP, Kasapis S. Glass-transition behaviour of plasticized starch biopolymer system – A modified Gordon–Taylor approach. *Food Hydrocolloids* 2011;25:114–21.
- [87] Koiwai R, Kawanowa H, Gotoh Y, Souda R. Characterization of water, ethanol, and 1-butanol films by interaction with C6F14. *ECOSS-24 Proceedings of the 24th European Conference on Surface Science* 2007;601:4557–61.
- [88] Hilfiker R. *Polymorphism: In the Pharmaceutical Industry*; 2006.
- [89] ZuWallack R, De Salvo, M. C., Kaelin T, Bateman ED, Park CS, Abrahams R, Fakhri F et al. Efficacy and safety of ipratropium bromide/albuterol delivered via Respimat® inhaler versus MDI. *Respiratory Medicine* 2010;104:1179–88.
- [90] Gelb AF, Karpel J, Wise RA, Cassino C, Johnson P, Conoscenti CS. Bronchodilator efficacy of the fixed combination of ipratropium and albuterol compared to albuterol alone in moderate-to-severe persistent asthma. *Special Section: Cystic Fibrosis Symposia* 2008;21:630–6.
- [91] Cazzola M, Molimard M. The scientific rationale for combining long-acting β_2 -agonists and muscarinic antagonists in COPD. *Pulmonary Pharmacology & Therapeutics* 2010;23:257–67.
- [92] Boehringer Ingelheim Pharma GmbH & Co. KG. Binger Straße 173, 55216 Ingelheim.
- [93] Cazzola M, Calzetta L, Page CP, Rogliani P, Facciolo F, Gavaldà A, Matera MG. Pharmacological characterization of the interaction between aclidinium bromide and formoterol fumarate on human isolated bronchi. *European Journal of Pharmacology* 2014;745:135–43.
- [94] Nials AT, Ball DI, Butchers PR, Coleman RA, Humbles AA, Johnson M, Vardey CJ. Formoterol on airway smooth muscle and human lung mast cells: a comparison with salbutamol and salmeterol. *European Journal of Pharmacology* 1994;251:127–35.
- [95] Brodka-Pfeiffer K, Langguth P, Graß P, Häusler H. Influence of mechanical activation on the physical stability of salbutamol sulphate. *European Journal of Pharmaceutics and Biopharmaceutics* 2003;56:393–400.
- [96] Chawla A, Taylor KMG, Newton JM, Johnson MCR. Production of spray dried salbutamol sulphate for use in dry powder aerosol formulation. *International Journal of Pharmaceutics* 1994;108:233–40.
- [97] Matera MG, Calzetta L, Rogliani P, Bardaro F, Page CP, Cazzola M. Evaluation of the effects of the R- and S-enantiomers of salbutamol on equine isolated bronchi. *Translation-*

- al Medicine Approaches to the Study of Pulmonary Diseases Translational Medicine Approaches to the Study of Pulmonary Diseases 2011;24:221–6.
- [98] Zhang X, Liu Q, Hu J, Xu L, Tan W. An aerosol formulation of R-salbutamol sulfate for pulmonary inhalation. *SI: Drug Delivery System and Pharmaceutical Technology* 2014;4:79–85.
- [99] Corrigan DO, Corrigan OI, Healy AM. Physicochemical and in vitro deposition properties of salbutamol sulphate/ipratropium bromide and salbutamol sulphate/excipient spray dried mixtures for use in dry powder inhalers. *International Journal of Pharmaceutics* 2006;322:22–30.
- [100] Su M, Song M, Zhuang Y, Wang Y, Hang T. Simultaneous determination of ciclesonide and its active metabolite desisobutyryl-ciclesonide in human plasma by LC–APCI-MS/MS: Application to pharmacokinetic study in healthy Chinese volunteers. *Journal of Pharmaceutical and Biomedical Analysis* 2011;55:230–5.
- [101] Boero S, Sabatini F, Silvestri M, Petecchia L, Nachira A, Pezzolo A, Scarso L et al. Modulation of human lung fibroblast functions by ciclesonide: Evidence for its conversion into the active metabolite desisobutyryl-ciclesonide. *Immunology Letters* 2007;112:39–46.
- [102] Schroeder S, Fleischer DM, Masterson JC, Gelfand E, Furuta GT, Atkins D. Successful treatment of eosinophilic esophagitis with ciclesonide. *The Journal of allergy and clinical immunology* 2012;129:1419–21.
- [103] Vogelmeier CF, Hering T, Lewin T, Sander P, Bethke TD. Efficacy and safety of ciclesonide in the treatment of 24,037 asthmatic patients in routine medical care. *Respiratory Medicine* 2011;105:186–94.
- [104] Murphy KR, Dhand R, Trudo F, Uryniak T, Aggarwal A, Eckerwall G. Therapeutic equivalence of budesonide/formoterol delivered via breath-actuated inhaler vs pMDI. *Respiratory Medicine*.
- [105] Xia M, Ding X, Qi J, Gu J, Hu G, Sun X. Inhaled budesonide protects against chronic asthma-induced neuroinflammation in mouse brain. *Journal of Neuroimmunology* 2014;273:53–7.
- [106] Hozawa S, Terada M, Hozawa M. Comparison of the effects of budesonide/formoterol maintenance and reliever therapy with fluticasone/salmeterol fixed-dose treatment on airway inflammation and small airway impairment in patients who need to step-up from inhaled corticosteroid monotherapy. *Pulmonary Pharmacology & Therapeutics* 2014;27:190–6.

- [107] da Costa, Alice Vieira, Calábria LK, de Souza Santos, Paula, Goulart LR, Espindola FS. Glibenclamide treatment modulates the expression and localization of myosin-IIB in diabetic rat brain. *Journal of the Neurological Sciences* 2014;340:159–64.
- [108] Serrano-Martín X, Payares G, Mendoza-León A. Glibenclamide, a blocker of K^+ (ATP) channels, shows antileishmanial activity in experimental murine cutaneous leishmaniasis. *Antimicrobial agents and chemotherapy* 2006;50:4214–6.
- [109] Dressman J, Butler J, Hempenstall J, Reppas C. The BCS: Where do we go from here? *Pharm. Technologie* 2001:68–76.
- [110] Wu L, Miao X, Shan Z, Huang Y, Li L, Pan X, Yao Q et al. Studies on the spray dried lactose as carrier for dry powder inhalation. *Asian Journal of Pharmaceutical Sciences* 2014;9:336–41.
- [111] Kho K, Hadinoto K. Dry powder inhaler delivery of amorphous drug nanoparticles: Effects of the lactose carrier particle shape and size. *Powder Technology* 2013;233:303–11.
- [112] Larhrib H, Martin GP, Marriott C, Prime D. The influence of carrier and drug morphology on drug delivery from dry powder formulations. *International Journal of Pharmaceutics* 2003;257:283–96.
- [113] Donovan MJ, Smyth, Hugh D. C. Influence of size and surface roughness of large lactose carrier particles in dry powder inhaler formulations. *International Journal of Pharmaceutics* 2010;402:1–9.
- [114] Antunes, A. E. C., Silva e Alves, A. T., Gallina DA, Trento, F. K. H. S., Zacarchenco PB, Van Dender, A. G. F., Moreno I et al. Development and shelf-life determination of pasteurized, microfiltered, lactose hydrolyzed skim milk. *Journal of Dairy Science* 2014;97:5337–44.
- [115] Rogachev AS, Moskovskikh DO, Nepapushev AA, Sviridova TA, Vadchenko SG, Rogachev SA, Mukasyan AS. Experimental investigation of milling regimes in planetary ball mill and their influence on structure and reactivity of gasless powder exothermic mixtures. *Powder Technology* 2015;274:44–52.
- [116] Ghosh J, Mazumdar S, Das M, Ghatak S, Basu AK. Microstructural characterization of amorphous and nanocrystalline boron nitride prepared by high-energy ball milling. *Materials Research Bulletin* 2008;43:1023–31.
- [117] Rehder S, Sakmann A, Rades T, Leopold CS. Thermal degradation of amorphous glibenclamide. *European Journal of Pharmaceutics and Biopharmaceutics* 2012;80:203–8.

- [118] Kozawa K, Seto T, Otani Y. Development of a spiral-flow jet mill with improved classification performance. *Advanced Powder Technology* 2012;23:601–6.
- [119] Sawpan MA, Holdsworth PG, Renshaw P. Glass transitions of hygrothermal aged pultruded glass fibre reinforced polymer rebar by dynamic mechanical thermal analysis. *Materials & Design* 2012;42:272–8.
- [120] Qiao JC, Cardinal S, Pelletier JM, Kato H. Insight on the process ability of bulk metallic glasses by thermo-mechanical analysis and dynamic mechanical analysis. *Journal of Alloys and Compounds* 2015;628:357–63.
- [121] Moreno-Hernandez D, Andrés Bueno-García J, Ascención Guerrero-Viramontes J, Mendoza-Santoyo F. 3D particle positioning by using the Fraunhofer criterion. *Research in Optics and Photonics at CIO, Mexico* 2011;49:729–35.
- [122] Ylä-Mäihäniemi PP, Heng, Jerry Y. Y., Thielmann F, Williams DR. Inverse gas chromatographic method for measuring the dispersive surface energy distribution for particulates. *Langmuir* 2008;24:9551–7.
- [123] Eisazadeh A, Kassim KA, Nur H. Morphology and BET surface area of phosphoric acid stabilized tropical soils. *Engineering Geology* 2013;154:36–41.
- [124] Harnby N. An engineering view of pharmaceutical powder mixing. *Pharmaceutical Science & Technology Today* 2000;3:303–9.
- [125] Taki M, Marriott C, Zeng X, Martin GP. Aerodynamic deposition of combination dry powder inhaler formulations in vitro: A comparison of three impactors. *International Journal of Pharmaceutics* 2010;388:40–51.
- [126] May S, Jensen B, Wolkenhauer M, Schneider M, Lehr CM. Dissolution Techniques for In Vitro Testing of Dry Powders for Inhalation. *Pharm Res* 2012;29:2157–66.
- [127] May S, Jensen B, Weiler C, Wolkenhauer M, Schneider M, Lehr C. Dissolution testing of powders for inhalation: influence of particle deposition and modeling of dissolution profiles. *Pharm Res* 2014;31:3211–24.
- [128] Kleppmann W. *Versuchsplanung - Produkte und Prozesse optimieren*. 7th ed.: Hanser; 2011.
- [129] Craig, Duncan Q. M, Royall PG, Kett VL, Hopton ML. The relevance of the amorphous state to pharmaceutical dosage forms: glassy drugs and freeze dried systems. *International Journal of Pharmaceutics* 1999;179:179–207.
- [130] Gurunath S, Pradeep Kumar S, Basavaraj NK, Patil PA. Amorphous solid dispersion method for improving oral bioavailability of poorly water-soluble drugs. *Journal of Pharmacy Research* 2013;6:476–80.

- [131] Petzoldt C, Bley O, Byard SJ, Andert D, Baumgartner B, Nagel N, Tappertzhofen C et al. An example of how to handle amorphous fractions in API during early pharmaceutical development: SAR114137 – A successful approach. *European Journal of Pharmaceutics and Biopharmaceutics* 2014;86:337–50.
- [132] Martínez LM, Videa M, López-Silva GA, de los Reyes, Carlos A., Cruz-Angeles J, González N. Stabilization of amorphous paracetamol based systems using traditional and novel strategies. *International Journal of Pharmaceutics* 2014;477:294–305.
- [133] Chikhalia V, Forbes RT, Storey RA, Ticehurst M. The effect of crystal morphology and mill type on milling induced crystal disorder. *European Journal of Pharmaceutical Sciences* 2006;27:19–26.
- [134] Müller T, Krehl R, Schiewe J, Weiler C, Steckel H. Influence of small amorphous amounts in hydrophilic and hydrophobic APIs on storage stability of dry powder inhalation products. *European Journal of Pharmaceutics and Biopharmaceutics* 2015;92:130–8.
- [135] Sun P, Wu S, Chin T. Melting point depression of tin nanoparticles embedded in a stable alpha-alumina matrix fabricated by ball milling. *Materials Letters* 2015;144:142–5.
- [136] Weiler C. Generierung leicht dispergierbarer Inhalationspulver mittels Sprühtrocknung; 2008.
- [137] Guo Y, Shalaev E, Smith S. Physical stability of pharmaceutical formulations: solid-state characterization of amorphous dispersions. *TrAC Trends in Analytical Chemistry* 2013;49:137–44.
- [138] Müller E, Bayer O, Meerwein, H., Ziegler, K. Houben-Weyl Methods of Organic Chemistry: Carbocyclic p-Electron Systems. 4th ed.: Thieme; 1975.
- [139] Li N, Taylor LS, Mauer LJ. The physical and chemical stability of amorphous (–)-epigallocatechin gallate: Effects of water vapor sorption and storage temperature. *Food Research International* 2014;58:112–23.
- [140] Tajber L, Corrigan DO, Corrigan OI, Healy AM. Spray drying of budesonide, formoterol fumarate and their composites—I. Physicochemical characterisation. *International Journal of Pharmaceutics* 2009;367:79–85.
- [141] Jones R, Pollock HM, Geldart D, Verlinden A. Inter-particle forces in cohesive powders studied by AFM: effects of relative humidity, particle size and wall adhesion. *Powder Technology* 2003;132:196–210.
- [142] Shah UV, Olusanmi D, Narang AS, Hussain MA, Tobbyn MJ, Heng, Jerry Y. Y. Decoupling the contribution of dispersive and acid-base components of surface energy on the

- cohesion of pharmaceutical powders. *International Journal of Pharmaceutics* 2014;475:592–6.
- [143] Lehto V, Tenho M, Vähä-Heikkilä K, Harjunen P, Päällysaho M, Väliisaari J, Niemelä P et al. The comparison of seven different methods to quantify the amorphous content of spray dried lactose. *Powder Technology* 2006;167:85–93.
- [144] Müller T, Schiewe J, Smal R, Weiler C, Wolkenhauer M, Steckel H. Measurement of low amounts of amorphous content in hydrophobic active pharmaceutical ingredients with dynamic organic vapor sorption. *European Journal of Pharmaceutics and Biopharmaceutics* 2015;92:102–11.
- [145] Young PM, Chiou H, Tee T, Traini D, Chan H, Thielmann F, Burnett D. The use of organic vapor sorption to determine low levels of amorphous content in processed pharmaceutical powders. *Drug Development and Industrial Pharmacy* 2007;33:91–7.
- [146] Rucker G, Neugebauer M, Willems GG. *Instrumentelle pharmazeutische Analytik: Lehrbuch zu spektroskopischen, chromatographischen, elektrochemischen und thermischen Analysemethoden*. 4th ed.: Wissenschaftliche Verlagsgesellschaft mbH Stuttgart; 2008.
- [147] Muhammad, Syed Anuar Fua'ad Syed, Langrish T, Tang P, Adi H, Chan H, Kazarian SG, Dehghani F. A novel method for the production of crystalline micronised particles. *International Journal of Pharmaceutics* 2010;388:114–22.
- [148] Weiler C, Egen M, Trunk M, Langguth P. *Force Control and Powder Dispersibility of Spray Dried Particles for Inhalation*. Wiley InterScience 2010:303–16.
- [149] Depalo A, Santomaso AC. Wetting dynamics and contact angles of powders studied through capillary rise experiments. *Colloids and Surfaces A: Physicochemical and Engineering Aspects* 2013;436:371–9.
- [150] Grasmeyer F, Frijlink HW, de Boer, Anne H. A proposed definition of the 'activity' of surface sites on lactose carriers for dry powder inhalation. *European Journal of Pharmaceutical Sciences* 2014;56:102–4.
- [151] Wagenseil L. *Untersuchungen zu Pulverstruktur und Deagglomerationsverhalten mikronisierter Pulverformulierungen zur Inhalation*; 2014.
- [152] Cordts E. *Advanced powder characterization techniques for inhalation powder mixtures*; 2014.
- [153] Zeng XM, Pandhal KH, Martin GP. The influence of lactose carrier on the content homogeneity and dispersibility of beclomethasone dipropionate from dry powder aerosols. *International Journal of Pharmaceutics* 2000;197:41–52.

- [154] Steckel H, Müller BW. In vitro evaluation of dry powder inhalers II: influence of carrier particle size and concentration on in vitro deposition. *International Journal of Pharmaceutics* 1997;154:31–7.
- [155] Dickhoff, B. H. J., de Boer, A. H., Lambregts D, Frijlink HW. The interaction between carrier rugosity and carrier payload, and its effect on drug particle redispersion from adhesive mixtures during inhalation. *European Journal of Pharmaceutics and Biopharmaceutics* 2005;59:197–205.
- [156] Rabinovich Y, Esayanur M, Johanson K, Lin C, Miller J, Moudgil BM. The flow behavior of the liquid/powder mixture, theory and experiment. I. The effect of the capillary force (bridging rupture). *Powder Technology* 2010;204:173–9.
- [157] Young PM, Price R. The influence of humidity on the aerosolisation of micronised and SEDS produced salbutamol sulphate. *European Journal of Pharmaceutical Sciences* 2004;22:235–40.
- [158] Harjunen P, Lankinen T, Salonen H, Lehto V, Järvinen K. Effects of carriers and storage of formulation on the lung deposition of a hydrophobic and hydrophilic drug from a DPI. *International Journal of Pharmaceutics* 2003;263:151–63.
- [159] Althaus TO, Windhab EJ, Scheuble N. Effect of pendular liquid bridges on the flow behavior of wet powders. *Powder Technology* 2012;217:599–606.
- [160] Zhu K, Tan, Reginald B. H., Kiong Ng W, Shen S, Zhou Q, Heng, Paul W. S. Analysis of the influence of relative humidity on the moisture sorption of particles and the aerosolization process in a dry powder inhaler. *Journal of Aerosol Science* 2008;39:510–24.
- [161] Aquino, Adelia J. A., Tunega D, Pašalić H, Schaumann GE, Haberhauer G, Gerzabek MH, Lischka H. Study of solvent effect on the stability of water bridge-linked carboxyl groups in humic acid models. *Advances of Molecular Modeling of Biogeochemical Interfaces in Soils* 2011;169:20–6.
- [162] Fung, W. W. S., Kwan, A. K. H. Effect of particle interlock on flow of aggregate through opening. *Powder Technology* 2014;253:198–206.
- [163] de Boer, A. H., Chan HK, Price R. A critical view on lactose-based drug formulation and device studies for dry powder inhalation: Which are relevant and what interactions to expect? *Lactose as a carrier for inhalation products* 2012;64:257–74.
- [164] Zellnitz S, Schroettner H, Urbanetz NA. Surface modified glass beads as model carriers in dry powder inhalers—Influence of drug load on the fine particle fraction. *Powder Technology* 2014;268:377–86.

- [165] de Boer, A. H., Dickhoff, B. H. J., Hagedoorn P, Gjaltema D, Goede J, Lambregts D, Frijlink HW. A critical evaluation of the relevant parameters for drug redispersion from adhesive mixtures during inhalation. *International Journal of Pharmaceutics* 2005;294:173–84.
- [166] Grisedale LC, Belton PS, Jamieson MJ, Barker SA, Craig DQM. An investigation into water interactions with amorphous and milled salbutamol sulphate: The development of predictive models for uptake and recrystallization. *International Journal of Pharmaceutics* 2012;422:220–8.
- [167] Son Y, McConville JT. Development of a standardized dissolution test method for inhaled pharmaceutical formulations. *International Journal of Pharmaceutics* 2009;382:15–22.
- [168] Informa Healthcare USA. *Pharmaceutical Dissolution Testing*; 2009.
- [169] Davies NM, Feddah MR. A novel method for assessing dissolution of aerosol inhaler products. *International Journal of Pharmaceutics* 2003;255:175–87.
- [170] Dokoumetzidis A, Macheras P. A century of dissolution research: From Noyes and Whitney to the Biopharmaceutics Classification System. *International Journal of Pharmaceutics* 2006;321:1–11.
- [171] Patton JS. Mechanisms of macromolecule absorption by the lungs. *Advanced Drug Delivery Reviews* 1996;19:3–36.
- [172] Grey VA, Hickey AJ, Balmer P, Davies NM, Dunbar C, Foster TS, Olsson BL et al. The Inhalation Ad Hoc Advisory Panel for the USP performance tests of inhalation dosage forms: *Pharmacopeial Forum* 34: 1068-1074; 2008.
- [173] Sabine May. *Dissolution Testing of Powders for Inhalation*; 2013.
- [174] Oh D, Curl RL, Amidon GL. Estimating the Fraction Dose Absorbed from Suspensions of Poorly Soluble Compounds in Humans: A Mathematical Model. *Pharm Res* 1993;264–70.
- [175] Ono A, Sugano K. Application of the BCS biowaiver approach to assessing bioequivalence of orally disintegrating tablets with immediate release formulations. *European Journal of Pharmaceutical Sciences* 2014;64:37–43.
- [176] Huang X, Brazel CS. On the importance and mechanisms of burst release in matrix-controlled drug delivery systems. *Journal of Controlled Release* 2001;73:121–36.
- [177] Imboden R, Imanidis G. Effect of the amphoteric properties of salbutamol on its release rate through a polypropylene control membrane. *European Journal of Pharmaceutics and Biopharmaceutics* 1999;47:161–7.

- [178] Zeng N, Dumortier G, Maury M, Mignet N, Boudy V. Influence of additives on a thermosensitive hydrogel for buccal delivery of salbutamol: Relation between micellization, gelation, mechanic and release properties. *International Journal of Pharmaceutics* 2014;467:70–83.
- [179] Ras M, Lefebvre D, Derlon N, Hamelin J, Bernet N, Paul E, Girbal-Neuhauser E. Distribution and hydrophobic properties of Extracellular Polymeric Substances in biofilms in relation towards cohesion. *Journal of Biotechnology* 2013;165:85–92.
- [180] Anderberg EK, Bisrat M, Nyström C. Physicochemical aspects of drug release. VII. The effect of surfactant concentration and drug particle size on solubility and dissolution rate of felodipine, a sparingly soluble drug. *International Journal of Pharmaceutics* 1988;47:67–77.
- [181] Sheng JJ, Sirois PJ, Dressman JB, Amidon GL. Particle diffusional layer thickness in a USP dissolution apparatus II: a combined function of particle size and paddle speed. *Journal of pharmaceutical sciences* 2008;4815–29.
- [182] Sertsou G. Analytical derivation of time required for dissolution of monodisperse drug particles. *Journal of pharmaceutical sciences* 2004;93:1941–4.

DANKSAGUNG

Die vorliegende Arbeit wurde von Oktober 2012 bis September 2015 im Pharmazeutischen Institut – Abteilung Technologie und Biopharmazie, an der Christian-Albrechts-Universität in Kooperation mit der Abteilung Respiratory Drug Delivery der Boehringer Ingelheim Pharma GmbH & Co. KG durchgeführt.

An erster Stelle möchte ich meinem verehrten Doktorvater, Herrn Prof. Dr. Hartwig Steckel, für die Stellung des Dissertationsthemas, die stetige Unterstützung und den vielen anregenden Diskussionen bei der Erstellung der Veröffentlichungen danken.

Weiterhin gilt mein Dank der Firma Boehringer Ingelheim für das Sponsoring dieses Projektes sowie Herrn Dr. Claudius Weiler für die angenehme Zusammenarbeit, für fachspezifische Anregungen und die stete Unterstützung. Herrn Dr. Jörg Schiewe danke ich für die Leitung des Projektes, das Interesse an den Ergebnissen und den Anregungen, die mir während zahlreicher Telefon-Konferenzen und Meetings gegeben wurden. Ebenfalls danke ich Herrn Dr. Markus Wolkenhauer für wertvolle Hinweise und Frau Dr. Sabine May für die Einführung in verschiedene analytische Messtechniken bei den praktischen Versuchen in Ingelheim.

Ebenso danke ich Frau Dr. habil. Regina Scherließ für die Betreuung und die wissenschaftliche Begleitung meiner Arbeit in den letzten Monaten.

Des Weiteren möchte ich mich bei allen Kollegen/-innen des Arbeitskreises für die gute Aufnahme und Unterstützung bedanken. Dies gilt besonders für die Anfertigungen von REM-Aufnahmen durch Gereon, Lars und Mathias, die Unterstützung der HPLC-Analytik durch Frau Regina Krehl und die Unterstützung bei der XRPD-Analytik sowie das Anfertigen verschiedener Abbildungen durch Herrn Rüdiger Smal. Ebenfalls möchte ich mich bei Herrn Dirk Böhme bedanken, der stets die Stickstoffversorgung für die DVS-Analytik sichergestellt hat. Herrn Felix Litty danke ich für Tipps aus der Pharmazeutischen Chemie. Weiterhin danke ich allen technischen Angestellten der Abteilung für zahlreiche Hilfeleistungen und technische Unterstützung. Außerdem danke ich Herrn Dr. Lars Wagenseil für das Korrekturlesen dieser Arbeit.

Ein herzliches Dankeschön geht an meine Freundin Lena, die mich stets unterstützt hat und die vorliegende Arbeit gelesen hat. Schließlich danke ich meinen Eltern und Geschwistern, die mich immer unterstützt haben und mit großem Interesse den Verlauf meiner Promotion verfolgt haben.

LEBENS LAUF**Persönliche Daten**

Nachname	Müller
Vorname	Thorsten Nicolas
Geburtsdatum	21. Dezember 1986
Geburtsort	Hamburg
Staatsangehörigkeit	deutsch

Schulbildung

1993 bis 1997	Herman-Löns Grundschule, Ellerbek
1997 bis 2006	Elsensee-Gymnasium, Quickborn
Juni 2006	Abitur
2006 bis 2007	Zivildienst (Johanniterhaus Quickborn)

Studium der Pharmazie

April 2007 bis März 2009	Pharmazie-Grundstudium an der Universität des Saarlandes (1. Abschnitt der Pharmazeutischen Prüfung)
April 2009 bis Mai 2011	Pharmazie-Hauptstudium an der Universität Kiel (2. Abschnitt der Pharmazeutischen Prüfung)
August 2012	Approbation als Apotheker (3. Abschnitt der Pharmazeutischen Prüfung)

Berufliche Erfahrung

Juli 2011 bis Dez. 2011	Pharmazeut im Praktikum, Wiking Apotheke, Laboe
Januar 2012 bis Juni 2012	Pharmazeut im Praktikum, Nordmark Arzneimittel GmbH & Co. KG, Uetersen
Seit September 2012	Promotion am Pharmazeutischen Institut der Universität Kiel, Abteilung Pharmazeutische Technologie und Biopharmazie, Arbeitsgruppe Prof. H. Steckel, in Kooperation mit Firma Boehringer Ingelheim Pharma GmbH & Co. KG

ERKLÄRUNG NACH § 8 DER PROMOTIONSORDNUNG

Hiermit erkläre ich gemäß § 8 der Promotionsordnung der Mathematisch-Naturwissenschaftlichen Fakultät der Christian-Albrechts-Universität zu Kiel, dass ich die vorliegende Arbeit, abgesehen von der Beratung durch meinen Betreuer, selbstständig und ohne fremde Hilfe verfasst habe. Weiterhin habe ich keine anderen als die angegebenen Quellen oder Hilfsmittel benutzt und die den benutzten Werken wörtlich oder inhaltlich entnommenen Stellen als solche kenntlich gemacht. Die vorliegende Arbeit ist unter Einhaltung der Regeln guter wissenschaftlicher Praxis entstanden und wurde bei keiner anderen Universität zur Begutachtung eingereicht.

Thorsten Müller

